ISBN 978-82-326-5479-6 (printed ver.)
ISBN 978-82-326-5626-4 (electronic ver.)
ISSN 1503-8181 (printed ver.)
ISSN 2703-8084 (electronic ver.)

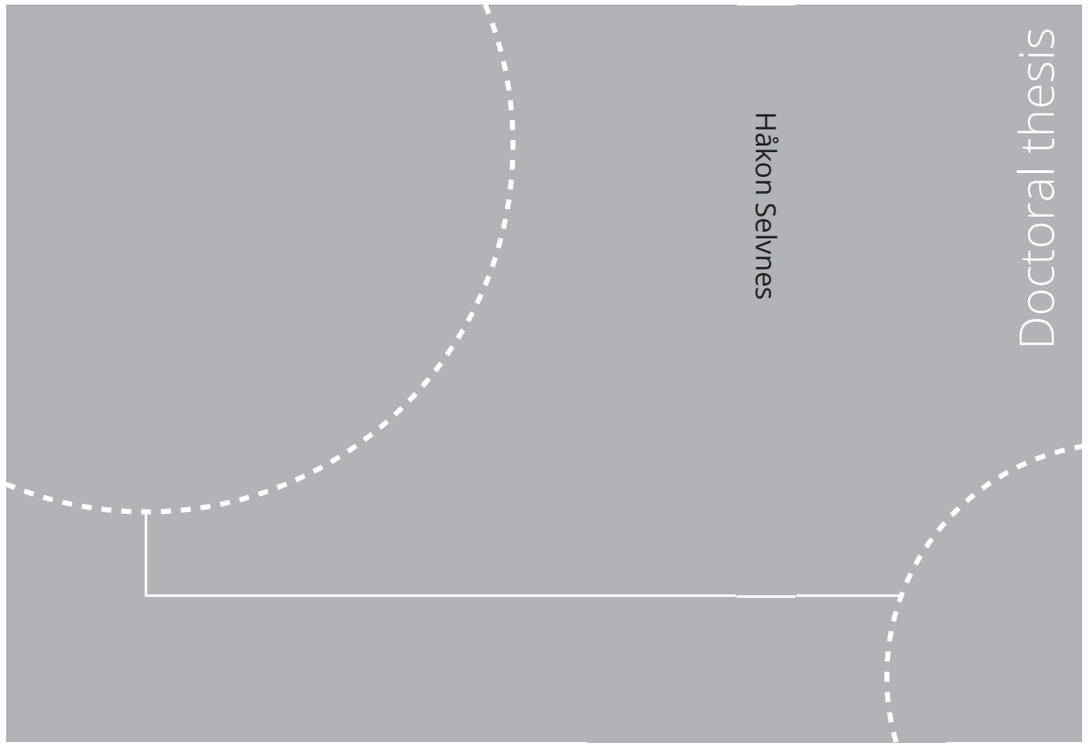

Doctoral theses at NTNU, 2022:387

Håkon Selvnes

Development of cold thermal energy storage for industrial refrigeration applications

NTNU
Norwegian University of
Science and Technology

Doctoral theses at NTNU, 2022:387

NTNU

NTNU
Norwegian University of
Science and Technology
Thesis for the degree of
Philosophiae Doctor
Faculty of Engineering
Department of Energy and Process Engineering

NTNU
Norwegian University of
Science and Technology

Håkon Selvnes

Development of cold thermal energy storage for industrial refrigeration applications

Thesis for the degree of Philosophiae Doctor

Trondheim, December 2022

Norwegian University of Science and Technology
Faculty of Engineering
Department of Energy and Process Engineering

NTNU
Norwegian University of
Science and Technology

NTNU
Norwegian University of Science and Technology

Thesis for the degree of Philosophiae Doctor

Faculty of Engineering
Department of Energy and Process Engineering

ISBN 978-82-326-5479-6 (printed ver.)
ISBN 978-82-326-5626-4 (electronic ver.)
ISSN 1503-8181 (printed ver.)
ISSN 2703-8084 (electronic ver.)

Doctoral theses at NTNU, 2022:387

PRINTED IN NORWAY
NO - 1598

NORDIC SWAN ECOLABEL
Printed matter
2041 0731

Printed by Skipnes Kommunikasjon AS

Preface

This thesis is submitted in partial fulfilment of the requirements for the degree of Doctor of Philosophy (Ph.D.) at the Norwegian University of Science and Technology (NTNU). The research described herein was carried out from August 2017 to May 2021 at the Department of Energy and Process Engineering of the Faculty of Engineering, with Professor Armin Hafner as the main supervisor and Associate Professor Yosr Allouche and Professor Trygve Magne Eikevik as co-supervisors. The present Ph.D. was funded by HighEFF: Centre for an Energy Efficient and Competitive Industry for the Future, under the FME-scheme (Centre for Environment-friendly Energy Research, 257632) with financial support from the Research Council of Norway and user partners of HighEFF.

Acknowledgments

I would like to express my deepest gratitude to all the people who have assisted and guided me along the path to completing this doctoral degree. Firstly, this thesis would not have been completed without the support and guidance of my supervisor, Professor Armin Hafner. I am forever thankful for the opportunity and your belief in me during all these years. Your knowledge and enthusiasm have truly been an inspiration to me. To my co-supervisor Dr. Yosr Allouche, thank you for your countless hours of discussion, guidance and corrections; I have learned so much from you. To my co-supervisor Professor Trygve Eikevik, thank you for always having an open door and sharing your knowledge. I would also like to thank Dr. Camila Barreneche and the group at the University of Barcelona for welcoming me and sharing their knowledge during a week in September 2019.

I would like to thank all my colleagues at NTNU for providing an inspiring and interesting work environment. Håvard Rekstad and Reidar Tellebon for sharing your deep experience and advice on refrigeration and experimental setups. To Lars Sørensen, Stein Skånøy and Hilde Faanes for constructing the test facility. A very special thanks to my good friends and fellow PhD students in the refrigeration group Silje Smitt, Ehsan Allymehr, Knut Ringstad and Marcel Ahrens. You created a welcoming and creative atmosphere I looked forward to every day.

I am forever grateful to my family for all the support and understanding during these years. To my brothers Eirik and Vegard - thank you for being there for me whenever I needed a timeout. To my parents, Kari and Per Arnfinn, thank you for all that you have done for me and for your unconditional support.

Finally, to my beautiful children Ida, Sverre and Åse - thank you for your endless love and for reminding me of the important things in life. To my dear Randi, thank you for always being by my side in life and supporting my decisions. This doctoral thesis is dedicated to you.

Summary

Refrigeration technology is a vital part of modern society, covering multiple applications from comfort cooling and process cooling of servers in data centres, to domestic, commercial, and industrial refrigeration systems. The market for refrigeration systems is continuously expanding, and space cooling is the fastest-growing end user of electricity in buildings today. Furthermore, refrigeration is essential in the food cold chain to preserve fresh and frozen goods and to prevent the important challenge of food loss. Refrigeration technology is crucial in every link of the cold chain, all the way from the processing plants, in transport, in retail and during the final stage at the consumer. Refrigeration systems are large electricity consumers, and some of these systems face high peak refrigeration loads and the associated high electricity consumption. Some examples of applications that experience large variations in the refrigeration load during the day are process cooling for the dairy industry and industrial freezing processes in food processing plants.

Thermal energy storage (TES) technology can be applied to refrigeration systems to decouple the supply of cooling from the refrigeration system and the demand for cooling from the consumer. When TES technology is applied to store thermal energy at sub-ambient temperatures, it is often called cold TES (CTES). The two methods of achieving CTES are sensible heat storage and latent heat storage. In the former method, CTES is achieved due to the change of temperature of a storage medium, such as water. In the latter method, CTES is achieved in the phase transition of a storage medium, often by melting and solidification. A substance capable of storing large quantities of thermal energy in the solid-liquid transition is often denoted as a phase change material (PCM). Common PCM for CTES application are paraffins and various salt-water solutions.

An in-depth review of applications of CTES using PCMs in refrigeration systems was carried out to identify the current research gaps and establish the state-of-the-

art. It was found that the interest in PCMs for the temperature range relevant to CTES applications has been increasing in the last few years, and commercial PCMs have become available on the market. It was found that research on the implementation of CTES technology in refrigeration has been carried out for multiple applications, including food transport and packaging, commercial refrigeration and various other refrigeration systems. Common to many of these applications is the pressing need to conduct experimental investigations of promising concepts studied theoretically in the past, such as for large-scale CTES systems for industrial cooling and freezing processes using ammonia or CO_2 as the refrigerant. Common ways to implement CTES in refrigeration systems in the past have consisted of using ice/water as the latent storage medium, particularly for space cooling and process cooling applications. These CTES systems are connected to the refrigeration plant by an intermediate heat transfer circuit with glycol. This concept reduces the efficiency of the refrigeration plant because the evaporation temperature must be reduced considerably compared to supplying the cooling directly at the consumer temperature. The cooling must be cascaded through the intermediate circuit and then to the consumer, while the charging process of the storage requires even lower supply temperatures. To improve the efficiency of CTES systems for refrigeration plants, it can be beneficial to integrate CTES units directly into the primary refrigerant circuit, effectively avoiding the secondary heat transfer circuit. However, the review revealed a research gap for CTES solutions suitable for industrial scale that can handle the operating pressure of refrigeration systems.

In the present research work, a novel concept for a CTES unit suitable for integration into the primary refrigerant circuit of a CO_2 refrigeration system has been developed. A lab-scale demonstration unit and an experimental test facility using CO_2 as the refrigerant was constructed. The novel concept is based on a special type of welded heat exchanger (HEX) plate called pillow plate (PP). The PPs are constructed of stainless steel and are stacked together to form a PP-HEX placed into a container. The container is filled with the PCM, immersing the PP-HEX into the storage medium. The PPs have flow channels inside for the refrigerant to exchange heat with the PCM outside the PPs. During the charging process of the CTES unit, the refrigerant evaporates due to heat extraction from the PCM, which solidifies on the PP surface. During the discharging process, the heat transfer direction is reversed so that the refrigerant condenses while the PCM is melting. The CTES unit is flexible by accepting various types of PCMs and refrigerants at multiple temperature levels.

The novel CTES unit has been tested experimentally by applying two types of storage media. Water/ice was first used as the PCM to provide the proof of concept, show the feasibility of operating the CTES unit in charging and discharging cycles and provide a benchmark for future PCMs. Then, a low-temperature commercial

PCM with a melting temperature of - 9.6 °C, suitable for the temperature requirement in food processing plants, was experimentally characterised using established methods before being tested in the CTES unit. Various refrigerant parameters and various PP-HEX geometries were tested. The experimental test campaigns on using water/ice and the commercial PCM have shown that the evaporation and condensation temperatures of the refrigerant are the most critical parameters influencing the performance of the charging and discharging cycles of the CTES unit, respectively. It was found that the charging time was mainly affected by the refrigerant evaporation temperature, while the discharging rate and discharged energy over the cycle increased with higher refrigerant condensing temperature. Furthermore, it was found that the distance between the PPs in the PP-HEX (plate pitch) influences the discharging characteristics of the CTES unit. A smaller plate pitch resulted in high discharge rates at the cost of lower thermal storage capacity. Increasing the plate pitch improved the thermal storage capacity, but the discharging cycle length increased. Hence, the average discharge rate was reduced.

In summary, the flexible design of the CTES unit allows the designer to select a discharge characteristic of the CTES unit that matches the refrigeration load curve of the refrigeration plant by changing the plate pitch. The present research work establishes the foundation for further improvement of the concept and considerations for up-scaling and industrial implementation in the future.

Table of contents

List of tables

List of figures

Nomenclature

$\dot{m}$	mass flow rate [kg/s]
$\dot{Q}$	heat flow [W]
b	thickness [m]
cp	specific heat capacity [J/(kg K)]
d	diameter [m]
h	enthalpy [J/kg]
l	length [m]
m	mass [kg]
n	number [-]
P	pressure [bar]
Q	heat [J]
s	welding spot pitch [m]
T	temperature [°C]
u	uncertainty [-]
V	volume [m^3]
W	work [J]

w width [m]

Greek letters

Δ difference [-]

δ distance, plate pitch [m]

$\dot{\gamma}$ shear rate [1/s]

η efficiency [-]

μ apparent viscosity [Pa s]

ρ density [kg/m^3]

τ shear stress [Pa]

θ volumetric storage capacity [J/m^3]

Subscripts

Ca carnot

CO_2 carbon dioxide

$cond$ condensaton

el electric

$evap$ evaporation

f final

fus fusion

g glycol

H high

i inflation

in initial

L low, longitudinal

lat latent

liq liquid

m melting

o outer

PCM phase change material

PP pillow plate

r reaction

sat saturation

$sens$ sensible

SP spot weld

$subcool$ subcooling

T transversal

tc thermochemical

TES thermal energy storage

tot total

w wall

Abbreviations

AC air conditioning

ACC auxiliary CO_2 circuit

CFC chlorofluorocarbon

CO_2 carbon dioxide

COP coefficient of performance

$CTES$ cold thermal energy storage

DP differential pressure

DSC differential scanning calorimetry

FT flow transmitter

GHC glycol heating circuit

GHG greenhouse gas

GWP global warming potential

$HCFC$ hydrofluorocarbon

HEX heat exchanger

HFO hydrofluoroolefin

IEA International Energy Agency

ODP ozone depletion potential

PCC primary CO_2 circuit

PCM phase change material

$PFAS$ polyfluoroalkyl substances

PID process and instrumentation diagram

PP pillow plate

PWM pulse-width modulation

RSW refrigerated sea water

SCC secondary CO_2 circuit

TC thermocouple

TES thermal energy storage

TFA trifluoroacetic acid

TPS transient plane source

VSD variable speed drive

1 Introduction

This chapter presents the motivation and objectives of the research within the scope of this doctoral work. The chapter presents the thesis structure and the list of scientific publications published within the scope of this thesis.

1.1 Motivation

Decarbonisation of the electricity generation, electrification of the industry, transport and the building sector, combined with a high focus on energy efficiency measures, are identified as key actions to limit global warming to the 1.5 °C target consistent with the Net Zero Emission by 2050 scenario [1]. Consequently, the demand for electricity and the peak power capacity required from the grid is predicted to increase substantially [2, 3, 4]. Refrigeration systems constitute an essential part of modern society. Refrigeration technology ensures the processing and preservation of food through the cold chain [5, 6], maintaining the temperature in our homes and workplaces at a comfortable level by air-conditioning (AC) [7] and keeps the server racks in data centres at optimum temperature for providing necessary IT services [8]. It has been estimated that about 15 % of global electricity use is related to refrigeration processes [9]. Furthermore, significant growth in the global demand for space cooling is predicted towards 2050, particularly in emerging economies [10]. Space cooling is the fastest-growing end-use in buildings today and has tripled since the 1990s. In many emerging economies, e.g. India, the middle class expands rapidly [11]. Consequently, the number of households that install AC units are rising, fuelled by the increased comfort requirement of the group. With the energy efficiency of AC units today, the International Energy Agency (IEA) predicts that space cooling will constitute 40-45 % of the total peak power demand in warm regions in 2050 [10].

About one-third of all food produced is wasted throughout the food chain [12], where lack of preservation methods and breaches in the cold chain is one example of a source of food waste. The food waste problem contributes largely to the global climate change issue due to the waste of energy resources spent for producing, harvesting, processing and transporting food products that are not utilised for human consumption. Refrigeration technology is central in the food production process, and about 40 % of all food products require refrigeration [6], either in processing, transport, cold storage, retail or domestic storage. Refrigeration systems must be designed to cover the peak refrigeration load it expects to encounter, usually occurring on the warmest day of the year. Chillers for AC applications are typically designed to provide a specific refrigeration capacity to the building during the warmest day of the year. Consequently, the refrigeration plant operates at part load conditions for most of the year, which is generally associated with a reduction in the energy efficiency of these systems. More efficient part load regulation technology for refrigeration systems has been introduced to the market in recent years, such as variable speed drive (VSD) regulation for compressor motors and cylinder unloading technology for compressor capacity regulation. Nevertheless, the refrigeration system must be sized to cover the peak demand, increasing the investment costs of the refrigeration plant.

Thermal energy storage (TES) technology can be applied to refrigeration systems to decouple the supply and demand of cooling [13]. TES technology applied to sub-ambient temperatures is often denoted as cold TES (CTES). The principle of CTES technology is to store the cold (remove the heat) in a storage material during a time of low load on the refrigeration plant and then utilise the accumulated cold during the high load hours to reduce the required capacity from the refrigeration system. This concept is often referred to as peak shifting. Hence the refrigeration plant can operate at a more even load throughout the day, decoupling the supply and demand of refrigeration. The general interest in TES technology increased following the energy crisis during the 1970s and early 1980s, alongside a general focus on energy efficiency. As a result, several demonstration plants of ice CTES connected to chillers by additional heat transfer circuits for serving AC loads in schools, offices and apartment buildings were constructed throughout the 1980s, and the 1990s [14]. Ice CTES systems for space cooling have an important drawback compared to producing the cooling on demand; the chiller needs to operate at a lower evaporation temperature during the ice production compared to producing chilled water directly. This drawback generally increases the power consumption of the chiller, making it less efficient. Many refrigeration processes require cooling at a temperature level considerably lower than what can be provided by melting ice, such as blast freezers for food products. Phase change material (PCM) is a common term for materials designed to store energy using the latent heat storage principle, i.e., storing heat in the solid-liquid phase transition [15]. It has been

considerable development in the number of different types of PCMs over the last decades, including PCM for CTES applications [16]. Current research and investigations on PCMs focus on developing advanced, multi-component mixtures and enhancing the performance of PCMs in terms of heat transfer and stability [17]. Moreover, the commercial market of PCMs in the sub-ambient temperature range has increased significantly. Several large chemical companies and niche manufacturers now offer PCMs in their portfolio, and a considerable selection of PCMs are commercially available [13].

CTES technology with PCM integrated into refrigeration systems can provide valuable flexibility to the system operator, save energy cost and reduce the maximum power draw from the electric grid [14]. However, to increase the efficiency and attractiveness of such systems, there is a need to develop technical solutions that limit the drawbacks of CTES technology. More specifically, concepts that can help reduce the additional energy spent for rejecting and extracting the thermal energy to the storage compared to directly producing the cooling need to be developed. Moreover, there is a need for research focusing on technical solutions that can be scaled for industrial-size refrigeration plants. Many of these plants have high peak load demands due to operation in batches, such as blast freezers in food processing plants. CTES systems can reduce the maximum power draw from the electrical grid during peak hours and make refrigeration plants more flexible to exploit intermittent renewable power from wind and solar. Developing efficient and high-performing CTES units with storage temperatures in the sub-ambient temperature range will be essential to ensure the possibility of transitioning refrigeration plants to the future energy system.

1.2 Objective and scope

The present work aims to develop and demonstrate the principle of novel CTES technology with PCMs suitable for industrial applications, investigating storage temperatures in the relevant temperature range. The main research objective can be divided into the following sub-goals:

- Investigate and identify state-of-the-art latent CTES technology applied to refrigeration systems and map the applications commonly investigated in the literature. Furthermore, the current commercially available PCM in the sub-ambient temperature range should be identified.

- Develop a concept for a latent CTES unit that can be integrated into the primary refrigerant circuit of industrial refrigeration systems, avoiding the

intermediate heat transfer circuits that reduce the efficiency of these storage systems.

- Design and construct a lab-scale demonstration CTES unit of sufficient size and capacity to be representable for an industrial-size unit. The design should be compact and allow for high heat transfer rates and storage capacity. The lab-scale unit must be flexible and allow for testing various geometry parameters.
- Design and develop an experimental test facility that allows for testing charging and discharging processes of the CTES unit with varying refrigerant parameters and the possibility to test several PCMs in the relevant temperature range.
- Test and demonstrate the proof-of-concept of CTES technology integrated into the primary refrigerant circuit of a refrigeration system. The testing should involve mapping the CTES performance, such as storage capacity and heat transfer rate for various PCMs, storage geometries and refrigerant parameters.

1.3 Structure of the thesis

The structure of this Doctoral thesis is presented as six chapters and a collection of three journal publications, where the main content in each chapter is described as follows:

- **Chapter 1** introduces the motivation and background of the doctoral work. The introduction presents the main benefits and advantages of installing CTES technology into refrigeration systems in the current and future energy market. Then the objective and scope of the research work are presented, followed by a list of the scientific publications achieved within the scope of the present doctoral work.
- **Chapter 2** presents the current status and provides the necessary technical background on refrigeration and CTES technology. The first part of the chapter focuses on refrigeration technology, including a brief history and development of refrigerants. Furthermore, the current status of industrial refrigeration is provided. The second part of the chapter presents a brief introduction to CTES technology using PCMs.
- **Chapter 3** explains the development of the novel CTES unit investigated in this doctoral work. The first part of the chapter includes the description

of the lab-scale demonstration CTES unit, including geometry, dimensions and material properties. The second part presents the experimental test facility developed for testing the operation and performance of the novel CTES unit, including the methodology of operating the facility in charging and discharging mode. The last part of the chapter presents the experimental apparatus and procedure used for the characterisation of the thermophysical properties of PCMs.

- **Chapter 4** summarises the research performed in the present doctoral work. The chapter is organised in separate sections for each journal publication included in the thesis. The main findings from each journal paper are summarised, and the contribution toward achieving the objectives of the doctoral work is indicated.

- **Chapter 5** discusses the main findings of the research work presented in Chapter 4 by comparing and evaluating the achievements concerning the research objectives and the impact of the present research. Additional aspects regarding the developed CTES technology are discussed.

- **Chapter 6** concludes the thesis by presenting the main results and the indicated impact of the present research work.

- **Chapter 7** presents the recommendations for further work on the research topic of CTES technology for refrigeration systems based on the experiences gained in the present doctoral work.

1.4 List of publications

The author of this thesis contributed to three journal papers and six conference papers on the subject of CTES applied to CO_2 refrigeration systems. The three journal publications are attached in the Appendix, while the conference papers are listed here for reference. The author contributions for each paper are detailed below, following the Contributor Roles Taxonomy (CRediT) classification [18].

1.4.1 Journal publications

Journal paper I

H. Selvnes, Y. Allouche, R.I. Manescu, A. Hafner (2021). "Review on cold thermal energy storage applied to refrigeration systems using phase change materials." In: *Thermal Science and Engineering Progress* 22, pp. 100807.
DOI: https://doi.org/10.1016/j.tsep.2020.100807

Author contributions: Conceptualization: H. Selvnes, Y. Allouche, R.I. Manescu, A. Hafner, Investigation: H. Selvnes, Formal Analysis: H. Selvnes, R.I. Manescu, Original Draft: H. Selvnes, R.I. Manescu, Writing - Review and Editing: H. Selvnes, Y. Allouche, Visualization: H. Selvnes, Supervision: Y. Allouche, A. Hafner.

Journal paper II

H. Selvnes, Y. Allouche, A. Hafner (2021). "Experimental characterisation of a cold thermal energy storage unit with a pillow-plate heat exchanger design." In: *Applied Thermal Engineering* 199, pp. 117507.
DOI: https://doi.org/10.1016/j.applthermaleng.2021.117507

Author contributions: Conceptualization: H. Selvnes, A. Hafner, Methodology: H. Selvnes, A. Hafner, Investigation: H. Selvnes, Software: H. Selvnes, Writing - Original Draft: H. Selvnes, Writing - Review and Editing: H. Selvnes, Y. Allouche, Visualization: H. Selvnes, Supervision: Y. Allouche, A. Hafner.

Journal paper III

H. Selvnes, Y. Allouche, I. Tolstorebrov, C. Schlemminger, A. Hafner (2022). "Cold thermal energy storage for industrial CO_2 refrigeration systems using phase change material: An experimental study." In: *Applied Thermal Engineering* xxx, pp. 118543.
DOI: https://doi.org/10.1016/j.applthermaleng.2022.118543

Author contributions: Conceptualization: H. Selvnes, Y. Allouche, A. Hafner, Methodology: H. Selvnes, Y. Allouche, I. Tolstorebrov, C. Schlemminger, A. Hafner, Investigation: H. Selvnes, Software: H. Selvnes, Writing - Original Draft: H. Selvnes, Writing - Review and Editing: H. Selvnes, Y. Allouche, I. Tolstorebrov, C. Schlemminger, Visualization: H. Selvnes, Supervision: Y. Allouche, A. Hafner.

1.4.2 Conference publications

The following conference papers are within the scope of the doctoral work and have been presented at international conferences and published in conference proceedings during the doctoral research period.

Conference paper I

H. Selvnes, A. Hafner, H. Kauko (2018). "Cold thermal storage integration in a large industrial refrigeration system." In: *Proceedings of the 13th IIR Gustav Lorentzen Conference on Natural Refrigerants*, València, Spain.
DOI: http://dx.doi.org/10.18462/iir.gl.2018.1383

Author contributions: Conceptualization: H. Selvnes, A. Hafner, H. Kauko, Methodology: H. Selvnes, A. Hafner, Investigation: H. Selvnes, Software: H. Selvnes, Writing - Original Draft: H. Selvnes, Writing - Review and Editing: H. Selvnes, A. Hafner, H. Kauko, Visualization: H. Selvnes, Supervision: A. Hafner.

Conference paper II

H. Selvnes, Y. Allouche, A. Sevault, A. Hafner (2019). "A CFD analysis for the performance assessment of a novel design of plates-in-tank latent storage unit for freezing applications" In: *Proceedings of the 8th IIR International Conference on Ammonia and CO_2 Refrigeration Technologies*, Ohrid, North Macedonia.
DOI: http://dx.doi.org/10.18462/iir.nh3-co2.2019.0041

Author contributions: Conceptualization: H. Selvnes, Y. Allouche, A. Hafner, Methodology: H. Selvnes, Y. Allouche, A. Sevault, A. Hafner, Investigation: H. Selvnes, Software: H. Selvnes, Writing - Original Draft: H. Selvnes, Writing - Review and Editing: H. Selvnes, Y. Allouche, A. Sevault, A. Hafner, Visualization: H. Selvnes, Supervision: Y. Allouche, A. Hafner.

Conference paper III

H. Selvnes, Y. Allouche, A. Sevault, A. Hafner (2019). "CFD modeling of ice formation and melting in horizontally cooled and heated plates" In: *Eurotherm Seminar 112 - Advances in Thermal Energy Storage*, Lleida, Spain.

Author contributions: Conceptualization: H. Selvnes, Y. Allouche, A. Hafner, Methodology: H. Selvnes, Y. Allouche, A. Sevault, A. Hafner, Investigation: H. Selvnes, Software: H. Selvnes, Writing - Original Draft: H. Selvnes, Writing - Review and Editing: H. Selvnes, Y. Allouche, A. Sevault, A. Hafner, Visualization: H. Selvnes, Supervision: Y. Allouche, A. Hafner.

Conference paper IV

H. Selvnes, A. Hafner, H. Kauko (2019). "Design of a cold thermal energy storage unit for industrial applications using CO_2 as refrigerant." In: *Proceedings of the 25th IIR International Congress of Refrigeration.* Montréal, Canada.
DOI: http://dx.doi.org/10.18462/iir.icr.2019.0139

Author contributions: Conceptualization: H. Selvnes, A. Hafner, H. Kauko, Investigation: H. Selvnes, Writing - Original Draft: H. Selvnes, Writing - Review and Editing: H. Selvnes, A. Hafner, H. Kauko, Visualization: H. Selvnes, Supervision: A. Hafner.

Conference Paper V

H. Selvnes, V. Büttner, A. Hafner (2020). "Evaluation of a pillow-plate heat exchanger for a pump-circulated CO_2 refrigeration system." In: *Proceedings of the 13th IIR Gustav Lorentzen Conference on Natural Refrigerants*, Kyoto (Online), Japan.
DOI: http://dx.doi.org/10.18462/iir.gl.2020.1094

Author contributions: Conceptualization: H. Selvnes, A. Hafner, Methodology: H. Selvnes, A. Hafner, Investigation: H. Selvnes, V. Büttner, Software: H. Selvnes, Writing - Original Draft: H. Selvnes, V. Büttner, Writing - Review and Editing: H. Selvnes, V. Büttner, A. Hafner. Visualization: H. Selvnes, Supervision: A. Hafner.

Conference Paper VI

H. Selvnes, Y. Allouche, A. Hafner (2021). "A cold thermal energy storage unit for CO_2 refrigeration using phase change material: First experimental results." In: *Proceedings of the 9th IIR Conference on Ammonia and CO2 Refrigeration Technologies.*, Ohrid (Online), North Macedonia.
DOI: http://dx.doi.org/10.18462/iir.nh3-co2.2021.0021

Author contributions: Conceptualization: H. Selvnes, A. Hafner, Methodology: H. Selvnes, A. Hafner, Investigation: H. Selvnes, Software: H. Selvnes, Writing - Original Draft: H. Selvnes, Writing - Review and Editing: H. Selvnes, Y. Allouche, Visualization: H. Selvnes, Supervision: Y. Allouche, A. Hafner.

2 Technical Background

2.1 Refrigeration

This chapter provides the fundamental background and thermodynamics that apply to refrigeration systems, focusing on vapour-compression refrigeration systems. Furthermore, a short introduction to the history of refrigerants and their current status is provided.

2.1.1 Vapour compression refrigeration basics

The target of a refrigeration cycle is to transfer heat from a reservoir of low temperature to a reservoir of high temperature, a process that requires energy. In the case of a vapour compression refrigeration system, energy is required in the form of mechanical work to operate a compressor to drive the process. Figure 2.1 shows the principle of operation of a refrigeration system operating between two thermal reservoirs with temperatures T_L and T_H, respectively. The highest theoretical performance of a refrigeration system operating between these reservoirs is called the Carnot Coefficient of Performance (COP_{Ca}) and is expressed by Equation 2.1:

$$COP_{Ca} = \frac{T_L}{T_H - T_L}. \tag{2.1}$$

In a real refrigeration system, the working fluid (refrigerant) is circulated in a closed loop to transfer heat from the cold source to the warm sink. Unlike the ideal cycle, real refrigeration systems have inherited losses that translate to lower system efficiencies, such as throttling losses in valves, pressure losses and heat exchange losses. The basic components of a refrigeration cycle are shown in Figure 2.2, while the corresponding ideal thermodynamic representation of the cycle is presented in a pressure-enthalpy diagram in Figure 2.3. The heat is absorbed from

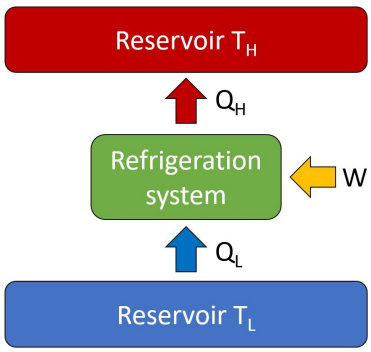

Figure 2.1: Illustration of a refrigeration system operating between two thermal reservoirs of temperature T_L and T_H.

the heat source (Q_L) to the refrigerant in the evaporator, and the liquid refrigerant evaporates (Point 4 to 1). The evaporated refrigerant vapour is then compressed to a superheated vapour state at high temperature and high pressure in the compressor (Point 1 to 2), using electricity to operate the compressor motor. The high-pressure refrigerant rejects its heat to the heat sink (Q_H), which is of lower temperature than the refrigerant, and the refrigerant condenses to the liquid state (Point 2 to 3). Finally, the high-pressure liquid refrigerant is throttled through an expansion valve to a low-pressure mixture of vapour and liquid to close the cycle (Point 3 to 4). In a real cycle, the refrigerant experiences pressure losses through the various components in the system, such as the piping, the evaporator and the condenser. The pressure losses on the low-pressure side of the refrigeration cycle translate to an increased pressure lift of the compressor, increasing its power consumption and reducing the overall system efficiency. Furthermore, the frictional losses and required clearances in the compressor geometry and heat losses further contribute to the diversion from the ideal cycle.

The evaluation of the performance of a real refrigeration system is done by calculating the real COP of the system. It is expressed as the amount of heat removed from the cold source (Q_L) divided by the electric power consumption of the compressor (W_{el}), as presented in Equation 2.2:

$$COP = \frac{Q_L}{W_{el}}. \tag{2.2}$$

The Carnot efficiency (η_{Ca}) is a valuable concept to evaluate how closely the refrigeration system performs compared to the ideal Carnot cycle operating between the same thermal reservoirs. It is expressed as the ratio between the real COP of the refrigeration system and the Carnot COP, as shown in Equation 2.3.

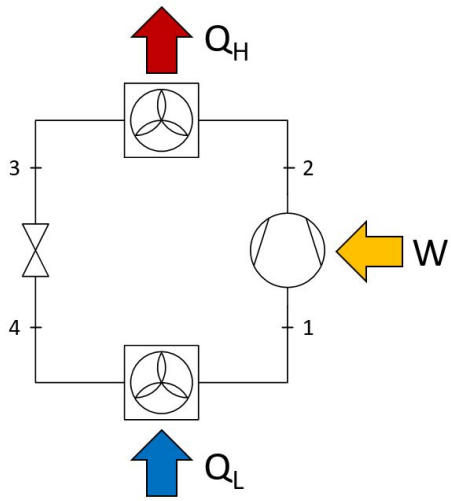

Figure 2.2: Illustration of a simple refrigeration system with an evaporator, compressor, condenser and expansion valve.

$$\eta_{Ca} = \frac{COP}{COP_{Ca}}. \tag{2.3}$$

2.1.2 Refrigerants

A crucial constituent of any refrigeration system is the refrigerant that circulates in the circuit to transfer heat from the heat source to the heat sink. Over the history of mechanical refrigeration, there have been several generations of working fluids. The first generation of working fluids used from the beginning of mechanical refrigeration in the 1830s were all natural refrigerants, mostly CO_2 (R744), ammonia (R717), diethyl ether (R610) and sulphur dioxide (R764) [19]. Natural refrigerants are substances that occur naturally in the environment. In essence, all the refrigerants used except for CO_2 were either flammable, toxic or both. With the technology at the time, the safety concerns for people and goods in air-conditioned spaces or rooms containing refrigeration systems were rising. Accidents were common and made the challenges with refrigerants at the time visible. In the early 1930s, the second generation of refrigerants was introduced to the market, the chlorofluorocarbon (CFC) refrigerants. These synthetic refrigerants were known under the brand name Freon. Better equipment and the efficient operation of these systems made them dominate the domestic and industrial market for many years. Although highly efficient, non-flammable and low toxicity, it was revealed during investigations in the 1970s and early 1980s that these refrigerants were causing a breakdown of the ozone layer. The Montreal Protocol on Substances that Deplete the Ozone

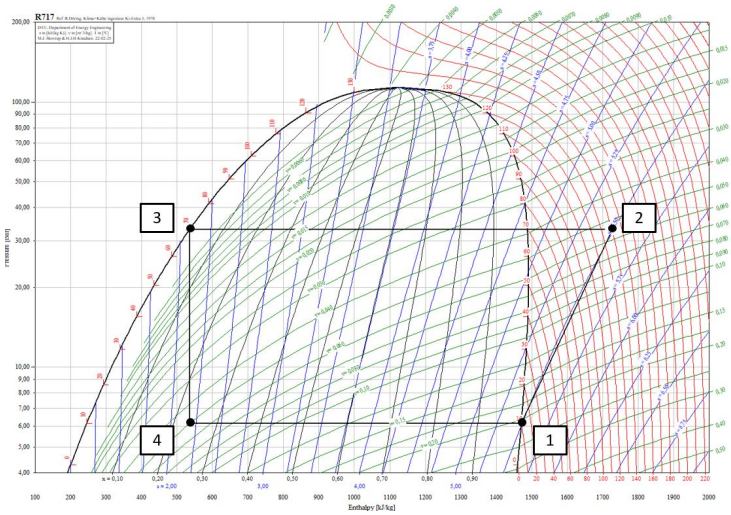

Figure 2.3: Specification of the operating points in a simplified refrigeration cycle, illustrated in a pressure-enthalpy diagram of R717 (ammonia) as the refrigerant. Numbers (states) corresponds to Figure 2.2.

Layer was adopted in 1987, effectively introducing a stepwise phase-down of these harmful substances. Ratified by nearly 200 states, the Montreal Protocol has been considered the most successful international agreement concerning environmental action. Although the target of the Montreal Protocol was the reduction of ozone-depleting substances, CFC refrigerants are also powerful greenhouse gases (GHG). It has been estimated that the climate protection of the Montreal protocol alone is larger than the reduction target of the first commitment period of the Kyoto Protocol [20].

Following the phase-down of the CFCs, the third generation of refrigerants was introduced, the Hydrofluorocarbons (HFCs). These refrigerants have no ozone depletion potential (ODP) but are very powerful GHG. Following the rising concern of climate change and the emission of GHGs into the atmosphere, the Kigali Amendment to the Montreal Protocol was put into action in 2019. The agreement ensured a stepwise phase down of HFC refrigerants having global warming potential (GWP) higher than thresholds presented in the amendment. The latest addition to combat the GWP challenges of HFCs was the introduction of hydrofluoroolefins (HFO) as the fourth-generation refrigerants. This group of synthetic refrigerants has no ODP and very low GWP due to a fast decomposition in the atmosphere. Nevertheless, there are rising concerns about the decomposition products from certain HFOs, including trifluoroacetic acid (TFA) and perfluoroalkyl and polyfluoroalkyl substances (PFAS) [21]. Parallel to the development of new generations of synthetic refrigerants, natural refrigerants have been available and partially used in specific

applications. In particular, ammonia has survived as an industrial refrigerant in fishing vessels and food processing plants. At the beginning of the 1990s, the revival of carbon dioxide (CO_2) as a refrigerant was proposed by professor Gustav Lorentzen at NTNU as a countermeasure for the introduction of new synthetic refrigerants [22]. Significant research on natural refrigerants has been carried out since then. They have become increasingly attractive for installations in the industry due to environmental concerns about synthetic refrigerants and achieving a competitive total cost of ownership. Transcritical CO_2 refrigeration systems have become the standard solutions for new supermarkets in Europe, with more than 30.000 systems installed per 2020 [23].

2.1.3 Industrial refrigeration systems

Industrial refrigeration systems refer to large-scale refrigeration systems utilised in applications requiring high capacities, such as the dairy industry, process cooling, food and beverage processing plants, fishing vessels, ice rinks and large air-conditioning systems. Ammonia (R717) is widely used as an industrial refrigerant and has been used since the middle of the 1800s. Ammonia has also become popular in industrial heat pump applications, such as providing process heat in the food and beverage industry [24] and for district heating systems [25]. It has favourable thermophysical properties that make it particularly efficient and attractive for large-scale systems, such as high latent heat of evaporation resulting in high refrigeration capacity per unit mass of refrigerant. However, for evaporation temperatures below -33.5 °C, the pressure of ammonia is below 1 bar. The resulting vapour density decreases rapidly, and the volume of refrigerant required to be compressed by the compressor increases, resulting in lower system efficiency. In cases where the evaporation temperature is -40 °C or lower, other system configurations such as cascades with CO_2 are likely to be more efficient [26].

Cascade refrigeration systems are commonly used in applications where the temperature difference between the refrigerated medium and the heat sink is substantial, such as blast freezers operating at air temperatures of -35 °C or lower. Cascade refrigeration systems are beneficial to use in applications where the designer wants to benefit from the different refrigerant properties at the various stages of the system or in the case where the temperature lift is too high for a single-stage system. There is often the need for both cooling and heating in many industrial plants in the food and beverage industry, such as cooling water and hot process water or steam. A combined heat pump/refrigeration system serving both these purposes would often require a temperature lift of 70-120 K, which is usually too high for a single-stage system. A propane/butane (R290/R600) cascade heat pump system for the simultaneous production of cold process water at 1-5 °C and hot process water up to 115 °C has been developed, tested and later demonstrated in a Norwegian dairy [27, 28]. NH_3/CO_2 cascade refrigeration systems have been investigated in-

tensively in the past and are commonly installed in applications where refrigeration is required at multiple temperature levels. Food processing plants are examples of such applications, where refrigeration is required for freezing processes, chilling and cold storage. Additionally, heat recovery to hot water for cleaning purposes on the high-temperature side of the system is beneficial for the overall system efficiency. Multi-stage systems are alternatives to cascade refrigeration systems, most often two-stage or booster configurations using the same refrigerant in the entire system.

Using CO_2 in the low-temperature stage of a cascade refrigeration system with ammonia has several benefits. CO_2 is non-toxic and non-flammable and can be safely used as a secondary pumped (evaporating) refrigerant in, e.g. blast freezers and freezing tunnels in food processing plants without concern of contaminating products. Furthermore, using an NH_3/CO_2 would limit the ammonia inside the machine room, greatly reducing the necessary charge of the toxic refrigerant in the plant [29]. Both theoretical and experimental studies have proved that an NH_3/CO_2 cascade is an attractive system solution. It has been shown through thermodynamic analysis that using ammonia in the high-temperature circuit of the cascade refrigeration system results in higher COP compared to using R404A under moderate superheating and subcooling conditions [30]. A parametric analysis of operational conditions in an NH_3/CO_2 cascade has shown that the optimal operation point of such systems depends on the CO_2 evaporation temperature, CO_2 condensing temperature, NH_3 condensing temperature, the temperature difference in the cascade heat exchanger, and the isentropic efficiencies of the compressors [31]. An experimental study of a 9 kW NH_3/CO_2 cascade refrigeration system connected to a plate freezer showed that using CO_2 as the refrigerant in the bottom cycle of the cascade resulted in an improvement of up to 19.5 % over a two-stage ammonia plant for evaporation temperatures below -40 °C [32]. According to a theoretical thermodynamic analysis, NH_3/CO_2 cascade systems show comparable efficiency to an R404A two-stage cycle for evaporation temperatures lower than -35 °C [33]. Furthermore, a multi-objective optimisation of an NH_3/CO_2 system revealed that a maximum exergetic efficiency of 45.86 % was achievable when operating with CO_2 evaporation temperature of -48.68 °C and a NH_3 condensing temperature of 40.1 °C [34]. NH_3/CO_2 cascades with several evaporation temperature levels on both the low and high-temperature stage of the system have been proposed as a suitable configuration for seafood processing plants in high ambient temperature climates [35].

2.2 Cold Thermal Energy Storage

Methods for TES can be classified based on the mechanism used to store and release the energy in the system. TES technology is commonly divided into sensible, latent, and chemical TES. Sensible heat is a well-known form of TES, which stores the heat by changing the temperature of the material with no change of phase during the process. The amount of energy that can be stored as sensible heat Q_{sens} depends on the mass m and specific heat capacity cp of the material, as well as the difference between the initial temperature T_i and final temperature T_f of the system according to Equation 2.4. A commonly used example of sensible thermal energy storage is storing hot water for process heating, cleaning or domestic use. In these applications, the difference between the initial temperature (return stream or cold city water) and the storage temperature can be 50-80 K. The larger the temperature difference in the substance used, the more energy is stored.

$$Q_{sens} = \int_{T_i n}^{T_f} m\, cp\, T\, dT \tag{2.4}$$

The temperature difference in many sensible TES systems is limited to a relatively narrow range, such as storing cold water for process cooling or AC applications. In these systems, the temperature difference of the storage medium is often in the range of 3-10 K. Using a storage medium with high heat capacity and high density becomes paramount for the attractiveness of the technology. Latent TES systems are designed to utilise the latent heat of fusion of the material to store and release heat, where the material transitions from one phase to another during the process of storing and releasing thermal energy. The phase change process can be solid-liquid, liquid-gas, solid-gas or solid-solid. Due to the significant volumetric expansion of the material in the liquid-gas phase change, most practical latent TES systems are designed to utilise the solid-liquid transition regime. The energy that can be stored or released in a latent TES Q_{lat} can be found from Equation 2.5:

$$Q_{lat} = m\, h_{fus}\ , \tag{2.5}$$

where h_{fus} is the enthalpy of fusion of the material. The equation assumes that all material in the system undergoes a phase change. Alternatively, a fraction can be included in the equation to compensate for the amount of material in the system that has not changed phase. There is often a combination of latent and sensible heat storage in latent TES systems. This statement indicates that during the heat release, the material is initially at a lower temperature than its melting temperature and the final temperature of the system is higher than the phase change

temperature of the material. Combining Equation 2.4 and 2.5 gives Equation 2.6, which can be used to find the total energy stored in a TES system Q_{TES}. The mass m is substituted by the product of the density ρ and the volume V of the storage material. The TES system here is taken from the initial temperature T_i to the final temperature T_f, and includes the phase change process:

$$Q_{TES} = \int_{T_in}^{T_{fus}} \rho\, V\, cp\, T\, dT + \rho\, V\, h_{fus} + \int_{T_{fus}}^{T_f} \rho\, V\, cp\, T\, dT \tag{2.6}$$

Although sensible and latent TES systems are the most popular and frequently installed systems, thermochemical energy storage is under development. This technology has a significant potential for storing thermal energy over long periods and is mentioned here for reference. This technology is currently at the laboratory and pilot scale in terms of maturity [36]. The amount of heat released and absorbed in these types of systems depends on the heat of reaction of the material. The heat exchange with the environment comes from forming and breaking molecular bonds in the material. The amount of energy that can be stored and released in thermochemical energy storage can be found using equation 2.7. This simplification assumes a complete reaction of all the material in the system. Alternatively, the fraction of material reacted could be included in the equation.

$$Q_{tc} = m\, h_r \tag{2.7}$$

2.2.1 Phase change materials

PCM is a common term given to a group of materials used in latent TES systems due to their relatively large enthalpy of fusion in the solid-liquid transition, making them attractive candidates for compact TES solutions. One way of classifying PCMs is according to their chemical composition. An overview of the material classification of PCM for TES systems is presented in Figure 2.4. It can be noted that sensible TES and thermochemical TES are presented in the figure for reference. The latent heat of vaporisation is generally higher than the enthalpy for fusion for most materials. However, the associated change in the volume of the substance during the liquid-vapour phase transition presents a major challenge for designing a practical and feasible TES system. The vapour formation creates considerable technical difficulties in terms of storage unit design and would require large equipment to deal with the volume changes. Consequently, from the technical and economic point of view, the solid-liquid phase change is more convenient for latent heat storage purposes.

PCM can generally be classified into three groups: Organic, inorganic and eutectic PCMs. Further details on the classification of PCM relevant for CTES applications,

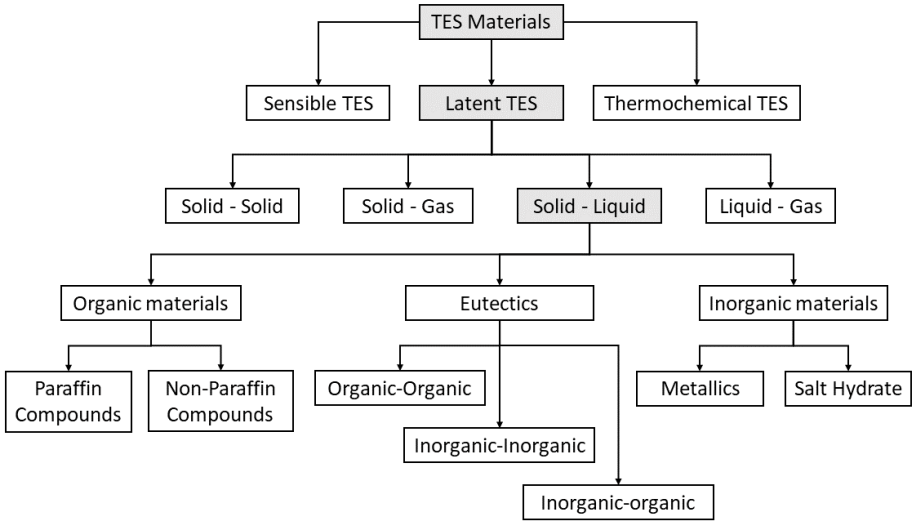

Figure 2.4: Overview of the various methods of thermal energy storage and further details on different groups of solid-liquid thermal energy storage materials.

properties and characteristics and methods for characterisation of thermo-physical properties are presented by the author in Journal paper 1: "Review on cold thermal energy storage applied to refrigeration systems using phase change materials" [13], which is included in its entirety in the Appendix. Furthermore, the review presents the main limitation of the various types of PCM and enhancement techniques commonly applied to improve the physical and thermal properties.

Although certain PCMs can have relatively high latent heat capacity, the density of the PCM might be relatively low. The limiting factor in many CTES applications is often the space available for installing the storage. For this reason, it is convenient to define a quantity that considers how much energy can be stored per unit volume of the PCM. The volumetric storage capacity θ_{PCM} is defined as the product of the latent heat capacity h_{fus} of the PCM and its density ρ, as presented in Equation 2.8:

$$\theta_{PCM} = h_{fus}\,\rho_{PCM} \tag{2.8}$$

The volumetric storage capacity is a suitable parameter for comparing and evaluating various PCM in applications where the space is restricted.

2.2.2 Application of CTES in refrigeration system

An extensive review of past research, description of current trends as well as identification of knowledge gaps within the application of CTES technology with PCMs in refrigeration systems is presented by the author in Journal paper 1: "Review on cold thermal energy storage applied to refrigeration systems using phase change materials" [13] (see Appendix).

3 Experimental Setup and Methodology

To demonstrate the feasibility of integrating CTES technology in the primary refrigerant circuit, it was necessary to design and construct a CTES unit and an associated test facility. A location was dedicated in the Thermal Engineering Laboratory at the Department of Energy and Process Engineering of the Norwegian University of Science and Technology to accommodate the experimental test facility.

3.1 Cold thermal energy storage unit

The aim of the research was to develop and test a CTES unit suitable for integration into industrial refrigeration systems, typically used in food processing plants. The industrial annotation indicates that the CTES unit must be designed in such a way that it can be easily scaled in size. At the same time, it is crucial that the lab-scale CTES unit is large enough that the obtained specific results (e.g. per unit area) from the test campaign are also representable for an industrial-scale unit. Regarding scalability, the laboratory demonstration unit must be large enough for any boundary effects of the heat exchanger (HEX) to be negligible but small enough for practical implementation regarding laboratory infrastructure requirements for heating, cooling and electric power. Since the research aims to couple the evaporation/condensation process of the refrigerant with the solidification/melting of the PCM in the CTES unit, the HEX inside the CTES unit needs to withstand the operating pressures of CO_2 refrigeration systems. The evaporation temperatures in industrial refrigeration systems ranges from approximately T_{sat} = -50 °C to 10 °C, which corresponds to a saturation pressure range of approximately P_{sat} = 7 bar to 45 bar for CO_2. The typical design pressure for the low-pressure side of CO_2 refrigeration systems is 60 bar and was used as a reference for the upper opera-

tional pressure for the CTES unit. The CTES unit is presented in Fig. 3.1. It is constructed on the plates-in-tank principle and is composed of HEX plates stacked horizontally and placed into a welded stainless steel container filled with the PCM. To make the CTES unit suitable for water-based PCMs and organic PCMs, stainless steel (316) was selected for components and hardware. Stainless steel has been proven to be the most suitable material for PCM-based CTES units, showing satisfying corrosion resistance for many different PCMs [37, 38]. The container could have been constructed of polymer materials to reduce the cost. However, these materials can be incompatible with certain paraffin PCMs in the long-term perspective [39]. Furthermore, constructing everything using stainless steel improves the structural integrity of the CTES unit under transportation and handling.

The plates-in-tank design was chosen over the tube-in-tank/coil-in-tank principle due to the possibility of practically reaching a high heat transfer area per unit volume of storage. Furthermore, it was of particular interest to create a design with relatively few connections, effectively minimising the potential leakage points in the unit. However, the plates needed to withstand an operating pressure of up to 60 bar. The market was scanned for available technology that could match these requirements, and a manufacturer that could produce such plates was identified locally in Trondheim. Skala Fabrikk AS designs and produces various products in metal, particularly for the dairy industry, and has been involved in research and development projects focusing on refrigeration systems together with NTNU and SINTEF Energy Research in the past. One outcome of a previous collaboration was an evaporator for a refrigerated sea water (RSW) system with CO_2 as the working fluid based on a welded dimple-plate HEX [40]. Inspired by the design of the HEX plates from the previous work, a new plate design was created in collaboration with the company. A picture of one of the new HEX plates is shown in Fig. 3.1a. These special welded HEX plates are called pillow plates (PP) due to their characteristic wavy surface. Each PP is made from two thin sheets of stainless steel, laser welded together in a repetitive circular welding pattern. The edge of each plate is then seam-welded to ensure a pressure-tight seal. A tube is welded to each end of the PP, serving as the inlet and outlet for the refrigerant. Furthermore, two longitudinal seam welds are added to the plate surface, as indicated by the two black lines in Fig. 3.1a. These seam welds generate three flow passes for the refrigerant through each plate to flow between the inlet and outlet tube. This design feature is used to direct the refrigerant flow and ensure better refrigerant distribution in the PP channels. After the PP is welded in the laser welding machine, it is inflated by applying a hydroforming process. During this process, the plate is fixed onto a frame, one refrigerant tube on the PP is blocked, and high pressure is applied to the inside channels using water or oil. The high pressure inflates the PP around the circular welds and creates flow channels for the refrigerant inside the PP, along with the wavy surface characteristic of these HEX plates. The higher the water/oil

pressure, the larger the resulting inflation height (maximum flow channel height). For an in-depth review of the geometry, challenges and potentials of PP and PP-HEX, the reader is directed to a recent review paper where the author was one of the contributors [41]. The important geometrical design parameters of a PP are (see Fig. 3.1a, d, and e): the spot weld diameter (d_{SP}), the transversal spot weld pitch (s_T), the longitudinal spot weld pitch (s_L), the PP wall thickness (b_w), the PP channel maximum inflation height (δ_i), the PP overall length (l_{PP}) and the PP overall width (w_{PP}). The selected spot weld diameter, the transversal spot weld pitch and the longitudinal spot weld pitch were selected to 10 mm, 30 mm and 50 mm, respectively. This selection results in a triangular welding pattern commonly found in the process industry.

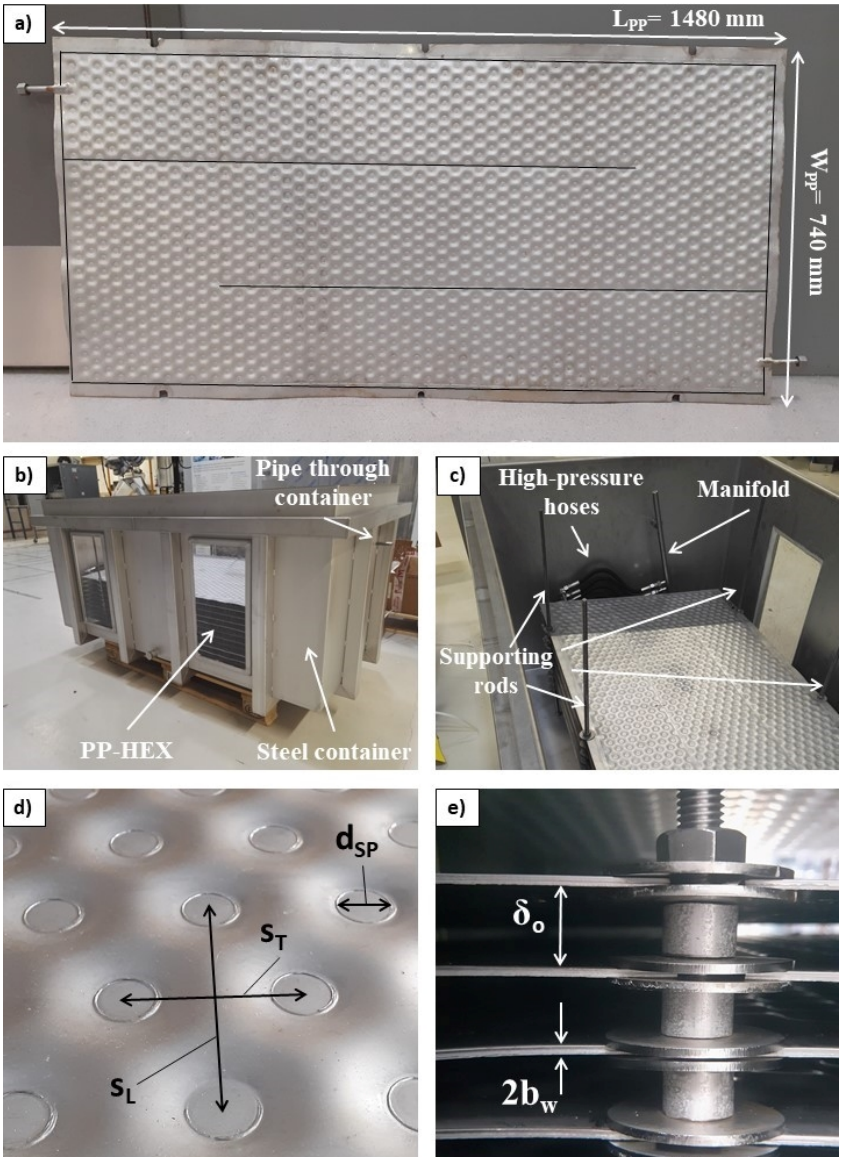

Figure 3.1: Overview of the novel CTES unit showing the details of a) one PP for CO_2 refrigeration with inlet/outlet tubes and the seam welds marked with black lines b) the CTES unit before assembly in the test facility c) view of the PP-HEX inside the container d) the wavy PP surface characteristic with the welding pattern parameters e) the PP-HEX stack in the CTES unit with vertical plate pitch.

To create the complete PP-HEX assembly, a square tube frame is welded together to accommodate the PPs. Six threaded rods are mounted on this frame, matching the slots that are cut along the edges of each PP (see Fig. 3.1a). The PPs are stacked on the threaded rods with washers and cylindrical spacers that govern the vertical distance between each plate (plate pitch δ_o, see Fig. 3.1e). The plate pitch can be varied by selecting a different length of cylindrical spacers. This parameter is an important design parameter for the CTES unit, directly influencing its storage capacity. A larger plate pitch translates into a larger volume of PCM between each pair of PPs, giving the potential for increased storage capacity by increasing the available volume of PCM subject to phase change. In this work, plate pitches of 15 mm, 30 mm and 45 mm were studied to investigate the effect on the performance characteristic of the CTES unit. The number of PPs was kept to ten in all configurations, resulting in a constant heat transfer area of approximately 21.90 m^2. The tubes welded to each end of the PPs are connected to a simple manifold on each end by high-pressure braided hoses. The two manifolds are connected to the rest of the experimental test facility by a tube passing through the container wall as indicated in Fig. 3.1b. Thus, only two connections link the PP-HEX assembly to the experimental test facility, allowing for simple removal and installation of the PP-HEX from the container using an overhead crane when modifications are required. A frame of square tube supports the welded container to counter the pressure exerted by the weight of the PCM on the inside, see Fig. 3.1b. Furthermore, the container is fitted with a lid to prevent the evaporation of the PCM. To easily observe the melting and solidification process of the PCM, the container is equipped with two windows of 10 mm acrylic plexiglass on each side. After installation of the container into the experimental test facility, it is insulated using extruded polystyrene plates to limit the heat loss from the PCM to the environment. A summary of the most important geometrical parameters of the PP-HEX is given in Table 3.1.

Table 3.1: Main geometrical parameters of the PPs and PP-HEX in the novel CTES unit

Parameter	**Value**
s_L	50 mm
s_T	30 mm
d_{SP}	10 mm
δ_i	4.3 mm
b_w	1.0 mm
l_{PP}	1480 mm
w_{PP}	740 mm
δ_o	15/30/45 mm
n_{PP}	10

3.2 Experimental test facility

The experimental test facility was designed to accommodate the novel CTES unit and enable testing of charging and discharging cycles with heat exchange between CO_2 as refrigerant and PCM as the storage medium. Figure 3.2 shows the CTES unit connected to the finished test facility. The main feature of the test facility is an oil-free pump-circulated CO_2 refrigeration cycle connected to the CTES unit. The facility is required to supply various refrigerant flow rates, refrigerant evaporation/condensation temperatures, and heat input/output from the oil-free CO_2 circuit. A piping and instrumentation diagram (P&ID) of the test facility is shown in Figure 3.4. During the test campaign, the operator can set and monitor the various operating parameters of the refrigerant (flow, temperature and pressure) to match the requirements of each specific test condition. It can be operated in two modes: Charging mode (indicated with green lines in Fig. 3.4) and discharging mode (indicated with purple lines in Fig. 3.4). For conveniently referring to the various parts of the test facility in the following text, four circuits are identified by name: The primary CO_2 circuit (PCC), the secondary CO_2 circuit (SCC), the glycol heating circuit (GHC) and the auxiliary CO_2 circuit (ACC). The PCC and the SCC together constitute the oil-free CO_2 test circuit. During the charging mode, the PCC and the ACC are in operation. During the discharging mode, the SCC and the GHC are in operation. The refrigerant tubing in the test facility (PCC, SCC and ACC) is constructed of brazed K65 alloy copper tubes, while the piping for the GHC is composed of copper tubing with Geberit Mapress fittings. The refrigerant tubing, heat exchangers, receiver and valves are insulated using Armaflex foam insulation products.

The circulation of the CO_2 refrigerant in the test facility is assured by a high-pressure hermetic centrifugal refrigerant pump (CO_2 pump) with an inverter to control the refrigerant flow rate (Hermetic Pumpen GmbH [42], see Fig.3.3). The CO_2 pump can be operated at a frequency of 35 to 50 Hz, while the flow can be throttled using a manual ball valve (V2, see Fig. 3.4) if lower flow rates are required for the specific experiment. From the outlet of the CO_2 pump, the refrigerant flow is split into two: One pipe is used to recirculate some of the liquid refrigerant to the liquid receiver, while the other supplies the CTES unit. The recirculation pipe is required to assure the minimum flow requirement of the CO_2 pump according to the manufacturer's specification, as well as installing a maximum and minimum flow orifice in the refrigerant pipe. During the charging process, heat needs to be removed from the PCC. This is achieved in the condenser (CO_2/CO_2 HEX, see Fig. 3.2), where the PCC is connected to an external CO_2 booster refrigeration system by the ACC. The ACC simulates the cascade HEX removing the heat from the low-temperature circuit in a cascade refrigeration system. The removal of heat

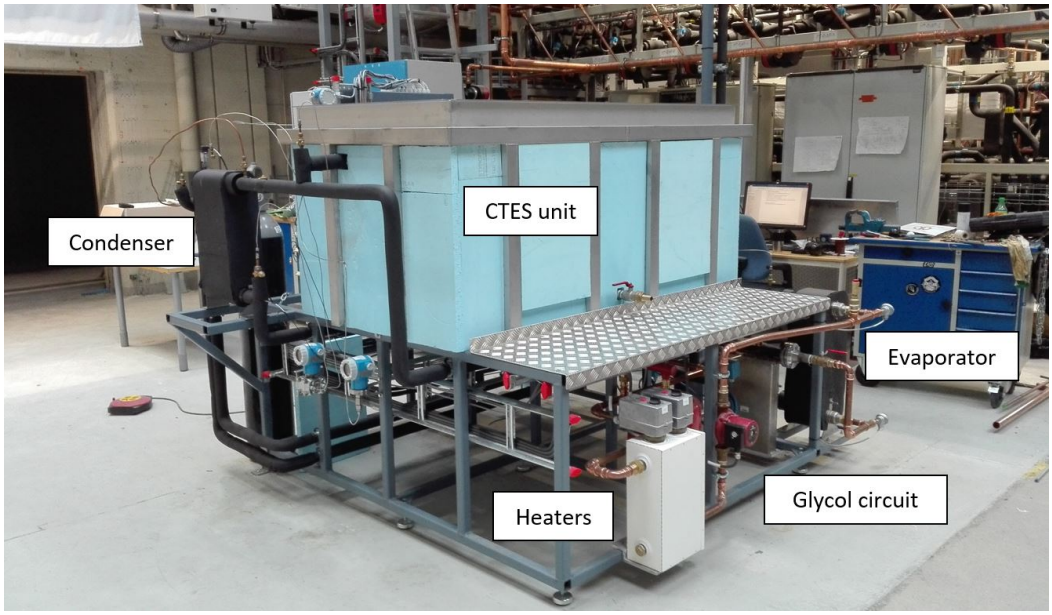

Figure 3.2: Overview of the experimental test facility with the novel CTES unit located in the refrigeration laboratory at NTNU.

from the PCC is achieved by supplying refrigerant from the ACC to the condenser through an electronic expansion valve (EEV 1). Furthermore, the ACC maintains standby pressure below 52 bar in the PCC/SCC when the system is not operating by supplying refrigerant to the subcooler installed on the refrigerant receiver by operating EEV 2. Both EEVs are operated by Danfoss superheat controllers. The ACC circuit is connected to the liquid and suction lines of a centralised CO_2 booster refrigeration system in the laboratory, which also serves several other test facilities and climatic chambers in the laboratory. The operator can select an evaporation level of -10 °C, -30 °C and -50 °C for the ACC by acting on a valve station (see Fig. 3.4). Moreover, the evaporation pressure of the ACC can be adjusted further by changing the opening degree of the electronic stepper valve (V5) on the suction line of the ACC. This valve then serves as a back-pressure valve, and reducing its opening degree will increase the evaporation pressure in the ACC.

The GHC supplies heat to the SCC during the discharging process, simulating the thermal load on the low-temperature CO_2 circuit in a cascade refrigeration system. The SCC is connected to the GHC by a plate HEX, operating as an evaporator for the SCC (see Fig. 3.2). In the evaporator, heat is transferred from the glycol to the refrigerant so that the CO_2 in the SCC exits the evaporator as a liquid/vapour mixture. The heat transfer fluid (HTF) used in the GHC was a mixture of 30 % propylene glycol (DowCal 200, DOW Chemicals) and water in the experiments

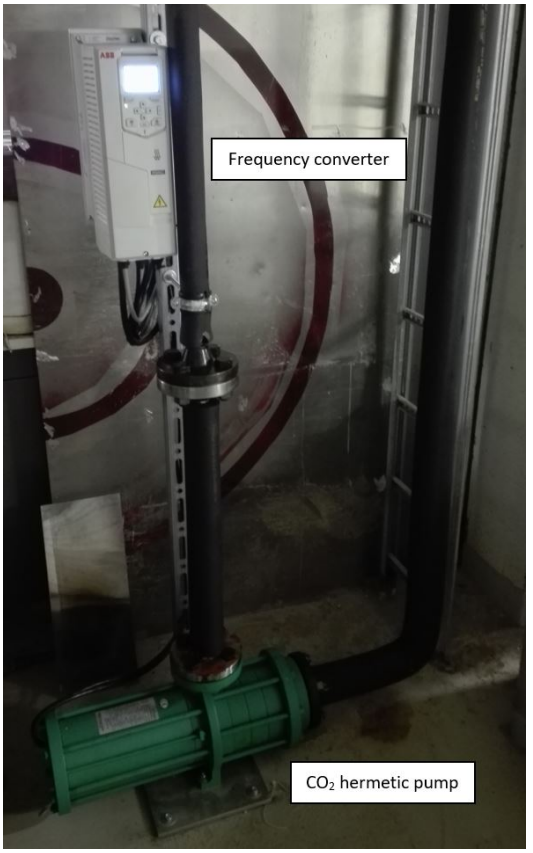

Figure 3.3: Hermetic CO_2 refrigerant pump with frequency control, supplying refrigerant circulation to the CTES unit.

using water/ice as the PCM. It was later replaced by a mixture of 47 % ethylene glycol (DowCal 100, DOW Chemicals) and water for the experiments using the low-temperature PCM as the storage medium. The concentration of the glycol mixtures was checked with an ATAGO Master refractometer. The glycol is supplied to the evaporator by a Grundfos circulation pump. The heat input to the GHC is achieved by two 9 kW electric immersion heaters installed in the GHC circuit, allowing the operator to simulate a thermal load up to 18 kW. Both heaters have individual thermostat control in the range of 0 °C to 50 °C. Furthermore, one heater is fitted with pulse-width modulation (PWM) control for precise regulation of the power output from 0 to 100 % so that the total output power can be continuously regulated from 0 to 18 kW according to either a temperature setpoint or a manual adjustment of the PWM output.

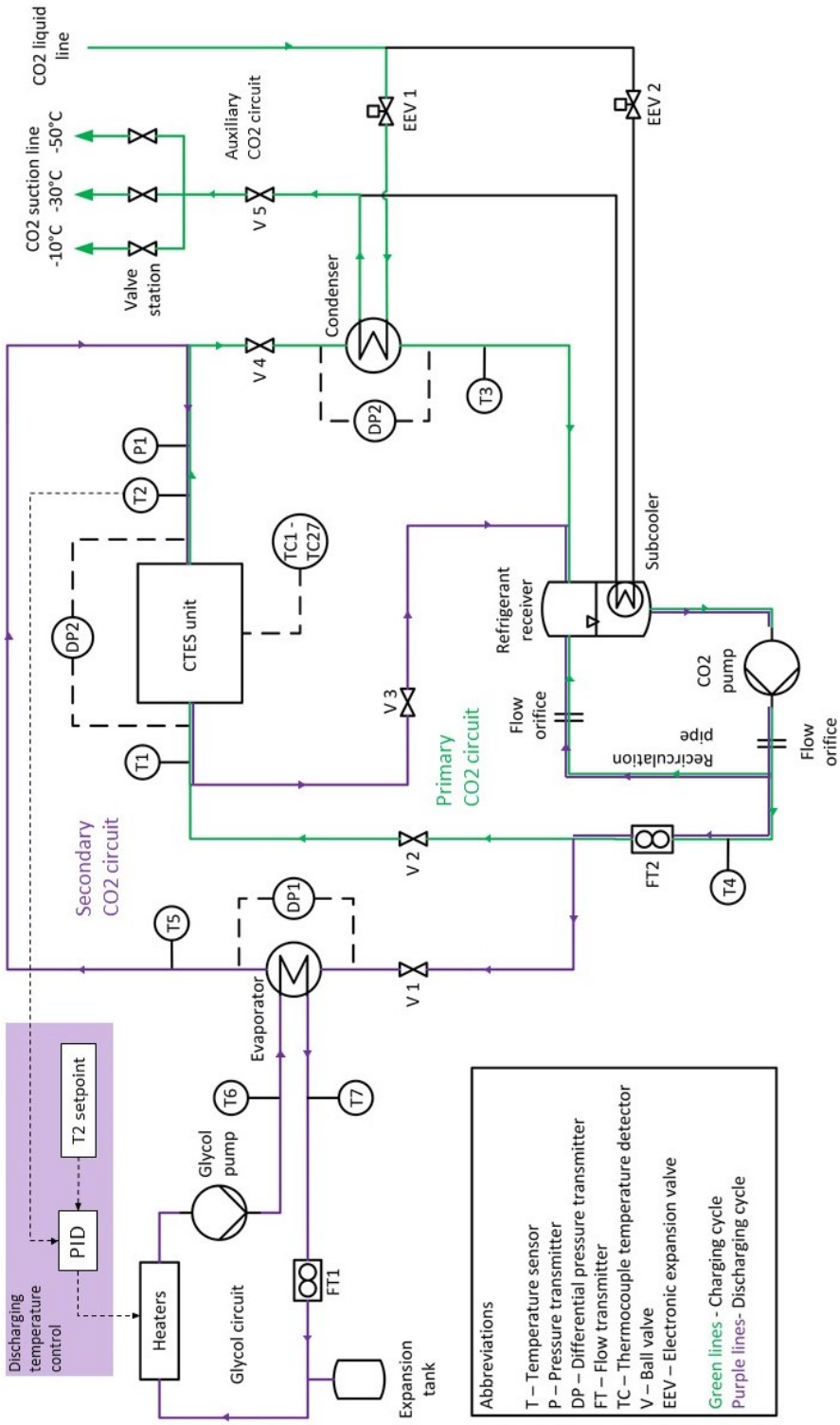

Figure 3.4: Piping and Instrumentation Diagram of the experimental test facility.

3.2.1 Instrumentation

The locations of the sensors for monitoring the mass flow rates, temperatures, pressures and differential pressures around the test facility are shown in the PID (Fig. 3.4). The mass flow rates of the glycol in the GHC (FT1) and the CO_2 refrigerant in the PCC and SCC (FT2) are measured by Coriolis flow meters. The pressure of the PCC and SCC is measured by an absolute pressure transmitter (P1) calibrated in the pressure range of 0-70 bar. Differential pressure (DP) sensors (calibrated in the range of 0.03 - 3 bar) are installed at three locations to measure the pressure drop across the evaporator HEX (DP1), CTES unit (DP2) and condenser HEX (DP3). The flow direction through the CTES unit is reversed between the charging and discharging cycle so that the inlet and outlet are swapped. The change of flow direction requires a switch of the high-pressure and low-pressure ports of the DP sensor measuring across the CTES unit (DP2). Two manual ball valves on the pressure lines exchange the high-pressure and low-pressure sides on the sensor when the test facility is switched from charging mode to discharging mode. The refrigerant temperature through both the charging and discharging processes in the PCC and SCC is measured by five RTD Pt100 temperature sensors as follows: inlet and outlet of the CTES unit (T1 and T2), outlet of condenser HEX (T3), outlet of CO_2 pump (T4) and outlet of the evaporator (T5). The PCM temperature in the CTES unit is measured by T-type thermocouples (TC), which are mounted on the top surface of three selected PPs in the stack.

Fig. 3.6 shows a schematic representation of one PP instrumented with TC temperature sensors, indicating the location of each sensor. The three PPs are selected according to their height in the plate stack, where PP 1 refer to the bottom PP in the stack, and PP 10 is the top PP in the stack. PP 2, PP 5 and PP 9 are instrumented in the PP-HEX, representing a low, middle and high position in the PP stack. Each of these PPs is equipped with a set of nine consecutively numbered TC, which are distributed on the surface as follows: TC00-TC08 are mounted on PP 2, TC09-TC17 are mounted on PP 5, and TC18-TC26 are mounted on PP 9. Fig. 3.6 shows a picture of how the TC sensors are mounted on the PP during the assembly of the PP stack. The TC wire is fixed to the PP surface using an adhesive sealant in such a way that the measurement point of the TC is 3-5 mm from the surface. The operator control of the test facility and the measurement data collection are achieved using a data acquisition system from National Instruments, coupled with the LabView software [43]. An overview of the measurement equipment and the indicated accuracy is given in Table 3.2.

3.2.2 Experimental procedure

The following two sections explain how the test series for the charging and discharging processes were carried out. The range in the parameters and test conditions

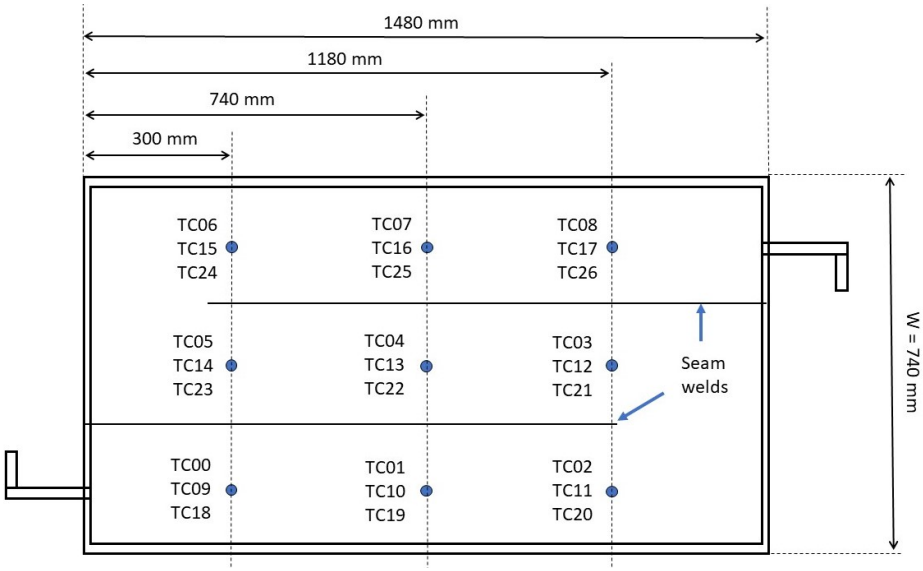

Figure 3.5: Top view of a PP: Locations of thermocouples on three selected PPs

applied during the test campaign using water/ice and PCM as the storage medium are summarised in Table 3.3.

Charging process

The purpose of the charging process is to extract heat (i.e. storing cold) from the storage material and transfer it to the refrigerant. In other words, the charging process is storing the cold in the storage medium for use later. During this process, the storage material solidifies (due to heat release), and the refrigerant evaporates (due to heat absorption). Liquid CO_2 refrigerant is supplied to the inlet of the CTES unit from the bottom of the liquid receiver by the CO_2 pump as described in Section 3.2. During the charging process, valves V1 and V3 are closed and valves V2 and V4 are open so that the PCC is active (see 3.4). The refrigerant enters the inlet of the CTES unit at a liquid state through valve V2. It then evaporates as it flows through the internal channels of the PP-HEX due to absorbing heat from the storage medium, which is at a higher temperature. At the outlet of the CTES unit, the refrigerant is a mixture of liquid and vapour, and the CTES unit is operated in overfed conditions. Most industrial refrigeration systems with pump circulation are operated in overfeed mode, meaning that more refrigerant is supplied to the evaporators than is evaporated in the HEX. Hence, the entire heat transfer area is utilised for two-phase heat transfer instead of superheating the vapour. This operating condition is replicated during the charging process in the test facility. The liquid/vapour CO_2 mixture is then condensed to the liquid state in a plate

Figure 3.6: Location of thermocouples close to the PP surface on plate number 2, 5 and 9 in the stack (PP2 shown in the figure).

HEX (Condenser) connected to the ACC. The liquid CO_2 is then brought from the outlet of the condenser to the refrigerant receiver. It is then drawn from the bottom of the receiver, and the cycle continues until the charging process is completed.

The charging process in each test was run until completion to compare the pressure drop of the CO_2 refrigerant, the temperature of the storage medium and the charging time of various operating conditions and plate pitches (full details in Table 3.3). The charging cycle is initiated with all the storage medium in the CTES unit in the liquid phase. The start of the charging process occurs when the average temperature of the storage medium (the mean temperature of TC00 to TC26) is measured below a certain threshold (e.g. below 0 °C when using the PCM as the storage medium). When the charging process is initiated, a layer of solid storage medium is formed on the PP surface, becoming thicker as the charging process progresses. This phenomenon continues until a complete block of solid storage medium is formed between two adjacent PPs, i.e. when the solid layer on the two PPs has overlapped. An illustration of a typical charging process is shown in Figure 3.7. When the solid layers of the storage medium have overlapped, the charging process continues as sensible energy storage until the temperature of the solid storage

Table 3.2: Measurement equipment utilised in the test facility

Component	Model	Producer	Indicated accuracy
Absolute pressure transmitter	Cerabar S PMP71	Endress+Hauser	± 0.25% of set span
Differential pressure transmitter	Deltabar S PMD75	Endress+Hauser	± 0.15% of set span
Temperature sensor CO_2 and glycol	Class B RTD Pt100	RS PRO	± 0.1 K
Temperature sensor PCM	Thermocouple type T	RS PRO	± 0.2 K
Mass flow meter glycol	RHM 15 Coriolis meter	Rheonik	± 0.2% of reading
Mass flow meter CO_2	RHM 06 Coriolis meter	Rheonik	± 0.2% of reading

Table 3.3: Test conditions applied in the test campaign using water/ice as the storage medium

Storage medium	**Water/ice**	**PCM**
Parameter	**Range**	**Range**
$T_{CO_2,\,evap}$	-2.5 to -15 °C	-12 to -23 °C
$T_{CO_2,\,cond}$	2.5 to 10 °C	-6.5 to 3.7 °C
$\dot{m}_{CO_2}$	4 to 10 kg/min	4 to 10 kg/min
δ_o	15, 30 and 45 mm	30 and 45 mm

medium block approaches the inlet refrigerant temperature. The charging process is completed when the difference between the mean temperature of the storage medium and the refrigerant temperature is less than 0.2 K.

The charging time is defined as the period from the mean temperature of the storage medium is measured below the defined threshold at the beginning, and to the point where the temperature difference of the PCM and the refrigerant is less than 0.2 K. During the charging process, the solidification of the storage medium on the PP surface can be observed through the plexiglass windows on each side of the CTES unit. The test conditions are varied according to Table 3.3. The refrigerant mass flow rate in the PCC is adjusted by controlling the frequency output of the variable speed drive on the $CO2_2$ pump in the range of 35 to 50 Hz. If the required mass flow rate is lower than the minimum frequency, the flow is throttled by partly closing valve V2 as described in 3.2. The evaporation temperature of the refrigerant in the PCC (and thereby in the PP channels in the CTES unit) is set by adjusting the cooling rate of the ACC in the condenser HEX. The pressure in the PCC is maintained at a constant level when the same heat rate extracted from the storage

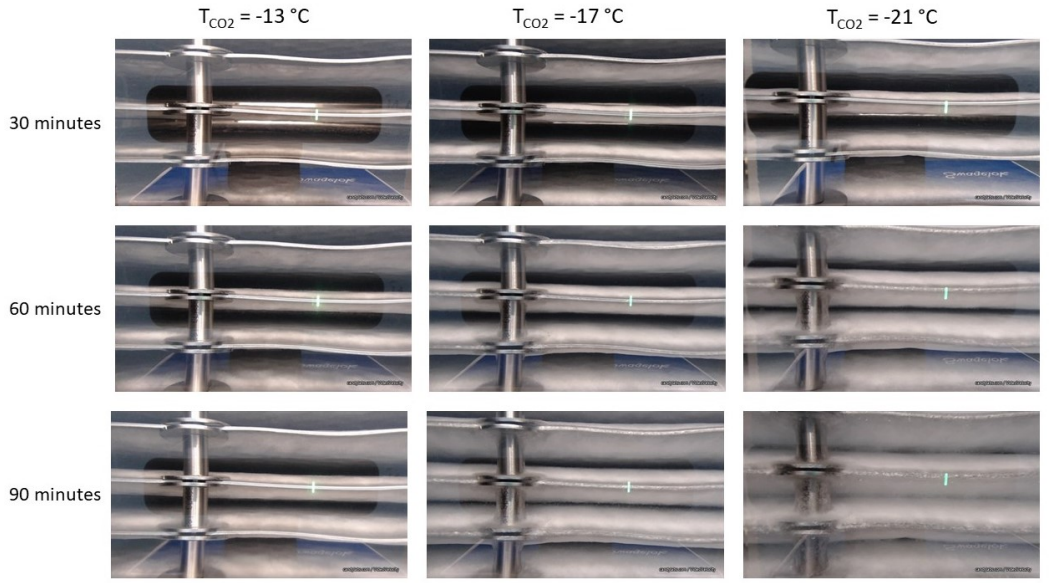

Figure 3.7: Example of the development of a solid PCM layer on the PP surface after 30, 60 and 90 minutes when using a CO_2 evaporation temperature of -13 °C, -17 °C and -21 °C. The example shown here is using a refrigerant mass flow rate of 8 kg/min and a plate pitch of 30 mm.

medium in the CTES unit is rejected to the ACC in the condenser. When the ACC in the condenser provides a higher cooling rate than extracted from the storage medium in the CTES unit, the pressure of the PCC will decrease. This balance is adjusted by choice of the appropriate suction temperature at the valve station of the ACC and further adjustment by using valve V5 to provide adequate heat transfer in the condenser.

Discharging process

The purpose of the discharging process is to reject heat from the refrigerant to the storage medium (i.e. releasing the cold) stored in the CTES unit during the charging process. During this process, the storage medium melts due to heat absorption, while the refrigerant condenses due to heat rejection. The discharging process is initiated immediately after the charging cycle is completed (described in Section 3.2.2) to minimise heat loss to the ambient from the CTES unit. During the discharging process, valves V2 and V4 are closed, and valves V1 and V3 are open so that the SCC is active (see 3.4). The GHC is also active by providing heat to the SCC. The liquid refrigerant is drawn from the bottom of the refrigerant receiver and circulated to the evaporator through valve V1 by the CO_2 pump. In the evaporator, heat is transferred from the glycol mixture in the GHC to the

refrigerant so that it exits the evaporator at a liquid/vapour state. The GHC simulates the thermal load to the CO_2 circuit, similar to the evaporators in an industrial plant. The two-phase CO_2 refrigerant mixture is then circulated to the CTES unit, where heat is transferred to the storage medium. When the refrigerant flows inside the PP channels, the heat is rejected to the storage medium until the refrigerant is completely condensed at the outlet manifold. Consequently, the storage medium absorbs the heat until it is completely melted. The liquid refrigerant is then returned to the refrigerant receiver through valve V3 to complete the cycle.

The refrigerant mass flow rate is controlled by the variable speed drive on the CO_2 pump and throttling of the flow using valve V1, identical to the procedure during the charging process. The heat input to the refrigerant from the GHC actively controls the pressure in the SCC during the discharging cycle. If the heat transferred to the CO_2 in the evaporator equals the heat rejected to the storage medium in the CTES unit, the pressure in the SCC remains constant. Consequently, the pressure in the SCC can be set to the required value by supplying more or less heat to the SCC. Since one of the heaters is equipped with PWM control, the output of the electric heaters can be controlled with high precision by the operator. The discharging cycle is a highly transient process, and a PI controller is therefore implemented in the LabVIEW software to continuously adjust the heater output to keep a constant pressure in the SCC according to the specifications of the experiment. The discharging process continues until all of the storage medium have completely melted or until the refrigerant in the SCC cannot reject any more heat to the CTES unit without increasing the pressure in the system. The discharging time is the period from starting the discharging cycle until one of the two criteria mentioned above occurs.

The discharging rate of the CTES unit is obtained by calculating the total heat transfer rate from the refrigerant to the storage medium in the CTES unit. The heat is first transferred from the GHC to the SCC in the evaporator, assuming no heat loss to the ambient occurs in the evaporator HEX. It is further assumed that the CO_2 enters the evaporator at a saturated liquid state since it is delivered from the bottom of the liquid receiver (see Figure 3.4). After the evaporator, the refrigerant enters the CTES unit as a two-phase mixture after about two meters of insulated pipe, where the heat loss to ambient is assumed to be negligible. After rejecting the heat to the storage medium in the CTES unit, the refrigerant exits at a subcooled condition. Consequently, it can safely be assumed that all the heat transferred from the glycol to the refrigerant in the evaporator HEX is rejected to the PCM in the CTES unit. The energy balance for the evaporator is given in Equation 3.1. The thermodynamic properties of the ethylene glycol mixture and propylene glycol mixture were taken from the datasheets of the manufacturer [44, 45], assuming a constant specific heat capacity of the fluid in the relevant

temperature range.

$$\dot{Q}_{CO_2,evap} = \dot{Q}_g = \dot{m}_g \; cp_g \; (T_{g,outlet} - T_{g,inlet}) \tag{3.1}$$

Where $\dot{Q}_{CO_2,evap}$ is the heat flow to the refrigerant in the evaporator, $\dot{Q}_g$ is the heat flow of the glycol, $\dot{m}_g$ is the mass flow rate of the glycol, cp_g is the specific heat capacity of the glycol, and $(T_{g,outlet} - T_{g,inlet})$ is the temperature difference from the inlet to the outlet of the glycol in the evaporator. Furthermore, the heat transfer required to cool the refrigerant from the condensation temperature (saturation temperature) to the outlet temperature (subcooled condition) is given in Eq. 3.2.

$$\dot{Q}_{CO_2,subcool} = \dot{m}_{CO_2} \; cp_{\,CO_2} \; (T_{CO_2,sat} - T_{CO_2,outlet}) \tag{3.2}$$

Where $Q_{CO_2,subcool}$ is the heat flow from the refrigerant to the PCM due to subcooling, $\dot{m}_{CO_2}$ is the mass flow rate of the refrigerant, $cp_{\,CO_2}$ is the specific heat capacity of the refrigerant, and $(T_{CO_2,sat} - T_{CO_2,outlet})$ is the difference between the saturation temperature and the outlet temperature of the refrigerant. The total discharge rate is then obtained by adding Eq. 3.1 and Eq. 3.2 together, as presented in Eq. 3.3.

$$\dot{Q}_{CO_2,tot} = \dot{Q}_{CO_2,evap} + \dot{Q}_{CO_2,subcool} \tag{3.3}$$

Where $Q_{CO_2,tot}$ is the total heat flow from the refrigerant to the PCM in the CTES unit. The total energy discharged over the cycle is obtained by numerical integration of the total discharge rate given in Eq. 3.3. All thermo-physical properties of the CO_2 are obtained using the thermodynamic database REFPROP 10 [46].

3.3 Uncertainty analysis

The output of the temperature sensors was checked with an ice water bath and validated to operate within ± 0.2 K (thermocouples TC01-TC27, see Fig. 3.4) and ± 0.1 K (RTD100 T1-T7, see Fig 3.4) at 0 °C. The uncertainty analysis was carried out by the method elaborated in [47], using a confidence level of 95 % (coverage factor of 2). The formulation used for the propagation of uncertainty is summarised below. Uncertainty for the mean PCM temperature on PP2, PP5, and

PP9 ($T_{PP2,mean}$, $T_{PP5,mean}$, and $T_{PP9,\ mean}$):

$$u(T_{\mathrm{PCM}}) = \sqrt{(1/9)^2 \cdot \sum_{i=1}^{9} u(T_i)} \ . \tag{3.4}$$

Uncertainty for the refrigerant saturation temperature:

$$u(T_{\mathrm{CO_2},sat}) = \sqrt{(\frac{\partial T_{\mathrm{CO_2},sat}}{\partial P_{\mathrm{CO_2},sat}})^2 \cdot u(P_{\mathrm{CO_2},sat})^2} \ . \tag{3.5}$$

From the Antoine equation, the relationship between saturation temperature and saturation pressure can be found. By derivation and inserting the coefficients for CO_2, it can be written as:

$$\frac{\partial T_{\mathrm{CO_2},sat}}{\partial P_{\mathrm{CO_2},sat}} = \frac{2273.66}{P_{\mathrm{CO_2},sat} \cdot (17.9834 - \ln(P_{\mathrm{CO_2},sat}))^2} \ . \tag{3.6}$$

Uncertainty in the heat flow from the glycol to the refrigerant in the evaporator:

$$u(\dot{Q}_{\mathrm{CO_2,\ evap}}) = \sqrt{(cp_g \cdot \Delta T_g \cdot u(\dot{m}_g))^2 + (\dot{m}_g \cdot cp_g \cdot u(\Delta T_g))^2} \ . \tag{3.7}$$

Uncertainty in the glycol temperature difference from inlet to outlet in the evaporator:

$$u(\Delta T_g) = \sqrt{u(T_{g,inlet})^2 + u(T_{g,outlet})^2} \ . \tag{3.8}$$

Uncertainty in the heat flow from the refrigerant to the PCM due to subcooling of the refrigerant:

$$u(\dot{Q}_{\mathrm{CO_2,\ subcool}}) = \sqrt{(cp_{CO_2,liq} \cdot \Delta T_{CO_2} \cdot u(\dot{m}_{CO_2}))^2 + (\dot{m}_{CO_2} \cdot cp_{CO_2,liq} \cdot u(\Delta T_{CO_2}))^2} \ . \tag{3.9}$$

Uncertainty in the refrigerant temperature difference from the saturation temperature to the outlet temperature from the CTES:

$$u(\Delta T_{CO_2}) = \sqrt{u(T_{\mathrm{CO_2},sat})^2 + u(T_{\mathrm{CO_2,\ outlet}})^2} \ . \tag{3.10}$$

Uncertainty in the total heat flow from the refrigerant to the PCM in the CTES unit:

$$u(\dot{Q}_{CO_2,tot}) = \sqrt{u(\dot{Q}_{\mathrm{CO_2,\ evap}})^2 + u(\dot{Q}_{\mathrm{CO_2,\ subcool}})^2} \ . \tag{3.11}$$

The uncertainty in the discharged energy over the cycle is estimated by integrating the uncertainty in the heat flow from the refrigerant to the PCM (Eq. 3.3) from the start to the end of the cycle. To investigate the repeatability of the experiments, tests with identical test conditions were carried out for the 30 mm and 45 mm plate pitches for the experiments using water as the storage medium and for the 15 mm and 30 mm plate pitches in the case of using the PCM RT-9HC as the storage medium. The charging time was used as the indicator for the charging cycle. In the case of using water/ice as the storage medium, the resulting range of charging time was found to be $<$ 10 minutes for both the 30 mm and 45 mm plate pitch. This corresponds to a repeatability of the charging time within $\pm$ 5.9 % and $\pm$ 3.3 % at T_{sat} = -5 °C and $\dot{m}_{CO_2}$ = 7 kg/min for the 30 mm and 45 mm plate pitch, respectively. For the experiments with RT-9HC, the resulting range of charging time was found to be $<$ 5 minutes for the 15 mm plate pitch and $<$ 10 minutes for the 30 mm configuration. This corresponds to a repeatability of the charging time within $\pm$ 6.7 % and $\pm$ 5.1 % at T_{sat} = -15.5 °C and $\dot{m}_{CO_2}$ = 8 kg/min for the 15 mm and 30 mm plate pitch, respectively.

For the discharging process, the mean discharge rate and discharged energy over the cycle were chosen as indicators for repeatability. For experiments using water/ice as the storage medium, the obtained range for the discharged energy over the cycle was $<$ 1 kWh for both configurations, corresponding to $<$ 5 % and $<$ 3 % of the discharged energy for the 30 mm and 45 mm plate pitch, respectively. For the experiments using RT-9HC as the storage medium, a range for the discharged energy over the cycle was $<$ 0.3 kWh for both configurations, corresponding to $<$ 4 % and $<$ 3 % of the discharged energy at the tested conditions for the 15 mm and 30 mm plate pitch, respectively. Regarding the mean discharge rate, a range of $<$ 0.25 kW was obtained for both experiments using water/ice and RT-9HC as the storage medium for all plate pitch configurations.

3.4 PCM characterisation

This section presents the selection of storage media used in the experimental campaign to characterise the performance of the novel CTES unit at different temperature levels. First, the selection process of the two storage media is explained. Then the experimental procedure for determining the thermo-physical properties of the PCM is given. The results of the PCM characterisation are presented in Journal paper III: Cold thermal energy storage for industrial CO_2 refrigeration systems using phase change material: An experimental study [48], which can be found in the Appendix.

3.4.1 Phase change material

It was decided that the first experimental campaign should be carried out using a well-known storage medium with established and well-documented thermo-physical properties. This decision was made based on first providing a proof-of-concept on operating the novel CTES unit in charging and discharging mode. Water/ice was selected as the storage medium due to its well-known properties and the established experience of being used as a storage medium both in research and in commercial/industrial applications in the past [13]. Furthermore, the phase transition temperature of water/ice fits well with the temperature requirements in industrial process cooling plants (0 to 15 °C) and chiller plants for AC (usually operating at a temperature between 7 and 12 °C). After verifying the concept and operational modes using water/ice as the storage medium, it is of great interest to explore storage materials with phase transition temperature applicable for low-temperature industrial refrigeration systems typically found in the food processing industry.

A screening of the commercially available PCMs in the temperature range of -65 °C to 10 °C was carried out to find suitable candidates for testing in the novel CTES unit. The list of commercially available PCMs at the time of publication can be found in the review paper: Review on cold thermal energy storage applied to refrigeration systems using phase change materials [13] and in Section 4.1. Since the present research focuses on sub-ambient TES, the PCMs used are in the liquid state at ambient temperatures. It enables immersion of the PP-HEX in liquid PCM in the container. Consequently, the PCM must be suitable for transitioning between the solid and liquid phases in bulk. Due to phase segregation issues commonly found in salt hydrate/water mixtures (and therefore often found as macroencapsulated products), it was decided that organic PCMs would be the most suitable option. This choice was made despite the generally lower latent heat capacities and lower thermal conductivity of organic PCMs. Among the available candidates, the selected PCM was the commercial paraffin PCM RT-9HC (Rubitherm Technologies GmbH [49]). It has a phase change temperature in the range of -9 °C and -10 °C [49]. The PCM was selected among other potential candidates as it has the highest latent heat capacity compared to the other PCMs. Furthermore, RT-9HC was selected thanks to its compatibility with the stainless steel used in the construction of the CTES unit.

3.4.2 Experimental procedure

The datasheet for the PCM provided by the manufacturer contains information on the thermo-physical properties of the material, but mainly at a single temperature point. For this reason, a thorough experimental characterisation of the PCM is required to fully explore and understand the behaviour of the heat transfer process within the PCM and between the PCM and the refrigerant. Established experimen-

tal characterisation techniques are applied to determine important PCM properties, such as the latent heat capacity, phase transition temperature and thermal conductivity. The methodology of each experimental characterisation technique utilised for RT-9HC is explained in the following paragraphs.

Latent heat capacity and phase transition temperature

The latent heat capacity of PCMs is one of the most important properties determining whether it is suitable to use in a CTES system since it directly affects the specific latent storage density (see Equation 2.8). For determining the latent heat capacity and the phase transition temperature of the PCM, the differential scanning calorimetry (DSC) technique is used. According to guidelines of the Quality and Testing Specifications for PCM RAL-GZ 896 [50], approved by the German Institute for Quality Assurance and Certification, DSC is the appropriate method for determining the phase change temperature and thermal storage capacity of PCMs. The reader is directed to the following reference for full details on the DSC technique [51]. DSC is typically used to measure transitions such as glass transition, melting, crystallisation and curing, as well as heat capacities of materials. In the heat flux DSC method, the sample is encapsulated into an aluminium pan and placed on a thermoelectric disk with an empty pan (reference). The sample and reference are surrounded by a furnace, in which the temperature is changed according to a specified program. Heat is transferred to/from the sample and the reference through the thermoelectric disk. The temperature difference between the sample and reference material is measured as a function of temperature [52]. For more in-depth information and description of DSC methods applicable to PCM characterisation, the reader is directed to the following reference [53]. The literature emphasises the importance of using low heating/cooling rates (typically 1 K/min or lower) to obtain reliable and accurate results when using DSC for PCM characterisation [53, 54, 55, 56]. Furthermore, the sample size could affect the characterisation results, as thermal resistance within the sample might shift the measured transition temperatures. However, it has been shown that the sample mass has less influence on the measured latent heat capacity than the heating rate [55].

The DSC apparatus used in the current research is a TA Instruments Q2000 DSC equipped with liquid nitrogen cooling (see Figure 3.8). Standard Tzero 40 μL aluminium pans/crucibles were utilised in the experiments to encapsulate the PCM samples. The empty pans and filled pans were weighed using a Mettler Toledo laboratory scale with a precision of ± 0.01 mg to determine the sample mass. Before the testing, the apparatus was calibrated and tested with an indium reference sample. The obtained melting enthalpy and melting temperature of indium were within 0.5 % of the values provided by the manufacturer [57, 58]. For further validation, a 10 mg sample of deionised water was tested and found to give a melting

enthalpy with less than 0.2 % deviation of tabulated values (333.55 kJ/kg). For investigating the characteristics of the selected PCM RT-9HC, two samples were prepared, weighted and encapsulated in aluminium pans. Two sample masses were prepared (7.914 mg and 13.351 mg) to investigate the effect of sample size on the results. The samples were then cycled from 30 °C to -40 °C in the DSC using a constant heating/cooling rate, often referred to as the dynamic DSC method. Each sample was cycled using heating and cooling rates of 10, 5, 2.5 and 1 K/min. The samples were subject to temperature equilibration and a 5-minute isothermal stage before and after each heating/cooling transition to/from 30 °C to -40 °C.

Figure 3.8: TA Instruments Q2000 differential scanning calorimetry equipped with liquid nitrogen cooling used for PCM characterisation

Thermal conductivity

The design of the CTES unit relies on the PCM being stagnant, i.e. no mechanical stirring, pumping or other forms of forced circulation of the PCM is occurring. Thus, the heat transfer process within the PCM in the CTES unit is expected to be dominated by conduction heat transfer. Some contributions from natural convection can be present, depending on the density difference with temperature in the liquid phase of the PCM. Therefore, the thermal conductivity of the PCM will have a significant impact on the heat transfer rate for both the charging and the discharging processes of the CTES unit. The thermal conductivity of the PCM RT-9HC is measured by a thermal constants analyser (TPS 2500s produced by manufacturer Hot Disk AB, shown in Figure 3.9), which is based on the transient

plane source (TPS) technique. For full details and description of this technology and measurement principles, the reader is directed to the following reference [59]. The TPS method utilises a flat sensor consisting of a thin metal spiral usually placed between two halves of the measured sample. Electrical current is passed through the spiral, increasing its temperature. The thermal conductivity can be calculated by recording the temperature response in the sensor over a given time. An illustration of a typical TPS sensor is shown in Figure 3.10. The metal spiral is covered in a special tape (Kapton), for which the thickness and specific heat capacity are compensated for in the calculations of the analyser. It is of interest to measure the thermal conductivity for both the liquid phase and the solid phase of the PCM. To achieve reliable results for both phases, the measurement sensor and setup have to be adjusted due to the different properties of the phases.

Figure 3.9: HotDisk TPS 2500S thermal constants analyser used for determining the thermal conductivity of PCM

For the liquid phase of the PCM, a liquid sample holder offered by the manufacturer of the thermal constants analyser (Hotdisk AB) was utilised to perform the measurements on the PCM. The liquid sample holder is designed to ensure appropriate test conditions for the sensor in the sample during the measurements. The liquid test cell consists of a block of aluminium divided into two pieces that are mounted together with a gasket in between. The two halves together hold a small sample volume inside. The TPS sensor is vertically inserted between the two halves of the liquid cell; see Figure 3.11. The plastic tubes connected to the two halves of the aluminium block are used to fill the test cell with the liquid PCM and bleed air out of the test chamber.

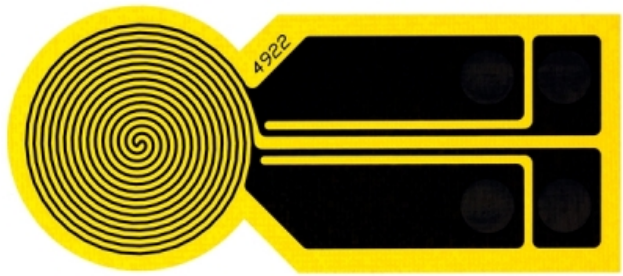

Figure 3.10: Example of a sensor for the TPS2500 (Hot Disk AB) thermal constants analyser

The liquid test cell was put into a metal sample holder and the assembly into a temperature-controlled thermal bath. A Pt100 temperature sensor connected to the TPS2500 was used to measure the sample temperature during the temperature stabilisation period. The bath temperature and the criterion for temperature stability of the sample can be programmed in the accompanying software of the TPS2500. The temperature of the thermal bath was changed from 25 °C to -9 °C, and a 6-hour stabilisation period was introduced at each temperature stage before the measurements were taken to ensure a thermal equilibrium within the sample. According to the manufacturer's recommendations, the thermal conductivity measurement in liquids should be carried out using a small sensor radius, applying low sensor heating power and limiting the measurement time to a few seconds to ensure the reliability and repeatability of the tests. These recommendations are given to avoid initiating natural convection within the sample that can affect the measurements. The reading will be false if convection occurs around the sensor during the measurement period.

A sensor with a radius of 2.0 mm (Kapton sensor 7577, Hotdisk AB), a sensor heating power of 25 mW and a measurement time of 2 seconds were applied to perform the measurements. The measurements were repeated four times at each temperature step, with a 20-minute holding time between each measurement. The holding time was introduced to ensure equilibrium within the sample after the heat input from the previous measurement. The mean value and standard deviation were calculated from the four measurements per temperature step. To verify the setup, a test series using distilled water in the liquid sample holder was first carried out in the temperature range 5 °C to 30 °C. The thermal conductivity obtained for distilled water was then compared to the correlation for water thermal conductivity proposed in [60]. The results were found to be within 3 % and 6.5 % of the correlation for a sample temperature below and above 20 °C, respectively. It can be noted that a more significant deviation from the correlation at the higher temperature may be due to the onset of convection as the viscosity reduces with higher

Figure 3.11: Experimental setup for measurement of thermal conductivity of liquid samples

temperatures. It is concluded that the results from the validation are acceptable for sample temperatures less than 20 °C.

For measuring the thermal conductivity of the solid phase of the PCM, another sample holder had to be made. The solid PCM sample holder is shown in Figure 3.12. It consists of a machined stainless steel cylinder, open at the top and closed at the bottom. The cylinder is split into two pieces at half of its height. The TPS sensor is inserted in between the two halves, which are then fixed together with fasteners and sealed with a gasket. Liquid PCM was then filled into the sample holder, ensuring no air was trapped. The whole sample holder was placed into a programmable freezer for the PCM to solidify completely so that the TPS sensor was embedded into the solid PCM. For the measurements in the solid phase, a sensor with a radius of 6.4 mm (Kapton sensor 5501, Hotdisk), a sensor heating power of 25 mW and a measurement time of 80 seconds was selected. Only two temperature points were measured in the solid phase due to the temperature restriction of the thermal bath and its stability at low temperatures.

Viscosity

Viscosity is the magnitude of internal friction in fluids, the resistance to change of shape or movement of neighbouring portions relative to one another. For liquids,

Figure 3.12: Experimental setup for measurement of thermal conductivity of solid PCM samples

viscosity could be translated to ease of flow or the more commonly known concept of the thickness of the liquid. For most liquids, the viscosity reduces with increasing temperature. For PCMs used in CTES units, the viscosity of the liquid phase can affect the significance of heat transfer due to natural convection during the discharging phase. For PCMs with lower viscosity, the onset of natural convection will occur at lower temperature differences within the fluid. In this work, the viscosity of the PCM in the liquid phase was experimentally determined using a Haake Mars III rotational rheometer (Thermo Fisher Scientific [61]). A concentric cylinder geometry DIN Z40 was selected for the experiments. In this setup, the liquid sample is confined between a rotating cylinder and a fixed cup. The cylinder is rotated at a set angular speed, and the resulting torque on the cylinder is measured. The shear stress and shear rate can be obtained using the geometric parameters of the cylinder and cup. The apparent viscosity is then determined by Equation 3.12:

$$\mu = \frac{\tau}{\dot{\gamma}} \,, \tag{3.12}$$

where μ is the apparent viscosity, τ is the shear stress applied to the liquid and $\dot{\gamma}$ is the shear rate. To determine the viscosity of the liquid PCM at different temperatures, the rheometer geometry is connected to a thermostatic circulation bath using glycol as the coolant. The thermal bath has a controller to manually set the requested coolant temperature delivered to the test section of the rheometer. The PCM was tested at temperatures of 8 °C, 0 °C and -8 °C, which is the expected practical operating temperature range of the PCM in the developed CTES unit. The experimental procedure consists of a sufficient holding period to ensure a homogeneous temperature within the sample. Then, a one-minute measurement period was conducted using a constant shear rate of $\dot{\gamma} = 10$ 1/s. The shear rate was then increased from $\dot{\gamma} = 10$ 1/s to $\dot{\gamma} = 100$ 1/s with increments of $\dot{\gamma} = 10$ 1/s over a total time of two minutes. Each test was repeated three times at the temperatures considered in this study, and the average of the collected data points was calculated.

Density

The density of the PCM is another essential property to consider in the selection process since it, together with the latent heat capacity, dictates the volumetric storage capacity of the PCM (see Equation 2.8). During the discharging process of the CTES unit, temperature gradients within the liquid PCM are expected due to the condensing temperature of the refrigerant will be higher than the melting temperature of the PCM. Consequently, the relative change in liquid PCM density as a function of its temperature will partly determine the significance of natural convection flow towards the total heat transfer between the refrigerant and the PCM. The contribution of natural convection during the discharging phase mainly depends on three factors previously discussed: the temperature gradients within the liquid PCM, the density change as a function of the temperature, and the viscosity of the PCM.

In this work, the density of the liquid PCM as a function of the temperature is determined by measuring the thermal expansion (i.e., the increase in volume) of a PCM sample placed in a thermostatic oil bath. The sample was held in a 25 ml measuring cylinder that was then placed in the thermal bath, where the temperature was varied from 30 °C to -9 °C with intervals of 5 K. Hence, the range of temperature covered the span from ambient temperature to just above the solidification temperature. A holding time of 30 minutes at each temperature was applied to ensure that the sample temperature was uniform before reading the measurement. The procedure was repeated for three samples with a mass of 14.82 gram, 16.38 gram and 17.90 gram, respectively. The sample mass was measured with a laboratory scale (Model ME4002, Mettler Toledo) having a precision of 0.01 grams.

4 Summary of research work

This chapter summarises the research performed in the present doctoral work. The chapter is organised in separate sections for each journal publication included in the thesis. The main conclusions from each paper are summarised, and the contribution towards achieving the sub-objectives of the doctoral work is given. The journal publications described here are intended to accomplish the sub-objectives of the doctoral work. All publications are enclosed in the appendix to provide the reader with complete insight into the topics covered in each respective publication.

4.1 Journal paper I: Review on cold thermal energy storage applied to refrigeration systems using phase change materials

This journal publication presents the current status regarding research on CTES technology with PCMs applied to refrigeration systems. The work is the outcome of the collection, reviewing and systematising the recent literature on the research topic, focusing on the applications in food transport and packaging, commercial refrigeration and other refrigeration applications.

The first part of the work focuses on the presentation and classification of PCMs relevant to CTES for refrigeration systems, herein the description of the important thermophysical properties of PCMs and a thorough description of recommended experimental characterisation methods for investigating these properties. Furthermore, the review paper describes various enhancement techniques to counter the main challenges and limitations of the various types of PCMs. An extensive list of commercially available PCMs in the temperature range of 10 °C to -65 °C at the time of publication is included in the publication. The list is provided to help the

reader get an overview of potential suppliers of low-temperature PCM relevant to CTES applications. The list is included in Table 4.1 for reference.

Table 4.1: Commercially available PCMs in the temperature range from -65 °C to 10 °C, sorted by melting temperature. All information is taken from the datasheet of the respective manufacturers.

Material	T_m [°C]	Latent heat [kJ/kg]	Type of product	Producer
E-65	-65	240	Inorganic	PCM Products
SP-50	-52 to -48	200	Inorganic	Rubitherm GmbH
E-50	-50	175	Inorganic	PCM Products
PureTemp-37	-37	145	Bio-based organic	PureTemp LCC
E-37	-37	225	Inorganic	PCM Products
E-34	-34	200	Inorganic	PCM Products
ATS-40	-33	300	Inorganic	Axiotherm GmbH
E-32	-32	225	Inorganic	PCM Products
va-Q-accu -32G	-32	243	n.a.	va-Q-tec
PCM-30	-30	150-160	Organic	Microtek Laboratories
HS30N	-30	224	Inorganic	PLUSS Advanced Technologies
E-29	-29	250	Inorganic	PCM Products
SP-30	-29 to -28	250	Inorganic	Rubitherm GmbH
SP-28	-29 to -28	260	Inorganic	Rubitherm GmbH
HS26N	-26	274	Inorganic	PLUSS Advanced Technologies
E-26	-26	265	Inorganic	PCM Products
SP-24	-25 to -23	285	Inorganic	Rubitherm GmbH
HS23N	-23	262	Inorganic	PLUSS Advanced Technologies
E-22	-22	305	Inorganic	PCM Products
CrodaTherm -22	-23	217	n.a	Croda Europe
va-Q-accu -21G	-21	234	n.a.	va-Q-tec
ClimSel C-21	-21	285	Inorganic	Climator AB
PureTemp -21	-21	239	Bio-based organic	PureTemp LLC
E-21	-21	285	Inorganic	PCM Products
ATS-21	-21	320	Inorganic	Axiotherm GmbH
SP-21	-21 to -19	285	Inorganic	Rubitherm GmbH

Material	T_m [°C]	Latent heat [kJ/kg]	Type of product	Producer
E-19	-19	300	Inorganic	PCM Products
HS18N	-18	242	Inorganic	PLUSS Advanced Technologies
ClimSel C-18	-18	288	Inorganic	Climator AB
SP-17	-18 to -17	300	Inorganic	Rubitherm GmbH
E-15	-15	320	Inorganic	PCM Products
HS15N	-15	308	Inorganic	PLUSS Advanced Technologies
PureTemp -15	-15	301	Bio-based organic	PureTemp LCC
ATS-12	-12	360	Inorganic	Axiotherm GmbH
E-11	-12	310	Inorganic	PCM Products
SP-11	-12 to -11	240	Inorganic	Rubitherm GmbH
SP-11 UK	-12 to -10	330	Inorganic	Rubitherm GmbH
PCM-10	-10	175-185	Organic	Microtek Laboratories
MPCM-10	-10	170-180	Organic	Microtek Laboratories
MPCM-10D	-10	170-180	Organic	Microtek Laboratories
HS10N	-10	290	Inorganic	PLUSS Advanced Technologies
RT-9 HC	-9	250	Organic	Rubitherm Technologies
HS7N	-7	296	Inorganic	PLUSS Advanced Technologies
SP-7	-7 to -5	290	Inorganic	Rubitherm GmbH
ATS-6	-6	360	Inorganic	Axiotherm GmbH
E-6	-6	300	Inorganic	PCM Products
RT-4	-4	180	Organic	Rubitherm GmbH
E-3	-4	330	Inorganic	PCM Products
HS3N	-3	346	Inorganic	PLUSS Advanced Technologies
ATS-3	-3	330	Inorganic	Axiotherm GmbH
PureTemp -2	-2	277	Bio-based organic	PureTemp LCC
E-2	-2	325	Inorganic	PCM Products
RT0	0	175	Organic	Rubitherm GmbH
E0	0	395	Inorganic	PCM Products
va-Q-accu +00G	0	330	n.a.	va-Q-tec

Material	T_m [°C]	Latent heat [kJ/kg]	Type of product	Producer
HS01	1	350	Inorganic	PLUSS Advanced Technologies
A2	2	230	Organic	PCM Products
ATP 2	2	215	Organic	Axiotherm GmbH
RT2 HC	2	200	Organic	Rubitherm GmbH
SP5 gel	2 to 7	155	Inorganic	Rubitherm GmbH
va-Q-accu +05G	2 to 8	240	n.a.	va-Q-tec
OM03	3	229	Organic	PLUSS Advanced Technologies
FS03	3	161	Organic (fatty acid)	PLUSS Advanced Technologies
RT3 HC	3	190	Organic	Rubitherm GmbH
A3	3	230	Organic	PCM Products
RT4	4	175	Organic	Rubitherm GmbH
PureTemp 4	5	187	Organic	PureTemp LLC
A4	4	235	Organic	PCM Products
RT5	5	180	Organic	Rubitherm GmbH
RT5 HC	5	250	Organic	Rubitherm GmbH
OM05P	5	216	Organic	PLUSS Advanced Technologies
A5	5	170	Organic	PCM Products
CrodaTherm 5	5	191	Bio-based organic	Croda
SP7 gel	5 to 8	155	Inorganic	Rubitherm GmbH
ATP 6	6	275	Organic	Axiotherm GmbH
A6	6	185	Organic	PCM Products
A6.5	6.5	190	Organic	PCM Products
CrodaTherm 6.5	6.8	184	Organic plant-based	Croda
Gaia OM PCM7	7	180	Organic	Global-E-Systems
ClimSel C7	8	123	Inorganic	Climator AB
A7	7	190	Organic	PCM Products
PureTemp 8	8	178	Organic	PureTemp LLC
OM08	8	175	Organic	PLUSS Advanced Technologies
RT8	8	175	Organic	Rubitherm GmbH
RT8 HC	8	190	Organic	Rubitherm GmbH
S8	8	130	Inorganic	PCM Products
A8	8	180	Organic	PCM Products
A9	9	190	Organic	PCM Products
CrodaTherm 9.5	9.7	186	Bio-based organic	Croda
RT10	10	160	Organic	Rubitherm GmbH
RT10 HC	10	200	Organic	Rubitherm GmbH
A10	10	210	Organic	PCM Products
S10	10	170	Inorganic	PCM Products
SP9 gel	10 to 11	155	Inorganic	Rubitherm GmbH

The second part of the review paper concerns the collection and systematisation of recent literature on CTES with PCMs applied to refrigeration systems. The results show that CTES technology has been proposed in nearly all links of the food cold chain. Examples of uses range from the processing plants at the start of the cold chain to domestic refrigeration at the consumer stage. Based on the number of reviewed publications on CTES technology using PCM in refrigeration systems, the relevant studies were classified into food transport and packaging, commercial refrigeration and other refrigeration applications. The main findings are summarised as follows:

Food transport and packaging include the use of PCM in various applications within the transport of perishable goods, either directly or indirectly integrated into a refrigeration system. Three methods of using PCMs in food transport and packaging were identified: i) integration into the walls of refrigerated vehicles, ii) into various product containers or packaging, iii) into an active thermal system working as a replacement for diesel-driven refrigeration systems usually found onboard refrigerated vehicles. The contributions of the research within this sector have shown that PCM-based multi-layer walls can reduce the heat flux of refrigerated compartments by up to 29 % in a Southern European climate context.

Commercial refrigeration has been of high interest for implementing CTES technology with PCM, where the research contribution can be grouped into two categories: i) integration of PCM-HEX units into the main air duct or the product shelf of refrigerated display cabinets, or ii) integrated into the supermarket refrigeration system itself in the case of a centralised system layout. Particular interest in the research community is related to implementing CTES technology in CO_2 supermarket refrigeration systems. The proposed solutions and locations for implementing CTES with PCM in these systems are given in Figure 4.1. In the case of integration of PCM-HEX units into the display cabinets, water/ice is by far the most frequently studied PCM. The reported benefits of this solution include the stabilisation of cabinet air temperature and lower product temperature, particularly for the open display cabinet designs. The reported research on integrating CTES technology with PCM on the system level in supermarkets primarily covers theoretical concepts with simplified storage models that need verification through experimental investigations.

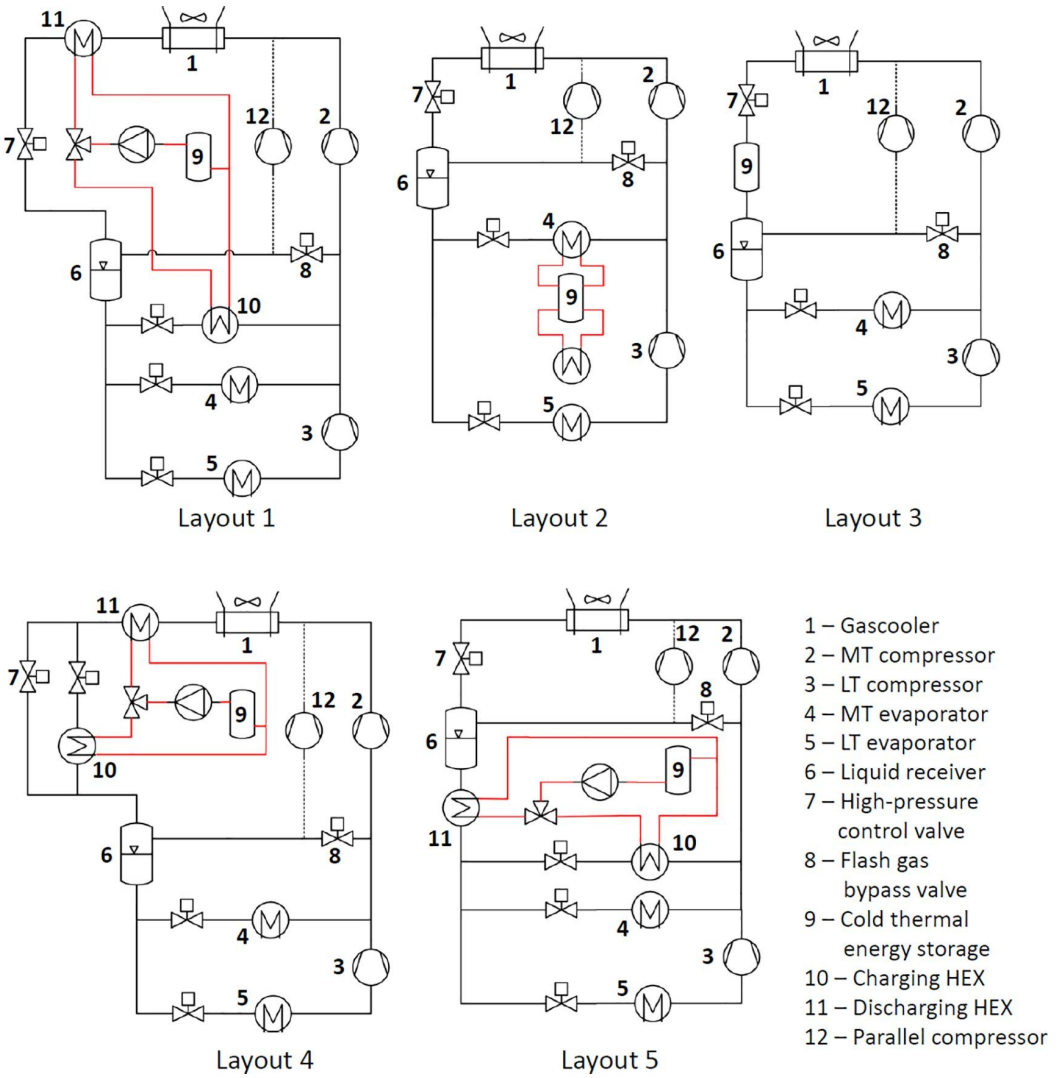

Figure 4.1: Integration of CTES into a CO_2 refrigeration system: 1) Downstream of the gascooler using ice/water as the PCM 2) into the MT display cabinet 3) Upstream of the pressure receiver and using ice/water as the PCM 4) Downstream of the gascooler, using a 15 °C PCM 5) Downstream of the pressure receiver. A dashed line indicates optional parallel compression in each configuration.

Other refrigeration systems, particularly AC systems/chillers for space cooling, have been considered potential candidates for implementing CTES units in the past. Generally, two methods of integrating CTES technology into refrigeration plants for peak shaving have been identified in the reviewed literature: i) the integration of the PCM-CTES unit in the secondary refrigerant cycle (glycol, brine, water) often

found in chillers for process cooling or AC application, and ii) direct integration of the PCM-CTES unit into the primary refrigerant circuit of the refrigeration plant, more commonly investigated in industrial refrigeration systems operating with considerably lower evaporation temperatures than chillers for AC applications. The principle of the two methods is explained in Figure 4.2.

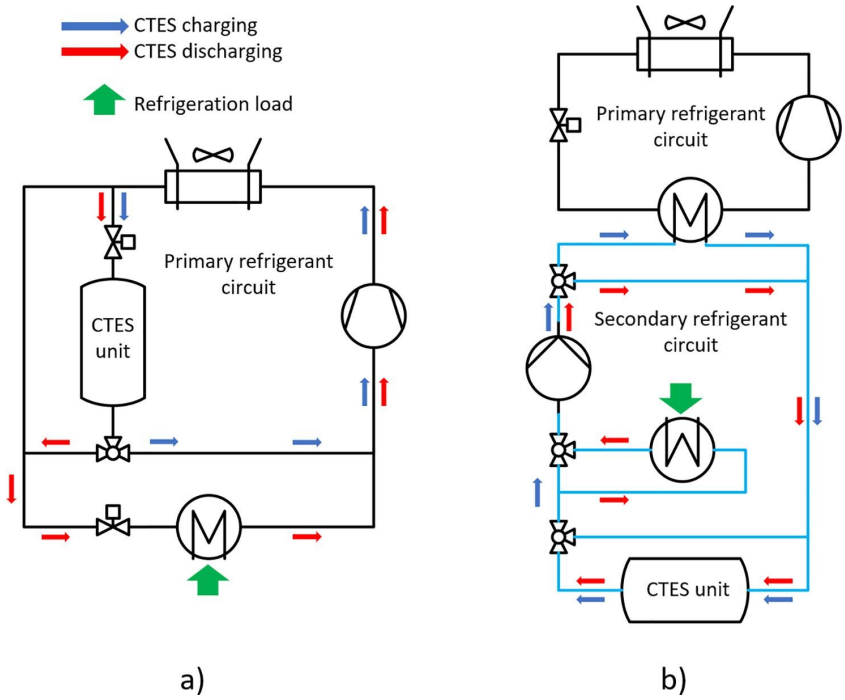

Figure 4.2: Strategies of CTES integration in a simplified refrigeration system: a) PCM/two-phase fluid heat exchange, b) PCM/single-phase fluid heat exchange

Common to all applications areas of CTES implementation using PCM in refrigeration systems is the pressing need to carry out experimental investigations of promising concepts studied theoretically in the past. Particularly the concept of replacing conventional diesel-driven refrigeration systems for refrigerated vehicles with a PCM-CTES unit would be of high interest to investigate further, along with large-scale CTES systems for industrial cooling and freezing processes.

4.2 Journal paper II: Experimental characterisation of a cold thermal energy storage unit with a pillow-plate heat exchanger design

In this second journal publication of the doctoral work, a design of a novel CTES unit suitable for industrial refrigeration plants is presented, and the performance is experimentally investigated and reported. The purpose of the newly designed CTES unit is to provide peak shifting of the refrigeration load by storing cold energy in the liquid-solid phase transition of a PCM at off-peak hours and providing a heat sink during peak hours. From the screened literature in the review paper (presented in Section 4.1), it was found that designing the CTES unit for integration directly into the primary refrigerant circuit would have several benefits compared to the integration into a secondary refrigerant circuit. When targeting peak shifting of industrial refrigeration systems, a large storage capacity and discharge rate will be required from the CTES unit. From the literature, the coil-in-tank or tube-in-tank were the most commonly investigated designs of CTES units. To achieve improved performance and reduce the required temperature differences between the PCM and the refrigerant in the CTES unit, it was decided to use a plate-in-tank design to ensure a high heat transfer area and improve compactness compared to conventional designs. CO_2 as a refrigerant is becoming increasingly popular in industrial refrigeration systems, either as the single refrigerant in a system or as the bottom cycle in a cascade system with ammonia (R717) in the high-temperature circuit. To withstand the relatively high operating pressure of CO_2 in refrigeration systems, PP-HEX plates were found to be suitable. A detailed description of the novel CTES unit is provided in Section 3.1. It was decided to use water/ice as the storage medium due to well-documented thermophysical properties and suitable phase change temperature targeting peak shifting for various process cooling purposes and AC systems.

An experimental test facility was established to accommodate the novel CTES unit, using pump circulation of an oil-free CO_2 refrigeration circuit to simulate the industrial refrigeration system. A detailed description of the experimental test facility and associated data acquisition system is provided in Section 3.2. The work presented in the paper aims to provide a proof of concept of pairing the evaporation/condensation process of the refrigerant inside the PP channels with the solidification/melting process of the storage medium on the outer surface of the PP during the charging and discharging cycles, respectively. The study provided the necessary proof of concept of operating a latent CTES unit integrated into a CO_2 refrigeration cycle, showing that the storage medium could be cycled between the liquid and solid phases by condensing and evaporating the refrigerant inside the PPs. Figure 4.3 shows the mean water temperature near three PPs through

the stack in the PP-HEX during the charging cycle. It was shown that a refrigerant mass flow rate of 7 kg/min was required to achieve adequate refrigerant distribution and even growth of the ice layer on the PPs during the charging process. Furthermore, the evaporation temperature of the CO_2 had a significant impact on the charging time of the CTES unit. Hence, the selection of evaporation temperature will be based on the cost of electricity and time available for charging the CTES unit since lowering the evaporation temperature decreases the overall performance of the refrigeration system.

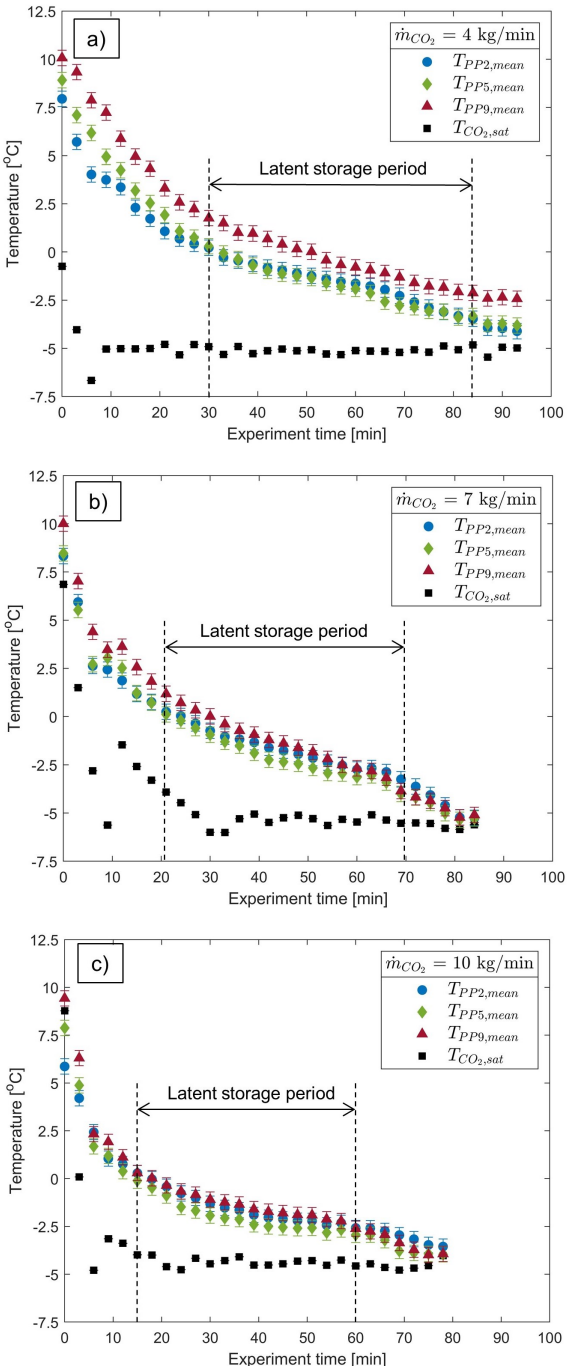

Figure 4.3: The mean PCM temperature close to PP 2, 5 and 9 in the stack during the charging cycle with plate pitch $\delta_o = 30$ mm for a refrigerant mass flow rate of a) 4 kg/min b) 7 kg/min and c) 10 kg/min.

It was shown that the characteristic discharging curve of the CTES unit was highly transient, providing a high heat transfer during the initial phase of the discharging process, see Figure 4.4. Furthermore, After the initial phase, the discharge rate decreases gradually towards zero to denote the end of the discharging cycle. Furthermore, it was shown that the selected CO_2 condensation temperature affected the discharging rate considerably. A condensing temperature of around 4-5 °C provided a low discharge rate for an extended period while increasing the condensation temperature resulted in a shorter discharging cycle with a higher discharge rate. Overall, the flexible design of the CTES unit proved to be suitable for achieving peak shifting of processes with several different load characteristics.

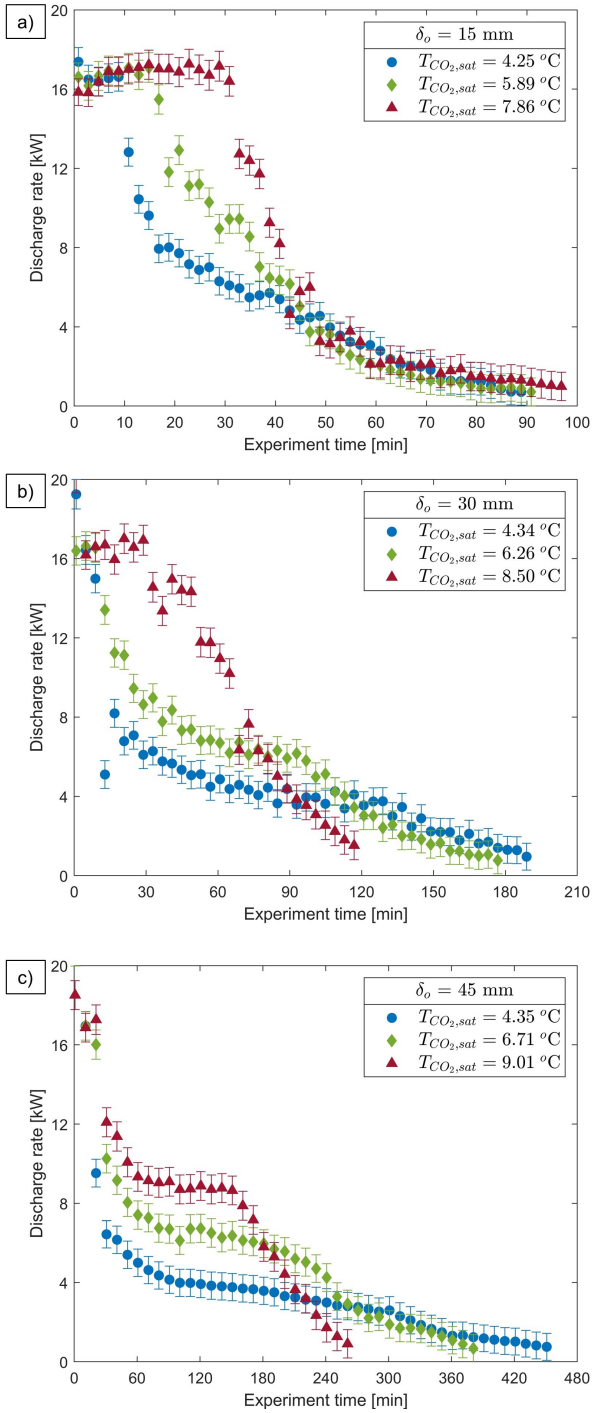

Figure 4.4: Discharging rate of the CTES unit over the discharging cycle using a refrigerant mass flow rate of 7 kg/min for various refrigerant condensation temperatures for a plate-to-plate pitch of a) 15 mm b) 30 mm c) 45 mm.

4.3 Journal paper III: Cold thermal energy storage for industrial CO_2 refrigeration systems using phase change material: An experimental study

In this third publication of the doctoral work, the experience obtained from the experimental testing of the newly designed CTES unit using water/ice as the storage medium is further extended to using a low-temperature PCM suitable for peak shifting in industrial refrigeration systems for cooling and freezing processes. Based on the screening of available commercial PCMs presented in the review paper (see Section 4.1), the organic PCM RT-9HC was selected, purchased and filled into the CTES unit. A thorough material characterisation using established methods was carried out to gain knowledge of the thermophysical properties of the PCM, particularly how the properties are affected by a change in temperature. The characterisation included investigation of the latent heat capacity and phase transition temperature, as well as the thermal conductivity, viscosity and density for various temperatures. An organic PCM was chosen due to not being corrosive to the metal PP-HEX and associated container and having no phase segregation or supercooling issues commonly experienced with inorganic PCMs. Due to the relatively low thermal conductivity of RT-9HC compared to water/ice, a plate pitch of 15 mm and 30 mm was selected for the experimental campaign based on the experience gained from previous experiments.

The first experimental tests for the 15 mm and 30 mm plate pitch configurations were carried out as a parametric study by varying the refrigerant mass flow rate and keeping the other parameters constant. The outcome of these test series was to determine the most appropriate refrigerant flow rate for the charging and discharging cycles. For the charging process, it was found that a refrigerant mass flow rate of 8 kg/min was required for uniform solidification of the PCM on the PP surface. For the discharging process, it was found that 5 kg/min and 7 kg/min provided the highest discharged energy over the cycle for the 15 mm and 30 mm PP configurations, respectively. The following charging test series were carried out by varying the refrigerant evaporation temperature from -12 °C to -23 °C, while the refrigerant mass flow rate was kept constant according to the findings in the first test series. Figure 4.5a shows the impact on charging time for both the 15 mm and 30 mm PP configurations. It was demonstrated that the charging time was reduced by 40-45 % when the refrigerant evaporation temperature was reduced from -13 °C to about -15.5 °C. It was also shown that the corresponding mean pressure drop through the PP-HEX unit over the charging cycle was nearly linearly increasing with a reduction in refrigerant evaporation temperature (see Figure 4.5b). The increase in pressure drop across the PP-HEX unit was most likely caused by an increased vapour fraction inside the PP channels with increasing heat transfer due

to the increasing temperature difference between the refrigerant and PCM. The increase in vapour fraction results in a higher mean velocity in the PP channel, resulting in higher pressure loss.

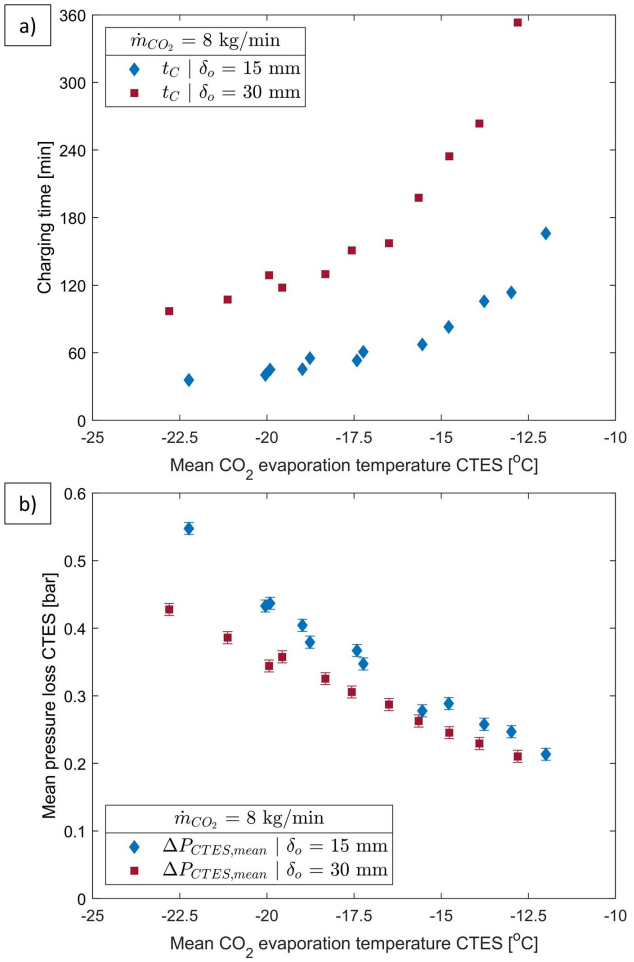

Figure 4.5: The effect of refrigerant evaporation temperature for the 15 mm and 30 mm configuration using a refrigerant mass flow rate of 8 kg/min on a) the charging time b) mean pressure loss.

The test series for the discharging process were carried out following a similar method as for the charging process. The mean refrigerant condensation temperature changed from about -6.4 °C to 3.7 °C. The results for the 30 mm PP configuration are presented in Figure 4.6. It can be observed that the mean discharge rate over the discharging cycle increases linearly with increasing refrigerant condensation, keeping in mind that the discharge rate is highly transient also when using

the PCM as the storage medium. The total discharged energy over the cycle also increases with elevated refrigerant condensation temperature for the temperature range considered in this study. A notable increase in the discharged energy over the cycle is evident when increasing the condensation temperature from about -6.5 °C to -4.5 °C. Based on this observation, -4.5 °C was identified as the lower practical limit of the temperature difference between the PCM and refrigerant to sustain the discharging cycle effectively. Below this limit, significant solid PCM was remaining in the CTES unit. Overall, the experimental research presented in this paper proved the feasibility of using an organic PCM in bulk as the storage medium for a PP-HEX CTES unit without experiencing any significant supercooling issues, segregation or deterioration of the PCM. Using a sub-zero PCM in the CTES unit expands the application area of the presented technology to industrial refrigeration plants. One example is the food processing industry, a sector that often experiences high peaks in refrigeration demand due to the nature of the batch processes.

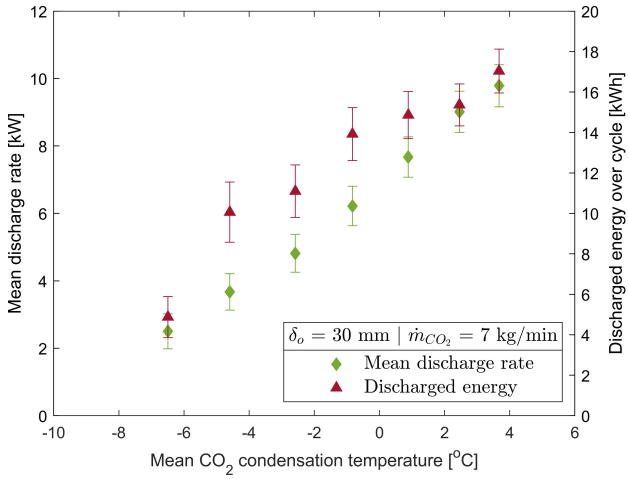

Figure 4.6: Mean discharging rate and discharged energy as a function of the refrigerant condensation temperature using a refrigerant mass flow rate of $\dot{m}_{CO_2} = 7$ kg/min and plate pitch $\delta_o = 30$ mm.

5 Discussion

This chapter discusses the most important results presented in Chapter 4 and the implications for the topic of CTES technology in the academic context and the refrigeration sector.

Choosing the appropriate storage medium is very important when designing a CTES system for refrigeration systems. The overall performance and compactness of the CTES system depend greatly on the properties of the selected storage medium. In the present doctoral work, two storage media were tested in the novel CTES. Experiments using water/ice were carried out to present the proof of concept using a storage medium with well-documented thermophysical properties. Furthermore, the melting temperature of water/ice fits well with the temperature requirement of numerous refrigeration applications such as space cooling and process cooling. To further test the relevance of the novel CTES unit for industrial refrigeration processes, a low-temperature storage medium was selected based on screening of commercially available PCM presented in the Journal paper 1 [13]. With a melting temperature of -9.6 °C, the selected PCM RT-9HC would be relevant for CTES purposes in low-temperature refrigeration systems, such as food processing plants with refrigeration demands for freezing and cooling. The summary and comparison of the most important thermophysical properties of water/ice and PCM RT-9HC are presented in Table 5.1. It can be observed that the volumetric storage capacity of RT-9HC is considerably lower (41.8 %) compared to water/ice, primarily due to the lower latent heat capacity of the PCM (39.2%, also see 2.8).

The drawback of using RT-9HC as the PCM compared to water is that it directly results in a less compact CTES system for the same storage capacity requirement when installed at an industrial site. Water/ice can, in many instances, be considered the benchmark for other PCMs for CTES applications due to its relatively

Table 5.1: Summary and comparison of important thermophysical properties of selected storage media for testing in the novel CTES unit. Water and ice properties are given at 20 °C and -10 °C, respectively.

Property	**Water/ice**	**PCM RT-9HC**
Melting temperature [°C]	0	-9.6
Latent heat capacity [kJ/kg]	333.6	202.6
Thermal conductivity liquid [W/(m K)]	0.598	0.175
Thermal conductivity solid [W/(m K)]	2.30	0.309
Density liquid [kg/m^3]	998.2	764.8
Density solid [kg/m^3]	918.9	880
Volumetric storage capacity [kWh/m^3]	85.15	49.52

high latent heat capacity, specific heat and thermal conductivity. However, for applications that require thermal energy storage at lower temperatures than 0 °C, other PCMs must be investigated.

The alternatives of PCM for CTES applications are dominated by the inorganic type, where the majority are mixtures of various concentrations of salts and water. A few examples of organic PCMs are commercially available in the temperature range below 0 °C. The organic PCMs in this temperature range are mostly petroleum-derived paraffins [62]. Using these PCMs increases our dependency on fossil resources, like crude oil. There should be a considerable focus on identifying more sustainable PCMs in both the academic and industrial segments. Some manufacturers advertise their products as bio-based organic PCMs, where most are non-paraffins derived from agricultural food sources, such as palm oil or coconut oil. With a growing world population, it is questionable to use food-grade resources to produce PCMs. Furthermore, palm oil production has been closely linked to deforestation and the resulting loss in biodiversity in tropical regions [63]. Researchers, designers, and system owners should carefully consider these aspects to evaluate the sustainability of CTES technology with organic PCM. Studies on the environmental impact and economic performance of applying PCM are still scarce [64], and a performing life cycle assessment of PCM would greatly support decision-makers and designers in selecting the most sustainable option.

Some batch-dominant refrigeration systems require evaporation temperatures below -40 degrees C, which is commonly found in the food processing industry. One example is tunnel freezers for deep freezing of food products, such as fish, seafood, meat and vegetables. Introducing CTES technology to these refrigeration plants could significantly mitigate the high peak power consumption of these batch processes. To implement CTES technology directly into these applications, a PCM with storage below -40 °C would be required. There are few studies conducted

in this temperature range, and the availability of PCMs is relatively limited [13]. Almost all available commercial PCMs in this temperature range are eutectic (salt hydrate/water) mixtures, which commonly suffer from supercooling, incongruent melting, phase segregation and being more corrosive to metals commonly used in heat exchangers [16]. Hence, it is a lack of PCMs suitable for use in this important temperature range. Therefore, it is necessary to investigate alternative technology to exploit the advantage of CTES in these applications.

CO_2 as a solid-liquid storage medium is an alternative proposed in the past, which seems to present considerable potential [65, 66]. The concept involves cycling the CO_2 between the saturated solid state (dry ice) and the saturated liquid state at a pressure level above the triple point pressure of 5.18 bar (-56.6 °C). Hence, CTES can be achieved at temperatures below -40 °C. The CO_2 needs to be cycled above the triple point pressure due to the sublimation process occurring at lower pressure. Sublimation is when the solid phase transitions directly to the vapour phase when the CO_2 absorbs heat. It is preferred to avoid this region due to the large difference in volume between the solid and vapour phases and instead let the CO_2 transition like other PCMs between the solid and liquid phases. Several benefits can be identified by using CO_2 as a storage medium. First, vast experience in research and applying CO_2 as a refrigerant exists in the academic community and the refrigeration industry [67]. Second, CO_2 has several advantageous characteristics: a relatively high latent heat capacity, high density, no ODP, low GWP, no toxicity or flammability issues, and it is readily available. Although using CO_2 as a solid-liquid storage medium has been proposed in the past for capacity enhancements of refrigeration systems, it is currently limited to theoretical concepts with a profound need for experimental validation.

The CTES unit designed and tested in the present work is defined as a lab-scale unit with a design capacity and size that could fit within a laboratory environment. During the design phase, it was important to size the PP-HEX and CTES unit sufficiently large so that its performance per unit area would be representable when scaling up to an industrial size suitable for integration into a refrigeration system in the field. As such, the performance and results from the experimental campaign can be utilised with higher confidence to predict the performance of an industrial-sized CTES unit following the same design principle. According to the manufacturer of the PPs, a maximum PP size of 3 m x 1.5 m can be produced with the current production equipment. That would increase the heat transfer area per PP by about four times compared to the current lab-scale design. The main production cost of PPs has been identified as the inflation process and welding of inlet/outlet pipes to the PPs. The laser welding process for the welding spots and seam welds is automated, and the PP size should be maximised to reduce the overall production costs. For practical considerations, the total width of the CTES

unit should be limited to fit standard transport options. For road transport, this would be about 2.3 m, resulting in an overall CTES unit size of 3.1 m x 1.6 m x 2.3 m when considering some 50 mm clearance around the PPs. In this way, a standardised minimum size unit can be defined. Depending on the requirement of the refrigeration plant, several CTES units can be installed in parallel to increase the overall storage capacity or the discharge rate of the CTES system.

The flow pass arrangement is a remaining question regarding scaling the unit to an industrial size. Since the flow length increases, the pressure drop is expected to increase for the same flow conditions in the PP channels. In an industrial-size CTES unit, it would be practical to have both the inlet and outlet pipes of the PP-HEX at the same end of the CTES unit. This arrangement would be more practical for connecting several CTES units to a common refrigerant distribution header for the supply and return line to the refrigeration plant. However, it is unclear whether most of the pressure loss measured in the lab scale unit occurs in the manifold, when the refrigerant flow turns around at the end of the flow pass or in the free-flowing length of the PP channel. Hence, a separate test section should be established for testing various flow pass arrangements, such as four or six passes, and the impact on the pressure loss. CO_2 as a refrigerant has a very low change in saturation temperature per unit pressure drop, with about 1 kelvin/1 bar pressure drop at 0 °C. The difference between the refrigerant condensing temperature and the melting temperature of the PCM was identified as the most important parameter for heat transfer. Hence, the pressure loss for CO_2 does not affect the driving force for heat transfer during the discharging process to the same extent as other refrigerants. Suppose the CTES concept is extended to using propane as the refrigerant. In that case, the saturation temperature drops about 7.5 kelvin/1 bar pressure loss at 0 °C. Consequently, the driving force for heat transfer during the discharging process across the PP length will be significantly reduced. Furthermore, the COP of the associated refrigeration system will be reduced by about 2-3 % per 1 bar pressure drop during the charging process of the CTES unit. Hence, a more careful evaluation of the impact of PP geometry on pressure loss should be carried out in the future.

The HEX plates used in the CTES unit presented in the current work are constructed of stainless steel. As described in Section 3.1, the choice was made based on material compatibility with common types of PCM and the required structural integrity of the plates used for the high operating pressures of CO_2 refrigeration systems. From the sustainability perspective, steel has significant CO_2 emissions associated with the production process. Over the last years, the direct CO_2 intensity of steel production has been stable at about 1.4 tons of CO_2 per ton of steel produced. According to the IEA, steel production is not on track toward the emission targets Net Zero Scenario by 2050 [68]. The weight of the ten PPs in the

lab-scale CTES unit is around 175 kg, using a sheet metal thickness of 1 mm. As described earlier, a suitable design of an industrial-size CTES unit would be using PPs with a dimension of 3 by 1.5 meters and a total CTES container width of 2.3 meters. These dimensions would allow for standard transport on the road. Such a unit with a vertical plate arrangement would fit approximately 75 PPs inside using a plate pitch of 30 mm, resulting in a total PP weight of about 5.4 tons. Reducing the plate pitch to 15 mm would result in a total PP weight of about 10.8 tons for an equally sized CTES unit. Based on these points, it should be investigated how much the thickness of the metal sheets used for the PPs can be reduced and still be suitable for operating pressures required in CO_2 refrigeration systems.

Aluminium is an interesting alternative to stainless steel in the production of PPs used in the described CTES unit design. Manufacturing PPs from aluminium would significantly reduce the weight of the PP-HEX, as its density is about one-third of stainless steel. The tensile strength of aluminium is lower than for stainless steel, but due to its lower density, the strength-to-weight ratio is higher for aluminium than for stainless steel. Aluminium HEX have been used with great success in the past for CO_2 refrigeration systems, as in mobile air-conditioning systems [69]. However, it needs to be investigated whether the laser welding and the following hydroforming process for PPs are feasible using aluminium metal sheets. A further benefit of aluminium is its high thermal conductivity. Regarding corrosion, aluminium is more resistant to oxidation in the presence of water/moisture compared to stainless steel. However, aluminium can be subject to corrosion in the presence of salts, commonly found in many low-temperature PCMs consisting of salt-water mixtures [38, 13]. Production of aluminium is, similar to steel, very energy-intensive, and there are significant CO_2 emissions associated with the consumption of carbon anodes and electricity use during the electrolysis process. On the other hand, research and field testing of the inert anode technology is ongoing. This method replaces the carbon anodes used in the conventional process with an inert anode, effectively removing CO_2 as a byproduct of the production [70]. Although this technology requires more electricity per ton of product than the currently used method [71], using renewable electricity in the production process enables a significant reduction in the carbon footprint of aluminium products.

6 Conclusions

The main objective of this research work has been to design and develop a novel CTES unit suitable for achieving peak shifting of the refrigeration load in industrial refrigeration systems. This objective involved developing a concept with high storage capacity and heat transfer rates while preserving a compact design. To fulfil the criterion of high storage capacity and compactness, it was decided to employ the latent heat storage principle using PCM. An in-depth investigation of the current state-of-the-art CTES technology applied to refrigeration systems was conducted to fulfil the research objective. A novel concept coupling the evaporation and condensation process of the CO_2 refrigerant with the solidification and melting process of the PCM in the same HEX was proposed. A lab-scale prototype of the CTES unit was developed and tested experimentally in a test facility using two types of PCM. The performance of the CTES unit was tested, and recommendations for the appropriate design for various applications were made. The following general conclusions can be summarised for the present research work.

A thorough investigation into the latest research and innovations on CTES applications with PCM in the refrigeration sector was carried out. It was established that the interest in PCMs in the temperature range relevant for CTES application has been increasing the latest years, and the availability of commercial PCMs has improved. Moreover, it was found that CTES technology with PCM has been applied in many segments of the refrigeration sector. Applications in the literature included food transport and packaging, commercial refrigeration and various other refrigeration systems such as chillers for space cooling and industrial refrigeration plants. For larger CTES systems, it could be distinguished between designs where the CTES unit was connected to the refrigeration by an intermediate heat transfer circuit and designs where the CTES unit was connected directly to the primary refrigerant circuit. The most popular design was found to be the first approach using an intermediate heat transfer circuit due to a more straightforward design

and avoiding a high operating pressure in the CTES unit. However, several novel concepts using the direct integration approach into the primary refrigerant circuit were proposed, although most designs were unsuitable for large-scale applications.

A CTES unit suitable for integration into pump circulated CO_2 refrigeration systems were made based on the plates-in-tank design principle. The CTES unit consists of a stack of welded HEX plates with flow channels for the refrigerant on the inside and are manufactured to withstand the operating pressure of CO_2 refrigeration systems. The PP-HEX is immersed in the storage medium to transfer heat between the refrigerant and the PCM. During the charging process of the CTES unit, the refrigerant evaporates due to heat extraction from the PCM, which solidifies on the PP surface. During the discharging process, the heat transfer direction is reversed so that the refrigerant condenses while the PCM is melting. The lab-scale CTES unit has a flexible design so that the PP-HEX geometry can be varied and the impact on its performance can be investigated. Furthermore, an experimental test facility was designed and constructed to host the novel CTES unit. The test facility can provide a range of refrigerant conditions by varying refrigerant parameters such as evaporation temperature, condensation temperature and flow rates.

The CTES unit was thoroughly tested in the experimental test facility using different PP-HEX geometries, refrigerant parameters and two different PCMs. The first test campaign was carried out using water/ice as the storage medium to provide proof of concept and establish the principle of operation. Based on the list of commercial PCMs established and presented in the technology review, a commercial low-temperature PCM with a melting temperature of -9.6 °C was selected, and its properties were experimentally determined using established methods. An organic PCM was favoured to avoid phase segregation and supercooling issues since the PCM is filled in bulk into the CTES unit. Then, a test campaign was carried out on the CTES unit using the low-temperature PCM as the storage medium. The experimental campaign showed that the evaporation and condensation temperatures of the refrigerant are the most critical parameters influencing the performance of the charging and discharging cycles of the CTES unit, regardless of the PCM applied. Furthermore, it was found that the charging time of the CTES unit was reduced significantly when the refrigerant evaporation temperature was reduced. However, the impact was found to be most important when employing evaporation temperatures close to the phase transition temperature of the PCM. The discharging rate and discharged energy over the cycle were found to increase with higher refrigerant condensing temperature. Furthermore, it was found that the plate pitch influences the discharging characteristics of the CTES unit. A smaller plate pitch resulted in high discharge rates but at the cost of lower thermal storage capacity. This geometry should then be applied to refrigeration systems facing high peaks in

the refrigeration load that last relatively short. Increasing the plate pitch improved the thermal storage capacity, but the discharging cycle length increased, and the average discharge rate was reduced. Hence, this design should be applied to systems with long periods of high refrigeration load by connecting several CTES units in parallel to match the load conditions.

7 Suggestions for further work

This thesis investigates the potential for using CTES technology with PCM in refrigeration systems to achieve peak shifting of the refrigeration demand. Based on the findings of this thesis and the discussions of the results, the recommendations for further research on the topic are presented.

Regarding the design of the CTES unit
The PPs utilised in the present study have a welding pattern of $s_T = 30$ mm and $s_L = 50$ mm, a triangular pattern commonly found in the industry. Furthermore, the refrigerant flow is directed in three passes through the plate length. In future studies, it would be of interest to investigate the impact of other welding patterns and other flow pass configurations on the performance of the CTES unit. In particular, the impact on pressure loss would be of high interest. Furthermore, it would be interesting to investigate the influence on the PP-HEX orientation in the container. In the present study, the PPs are stacked horizontally for practical modification of the plate pitch between test series. An enhancement in natural convection heat transfer is expected for a vertical arrangement due to creating a flow length across the entire PP height for the liquid PCM.

Regarding the experimental setup and test matrix
The current configuration of the experimental setup requires that all the heat provided by the glycol heating circuit is transferred from the CO_2 refrigerant to the PCM in the CTES unit to keep the pressure (and thereby the discharging operating conditions) constant. It would be interesting to rebuild the test facility so that the discharging tests could be operated with a constant refrigerant vapour fraction at the inlet of the CTES. This modification would allow for investigating the performance of the CTES unit in a more relevant industrial scenario, where the CTES unit could be connected to the return line from the evaporators of the refrigeration plant. To evaluate the discharge rate in the modified experimental

setup, an additional separator at the outlet of the CTES unit would be required, as well as two additional mass flow meters to measure the liquid and vapour streams from the separator. Consequently, the remaining refrigerant vapour, which is not condensed in the CTES unit, could be condensed in the CO_2/CO_2 HEX.

Regarding the overall performance of a refrigeration system with CTES
The experimental work carried out in this study focuses separately on the charging and discharging processes of the CTES unit, mapping the characteristics and performance of each cycle. A more holistic approach must be considered in the practical application and for selecting operational parameters of the CTES system. A suggestion for further work is developing a numerical model representing the CTES unit that can be used in a simulation environment such as Dymola/Modelica. The model can be validated with the experimental data from the current study and coupled into a simulation model of a refrigeration plant. Following this approach, the overall response and performance of a refrigeration system integrated with a CTES system can be investigated to find the optimal storage medium, phase change temperature, charging and discharging conditions.

General recommendations for advancing the field of CTES integration into refrigeration systems and market penetration of CTES technology
The current research has advanced the maturity of CTES technology with PCM for refrigeration systems to the level of demonstration in a laboratory environment. To further advance the maturity of the described technology, demonstration of a pilot installation in the field should be the next step. A fully instrumented, industrial-scale CTES unit installed in a suitable environment would provide valuable feedback and operational experience on the benefits of CTES technology. Some aspects need careful attention for this step to be successful and maximise the benefits. First, a control strategy for the CTES unit should be developed. This strategy includes decisions on which signals to use for initiating and ending the charging and discharging cycles, particularly when installing several CTES units in parallel for increased capacity. The control strategies applied to the CTES system can range from simple time-scheduled operation modes to more advanced solutions incorporating predictive control based on electricity price forecasting or a weather forecast. The second option could reduce the payback time and maximise the benefits of CTES technology to a much larger extent. Second, an optimal selection of PP-HEX geometry, size and material would reduce the cost of the CTES unit. As discussed in Chapter 5, it is recommended to investigate the possibility of using aluminium for the PP-HEX to reduce weight and evaluate any performance benefits and reduction in cost.

References

[1] International Energy Agency, IEA. *World Energy Outlook 2021*. 2021.

[2] Wencong Su, Habiballah Eichi, Wente Zeng, and Mo-Yuen Chow. "A survey on the electrification of transportation in a smart grid environment". In: *IEEE Transactions on Industrial Informatics* 8.1 (2011), pp. 1–10.

[3] Stefan Lechtenböhmer, Lars J Nilsson, Max Åhman, and Clemens Schneider. "Decarbonising the energy intensive basic materials industry through electrification–Implications for future EU electricity demand". In: *Energy* 115 (2016), pp. 1623–1631.

[4] Maria Taljegard, Lisa Göransson, Mikael Odenberger, and Filip Johnsson. "Impacts of electric vehicles on the electricity generation portfolio–A Scandinavian-German case study". In: *Applied Energy* 235 (2019), pp. 1637–1650.

[5] Eirik Starheim Svendsen, Kristina Norne Widell, Guro Møen Tveit, Tom Ståle Nordtvedt, Solveig Uglem, Inger Standal, and Kirsti Greiff. "Industrial methods of freezing, thawing and subsequent chilled storage of whitefish". In: *Journal of Food Engineering* 315 (2022), p. 110803.

[6] SJ James and CJFRI James. "The food cold-chain and climate change". In: *Food Research International* 43.7 (2010), pp. 1944–1956.

[7] Kian Jon Chua, Siaw Kiang Chou, WM Yang, and Jinyue Yan. "Achieving better energy-efficient air conditioning–a review of technologies and strategies". In: *Applied Energy* 104 (2013), pp. 87–104.

[8] Alfonso Capozzoli and Giulio Primiceri. "Cooling systems in data centers: state of art and emerging technologies". In: *Energy Procedia* 83 (2015), pp. 484–493.

[9] D Coulomb. “Refrigeration and cold chain serving the global food industry and creating a better future: two key IIR challenges for improved health and environment”. In: *Trends in food science & technology* 19.8 (2008), pp. 413–417.

[10] F Birol. “The future of cooling: opportunities for energy-efficient air conditioning”. In: *International Energy Agency* (2018).

[11] Homi Kharas. “The unprecedented expansion of the global middle class: An update”. In: (2017).

[12] Jenny Gustavson, Christel Cederberg, Ulf Sonesson, Robert Van Otterdijk, and Alexandre Meybeck. “Global food losses and food waste”. In: *Swedish Institute for Food and Biotechnology (SIK), Gothenburg, Sweden* (2011), pp. 1–37.

[13] Håkon Selvnes, Yosr Allouche, Raluca Iolanda Manescu, and Armin Hafner. “Review on cold thermal energy storage applied to refrigeration systems using phase change materials”. In: *Thermal Science and Engineering Progress* 22 (2021), p. 100807.

[14] Ibrahim Dincer and Marc A Rosen. *Thermal energy storage systems and applications*. John Wiley & Sons, 2021.

[15] Harald Mehling and Luisa F Cabeza. “Heat and cold storage with PCM”. In: *Heat and mass transfer* (2008), pp. 11–55.

[16] Gang Li, Yunho Hwang, Reinhard Radermacher, and Ho-Hwan Chun. “Review of cold storage materials for subzero applications”. In: *Energy* 51 (2013), pp. 1–17.

[17] Xinghui Zhang, Qili Shi, Lingai Luo, Yilin Fan, Qian Wang, and Guanguan Jia. “Research Progress on the Phase Change Materials for Cold Thermal Energy Storage”. In: *Energies* 14.24 (2021), p. 8233.

[18] Marcia K McNutt, Monica Bradford, Jeffrey M Drazen, Brooks Hanson, Bob Howard, Kathleen Hall Jamieson, Véronique Kiermer, Emilie Marcus, Barbara Kline Pope, Randy Schekman, et al. “Transparency in authors’ contributions and responsibilities to promote integrity in scientific publication”. In: *Proceedings of the National Academy of Sciences* 115.11 (2018), pp. 2557–2560.

[19] James M Calm. “The next generation of refrigerants–Historical review, considerations, and outlook”. In: *international Journal of Refrigeration* 31.7 (2008), pp. 1123–1133.

[20] Guus JM Velders, Stephen O Andersen, John S Daniel, David W Fahey, and Mack McFarland. “The importance of the Montreal Protocol in protecting climate”. In: *Proceedings of the National Academy of Sciences* 104.12 (2007), pp. 4814–4819.

[21] Armin Hafner and Risto Ciconkov. “Current state and market trends in technologies with natural refrigerants”. In: *9th Conference on Ammonia and CO2 Refrigeration Technologies Ohrid, R. Macedonia September 16-17, 2021 Proceedings*. International Institute of Refrigeration. 2021.

[22] Gustav Lorentzen. “Revival of carbon dioxide as a refrigerant”. In: *International journal of refrigeration* 17.5 (1994), pp. 292–301.

[23] Ilana Koegelenberg. “World Guide to Transcritical CO2 Refrigeration”. In: *sheccoBase* (2020).

[24] Marcel Ulrich Ahrens, Sverre Stefanussen Foslie, Ole Marius Moen, Michael Bantle, and Trygve Magne Eikevik. “Integrated high temperature heat pumps and thermal storage tanks for combined heating and cooling in the industry”. In: *Applied Thermal Engineering* 189 (2021), p. 116731.

[25] Zahid Ayub. “World’s largest ammonia heat pump (14 MWh) for district heating in Norway—a case study”. In: *Heat Transfer Engineering* 37.3-4 (2016), pp. 382–386.

[26] Andy Pearson. “Refrigeration with ammonia”. In: *International journal of refrigeration* 31.4 (2008), pp. 545–551.

[27] O Bamigbetan, Trygve Magne Eikevik, Petter Nekså, Michael Bantle, and Christian Schlemminger. “The development of a hydrocarbon high temperature heat pump for waste heat recovery”. In: *Energy* 173 (2019), pp. 1141–1153.

[28] Christian Schlemminger, Eirik Starheim Svendsen, Sverre Stefanussen Foslie, Michael Bantle, Opeyemi Olayinka Bamigbetan, and Petter Nekså. “Performance of high temperature heat pump for simultaneous and efficient production of ice water and process heat”. In: *Proceedings of the 25th IIR International Congress of Refrigeration. Montréal, Canada, August 24-30, 2019*. IIR. 2019.

[29] Dennis Jankovich and Krešimir Osman. “A feasibility analysis of replacing the standard ammonia refrigeration device with the cascade NH3/CO2 refrigeration device in the food industry”. In: *Thermal Science* 19.5 (2015), pp. 1821–1833.

[30] HM Getu and PK Bansal. “Thermodynamic analysis of an R744–R717 cascade refrigeration system”. In: *International journal of refrigeration* 31.1 (2008), pp. 45–54.

[31] J Alberto Dopazo, José Fernández-Seara, Jaime Sieres, and Francisco J Uhıa. “Theoretical analysis of a CO2–NH3 cascade refrigeration system for cooling applications at low temperatures”. In: *Applied thermal engineering* 29.8-9 (2009), pp. 1577–1583.

[32] J Alberto Dopazo and José Fernández-Seara. “Experimental evaluation of a cascade refrigeration system prototype with CO2 and NH3 for freezing process applications”. In: *International journal of refrigeration* 34.1 (2011), pp. 257–267.

[33] Antonio Messineo. “R744-R717 cascade refrigeration system: performance evaluation compared with a HFC two-stage system”. In: *Energy Procedia* 14 (2012), pp. 56–65.

[34] Mehdi Aminyavari, Behzad Najafi, Ali Shirazi, and Fabio Rinaldi. “Exergetic, economic and environmental (3E) analyses, and multi-objective optimization of a CO2/NH3 cascade refrigeration system”. In: *Applied Thermal Engineering* 65.1-2 (2014), pp. 42–50.

[35] Santosh Kumar Saini, Mani Sankar Dasgupta, Kristina N Widell, and Souvik Bhattacharyya. “Comparative analysis of a few novel multi-evaporator CO2-NH3 cascade refrigeration system for seafood processing & storage”. In: *International Journal of Refrigeration* 131 (2021), pp. 817–825.

[36] Fenil Desai, Jenne Sunku Prasad, P Muthukumar, and Muhammad Mustafizur Rahman. “Thermochemical energy storage system for cooling and process heating applications: A review”. In: *Energy Conversion and Management* 229 (2021), p. 113617.

[37] Eduard Oró, Laia Miró, Camila Barreneche, Ingrid Martorell, Mohammed M Farid, and Luisa F Cabeza. “Corrosion of metal and polymer containers for use in PCM cold storage”. In: *Applied energy* 109 (2013), pp. 449–453.

[38] Pere Moreno, Laia Miró, Aran Solé, Camila Barreneche, Cristian Solé, Ingrid Martorell, and Luisa F Cabeza. “Corrosion of metal and metal alloy containers in contact with phase change materials (PCM) for potential heating and cooling applications”. In: *Applied Energy* 125 (2014), pp. 238–245.

[39] A López-Navarro, J Biosca-Taronger, JM Corberán, C Peñalosa, A Lázaro, P Dolado, and J Payá. “Performance characterization of a PCM storage tank”. In: *Applied Energy* 119 (2014), pp. 151–162.

[40] Rekstad, H. and Eikevik, T., and Jensen, S. “Dimple plate heat exchangers for a sea-water chiller using CO2 as refrigerant, design and testing”. In: *24th IIR International Congress of Refrigeration Proceedings* (2015).

[41] Mahmood Mastani Joybari, Håkon Selvnes, Alexis Sevault, and Armin Hafner. “Potentials and challenges for pillow-plate heat exchangers: State-of-the-art review”. In: *Applied Thermal Engineering* (2022), p. 118739.

[42] HERMETIC Pumpen GmbH. *HERMETIC refrigeration pumps*. 2021. URL: https://kaelte.hermetic-pumpen.com/en/pump-types.

[43] Jeffrey Kodosky. “LabVIEW”. In: *Proceedings of the ACM on Programming Languages* 4.HOPL (2020), pp. 1–54.

[44] DOW Chemical Company. *DOWCAL 100 Heat Transfer Fluid Technical Data Sheet*. 2021. URL: https://www.dow.com/en-us/document-viewer.html?ramdomVar=5550034686195609151&docPath=/content/dam/dcc/documents/en-us/productdatasheet/180/180-01588-01-dowcal-100-heat-transfer-fluid-tds.pdf.

[45] DOW Chemical Company. *DOWCAL 200 Heat Transfer Fluid Technical Data Sheet*. 2021. URL: https://www.dow.com/en-us/document-viewer.html?ramdomVar=2372344082032526391&docPath=/content/dam/dcc/documents/en-us/productdatasheet/180/180-01589-01-dowcal-200-heat-transfer-fluid-tds.pdf.

[46] EW. Lemmon, IH Bell, ML Huberm, and MO McLinden. *NIST Standard Reference Database 23: Reference Fluid Thermodynamic and Transport Properties-REFPROP, Version 10.0, National Institute of Standards and Technology*. 2018. URL: https://www.nist.gov/srd/refprop.

[47] IEC ISO and BIPM OIML. “Guide to the Expression of Uncertainty in Measurement”. In: *Geneva, Switzerland* 122 (1995), pp. 16–17.

[48] Håkon Selvnes, Yosr Allouche, Armin Hafner, Christian Schlemminger, and Ignat Tolstorebrov. “Cold thermal energy storage for industrial CO2 refrigeration systems using phase change material: An experimental study”. In: *Applied Thermal Engineering* 212 (2022), p. 118543.

[49] Rubitherm Technologies GmbH. *Data sheet RT-9HC*. 2020. URL: https://www.rubitherm.eu/media/products/datasheets/Techdata_-RT-9HC_EN_29092020.PDF.

[50] German Institute for quality assurance and certification. *Phase change materials, Quality Assurance RAL-GZ 896*. 2018. URL: https://www.pcm-ral.org/pdf/RAL_GZ_896_Phase_Change_Material_Edition_March_2018.pdf.

[51] Günther Höhne, JL McNaughton, Wolfgang Hemminger, H-J Flammersheim, and H-J Flammersheim. *Differential scanning calorimetry*. Springer Science & Business Media, 2003.

[52] R Danley, T Kelly, and J Groh. "Improved DSC performance using Tzero technology". In: *International laboratory* (2001), pp. 30–31.

[53] Camila Barreneche, Aran Solé, Laia Miró, Ingrid Martorell, A Inès Fernández, and Luisa F Cabeza. "Study on differential scanning calorimetry analysis with two operation modes and organic and inorganic phase change material (PCM)". In: *Thermochimica Acta* 553 (2013), pp. 23–26.

[54] Stefan Gschwander, Thomas Haussmann, Georg Hagelstein, Camila Barreneche, G Ferrer, L Cabeza, G Diarce, W Hohenauer, D Lager, Christoph Rathgeber, et al. "Standardization of PCM characterization via DSC". In: *Proceedings of SHC 2015 International Conference on Solar Heating and Cooling for Buildings and Industry*. 2015, pp. 2–4.

[55] Guohui Feng, Kailiang Huang, Hailun Xie, Huixing Li, Xin Liu, Shibo Liu, and Chihong Cao. "DSC test error of phase change material (PCM) and its influence on the simulation of the PCM floor". In: *Renewable energy* 87 (2016), pp. 1148–1153.

[56] Mona Nazari Sam, Antonio Caggiano, Christoph Mankel, and Eddie Koenders. "A comparative study on the thermal energy storage performance of bio-based and paraffin-based PCMs using DSC procedures". In: *Materials* 13.7 (2020), p. 1705.

[57] K-H Breuer and W Eysel. "The calorimetric calibration of differential scanning calorimetry cells". In: *Thermochimica acta* 57.3 (1982), pp. 317–329.

[58] TA Instruments. *Enthalpy of Melting for Standards*. 2021. URL: `https://www.tainstruments.com/pdf/literature/TN11.pdf`.

[59] Silas E Gustafsson. "Transient plane source techniques for thermal conductivity and thermal diffusivity measurements of solid materials". In: *Review of scientific instruments* 62.3 (1991), pp. 797–804.

[60] John C Dixon. *The shock absorber handbook*. John Wiley & Sons, 2008.

[61] Thermo Scientific. *Haake Mars III rotational rheometer*. 2022. URL: `http://www.rheologysolutions.com/downloads/product%20brochures/Thermo%20Scientific%20HAAKE%20MARS%20III.pdf`.

[62] Otu Okogeri and Vassilis N Stathopoulos. "What about greener phase change materials? A review on biobased phase change materials for thermal energy

storage applications". In: *International Journal of Thermofluids* 10 (2021), p. 100081.

[63] Elıas Cisneros, Krisztina Kis-Katos, and Nunung Nuryartono. "Palm oil and the politics of deforestation in Indonesia". In: *Journal of Environmental Economics and Management* 108 (2021), p. 102453.

[64] Elli Kyriaki, Christina Konstantinidou, Effrosyni Giama, and Agis M Papadopoulos. "Life cycle analysis (LCA) and life cycle cost analysis (LCCA) of phase change materials (PCM) for thermal applications: A review". In: *International Journal of Energy Research* 42.9 (2018), pp. 3068–3077.

[65] Armin Hafner, Tom Ståle Nordtvedt, and Ingrid Rumpf. "Energy saving potential in freezing applications by applying cold thermal energy storage with solid carbon dioxide". In: *Procedia Food Science* 1 (2011), pp. 448–454.

[66] Espen Halvorsen Verpe, Ignat Tolstorebrov, Alexis Sevault, Armin Hafner, and Yves Ladam. "Cold thermal energy storage with low-temperature plate freezing of fish on offshore vessels". In: *Proceedings of the 25th IIR International Congress of Refrigeration. Montréal, Canada, August 24-30, 2019*. IIR. 2019.

[67] Paride Gullo, Armin Hafner, and Krzysztof Banasiak. "Transcritical R744 refrigeration systems for supermarket applications: Current status and future perspectives". In: *International Journal of Refrigeration* 93 (2018), pp. 269–310.

[68] IEA. *Iron and Steel*. 2021. URL: `https://www.iea.org/reports/iron-and-steel`.

[69] J Pettersen, A Hafner, G Skaugen, and H Rekstad. "Development of compact heat exchangers for CO2 air-conditioning systems". In: *International journal of refrigeration* 21.3 (1998), pp. 180–193.

[70] Yong He, Ke-chao Zhou, Yan Zhang, Hui-wen Xiong, and Lei Zhang. "Recent progress of inert anodes for carbon-free aluminium electrolysis: a review and outlook". In: *Journal of Materials Chemistry A* (2021).

[71] Asbjørn Solheim. "Inert anodes—the blind alley to environmental friendliness?" In: *TMS Annual Meeting & Exhibition*. Springer. 2018, pp. 1253–1260.

Appendix

Paper I

H. Selvnes, Y. Allouche, R.I. Manescu, A. Hafner (2021). "Review on cold thermal energy storage applied to refrigeration systems using phase change materials" *Thermal Science and Engineering Progress* Volume 22, 100807.
DOI: https://doi.org/10.1016/j.tsep.2020.100807.

New Journal and we have not received input yet 22 (2021) 100807

Contents lists available at ScienceDirect

Thermal Science and Engineering Progress

journal homepage: www.sciencedirect.com/journal/thermal-science-and-engineering-progress

Review on cold thermal energy storage applied to refrigeration systems using phase change materials

Håkon Selvnes *, Yosr Allouche, Raluca Iolanda Manescu, Armin Hafner

Norwegian University of Science and Technology, Department of Energy and Process Engineering, Kolbjø rn Hejes vei 1B, NO-7491 Trondheim, Norway

ARTICLE INFO

Keywords:
Cold thermal energy storage
Phase change materials
Refrigeration
Supermarket
Transport
Air conditioning

ABSTRACT

This paper presents a thorough review on the recent developments and latest research studies on cold thermal energy storage (CTES) using phase change materials (PCM) applied to refrigeration systems. The presented study includes a classification of the different types of PCMs applied for air conditioning (AC) systems (20 °C) to low-temperature freezing of food (−60 °C). An overview of the influencing thermophysical properties of PCMs, as well as their respective characterisation methods, are presented. The current available PCMs on the market in the temperature range 10 °C to −65 °C are listed. Finally, research on CTES using PCMs in refrigeration systems are reviewed and grouped into applications for food transport and packaging, commercial refrigeration and various other refrigeration systems. The findings show that using ice/water as PCM for AC applications is the most commonly studied system, due to widespread use of these systems, expected growth in the future and low cost of using water as the PCM. Over the last ten years the published research integrating CTES in different parts of the food cold chain, using water-salt solutions and paraffin PCM in both active and passive methods, has increased. Suggestions for the integration of CTES in supermarkets and industrial applications are also emerging. The technology has received increased interest from the scientific community the last five years, due to the benefits of achieving peak shaving of the refrigeration demand, exploiting low-cost electricity hours and offering backup refrigeration in case of blackouts.

1. Introduction

Climate change is the biggest challenge faced by our society today. The need for a transition towards more sustainable energy sources is immediate. An increased focus on energy efficiency in transport, industry, and the building sector is observed as they are characterized by high energy consumption and emissions [1]. Energy efficiency has the potential to account for 44% of the required reduction of CO_2 emissions in 2040, which is a level consistent with the two-degree scenario set by the Paris Agreement [1]. Decarbonisation of industry and transport is another important measure to reduce CO_2 emissions and is contributing to an increase in the demand for electricity [2,3]. The demand pattern is characterized by peaks and valleys, which is challenging to the electrical grid. The demand profile is becoming more and more pronounced. Indeed, air conditioning (AC) for residential and commercial buildings is expected to have a significant impact on the peak power use towards 2050 [4]. The International Energy Agency predicts that AC will contribute with a share of 40% of the total peak power demand in hot climates such as India and certain parts of South-East Asia in 2050. Peak shaving is one of the key features of thermal energy storage (TES), working from a diurnal to a seasonal timescale [5]. An overview of the potential load reductions, energy savings and reduction in CO_2 emissions using TES technology in Spain, Germany and the European context was presented by Arce et al. [6]. Focusing on a realistic implementation rate in the industrial and building sector the potential thermal load reduction was found to be 8% and 9% in Germany and Spain, respectively. The study also estimates potential energy savings of 7.5% and a reduction in CO_2 emissions of 7.5% in the European Union. This demonstrates the importance of integrating TES in the design of thermal energy systems energy system.

Latent heat storage (LHS) is characterized by a high volumetric thermal energy storage capacity compared to sensible heat storage (SHS). The use of LHS is found to be more competitive and attractive in many applications due to the reduction in the required storage volume [7,8]. The use of LHS is advantageous in applications where the high volume and weight can limit the energy efficiency, such as in transport applications. A considerable part of the research on applications of phase change material (PCM) has been focused around integrating PCMs in building applications. PCMs can be integrated into building materials,

* Corresponding author.
E-mail address: hakon.selvnes@ntnu.no (H. Selvnes).

https://doi.org/10.1016/j.tsep.2020.100807

Available online 26 December 2020

Nomenclature

AC	Air-Conditioning
TES	Thermal Energy Storage
CTES	Cold thermal energy storage
PCM	Phase change material
MPCM	Micro-encapsulated phase change material
HEX	Heat exchanger
HTF	Heat transfer fluid
HVAC	Heating, ventilation, and air conditioning
DSC	Differential Scanning Calorimetry
LHS	Latent heat storage
SHS	Sensible heat storage
COP	Coefficient of performance
MT	Medium temperature

such as concrete or gypsum boards, to reduce heat transfer to/from the inside of the building. Integrating PCMs into building envelopes is an application of TES where the process of storing and releasing energy is not actively controlled but occurs as a consequence of a change in the ambient temperature. This technique is applied both in hot and cold climates. An extensive review of the integration of PCM in building materials since 1980 can be found in [9]. An overview of PCMs suitable for cooling and heating of buildings is presented by Cabeza et al. [10]. The reviews by Baetens et al. [11] and Zhou et al. [12] give an overview of the suitable PCMs and various methods for implementation of PCM in building materials. The performance enhancement in buildings using PCMs considering the implementation of both active and passive methods was presented by [13]. Based on the reviewed literature from 2004 to 2017, the authors stated that more research has to be conducted on microencapsulated PCMs (MPCMs), heat transfer enhancement techniques and implementation of alternative control strategies of heating, ventilation and, air conditioning (HVAC) equipment after integrating PCMs.

The focus of the present review is on latent TES systems using PCM for the temperature range covering AC applications (20 °C) to low-temperature freezing of food (−60 °C). For these applications, the integrated TES units are commonly referred to as cold thermal energy storage (CTES) systems. CTES using PCM has gained attention both scientifically and commercially over the last two decades, but a widespread implementation in refrigeration is still lacking. The use of PCM TES is more common in high-temperature applications, such as solar process heating [14] and concentrated solar thermal power plants [15] when compared to low-temperature applications. This is probably because of the high initial costs of the low-temperature integrated system and the challenging system design, such as for transport application. Over the last decade, intensive research was carried out on the identification of the appropriate PCMs for refrigeration applications. Several reviews on PCMs specifically for low-temperature applications were performed over this period [16–18]. The study performed by Oró et al. [16] includes a comprehensive list of commercially available PCMs in 2012 with phase change temperature from 20 °C to −50 °C.

For the past twenty years, CTES technology has received increased attention as a way to cope with high peaks in refrigeration demands in various applications. CTES provides attractive solutions to reduce the required installed capacity of the refrigeration equipment and offers a backup solution in case of system failure. The identification of a peak/off-peak demand structure is one of the most important requirements to make a successful CTES implementation in a refrigeration system [5]. To date, most of the published work on CTES focused on small-scale applications, such as domestic refrigeration [18,19] and domestic heat pump/AC systems [20]. Systems involving large-scale CTES are less studied, especially for commercial and industrial refrigeration. This might be due to the space inconvenience and the requirements for high capacity infrastructure when conducting experimental characterisation on larger systems in the laboratory. Another reason might be the high generated costs and lack of full-scale installations fitted with measurement equipment for detailed performance monitoring. First, this review paper gives an overview of the different types of PCMs, the important thermophysical properties for PCMs, and the most commonly used material characterisation techniques reported up to this date. Then, a thorough and complete overview of CTES systems applied to food transport and packaging, supermarkets, commercial refrigeration systems and various refrigeration systems with capacities larger than 5 kW is presented.

2. Phase change materials

2.1. Classification of phase change materials

PCMs are a group of latent TES materials that takes advantage of the solid/liquid phase transition for storing energy. The liquid/gas and solid/gas phase transitions are not preferred due to the technical difficulties in handling the large volume change. PCMs are generally classified into three groups: organic, inorganic, and eutectic materials (please see overview given by Sharma et al. [21]). Organic PCMs can be further classified into paraffin and non-paraffin compounds. Paraffins are chains of hydrocarbon molecules of different length, while non-paraffins covers the other organics substances that can be used as PCMs e.g. sugars alcohols and fatty acids [7,16]. The inorganic PCMs can be divided into salt hydrates and metallics. The eutectics include any compound created by a combination of organic and/or inorganic PCMs. The two most frequently studied groups of PCMs for subzero applications are eutectic water-salt solutions and paraffins. In this range, paraffins have an available operating range down to −53.5 °C. Sugar alcohols and fatty acids have melting points above 0 °C. Eutectic water-salt solutions are available down to −62 °C, but some commercial products have melting points as low as −114 °C [17]. Li et al. [17] presented a thorough overview of the latent heat of fusion and phase change temperature of PCMs in the temperature range from 0 °C to −120 °C. The reader is directed to Sharma et al. [21] for a detailed description of the chemical composition of the three groups of PCMs.

Table 1 gives an overview of the important properties of the most commonly used types of PCMs for CTES in the temperature range from 0 °C to −62 °C. Generally, the inorganic PCMs have higher thermal conductivity and larger heat storage capacity than the organic PCMs. But their main drawbacks are that they suffer from a high degree of supercooling and phase segregation when compared to organic PCMs. On the other hand, the organic PCMs have low supercooling due to self-nucleating properties, no phase segregation and a congruent phase change. However, the main challenge of organic PCMs is the low

Table 1
Comparison of the thermophysical properties of some groups of PCMs for CTES in the subzero temperature range [26,27,21,17].

Property	Organics		Inorganics	
	Paraffins/ Paraffin mixtures	Alkanones	Eutectic water-salt solution	Alcohol solutions (70–100 wt% H_2O)
Phase change temperature [°C]	−0.5 to −53.5	−3.8 to −55.4	−1.6 to −62	0 to −20
Heat of fusion [kJ kg^{-1}]	110 to 216.2	134.5 to 190.4	116.84 to 314.1	250 to 334
Phase segregation	Low	Low	High	Low
Supercooling	Low	Low	High	High
Flammability	Yes	Yes	No	No

thermal conductivity and flammability [12]. The eutectic PCMs generally have high storage capacity, but the access to data about their thermophysical properties is generally limited [22–25].

2.2. Properties and characterization methods of PCMs

This section summarizes the most important selection criteria for PCMs based on thermophysical properties relevant to refrigeration applications. The reader is guided to the recommended characterisation techniques for each property. The different enhancement strategies to tackle the most significant drawbacks of the PCMs are discussed. Table 2 gives an overview of the important selection criteria classified into thermal, physical, kinetic, chemical, economic and environmental aspects that need to be considered when selecting a PCM [5,7,21]. These characteristics should be carefully addressed when selecting a PCM for a particular application.

2.2.1. Latent and specific heat capacities

A high latent heat capacity and a suitable phase change temperature of the PCM are the first selection criteria to satisfy when selecting a PCM [28,7,17]. The most common way of measuring the latent heat capacity and specific heat capacity of PCMs is the Differential Scanning Calorimetry (DSC) technique [29]. For latent heat capacity measurements, the two recommended methods applied to PCMs are the dynamic method and the step method. The dynamic method involves heating/cooling the sample at a constant rate, e.g. increasing/decreasing the temperature by 0.5, 1 or 5 K min^{-1}. In the step method, the heating or cooling is not continuous. The sample is heated in short periods, followed by periods of constant temperature to allow the sample to reach thermal equilibrium at each step. A varying heating/cooling rate is often utilised, with slower ramping of temperature around the phase change temperature. For a detailed description of both methods applied for PCMs, the reader is directed to Castellón et al [30] and Barreneche et al. [31]. Both methods show comparable results for melting temperatures for salt hydrate and paraffin PCMs. However, considerable deviations between the two methods have been found for melting enthalpies of paraffin PCMs [31]. Generally, the dynamic method is preferred over the step method because the analytical procedure is time-saving when analyzing the DSC curves [31]. When using a DSC for the PCM characterization, a low heating/cooling rate is preferred. Scanning rates of 1 K min^{-1} or lower is recommended to be applied after each thermal equilibrium in the sample to achieve good accuracy and repeatability of the results [32–34].

The specific heat capacity of the PCM is identified for both liquid and solid phases using one of the three available operation modes using the DSC technique: dynamic, isostep and areas method. In the dynamic method the sample is heated with a constant heating rate, but normally with higher heating rates than for latent heat capacity measurements (10 to 20 K min^{-1}). The isostep method consists of many short segments of dynamic stages from the starting temperature to the final temperature. Before and after each dynamic step, there are isothermal segments to stabilise the temperature within the sample. The heating rate during the dynamic step is normally low (1–2 K min^{-1}). The areas method consists of isothermal segments without any dynamic heating stages between each step. The temperature is increased rapidly by 1 K between each isotherm. A thorough description of all three methods can be found in Ferrer et al. [35]. The areas method was proven to give the most accurate results (maximum 3% error to tabulated values) for three common sensible TES materials (water, rock and potassium nitrate) [35].

Table 2
Selection criteria for PCM [5,7,21].

Category	Property
Thermal	Suitable phase change temperature; High latent heat capacity; Good heat transfer characteristics
Physical	Favorable phase equilibrium; High density; Small volume change; Low vapour pressure
Kinetic	No supercooling; Sufficient crystallisation rate
Chemical	Long term stability; Compatibility of PCM with other materials; No toxicity; No flammability concerns
Economic and environmental	Abundant; Available; Cost-effective; Good recyclability

2.2.2. Thermal conductivity

The thermal conductivity characterisation of PCMs is necessary to evaluate the heat transfer and properly design the heat exchanger (HEX) of the CTES system for increased performance. PCMs, and mainly the organic ones, suffer from low conductivity. A high thermal conductivity results in a higher heat transfer rate of the storage unit [29]. Three common methods are generally used to determine the thermal conductivity of PCMs: The laser flash, transient hot wire and transient hot disk technique [36]. The selection of the appropriate experimental method depends on the state of the material and its physical properties, such as viscosity. The reader is directed to Table 3 representing the appropriate methods to characterise different groups of PCMs. The laser flash method is a direct, non-steady-state technique which is well described by Parker et al. [37] and dos Santos et al. [38]. In this method, the specimen is disc-shaped and its front face is exposed to a uniform heat pulse of short duration. The temperature rise on the rear face is then recorded. The hot wire technique involves measurement of the temperature rise of a thin metal wire when a step voltage is applied to it. The wire is either immersed or embedded in the sample to be measured. A detailed description of the hot wire method can be found in [39] and [40]. The hot disc method uses a flat sensor consisting of a thin metal spiral that is put between two halves of a disc-shaped sample. Electrical current is passed through the spiral, increasing its temperature. By recording the temperature response in the sensor over a given time, the thermal conductivity can be calculated. For details on the hot disk method, the reader is directed to the work by Gustafsson [41]. Favourable features of the hot disk method are the possibility to measure powders of varying particle size, heterogeneous samples and highly conducting materials [42]. However, the equipment is more expensive than for the hot wire method [43].

2.3. Main PCM limitations

Some PCMs, especially inorganic salt hydrate PCMs, experience phase segregation/separation. The phase separation of the PCM results in two or more phases that can be observed in the TES unit after a melting - solidification process [55]. Semi-congruent or in-congruent melting occurs when the phase with the higher density sinks to the

Table 3
Recommended method for thermal conductivity measurement of different materials, including some examples references from the literature.

Method	Application domain	Examples of characterised materials	References
Laser flash	Solids	Erythirol	[44]
	Composites	Paraffin w/nanoparticle	[45]
Hot wire	Solids	Various paraffins	[46]
	Composites	Paraffin w/graphite	[47]
	Liquids	Various paraffins	[46]
	Slurries	MPCM suspension	[8]
	Granular solids	Construction sand	[48]
Hot disk	Solids	Ice	[49]
	Composites	Paraffin and nano-graphite	[50]
		Paraffin and expanded graphite	[51]
		Fatty acid w/ fibers/clay/ graphite	[52]
	Liquids	Water	[49]
		Ethylene glycol	[53]
		Methanol	[53]
	Powders	Various metal powders	[54]

bottom of the storage, while the phase with the lower density travels to the top [56].

Supercooling is another limiting factor, it refers to the phenomena where the temperature of the PCM is decreased below its solidification temperature and not initiating the nucleation process within the material which enables the phase change [5,7,57]. Supercooling is an undesirable effect that makes practical use of the PCM challenging, as the CTES system is often designed to work within a narrow temperature range. In integrated systems, a solution could be the decrease of the evaporation temperatures in the refrigeration system to initiate the solidification process. However, this may result in a reduced coefficient of performance (COP) of the refrigeration system.

2.4. Enhancement techniques for PCMs

2.4.1. Physical properties enhancements

Different methods are applied to prevent the phase separation including gelling, adding thickening agents or mechanical stirring [7]. Gelling additives, such as cellulose derivatives, will form a three-dimensional matrix inside the PCM that acts as a barrier in the phase separation process [10,56]. Thickening is a technique used to increase the viscosity of the material by adding thickening agents without changing the melting point of the PCM. However, adding thickening agents could result in a significant reduction in the latent heat capacity. The reported reduction in the latent heat capacity is ranging from about 4% [58] up to 20–35% [59]. The reduction in latent heat capacity depends on the amount of thickening material added to the PCM. It is reported that the introduction of small amounts of thickening and nucleating agents (0.5% to 4%) are sufficient to reduce supercooling and prevent phase separation in inorganic salt PCMs while preserving the latent heat capacity [60,61]. According to Farid et al. [55], the thermal conductivity of the PCM might also be reduced when adding thickening agents.

The encapsulation technique of PCM is another reported solution to enhance the properties of the PCMs. It also prevents the PCM from undergoing phase segregation. The PCMs can be macro-encapsulated or micro-encapsulated, depending on the size of the holder. More detailed information about the encapsulation technique and its effect on the thermal performance of PCMs are available in [62]. Macro-encapsulation refers to the process of filling PCM in containers of various geometrical shapes (e.g. spheres, slabs or tubes) and materials (e.g. polymers or metals) [7]. The size of these containers is usually larger than 1 cm [10]. Microencapsulation consists of filling PCM in a small solid shell with a size ranging from 1 μm to 1000 μm, which creates a fine powder of MPCM. The MPCM is often mixed with water or another liquid to create a suspension to be used in CTES systems. The concentration of MPCM in the suspension is typically ranging from 5% to 40% [57]. A low concentration of MPCMs is often preferred where the suspensions are used as a pumpable heat transfer fluid (HTF) due to the increased pressure drop associated with higher MPCM concentration [63]. For more details about the micro-encapsulation techniques and property characterisation of organic PCMs, the reader is directed to Khadiran et al. [64]. A detailed overview of microencapsulation and macroencapsulation techniques for inorganic PCMs is also presented by Milian et al. [65].

Intensive research has also been performed to limit the supercooling effect. Generally, two methods are applied: Active and passive methods. The passive method involves the addition of nucleating agents that has a similar crystal structure as the PCM itself. The nucleating agent acts as initial support for the crystal growth of the PCM once it reaches its solidification temperature. This method was found to be the most efficient and has shown a reduction in the supercooling of PCMs up to 90% using only 1 wt% nucleators [66]. The active methods are procedures to initiate the solidification process of the liquid PCM by applying an external force such as mechanical stirring, high-pressure air injection or ultrasonic waves. Injection of high-pressure air is a technique to agitate the liquid PCM in order to induce the nucleation process, i.e formation of the first stable crystal that can support further crystal growth [67]. Ultrasound irradiation also consists of creating agitation in the liquid PCM to initiate nucleation [68]. Both active and passive strategies are thoroughly described by Beaupere et al. [66].

2.4.2. Thermal properties enhancements

Low thermal conductivity is one of the major barriers for a widespread use of PCMs in TES systems, mainly for the organic PCMs. For this reason, developing new techniques for thermal conductivity enhancement has been attracting researchers over the last decade. The common solution consists of adding highly conductive materials to the PCM to enhance its thermal conductivity. The additive materials are classified into three groups; carbon-based, metal-based and other materials [69,70]. The inserts/additives can further be grouped in 3D (networks/foam), 2D (layered and flake materials), 1D (Fibers, nanotubes) and zero-dimensional (nanoparticles) structures [71]. The addition of carbon-based nanostructures to PCMs is reported to achieve greater enhancement of thermal conductivity compared to metallic-based particles. This is due to the high aspect ratio (length to width ratio) of the carbon nanostructures, creating highly conductive paths within the PCM [72]. It was shown that introducing a mass fraction of various carbon nano-additives from 0.1% to 10% increased the thermal conductivity of paraffin PCM in the range from 5% to 45% [73]. For a more detailed overview on thermal conductivity enhancement of paraffin-based PCMs, the reader is directed to Bose and Amirtham [73]. A recent review published by Wu et al. [71] covered the detailed theory and mechanisms of thermal conductivity, as well as the different types of inserts and additives applied to PCMs. It was concluded that graphite networks, graphene and titanium oxide foam, as well as boron nitride nanoparticles, were the most performant additives for increasing the thermal conductivity of PCMs. Enhancing the thermal performance of a TES unit can be performed by acting on the thermal properties of PCMs or by optimising the HEX geometry of the storage unit, such as adding fins. This second enhancement solution is not covered in this review but is available in [74].

2.5. PCMs on the market

The number of available PCM on the market has been continuously growing over the last years, including new types of PCMs and a substantial increase in the number of suppliers. Table 4 gives a current overview of the commercially available PCM with melting temperature in the range from −65 °C to 10 °C. The PCMs are available in different forms, e.g. in bulk, macro-encapsulated or as a dry micro-encapsulated powder. Because the market is continuously expanding, it is difficult to provide a complete list of the PCMs. To help the reader making the selection of the appropriate PCM for a specific application, an updated list of the available PCMs in the market until the date is given in Table 4. The table provides information on the different existing PCMs, their melting temperature, latent heat capacity, classification and the available suppliers.

3. Applications of PCM

PCM used as an LHS medium has gained a large interest over the years. The current research is focusing on integration into domestic refrigeration, AC applications, refrigerated transport, supermarket refrigeration systems and into large-scale industrial refrigeration systems. Over the past 15 years, investigations on PCM application was mainly dedicated to building applications [11,9,10,12,75,76] and domestic refrigeration [77,18,19]. Therefore, the authors will in this review provide the reader with the latest PCM integration technology applied to refrigerated transport and packaging, supermarket refrigeration and various other refrigeration systems.

Table 4
Commercially available PCMs in the temperature range from −65 °C to 10 °C, sorted by melting temperature. All information taken from the datasheet of the respective manufacturers.

Material	T_m [°C]	Latent heat [kJ/kg]	Type of product	Producer
E-65	−65	240	Inorganic	PCM Products
SP-50	−52 to −48	200	Inorganic	Rubitherm GmbH
E-50	−50	175	Inorganic	PCM Products
PureTemp-37	−37	145	Bio-based organic	PureTemp LCC
E-37	−37	225	Inorganic	PCM Products
E-34	−34	200	Inorganic	PCM Products
ATS-40	−33	300	Inorganic	Axiotherm GmbH
E-32	−32	225	Inorganic	PCM Products
va-Q-accu −32G	−32	243	n.a.	va-Q-tec
PCM-30	−30	150–160	Organic	Microtek Laboratories
HS30N	−30	224	Inorganic	PLUSS Advanced Technologies
E-29	−29	250	Inorganic	PCM Products
SP-30	−29 to −28	250	Inorganic	Rubitherm GmbH
SP-28	−29 to −28	260	Inorganic	Rubitherm GmbH
HS26N	−26	274	Inorganic	PLUSS Advanced Technologies
E-26	−26	265	Inorganic	PCM Products
SP-24	−25 to −23	285	Inorganic	Rubitherm GmbH
HS23N	−23	262	Inorganic	PLUSS Advanced Technologies
E-22	−22	305	Inorganic	PCM Products
CrodaTherm −22	−23	217	n.a	Croda Europe
va-Q-accu −21G	−21	234	n.a.	va-Q-tec
ClimSel C-21	−21	285	Inorganic	Climator AB
PureTemp −21	−21	239	Bio-based organic	PureTemp LLC
E-21	−21	285	Inorganic	PCM Products
ATS-21	−21	320	Inorganic	Axiotherm GmbH
SP-21	−21 to −19	285	Inorganic	Rubitherm GmbH
E-19	−19	300	Inorganic	PCM Products
HS18N	−18	242	Inorganic	PLUSS Advanced Technologies
ClimSel C-18	−18	288	Inorganic	Climator AB
SP-17	−18 to −17	300	Inorganic	Rubitherm GmbH
E-15	−15	320	Inorganic	PCM Products
HS15N	−15	308	Inorganic	PLUSS Advanced Technologies
PureTemp −15	−15	301	Bio-based organic	PureTemp LCC
ATS-12	−12	360	Inorganic	Axiotherm GmbH
E-11	−12	310	Inorganic	PCM Products
SP-11	−12 to −11	240	Inorganic	Rubitherm GmbH
SP-11 UK	−12 to −10	330	Inorganic	Rubitherm GmbH
PCM-10	−10	175–185	Organic	Microtek Laboratories
MPCM-10	−10	170–180	Organic	Microtek Laboratories
MPCM-10D	−10	170–180	Organic	Microtek Laboratories
HS10N	−10	290	Inorganic	PLUSS Advanced Technologies
RT-9 HC	−9	250	Organic	Rubitherm Technologies
HS7N	−7	296	Inorganic	PLUSS Advanced Technologies
SP-7	−7 to −5	290	Inorganic	Rubitherm GmbH
ATS-6	−6	360	Inorganic	Axiotherm GmbH
E-6	−6	300	Inorganic	PCM Products
RT-4	−4	180	Organic	Rubitherm GmbH
E-3	−4	330	Inorganic	PCM Products
HS3N	−3	346	Inorganic	PLUSS Advanced Technologies
ATS-3	−3	330	Inorganic	Axiotherm GmbH
PureTemp −2	−2	277	Bio-based organic	PureTemp LCC
E-2	−2	325	Inorganic	PCM Products
RT0	0	175	Organic	Rubitherm GmbH
E0	0	395	Inorganic	PCM Products
va-Q-accu + 00G	0	330	n.a.	va-Q-tec
HS01	1	350	Inorganic	PLUSS Advanced Technologies
A2	2	230	Organic	PCM Products
ATP 2	2	215	Organic	Axiotherm GmbH
RT2 HC	2	200	Organic	Rubitherm GmbH
SP5 gel	2 to 7	155	Inorganic	Rubitherm GmbH
va-Q-accu + 05G	2 to 8	240	n.a.	va-Q-tec
OM03	3	229	Organic	PLUSS Advanced Technologies
FS03	3	161	Organic (fatty acid)	PLUSS Advanced Technologies
RT3 HC	3	190	Organic	Rubitherm GmbH
A3	3	230	Organic	PCM Products
RT4	4	175	Organic	Rubitherm GmbH
PureTemp 4	5	187	Organic	PureTemp LLC
A4	4	235	Organic	PCM Products
RT5	5	180	Organic	Rubitherm GmbH
RT5 HC	5	250	Organic	Rubitherm GmbH
OM05P	5	216	Organic	PLUSS Advanced Technologies
A5	5	170	Organic	PCM Products
CrodaTherm 5	5	191	Bio-based organic	Croda
SP7 gel	5 to 8	155	Inorganic	Rubitherm GmbH
ATP 6	6	275	Organic	Axiotherm GmbH
A6	6	185	Organic	PCM Products
A6.5	6.5	190	Organic	PCM Products
CrodaTherm 6.5	6.8	184	Organic plant-based	Croda
Gaia OM PCM7	7	180	Organic	Global-E-Systems
ClimSel C7	8	123	Inorganic	Climator AB
A7	7	190	Organic	PCM Products
PureTemp 8	8	178	Organic	PureTemp LLC
OM08	8	175	Organic	PLUSS Advanced Technologies
RT8	8	175	Organic	Rubitherm GmbH
RT8 HC	8	190	Organic	Rubitherm GmbH
S8	8	130	Inorganic	PCM Products
A8	8	180	Organic	PCM Products
A9	9	190	Organic	PCM Products
CrodaTherm 9.5	9.7	186	Bio-based organic	Croda
RT10	10	160	Organic	Rubitherm GmbH
RT10 HC	10	200	Organic	Rubitherm GmbH
A10	10	210	Organic	PCM Products
S10	10	170	Inorganic	PCM Products
SP9 gel	10 to 11	155	Inorganic	Rubitherm GmbH

3.1. PCM applications in food transport and packaging

The research interest into the food cold chain has increased substantially over the last few years [78]. A homogeneous temperature through the cold chain is essential to preserve the food quality and avoid microbial growth [79]. Relevant studies have demonstrated a significant variation of temperature and humidity through the many links of the food cold chain, especially during transportation [80,81]. The use of

temperature loggers in packaged food products revealed that the food product temperature is on average 2 °C higher than the recommended values for 30% of the products when located in the display cabinet, 70% during transport to consumer and 40% in the domestic refrigerator [82]. These findings demonstrate the advantage of using PCMs when it comes to the product temperature stabilisation during the different links of the cold chain, mainly at the transport phase. The findings in the literature suggest different approaches to integrate PCMs in the transport link of the cold chain. The application of PCMs has been performed in the walls of the refrigerated vehicle, in the product packaging, or including an active PCM system externally to the storage space. A summary of the reported findings is presented in Table 5, including a description of the application and the applied PCMs. It has been shown that using PCMs in the walls of refrigerated transport vehicles is a highly performant strategy to reduce both peak and average heat transfer. PCM packaging for frozen foodstuff is deeply investigated by the scientific community and was proven to guarantee the thermal protection of the goods during the transport phase.

3.1.1. PCM integration into the walls of refrigerated vehicles

The strategy consists of limiting the heat flux through the walls of the refrigerated vehicle by integrating a PCM in the wall in order to absorb the heat exchanged with the environment. The long experience gained on PCM integration in building materials over the last years is believed to add considerable input when investigating PCM integration in the walls of refrigerated vehicles. The topic though has not gained the same interest as PCMs for buildings, but the interest has been growing through the recent years due to the urgent need to protect the cold chain of the higher recorded ambient temperatures. The required temperature for food transportation in refrigerated transport ranges from −25 °C (ice cream) to 15 °C (tropical fruits) [83]. PCM can be integrated either by including PCM layers in the insulating walls [84–86] or by creating a composite insulation material and dispersing an MPCM into traditional insulation material [87,88]. The main objective of integrating PCM in the walls of refrigerated vehicles is to reduce the peak and average heat transfer rate from the external environment to the refrigerated enclosure. This allows for a more uniform distribution of incoming heat flux from the environment to the refrigerated enclosure during the day. It was showed that integrating PCMs in the container wall can reduce the peak and average heat transfer rate by up to 29.1% and 16.3%, respectively [89]. Moreover, this technique was found to achieve a delay in the heat transfer peak between the external environment and the refrigerated enclosure due to the absorption of the incoming heat load in the PCM. The reported shifts in the heat transfer peak are ranging from 2 to 2.5 h when employing PCM-filled copper pipes inside the wall [89] and from 3 to 4.5 h when using a multi-layer PCM wall [86,85].

Ahmed et al. [89] investigated the reduction of peak and average heat transfer rates by integrating RT-5 [90] as a PCM filled into copper pipes in the walls of a refrigerated vehicle. The experimental work showed a reduction in average peak heat transfer rate of 29.1% and a reduction in daily heat transfer rates of 16.3%. Glouannec et al. [84] proposed to add a 5 mm layer of Energain PCM plates to a standard wall for a refrigerated vehicle. Starting from the inside wall of the refrigerated enclosure, the wall consisted of a polyester and fibreglass composite, polyurethane foam insulation, the PCM panel, an air gap and finally the outer steel plate of the vehicle. An experimental comparison showed that the PCM wall limited the increase in peak heat flux to 3.2 W m^{-2}, while the peak heat flux of the reference wall increased by 7.5 W m^{-2}. A reduction in average daytime energy consumption of 25% was demonstrated. However, the experimental tests were carried out for a total of 8 h and only considering 4 h to be daytime operation (30 °C).

Copertaro et al. [86] numerically investigated nine different PCMs as the outer layer in the sandwich wall of a standard 20 ft ISO refrigerated container using the software COMSOL Multiphysics. The PCMs were selected according to the Italian climate conditions. The most promising PCM was found to be RT35HC [90]. A peak heat transfer rate reduction between 20.01% and 25.01% and a daily energy rate reduction of 4.55–4.74% compared to a standard vehicle wall were recorded for summer climate conditions in Milan, Ancona and Palermo. The experimental results were found to be in good agreement with the numerical results considering the measured and simulated incoming heat fluxes through the wall (mean absolute error 4.23% during 24 h) using the PCM RT35HC. Fioretti et al. [85] employed a similar multi-layer wall

Table 5
Main results from use of PCM in food transport and packaging.

Application	Theoretical (T) Experimental (E)	PCM (T_m [°C])	Main result (value)	Reference
Wall for refrigerated vehicle	E	RT5 (5)	Peak shift (2 to 2.5 h); Peak heat transfer reduction (29.1%); Average heat transfer reduction (16.3%)	[89]
Wall for refrigerated vehicle	T/E	Energain PCM panel (21)	Average heat transfer reduction daytime (25%)	[84]
Wall of 20 ft ISO container	T/E	RT35HC (35)	Peak shift (3 h); Peak heat transfer reduction (20%); Average heat transfer reduction (about 4.5%)	[86]
Wall for refrigerated vehicle	T/E	RT35HC (35)	Peak shift (3.5 to 4.5 h); Peak heat transfer reduction (5.5 to 8.5%)	[85]
Wall for refrigerated vehicle	T/E	Composite PU/PCM C18 Inertek (18)	Average heat transfer reduction (0.3 to 4.1%)	[88]
Storage container for cold/hot food	T/E	RT-2 (2); PT-15 (-15); PT-63 (63)	Increase in storage time (320% to 400%)	[91]
Storage container for ice cream	T/E	E-21 (-21)	Decrease in product temperature when stored in room temperature (10 K)	[92]
Storage container for ice cream	E	E-21 (-21)	Decrease in product surface temperature during heat load test (17 K)	[93]
Packaging for chilled food	T/E	RT5 (5)	Increase in thermal buffering capacity; Increased shelf life of ham (6.7%)	[96]
Packaging for blood bags	E	Mixture of n-alkanes (4.8)	Correct storage temperature for 6 h (8 times increase)	[98]
PCM-HEX system for refrigerated transport	T/E	Inorganic salt-water solution (−26.8)	Reduction in annual cost (51 to 86.4%); Storage space kept at −18 °C for 10 h	[99,100]

construction using the same PCM (RT35HC) and PCM thickness for a refrigerated container considered by Copertaro et al. [86]. From the inside of the container, the wall consists of an internal metal sheet, a polyurethane foam insulation layer, the PCM placed in a polyethylene panel, a polyvinyl chloride film and finally an external metal sheet (see Fig. 1). The experimental results relative to two days of experiments under summer climate conditions in Ancona showed a reduction in peak heat transfer rate between 5.55% and 8.57%.

Michel et al. [88] presented a numerical model of a multi-layer wall using COMSOL software. One of the layers is a composite material which consists of a PCM/polyurethane (PU) foam, combining both the standard insulation layer and the PCM layer. The PCM layer is placed between two layers of PU foam so that the total thickness of the multi-layer wall is 6 cm. The study was carried out using various thicknesses of the PU-PCM layer (from 1.5 cm to 2 cm) and the two PU layers (from 0.5 to 4 cm), always adding up to a total of 6 cm. The change in thickness of the two PU layers affects the position of the PU-PCM layer within the wall, which is done to evaluate the effect of the PCM layer position on the heat transfer through the multi-layer wall. The deviation in heat flux through the composite plate between the numerical and experimental results were found to be acceptable (less than 2% during steady-state periods and less than 8.5% overall). The results from the numerical study have shown that the achieved reductions of the heat transfer exchange rate were in the range of 0.3% to 4.1%. It was also shown that the closer the PCM multi-layer plate to the external wall of the vehicle, the more important the heat transfer reduction is (4.1%). This results is found to be in accordance with those found by Copertaro et al. [86] where the maximum reductions were recorded in the range from 4.55% to 4.74% when the PCM layer is located close to the external surface. Through the investigated literature, it was observed that the largest reductions in the heat transfer rate are recorded when the PCM is placed towards the external wall of the refrigerated vehicle in PCM multi-layer walls. Only a few studies were focusing on the effect of PCM location inside the vehicle wall on the heat transfer rate, therefore, more research is needed to present the optimal design.

3.1.2. PCM integration into products packaging and containers

Integrating PCM into the storage containers and food packaging has been found as a suitable solution to increase the thermal mass of packaging so that the storage temperature is kept stable for longer periods. Ice cream is a very temperature-sensitive product. Therefore, it has been found to be a popular application that has attracted researchers to investigate the performance of PCM packaging [91–93]. Oró et al. [91] investigated both experimentally and numerically the benefits of using different PCMs as an additional layer in an insulated bin to store hot or cold food, as described in Fig. 2. The numerical model was solved using the fully implicit finite volume method and the numerical results were found to have an acceptable agreement with the experimental data. The results using the PCMs PT-15 and PT-63 [94] have shown an increased safe time for transportation of 400% and 320% in the case of ice cream and hot water storage, respectively. Scoop ice cream sold in restaurants and bars are often kept in 5-litre rectangular steel ice cream trays to fit in the display freezers, typically keeping the ice cream below −8 °C after it has been removed from the storage freezer. Oró et al. [92] proposed to add a layer of the PCM E-21 [95] around the sides of the tray to increase its thermal mass. The PCM occupied the volume between the trays that is available when they are placed side by side in the display freezer so that no extra freezer space was required. The experimental results demonstrated that after 3 h under 25 °C ambient conditions, the temperature increase in the centre and outer part of the ice cream was reduced by 3 °C and 10 °C, respectively.

Packaging for transport and ice cream storage using a salt-hydrate PCM was proposed by Leducq et al. [93]. The design was compared to a standard cardboard box and a box with expanded polystyrene as insulation materials. After 40 min of heat load test under ambient temperature conditions, it was found that the product surface temperature increased by 18 °C for the cardboard box, 9 °C for the conventional insulation and 1 °C for the PCM packaging. Hoang et al. [96] studied the thermal behaviour of the organic PCM RT5 [90]) encapsulated in a biodegradable polyester plate to be used in packaging for transportation of chilled food. A numerical heat transfer model was developed and experimentally validated. The model showed good agreement with experimental results with a maximum temperature deviation of less than 0.8 °C and 1.9 °C at the PCM plate centre and surface, respectively. A time-dependent air temperature profile representing different parts of the meat cold chain was used as an input to the simulation. The thermal

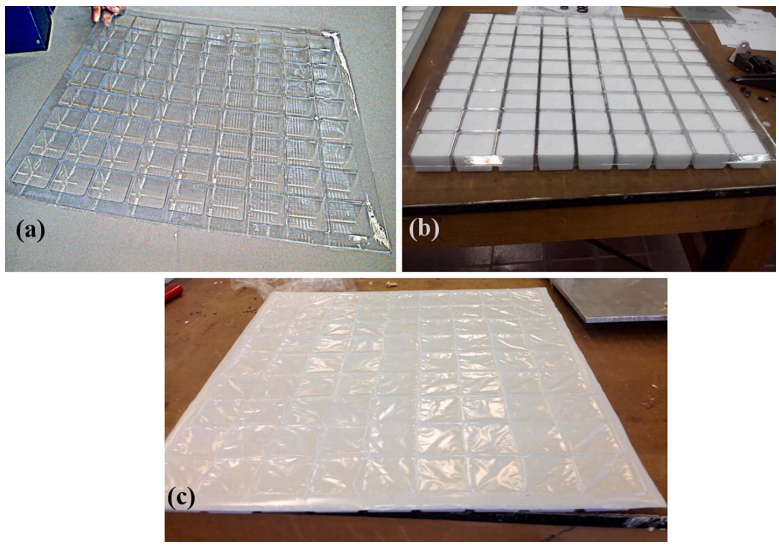

Fig. 1. Constructon of a PCM layer for a multi-layer wall: (a) polyethylene panel, (b) RT35HC encapsulation (PCM), (c) polyvinyl chloride closing layer [85]. Reprinted from Energy conversion and management, 122, Fioretti, R., Principi, P., Copertaro, A refrigerated container envelope with a PCM (phase change material) layer: Experimental and theoretical investigation in a representative town in central Italy, 131–141, Copyright (2016), with permission from Elsevier.

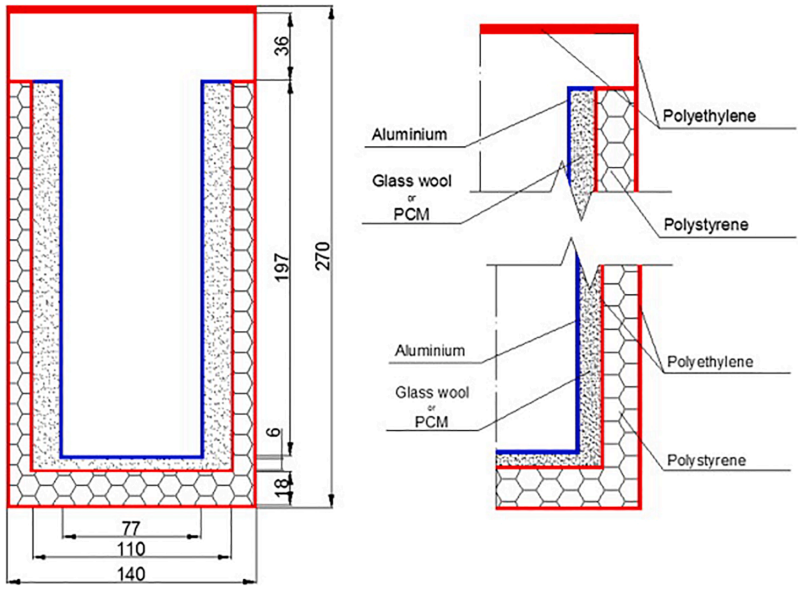

Fig. 2. Bin with PCM for transport and storage of food [91]. Reprinted from Applied Thermal Engineering, 58, Oró, E., Cabeza, L.F., Farid, M.M., Experimental and numerical analysis of a chilly bin incorporating phase change material, 61–67, Copyright (2013), with permission from Elsevier.

performance benefits of PCM packaging for foodstuff is well demonstrated. Indeed better thermal buffering characteristics were found when compared to a standard cardboard packaging. The surface peak temperature was reduced by 12.5 °C when using the PCM packaging. One way to improve the competitiveness of such system is to examine the safety aspect when using PCM for food storage application. Indeed, a PCM leakage from packaging can result in food contamination. In this review, the authors point out that food safety during transport does not only depend on the storage temperature, but also on a performant system design which prevents PCM leakage issues.

Transport and storage of biological material and vaccines require careful temperature control through the cold chain. Many vaccines are heat sensitive, which can affect their efficiency. A new generation of vaccines is nowadays available, which has an improved resistance experiencing temperature fluctuations. However, some of the new vaccines are freeze sensitive, proving that stable temperature during transport and storage is essential [97]. In this review, the authors report the only available research dedicated to medical and biological goods packaging including PCM [98]. The authors suggested using a mixture of n-alkanes as the PCM in a package device for transport of blood bags. The packaging could keep the blood samples below 10 °C during 6 h under 22 °C ambient temperature conditions. Until the date, research on packaging using PCM for foodstuff has been more attractive than for biomedical goods. Another urgent reason to increase the interest on investigating vaccines and biomedical goods storage, is the need of many countries with difficult climate conditions (high temperature and high humidity ratio), due to the limited access to electricity and refrigeration equipment to a secure and sustainable health care system.

3.1.3. Active PCM systems

An alternative approach of using PCM in refrigerated vehicles was proposed by Liu et al. [99]. The authors presented a novel design of a refrigeration system for the vehicle as represented in Fig. 3. The conventional diesel-driven refrigeration unit usually installed above the driver compartment is replaced by a phase change thermal storage unit (PCTSU). The PCM consists of a water-salt solution which has a melting point of −26.8 °C. The PCM is macro-encapsulated in thin and flat plastic capsules and stacked with 6 mm distance into an insulated

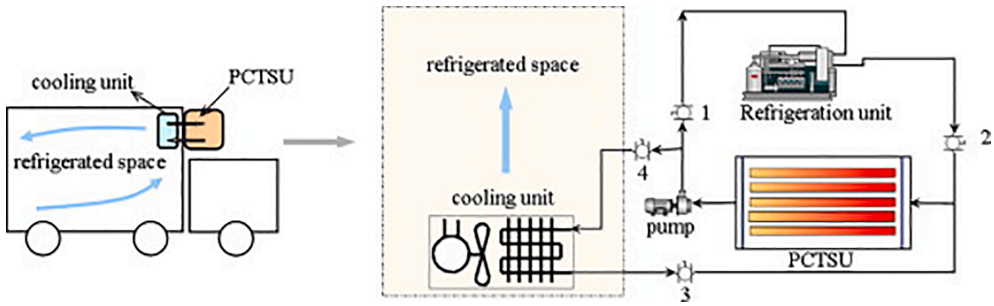

Fig. 3. System design of an on-board PCM unit integrated in the refrigeration system of a refrigerated vehicle [99]. Reprinted from Applied Energy, 92, Liu, M., Saman, W., Bruno, F., Development of a novel refrigeration system for refrigerated trucks incorporating phase change material, 336–342, Copyright (2012), with permission from Elsevier.

container. The secondary refrigerant (Dynalene HC-40) is pumped into the PCTSU to reject heat to the PCM. The cold HTF then circulates the air HEX in the refrigerated space to maintain the desired air temperature during transportation. Once the vehicle is stationary at a warehouse or depot, the PCTSU can be charged by connecting the system to an external refrigeration system through valves 1 and 2 as described in Fig. 3. The secondary refrigerant is cooled by the refrigeration system and circulates through the PCTSU to ensure the cold charging process. A prototype of the PCTSU was constructed and experimentally tested in a secondary refrigerant circuit connected to a cold room representing the refrigerated vehicle. The results revealed that the storage capacity of the PCTSU prototype was insufficient to keep −18 °C in the refrigerated space for the requested 10 h. To cover the daily energy demand of about 15 kWh of the refrigerated vehicle, the authors calculated the required amount of PCM to be 360 kg. Calculations showed that using an external refrigeration system which has a COP ranging from 1.0 to 1.5, the novel PCM-based system demonstrates important cost savings in the range of 51.0% to 86.4% under Australian ambient conditions. In a further work [100], a numerical model was developed using TRNSYS software to simulate the performance of the entire system. The one-dimensional model of the PCTSU was validated and showed reasonable agreement with the experimental results considering the heat transfer rates and HTF outlet temperature during the discharging process [101]. The results from the system simulation revealed that the refrigerated space could be kept at −18 °C for the requested 10 h during the warmest day of the year [100]. During door openings of the vehicle, the temperature inside the refrigerated space increased by about 8 K, and it would take 30 min for the system to restore it to the setpoint temperature (−18 °C). The authors recommended using a PCM with a lower melting point (−32 °C) in the PCTSU to limit the peak temperature during the door opening and provide higher cooling rate during the following pull-down period. These findings demonstrate again the ability of this technology to present a promising solution for typical refrigerated transport routes.

3.1.4. Summary and discussion

A summary of the reviewed literature on PCM applications in food transport and packaging is given in Table 5. For the past ten years, PCM integration into the walls of refrigerated vehicles and containers has been extensively investigated by applying both experimental and numerical methods. A special focus was dedicated to the development of multi-layer insulation materials including PCMs in order to replace the standard sandwich wall in refrigerated vehicles [84–86,88]. From the reviewed literature, it was shown that using a multi-layer PCM wall is an efficient technique to reduce the peak heat transfer rate from the environment to the refrigerated space. However, the most promising wall design in terms of performance looks to be the standard sandwich wall inserted with PCM-filled copper pipes as presented by Ahmed et al. [89]. This design demonstrated up to 29.1% and 16.3% reductions in the peak and the average heat transfer rates, respectively. For multi-layer PCM walls, the highest energy savings are demonstrated when the PCM layer is located closest to the external wall. On the other hand, the copper pipe wall design showed significant reductions in the average heat transfer rate by placing the PCM-filled copper pipes close to the internal wall. The PCM applied in this study had a melting temperature of 5 °C, which is close to the air temperature of the refrigerated space. This contrasts with the PCM selection for the multi-layer wall configurations. When the PCM layer was located closest to the external side of the wall, the selected PCMs had melting points closer to the ambient temperature (18 °C to 35 °C). Few studies can be reported combining different melting temperatures and the location of the PCM inside the wall, and a complete understanding of the effect of these parameters is still missing. A comparison between the PCM-wall and the standard insulated wall in terms of production cost and weight has to the authors knowledge not yet been carried out. The experimental procedure presented by Fioretti et al. [85] and Ahmed et al. [89] gives a very good representation of the real-life performance of the PCM-walls by considering a full-size container tested in real ambient conditions for up to 1 month, side-by-side of a standard container. Although the full-scale procedure is clearly more complex and costly compared to investigating a small section of a PCM multi-layer wall, the former demonstrates the real-life performance needed to increase the confidence of manufacturers to consider this novel technology as a viable alternative to traditional insulation materials.

PCMs used for food packaging and containers are reported for a broad range of melting temperatures, from −26.8 °C to 5 °C. PCM packaging of temperature-sensitive goods was proven to provide sufficient thermal comfort to the goods during high-temperature exposure and thus guarantees the food quality between the links of the cold chain, e.g. from the food supplier warehouse to the supermarket refrigerated display cabinets [98,92,93]. In the light of the recent outbreak of the pandemic COVID-19 [102], PCM packaging of medical goods could have played an important role for safe and urgent transport of temperature-sensitive medical goods such as medications, blood samples and vaccines to hospitals between countries. This would be particularly important in developing countries where access to electricity and refrigeration is limited.

The fundamentally new approach for the refrigeration system for refrigerated vehicles using an onboard PCM-HEX and a pumped HTF circuit presented by Liu et al. [101] looks to be very promising. It is clear that the system presents significant environmental benefits by replacing the standard diesel-driven refrigeration system on the vehicle by an active PCM-HEX unit. Instead of burning diesel to maintain the adequate temperature in the refrigerated space, the PCM-HEX unit can be charged by an external refrigeration system at the warehouse with higher efficiency and preferably powered by renewable energy. Also, the authors state that the novel system will reduce the local pollution of NO_X and particulate matter which is a known issue for diesel engines [103].

3.2. PCM application in commercial refrigeration

Refrigeration is typically responsible for 35–60% of the total energy consumption in supermarkets, depending on location, size and share of frozen/chilled food in the retail area [104,105]. Commercial refrigeration systems cover a wide range of different equipment from small plug-in vending machines, food service coolers and display cabinets to large centralised supermarket refrigeration systems. In this review, a presentation of the different integration scenarios of CTES into supermarket refrigeration systems is given. Two approaches of PCM integration in supermarkets are commonly investigated: A distributed storage which is directly integrated into the display cabinets and a centralised storage integrated into the main refrigeration system circuit. The latest research on PCM integration in various refrigerated vending machines and beverage coolers is also presented. A summary of the reviewed literature on PCM implementation related to commercial refrigeration is given in Table 6. The possibility of implementing a storage in the supermarket is becoming popular as it is often reported to be a cost-effective way to reduce the share of refrigeration in the total energy consumption and energy savings up to 6.4% is reported [106]. The implementation of CTES in CO_2 supermarket refrigeration was reported by Gullo et al. [107] as a key factor for energy efficiency enhancements of these systems, and up to 5.6% reduction in the daily energy consumption is reported in the literature [108]. Furthermore, experimental studies have shown that cold storage can offer a control strategy to stabilise the air temperature inside the display cabinet [109,110].

Key benefits of integrating CTES into commercial refrigeration systems are the possibility to shift energy purchases to low-cost periods by using the storage to achieve peak shaving of the refrigeration demand. Consequently, the power consumption stabilisation through the day will be achieved [111]. Furthermore, the use of local renewable electric energy production (e.g. installing photovoltaic panels on the roof) is increasing in the supermarket sector. The use of CTES can correct the mismatch between energy availability and demand, thereby maximising

Table 6
Main results of PCM application in commercial refrigeration.

System Configuration	Theoretical (T) Experimental (E)	PCM (T_m [°C])	Main results (Value)	Reference
Cabinet shelf with heat pipes and PCM	E	De-ionized water with 2% borax (−0.5)	Food temperature reduction during defrost (3.5 K); Reduced temperature peak during defrost (1.5 K)	[109]
Cabinet shelf with heat pipes and PCM	E	RT3 (2.5); RT4 (3.8); RT5 (5.2)	Product temperature fluctuation reduction (83.3%); Product temperature difference reduction (80%))	[117]
Radiator PCM-HEX in cabinet air duct	T/E	Water with nucleating agent (−2)	Energy savings (up to 5%); Reduction in the maximum cabinet temperature (2 K); Reduced start/stop cycles of compressor (27%)	[110,106]
Fin-tube PCM-HEX in cabinet air duct	E	Water/ice (0)	Reduction in the maximum cabinet temperature (1 K)	[119]
Three-fluid PCM-HEX in cabinet air duct	T	Water/ice (0)	PCM-HEX cooling duty (1.7 kW); High storage capacity (6 kWh per meter width)	[120]
Three-fluid PCM-HEX in cabinet air duct	T	Water/ice (0)	Reduction in the maximum cabinet air temperature during defrost (10 K)	[121]
CTES integrated into CO_2 refrigeration system	T	Water/ice (0)	Peak compressor power reduction (50%); Total energy consumption reduction (14.4%)	[129]
CTES integrated into CO_2 refrigeration system	T	Water/ice (0); PCM (15)	Peak compressor power reduction (15%); Total energy consumption reduction (5.6%)	[108]
CTES integrated into CO_2 refrigeration system	T	Water/ice (0)	Compressor power reduction during discharge (5% to 68%)	[111]
PCM-HEX in air duct of a bottle cooler	E	Water/ice (0); RT4 (4)	Energy consumption reduction (4–10%); Increase in compressor cycle time (118%)	[130]
PCM slab on evaporator of a bottle cooler	T/E	Water/ice (0)	Reduced compressor on/off ratio (36% to 26%)	[131]
CTES for dispenser beverage cooler	E	Water/ice (0)	Energy consumption reduction (15%)	[132]

the potential of the local energy production. Last but not least, the cold storage can increase the system reliability by supplying the cooling capacity under different unforeseen conditions such as a power blackout situation or component failure in the refrigeration system. There are three strategies to operate a CTES that is integrated into a refrigeration system. The three scenarios are: The full storage (Fig. 4a), partial storage with load levelling (Fig. 4b) and partial storage with load limiting (Fig. 4c). In the full storage scenario, the storage can cover the entire refrigeration load during peak hours, while a high capacity refrigeration system is required to fully charge the CTES during off-peak hours. In the load levelling scenario, the capacity of the storage and the refrigeration system is designed so that the refrigeration system operates at a near-constant load through the day. The load limiting scenario represents the case where the capacity of the storage is designed to cover a certain refrigeration load so that the power consumption of the refrigeration system does not exceed a given value during peak hours (e.g. to avoid an electricity tariff). In most applications, the load-levelling or load-limiting strategies will be the most favourable, due to reasonable investment costs for the CTES and the possibility to reduce the capacity requirement of the refrigeration system [5].

3.2.1. *Supermarket display cabinets*

Two main types of display cabinets are installed in supermarkets: The open style cabinet and the closed style display cabinet with glass doors. In the open type, one or more air curtains isolate the foodstuff from the external environment. About 70% of the cooling load of refrigerated display cabinets originates from air infiltration [112,113]. Replacing the open type cabinets by cabinets with glass doors can reduce the energy consumption in the range of 30 to 40 % [114,115]. A reduction in warm air entering the cabinets reduces the frost formation on the evaporator coils, resulting in less frequent defrost cycles. Despite these obvious benefits, the open type cabinets are frequently installed, mainly because it gives the customers easy access to the products. Nevertheless, it has been demonstrated that fitting doors to an open display cabinet have no negative effect on the product sales [116]. An efficient way to reduce the high energy consumption of these types of display cabinets is to integrate PCM cold storage. There are commonly two investigated strategies of integration: Into the cabinet shelf [109,117], or integrating an additional PCM storage at the rear wall of the cabinet [110,106]. The product temperature for chilled food in supermarket display cabinets normally range between 0 °C and 5 °C, and avoiding temperature fluctuations is key to preserve the food quality [79]. Suitable PCMs for this application have a melting temperature in the range from −5 °C to 5 °C, depending on the main objective of the CTES. Lu et al. [118] identified water-based PCMs as the most suitable candidates for implementing in display cabinets for chilled food. Water-based PCMs are preferred over paraffin PCMs due to their higher latent heat capacity and better thermal conductivity. Water has 2.5 times the latent storage capacity and about 2.7 times higher thermal conductivity compared to paraffin RT-2 and RT-4 [118,90].

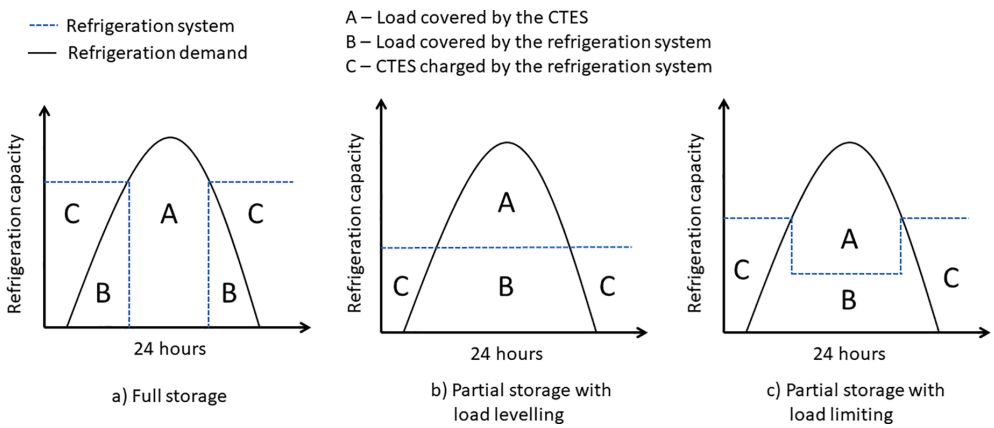

Fig. 4. Different strategies for operating a CTES system integrated into a refrigeration system.

Lu et al. [109] presented a new design of a cabinet shelf in an open type display cabinet, represented in Fig. 5a. The novel cabinet shelf was 30 mm thick and composed of 8 heat pipes that were evenly distributed over the width of the shelf, and the PCM was included between them (See Fig. 5b). The applied PCM consisted of de-ionized water with an addition of 2% borax which has a melting point of −0.5 °C. The objective of the study was to decrease the temperature difference between the products placed at the first row and last row of one shelf and between the products placed at the left, middle and right of the shelf. Furthermore, the objective was to decrease the product temperature peak that occurs during the defrosting process. The experimental results showed a reduction in the front-back and right-left product temperature variation compared to the standard shelf of 1.4 K (47%) and 1.7 K (68%), respectively. Furthermore, the rise in food temperature during the defrosting process was reduced by 1.5 K, while no increase in cabinet power consumption was recorded.

A similar design to that proposed by Lu et al. [109] was investigated by Wu et al. [117] using a shelf thickness of 20 mm and heat pipe spacing of 150 mm, whereas Lu et al. [109] used a shelf thickness of 30 mm and heat pipe spacing of 230 mm. Different organic PCMs were experimentally tested: RT3, RT4 and RT5 which have a melting temperature of 3 °C, 4 °C and 5 °C, respectively [90]. The results showed that integrating RT4 into the shelf provided the best overall results. Indeed, the temperature difference between packages in the left–right direction was reduced by 80% compared to a standard shelf. However, the novel shelf was not able to reduce the temperature difference between the packages in the front to back direction. The average food package temperature and food temperature fluctuation were decreased by 32% and 83.3%, respectively. The highest reduction in food package temperature variation in the width direction was obtained by Wu et al. [117], whereas the shelf design presented by Lu et al. [109] also gave important reductions in both depth (47%) and width (68%) directions.

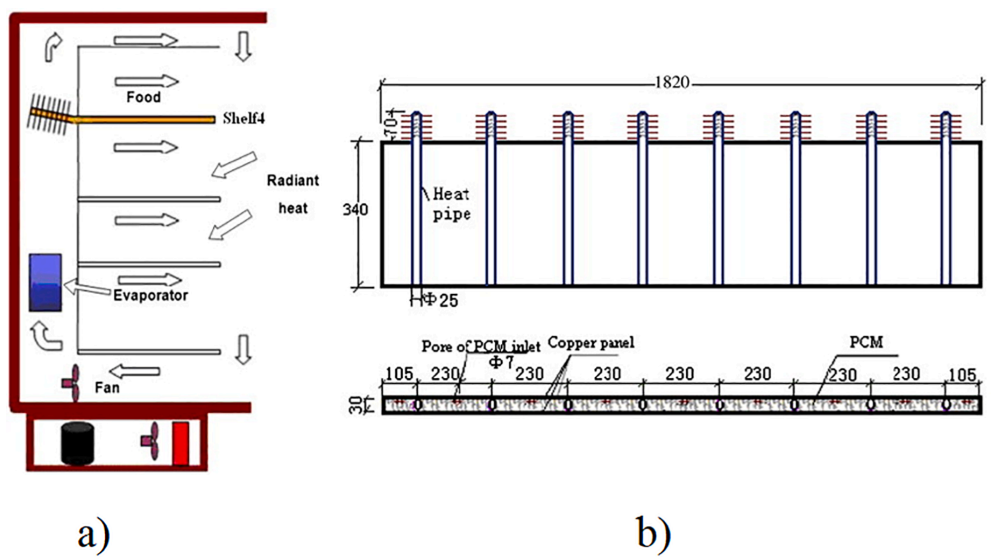

Fig. 5. Open display cabinet employing a cabinet shelf with heat pipes and PCM: a) Display cabinet b) Novel cabinet shelf [109]. Reprinted from Applied Thermal Engineering, 30, Lu, Y., Zhang, W., Yuan, P., Xue, M., Qu, Z., Tao, W., Experimental study of heat transfer intensification by using a novel combined shelf in food refrigerated display cabinets (experimental study of a novel cabinets), 85–91, Copyright (2010), with permission from Elsevier.

This can be attributed to the higher thermal conductivity and the lower melting point of the water-based PCM used by Lu et al. [109], obtaining comparable results to Wu et al. [117] while applying an 80 mm longer distance between each pipe in the shelf. Further investigations considering the selection of the appropriate PCM and the optimum location of the heat pipes for the cabinet shelf to clarify the effect of these parameters and to find the optimal design.

Another strategy to implement cold storage in display cabinets is to integrate a PCM-HEX in the air circulation duct. This configuration was experimentally investigated by Alzuwaid et al. [110] to reduce the energy consumption and decrease both the food product and air temperature in the cabinet. In this study, two single-panel radiators were filled with the PCM which consists of a mixture of water and a nucleating agent with a melting temperature of −2 °C. As it can be seen in Fig. 6, the PCM-HEX unit was installed downstream of the evaporator at the back of the cabinet and referred to as a radiator. The charging process is initiated when cold air from the evaporator flows across the surface of the PCM-HEX unit during the compressor ON period. During the compressor OFF period (e.g. during the defrosting period) the air temperature in the cabinet rises above the melting temperature of the PCM. The cabinet air is circulated through the PCM-HEX unit by using the fan. The air temperature decreases as soon as it is in contact with the charged PCM-HEX unit until it is completely discharged (when the PCM temperature exceeds the inlet air temperature). The results have shown a reduction of 5% in the energy consumption over 24 h. Furthermore, the maximum cabinet temperature during the compressor off-period was also reduced by 2 K. The authors completed their work by experimental validation of a numerical 2D CFD model developed for the entire system using ANSYS Fluent software [106]. The findings have shown a potential energy saving of 6.4% compared to the standard cabinet without a PCM storage. The compressor lifetime was found to be enhanced as the number of compressor cycles (ON/OFF function) was reduced by 27%.

Ben-Abdallah et al. [119] used a fin-and-tube HEX design for a PCM storage unit located in the rear air duct of an open display cabinet. The PCM-HEX unit has a total heat transfer area of 25 m^2 and 7 kg of water is used as the PCM. The experimental results have shown that during a 2 h compressor OFF period, the integration of the PCM-HEX unit has limited the product temperature rise to 1 K. In the case of a cabinet without PCM integration, a 2 K increase of the product temperature was observed under the same operating conditions. Moreover, it was also found that the PCM charging process is approximately two times longer than the discharging process due to the larger temperature difference between the air and the PCM during discharging of the storage.

Until the date, research focusing on PCM storage integration into closed-style display cabinets are limited to theoretical studies. Sevault et al. [120] presented a design of a cold storage unit using water as the PCM, located in the air circulation duct of the cabinet (Fig. 7). The storage consists of a container composed of CO_2 refrigerant coils with integrated small air ducts to ensure the charging and discharging processes, respectively. A 2D CFD study in Ansys Fluent was performed to evaluate the influence of the distance between the air ducts and the CO_2 coils on the heat transfer, charging and discharging time. The results have shown that a 20 mm centre-to-centre distance of the coils and air passages was suitable to cover defrost periods. The storage demonstrated a maximum cooling duty of about 1.7 kW and a total capacity of 6 kWh per meter width.

A similar concept using water as the PCM was investigated theoretically by Jokiel et al. [121]. The storage unit consists of a PCM container composed of horizontal tubes where the refrigerant circulates and vertical tubes for the cabinet air circulation to charge and discharge the storage. The PCM-HEX was placed downstream of the evaporator in the air duct of the cabinet. Dynamic simulations of the cabinet with a novel integration of the PCM-HEX unit were performed in the software Dymola. The results have shown a reduction in the maximum cabinet air temperature during the defrosting period of up to 10 K compared to the cabinet without PCM storage. Even though both studies performed by Sevault et al. [120] and Jokiel et al. [121] show interesting strategies to implement active PCM storages in display cabinets, they obviously need to be completed with experimental studies to validate the theoretical results.

3.2.2. PCM integration into supermarket refrigeration system

The second strategy for a successful implementation of CTES in supermarkets involves the integration of a centralised storage into the central or main refrigeration circuit. The use of SHS storage units has been a popular choice among researchers over the last ten years [122–126]. However, the use of PCMs as LHS mediums for cold storage was found to be rarely investigated for supermarkets refrigeration systems, even though they are commercially available (water/ice as the storage medium), e.g. from Calmac Corp. [127] and Viessmann

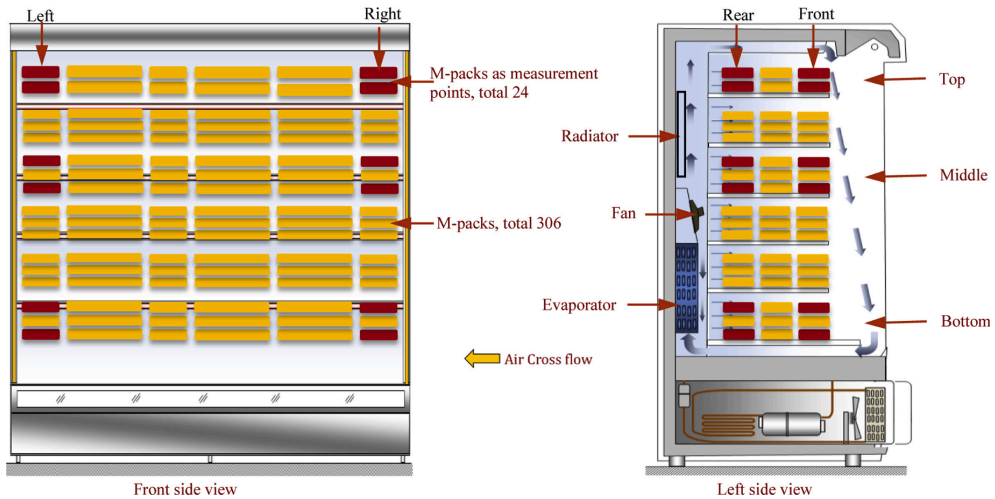

Fig. 6. Open display cabinet with integrated PCM-HEX (radiator) at the back wall [110]. Reprinted from Applied Thermal Engineering, 75, Alzuwaid, F., Ge, Y., Tassou, S., Raeisi, A., Gowreesunker, L., The novel use of phase change materials in a refrigerated display cabinet: An experimental investigation, 770–778, Copyright (2015), with permission from Elsevier.

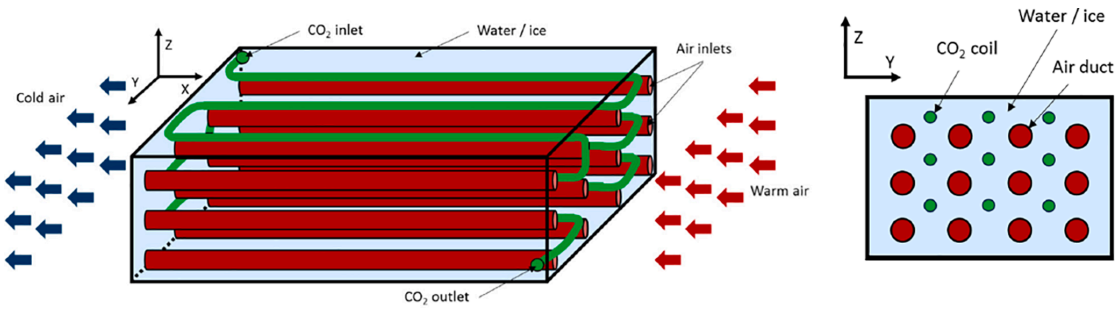

Fig. 7. PCM-HEX unit with air ducts and refrigerant tubes [120]. ©IIF/IIR. Published with the authorization of the International Institute of Refrigeration (IIR): www.iifiir.org.

Refrigeration Solutions [128]. Only a few investigations on the integration of CTES into CO_2 supermarket refrigeration systems have been performed the last five years. For a detailed overview of CO_2 refrigeration technology for supermarkets, the reader is directed to Gullo et al. [107]. The most common objective of the storage integration is to improve the system COP by reducing the throttling losses under unfavourable environmental conditions, such as high ambient temperatures. Fig. 8 presents an overview of the different configurations to

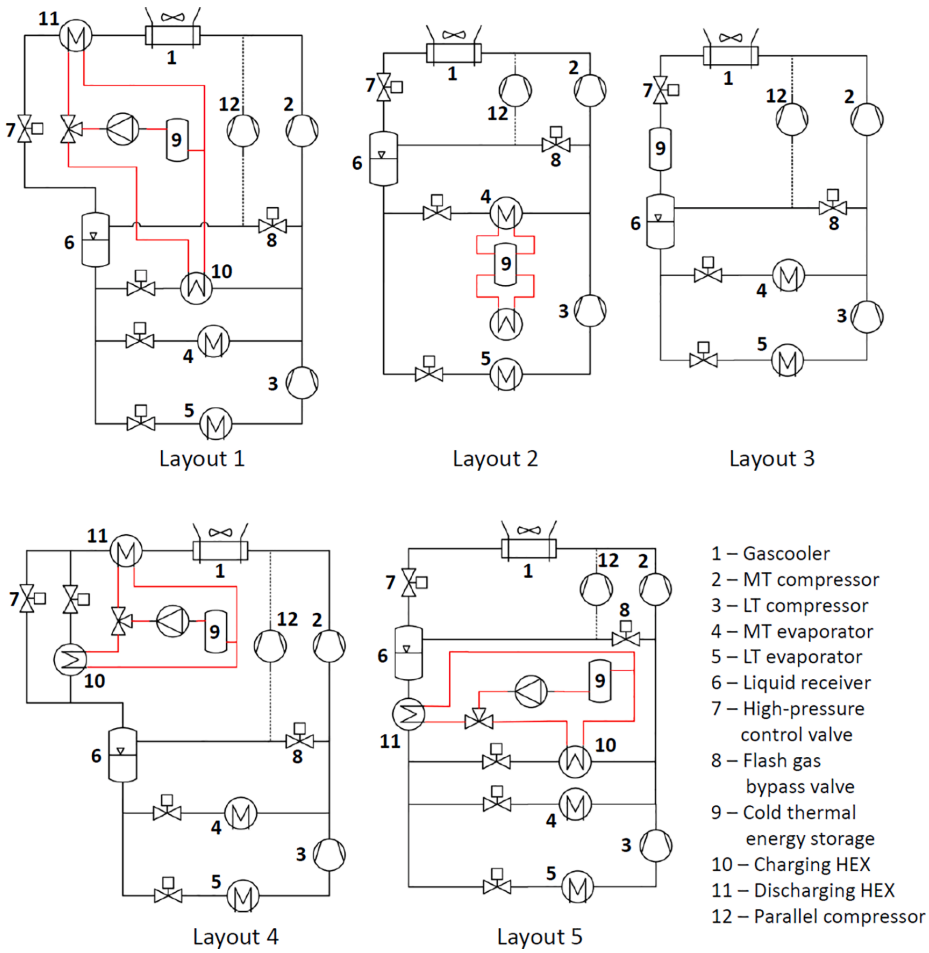

Fig. 8. Integration of CTES into a CO_2 refrigeration system: 1) Downstream of the gascooler using ice/water as the PCM 2) into the MT display cabinet 3) Upstream of the pressure receiver and using ice/water as the PCM 4) Downstream of the gascooler, using a 15 °C PCM 5) Downstream of the pressure receiver. Optional parallel compression indicated by a dashed line in each configuration.

integrate CTES into a transcritical CO_2 booster refrigeration system found in the literature. The most important components of the refrigeration system and the CTES system is indicated in Fig. 8. The possibility to include parallel compression is shown by a dashed line in all the layouts.

Heerup and Green [129] suggested to integrate a coil-in-tank LHS using ice as the storage medium between the high-pressure control valve and the liquid receiver (Layout 3 in Fig. 8, without parallel compression). The storage capacity is 144 kWh, which is equivalent to 33% of the cooling load for 6 h. The CO_2 circulates directly through the coil which is immersed in water. The charging and discharging processes are achieved by varying the liquid receiver pressure corresponding to −5 °C and 5 °C, respectively. The objective of the storage integration is to achieve energy and cost savings by shifting the refrigeration load from the day to the night, taking advantage of the difference in the ambient temperature conditions and the electricity pricing. The load is reduced during the daytime operation by condensing the flash gas that is formed after the expansion through the high-pressure control valve, reducing the load on the medium temperature (MT) compressors. Theoretical calculations using climate data from Denmark (cold) and San Francisco (warm) have revealed that the annual energy savings from implementing the ice storage are ranging from 4% (cold climate) to 14.4% (warm climate), as well as a reduction in peak power consumption of 50% during the warmest days of the year. The payback period was found to be more than 5 years, which is generally longer than accepted by the supermarket sector. The study did not evaluate the possibility to reduce the size of the other components (e.g. gas cooler, compressor pack) in the refrigeration system due to reduction of peak load by 50%. Taking this factor into account could possibly reduce the payback time of the system further.

Fidorra et al. [108] presented two different configurations to integrate CTES into a transcritical CO_2 booster refrigeration system with parallel compression (Layout 1 and 4 in Fig. 4). In both configurations, the storage is connected to the CO_2 refrigeration system employing a secondary HTF circuit via a charging and a discharging HEX. The discharging HEX is located downstream of the gascooler in both configurations. The objective of the storage integration is to decrease the temperature of the refrigerant downstream of the gas cooler during periods of high ambient temperatures, and consequently reducing the throttling losses and increasing the system COP. The first configuration (Layout 1, Fig. 4) utilises ice/water as the storage medium, and the charging HEX is therefore operated at the MT evaporation temperature (−8 °C). In the second configuration (Layout 4, Fig. 4), a PCM with a melting point of 15 °C is selected. An additional evaporation level at the liquid receiver pressure level (40 bar, 5.3 °C) is included upstream the pressure receiver to charge the PCM storage through the charging HEX. The load from the charging process is handled by the auxiliary compressor. Case studies applying different ambient conditions and storage capacities were simulated using a commercial dynamic simulation software (TIL-library/Modelica), and the results were compared to the system without storage. The results have shown that the reduction in daily energy consumption for layout 1 and 4 was up to 3.5% and 5.6%, respectively. The more important energy saving in layout 4 is due to the higher charging temperature compared to layout 1 (5.3 °C compared to −8 °C). Furthermore, up to 15% reduction in maximum compressor power was achieved for both configurations. This study shows again the potential for improving the efficiency of the refrigeration systems in supermarkets. A more detailed modelling of the heat transfer mechanisms of the storage and introducing thermophysical PCM properties into the numerical model is recommended to further improve the confidence in the results. Furthermore, a validation of this study by experimental results is currently missing.

Fidorra et al. [111] extended the previous work by carrying out a simplified thermodynamic analysis comparing the reduction in energy consumption and peak compressor power of four different configurations of CTES integration into a transcritical CO_2 refrigeration system under various ambient conditions. All the configurations use ice/water as the LHS medium. The four studied configurations for the implementation of CTES are layout 1, 2, 3 and 5 as presented in Fig. 4, but without parallel compression. Layout 1 is equal to the first configuration in Fidorra et al. [108] and was explained previously. In layout 2 the storage is located inside the display cabinet where the MT evaporator satisfies both the cooling needs and the PCM storage charging process. In layout 3 the storage is located upstream of the liquid receiver, similar to the configuration presented by Heerup and Green [129]. During the discharging process, the refrigerant liquid–vapour separation process is further enhanced by the integration of the CTES, where a part of the flash gas resulting from the throttling through the high-pressure valve is condensed thus the power consumption due to the compression of the flash gas is reduced. Layout 5 is equal to layout 1 except for the location of the discharging HEX, which is now located at the liquid receiver outlet. During the discharging process, the liquid CO_2 is subcooled before the expansion valves at the MT and low temperature (LT) evaporators to increase the evaporation capacity and thereby increase the system COP. The results have indicated that the highest reduction in the compressor power for high ambient temperature (40 °C) is achieved using layout 2 presented in Fig. 4. In fact, up to 68% power reduction was obtained assuming that the storage could cover the entire cooling load of the display cabinet. The maximum reduction in compressor peak power was 45.2%, 41.8% and 5.7% for layout 1, 3 and 5, respectively. The results for layout 3 is reasonably consistent with the findings reported by Heerup and Green [129], which showed up to 50% reduction in the compressor peak power. Transient numerical modelling of the storage taking into account the heat transfer in the CTES unit, supported by experimental validation of the results, should be further developed.

The largest performance penalty of CO_2 refrigeration system occurs during operation under high ambient temperature conditions, as a consequence of the throttling losses through the high-pressure control valve. Consequently, a centralised storage connected downstream the gas cooler is likely to limit this drawback most effectively. For this reason, layout 5 will not offer any benefits at higher ambient temperature conditions. This configuration will most likely be too costly compared to the achieved reduction in energy consumption (5.7%). Layout 1 and 4 presented in Fig. 4 utilises a secondary HTF circuit to achieve the charging and discharging processes of the storage. To reduce the investment costs and the payback period for the LHS, it could be beneficial to investigate a storage design where the primary refrigerant circulates through the LHS itself, without a secondary HTF circuit. This is believed to reduce the number of additional components and avoid heat transfer across multiple temperature levels via the secondary HTF circuit, thus improving the efficiency of the storage.

3.2.3. PCM integration into beverage coolers and vending machines

PCM cold storage integration into bottle coolers is an interesting application. Introducing CTES in these units could give multiple benefits, such as enabling operation of the cooler independently from the electrical grid, thermal protection of the goods in case of component failure in the refrigeration system or a blackout situation and stabilisation of the product temperature. Extensive research on PCM integration into domestic refrigerators and freezers has been carried out in the past [18,19]. Since the size and structure of bottle coolers and refrigerated vending machines are similar to a domestic refrigerator, some of the reported advantages could be transferable to bottle coolers. A few examples of reported benefits of integrating PCM into the evaporator section of domestic refrigerators are the decreased fluctuation of the air temperature inside the refrigerator and more stable conditions against thermal load variations [18].

Beek and Jong [130] presented a study aiming to develop and build a standard-size 350 dm^3 bottle cooler vending machine integrated with PCM, keeping the bottles at a temperature of 2.5 °C. Water and the paraffin RT4 (melting point 4 °C [90]) was considered as the PCMs in the storage. The main purpose of the storage is to provide the peak cooling

demand during the cooling down of new products when they are placed in the cooler (pull-down load) so that the refrigeration system can be sized for the average refrigeration load rather than the peak load. The novel vending machine is composed of a triple-layer glass door and vacuum insulated panels on the three other sides to reduce the heat transfer and air infiltration from the ambient, thereby reducing the cooling load. The PCM storage consists of three PCM-HEX units located at the rear wall of the cabinet as represented in Fig. 9a. A PCM-HEX is represented in Fig. 9b and consists of a tube-and-plate HEX placed inside a thin metal container. The tube-and-plate HEX consists of copper tubes where the refrigerant circulates, attached to a conducting plate. During the charging process, the PCM storage unit acts as an additional evaporator to the main evaporator located at the bottom of the cabinet. The discharging process takes place during the pull-down load where the fan circulates the cabinet air over the PCM-HEX, while simultaneously all the refrigerant is circulating through the main evaporator to maximise its cooling capacity. The numerical results revealed that using water as the PCM resulted in shorter time required to reduce the product temperature to 2.5 °C during the pull-down period compared to PCM RT4 for all conditions and compressor sizes. Consequently, water was selected as the PCM for the experimental study. The experimental results showed a 77% decrease in the total energy consumption compared to a standard glass door beverage cooler. The PCM integration share was calculated to 4–10%, while the rest was ensured by the cooling load reducing measures such as improved insulation in the walls. Furthermore, integrating the PCM storage allowed for a smaller compressor size to be used in the novel bottler cooler compared to the standard model, increasing the compressor cycle time by 118%.

Ezan et al. [131] numerically investigated the use of water as a latent storage medium to increase the compressor OFF-period in a commercial closed beverage cooler. The bottle cooler and its main components are represented in Fig. 10a. A 3D CFD model was developed in ANSYS FLUENT and validated with experimental results. The PCM storage is displayed in Fig. 10b and consists of a flat container that is attached to the surface of the evaporator which is located at the rear wall of the bottle cooler. The thickness of the PCM container was varied from 2 mm to 10 mm, and the effect on the energy consumption and the thermal stability was compared to a bottle cooler without PCM storage. The integration of a 6 mm thickness PCM storage has revealed a reduction in the ratio of compressor ON to OFF period from 36% to 26% compared to the model without storage. Nevertheless, only the model without storage was experimentally validated. Consequently, there is a need to complete this promising study by experimental validation of the numerical model performed for the case with the storage. The numerical results reveal that the storage was never fully charged, it was partly liquid at the upper part even at the end of the compressor ON period. This indicates that this storage design is sub-optimal, and the PCM-HEX design with integrated refrigerant tubes proposed by Beek and Jong [130] is a better configuration to ensure complete charging of the storage.

Beverage dispensers installed in e.g. catering facilities uses another type of cooling system to serve the beverage at the correct temperature. Some of these beverage coolers have an LHS using water as the storage medium to increase the cooling capacity during hours of high demand for cold beverage. This type of beverage cooler was experimentally investigated by Mađerić et al. [132], and an overview of the system is

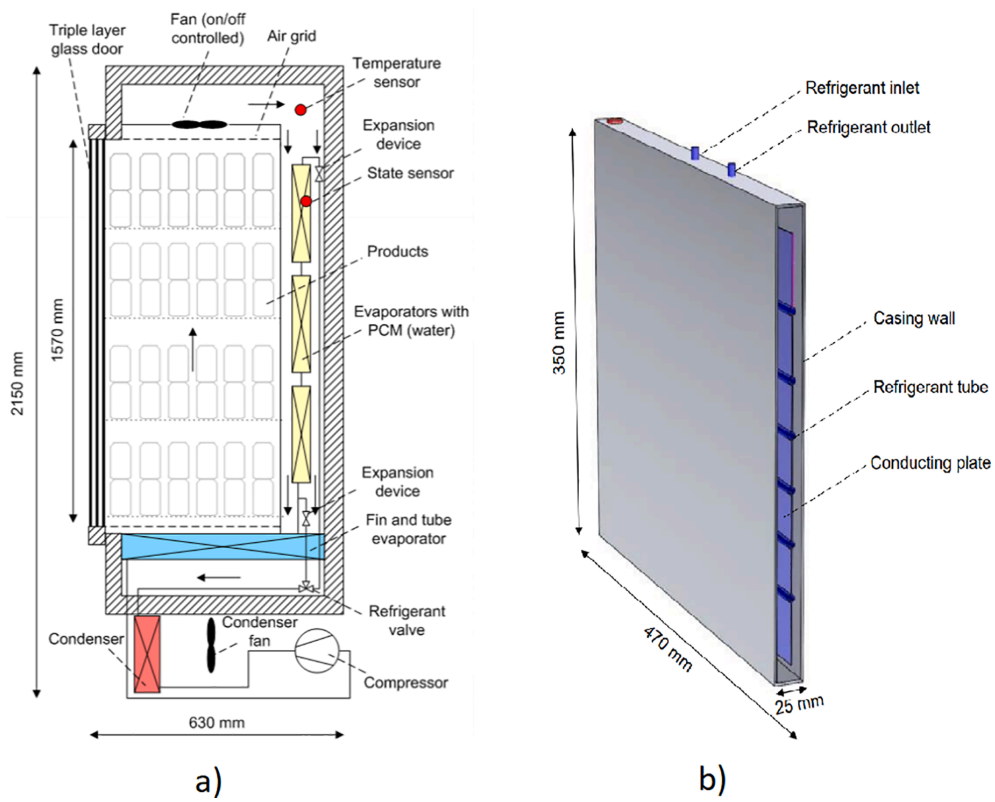

Fig. 9. Beverage cooler vending machine with an integrated PCM evaporator: a) System principle sketch, b) PCM evaporator [130]. Copyrightcopyright IIF/IIR. Published with the authorization of the International Institute of Refrigeration (IIR): www.iifiir.org.

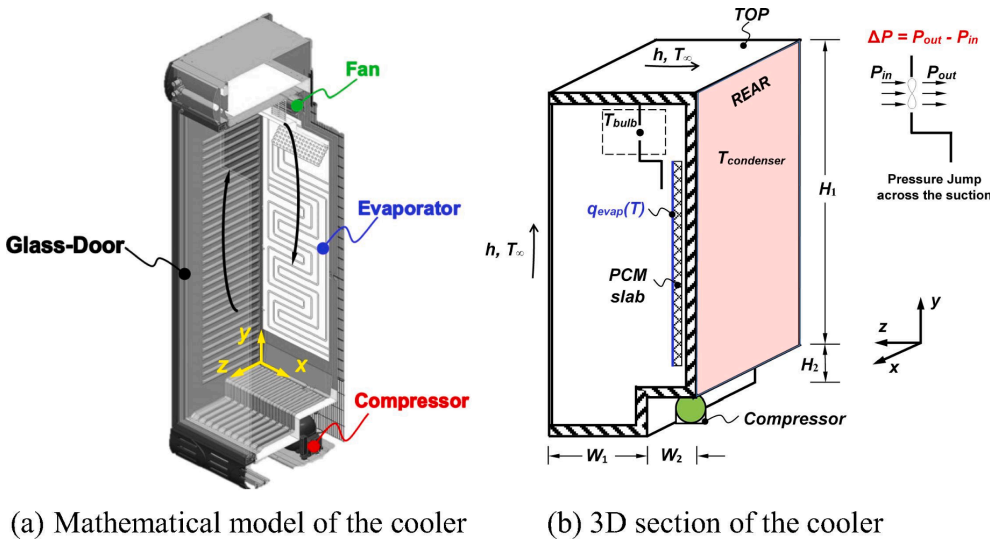

Fig. 10. Beverage cooler vending machine with integrated PCM storage unit: a) Mathematical model of the cooler b) 3D section of the cooler [131]. Reprinted from Energy conversion and management, 142, Ezan, M.A., Doganay, E.O., Yavuz, F.E., Tavman, I.H., A numerical study on the usage of phase change material (PCM) to prolong compressor off period in a beverage cooler, 95–106, Copyright (2017), with permission from Elsevier.

presented in Fig. 11. Referring to Fig. 11, the beverage is first drawn from containers and through tubes by using pressurized CO_2 gas as the driving force. The beverage is then cooled by circulating it inside coils that are immersed in a cold water bath before being served at the dispensing tower. The water bath is cooled by a small refrigeration system. The conventional thermostat in the cold water bath was replaced by an ice bank relay to measure the ice thickness. It was found that compared to using a thermostat-controlled charging and discharging process of the LHS, the energy consumption was reduced by 15%.

3.2.4. Summary and discussion

The results from the reviewed literature on PCM integration in commercial refrigeration applications is presented in Table 6. The common objective of these studies is to determine the optimal design, which results in the appropriate PCM selection to satisfy the cabinet air temperature conditions and limit the temperature fluctuations occurring during the evaporator defrosting periods. The most commonly applied PCM in commercial refrigeration systems was found to be the water/ice solution. The melting temperature of ice satisfies the required temperature conditions for chilled food in the supermarket display cabinets (0 °C to 5 °C. Moreover, water/ice solution is characterized by good heat

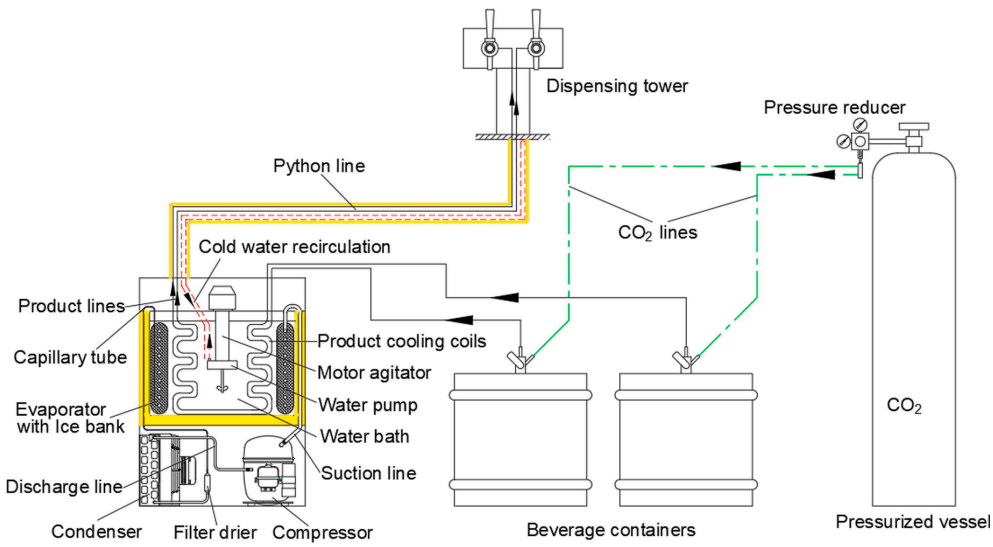

Fig. 11. Beverage cooler for a dispensing tower using a water LHS [132]. Reprinted from Applied Thermal Engineering, 148, Maerić, D., Pavković, B., Lenić, K., An experimental research on energy efficiency of a beverage cooler with the latent heat storage, 270–277, Copyright (2019), with permission from Elsevier.

transfer properties compared to the other commonly used PCM for this type of applications (e.g paraffin-based PCMs). The use of water as a PCM is also safe and non-toxic which preserve food from any damage in case of any leakage. The reviewed literature has shown two different strategies for implementing PCM storage units in the display cabinet: A direct integration into the cabinet shelves or through the installation of a PCM-HEX unit in the main air circulation duct. A PCM-shelf based design in combination with heat pipes was proven to be a performant strategy to reduce product temperature fluctuations (up to 83.3%) [117].

On the other hand, the integration of a PCM-HEX unit in the main air circulation duct of the cabinet was a more popular application over the last 5 years [110,106,120,121,119]. This might be because these PCM-HEX units are more technically feasible, easier to install and requires fewer modifications on the display cabinet itself. In the case of the PCM-shelf design, the shelf will become considerably heavier when including PCM and heat pipes and might require reinforcement of the shelf support. In case of a PCM leakage, the food could be damaged despite using water as the PCM in the shelves. The commonly set performance criteria to evaluate the appropriate display cabinet with an integrated PCM cold storage unit are: Reduction in the energy consumption by up to 5% and reduction in the peak cabinet air temperature during the defrosting period by up to 2 K. There are currently new proposed emerging concepts for PCM-HEX unit designs allowing the display cabinet to be disconnected from the main refrigeration system during the discharging process of the storage [133,121]. These PCM-HEX units can cover the entire refrigeration demand of the cabinet during its discharging process so that each cabinet can operate as a stand-alone unit. Nevertheless, experimental validation needs to be carried out to prove the feasibility of these concepts. Furthermore, the question regarding the optimum location of the PCM-HEX storage in the cabinet remains. This is also a practical matter since the available space to integrate a PCM-HEX unit in the display cabinet is limited, hence restricting the capacity of the storage. Furthermore, a clear description of the control strategy for the discharging process in these emerging concepts is not available to this date.

Although extensive research was carried out on the integration of CTES into the supermarket refrigeration system itself, most of the reported analysis has been limited to analytical approaches only and there is obviously a need for experimental studies to prove the overall system performance and reliability. Investigating a real-scale supermarket refrigeration system at a laboratory level is costly and a complex procedure compared to refrigerated display cabinets and vending machines, although all-in-one CO_2 refrigeration system for supermarkets is explored by Pardiñas et al. [134,135] considering an integrated ice storage into the display cabinets. To the date, few real-scale test facilities are available as this technology should be mature enough to gain more confidence by retail industry and refrigeration system manufacturers. The only way to achieve this goal is to perform more reliable experimental research on this topic. The energy consumption reduction, as well as a lower ON/OFF compressor cycles frequency, are reported to be the main benefits obtained by the PCM cold storage integration into the small commercial refrigeration units. Due to many system and design similarities with domestic refrigerators, where the integration of PCM cold storage has been extensively investigated, more interest should be attributed by the research community in this topic into the development of a new design of bottle coolers and vending machines with an integrated PCM cold storage.

3.3. PCM applications in various refrigeration systems

This section gives an overview of CTES integration into AC chillers systems, refrigerated warehouses and large industrial refrigeration systems. In this section, the refrigeration systems with integrated PCM-CTES are classified into two categories: CTES units integrated into the primary refrigeration circuit based on a PCM/two-phase fluid heat exchange design, and CTES units integrated into the secondary refrigeration circuit based on a PCM/single-phase fluid heat exchange design. The principle of CTES integration for the two categories is illustrated in Fig. 12.

In the first-mentioned category (PCM/two-phase fluid design, Fig. 12a), the CTES unit is directly integrated into the primary refrigerant circuit. During the charging process, the CTES unit acts as an evaporator where the refrigerant extracts heat from the PCM storage unit and evaporates. During the discharging process, the storage acts as a heat sink and the PCM is melting while it absorbs heat from the refrigerant. The refrigerant either condenses or its temperature is decreased, depending on whether the storage is designed to work as a condenser or a subcooler. A simplified refrigeration cycle with a CTES unit integrated as a subcooler is shown in Fig. 12a. In the second category (PCM/single-phase fluid design, Fig. 12b), the storage is integrated into the secondary refrigerant circuit. During the charging process, the temperature of the secondary refrigerant is set below the phase change temperature of the PCM. The temperature of the secondary refrigerant increases as it absorbs heat from the PCM, which solidifies. During the discharging process, the secondary refrigerant is heated by absorbing the refrigeration load. It is cooled down again by circulating it through the storage, which acts as the heat sink. The PCM in the storage is then melting as a result of absorbing the heat from the secondary refrigerant.

A summary of the reviewed literature of the PCM/two-phase fluid design and the PCM/single-phase fluid design are presented in Table 7 and 8, respectively. The presented studies cover CTES integration into AC systems, district cooling systems, refrigerated warehouses, industrial refrigeration systems and low-temperature food processing plants [136–140]. Few researchers report on the overall system performance when integrating a CTES unit into the refrigeration system. It is far more common to evaluate only the performance of the storage itself in terms of efficiency and storage capacity. CTES integration into AC applications has been extensively researched over the last two decades. Large AC systems often apply a secondary refrigerant circuit to reduce the amount of primary refrigerant in the system. For this reason, the majority of the research has been devoted to the development and integration of CTES units based on the PCM/single-phase fluid design. CTES based on the PCM/two-phase fluid design has become increasingly popular over the last five years due to interest of integrating CTES in refrigeration applications without secondary refrigerants. Many promising novel concepts are presented, but still require extensive experimental investigations [141,140]. Technical and economical studies should be carried out to make these systems commercially viable.

3.3.1. PCM-HEX integration into the primary refrigerant circuit

Wang et al. [136] experimentally investigated three possible locations to integrate a shell-and-tube PCM-HEX in the refrigerant cycle of a 5 kW air-to-air AC unit. The alternatives consist of the integration of the PCM-HEX as a pre-condenser located between the compressor and the condenser (Fig. 13a), as a subcooler between the condenser and the expansion valve (Fig. 13b) or as a desuperheater between the evaporator and the compressor (Fig. 13c). In alternative A and B, the PCM-HEX is integrated on the high-temperature side of the refrigeration cycle. For this reason, a eutectic PCM with a melting point of 21 °C is selected so that the storage can passively recharge overnight by releasing the stored heat to the cold ambient air. In alternative C a eutectic PCM with a melting temperature of 8 °C was selected according to the evaporation temperature and superheat of the refrigeration system. The purpose of the PCM-HEX in alternative A is to act as an extra condenser to reduce the condensing pressure of the cycle. For alternative B the purpose of the PCM-HEX is to decrease the liquid refrigerant temperature before the expansion valve, increasing the evaporation capacity. The purpose of the PCM-HEX in alternative C is to reduce the superheat of the refrigerant before entering the compressor.

For alternatives A and B, it was found that the COP was increased by 6 and 8% compared to the system without PCM storage, respectively. No

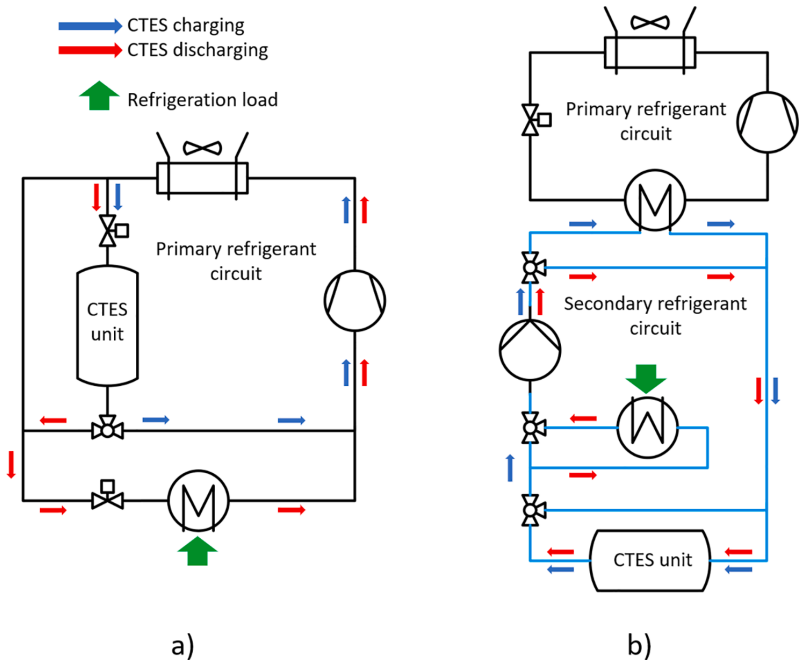

Fig. 12. Strategies of CTES integration in a simplified refrigeration system: a) PCM/two-phase fluid heat exchange, b) PCM/single-phase fluid heat exchange.

Table 7
Main results from application of CTES using PCM/two-phase fluid heat exchange.

Application	Theoretical (T) Experimental (E)	PCM (T_m [°C])	Main result (value)	Reference
Air-to-air heat pump	T/E	No info (8 and 21)	COP increase (6–8%); Stabilize system fluctuations	[136,142,143]
Tube-in-tank CTES for multi-split AC	E	RT28HC (28)	Mean cooling duty discharge of CTES (1.5 kW)	[146]
Tube-in-tank subcooler for multi-split AC	T/E	Parafol 16–97/ graphite mixture (18)	Evaporation capacity increase during discharge (18%); Evaporation capacity increase in high ambient temperature (40%)	[144]
CTES for industrial CO_2/NH_3 cascade	T	Water/ice (0); Adblue (-11)	Peak load reduction (19%)	[141,147]
PCM plates in refrigerated warehouse	T	Water/ice (0)	Even discharge of cold energy; Reasonable payback time (2.6 years)	[138]
CTES for low-temperature freezing processes	T	CO_2 /dry ice (below −50)	Reduced electricity consumption for the same capacity (30%)	[148]
CTES for low-temperature fish freezing process	T	CO_2 /dry ice (−57)	Reduced fish freezing time (3.2%)	[140]

Table 8
Main results from applications utilising PCM/single-phase fluid heat exchange.

Application	Theoretical (T) Experimental (E)	PCM (T_m [°C])	Main contribution (value)	Reference
Coil-in-tank CTES with 8 kW chiller	E	RT8 (8)	High storage capacity in tank (40 kWh); Highest COP for low HTF supply temperature	[161]
CTES tank with 4.2 kW chiller	E	S10 salt hydrate (10)	Storage capacity enhancement compared to water SHS (35.5%)	[165]
CTES tank with 15 kW chiller	E	RT15 MPCM 45% suspension (15)	Storage capacity enhancement compared to water SHS (53%)	[8]
District cooling system with storage	T	Water/ice (0)	Annual energy savings (0 to 4%); Long payback time (22 to 30 years)	[137]
PCM-HEX and AC system	T	Calcium chloride hexahydrate (29)	COP of the combined system (3.07); PCM-HEX show lowest relative irreversibility (6.0%)	[167]
CTES tank with 2000 kW chiller	T	Water/ice (0); RT3HC (3)	Exergy efficiency highest for PCM system (53.44%); Reduced power consumption using PCM (7.58%)	[168]
CTES tank for AC in hypermarket	T	Water/ice (0)	Short payback times (1.5–3.1 years); Highest cost savings for full storage scenario (1.45 mill USD)	[169]

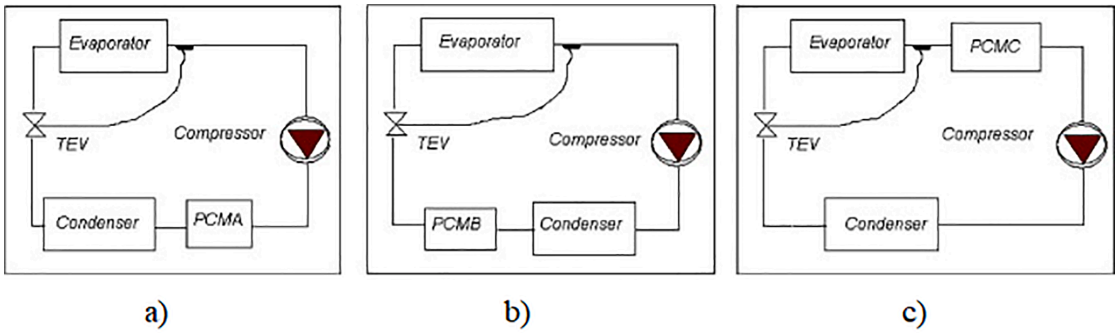

Fig. 13. Different integration scenarios of a PCM-HEX in a refrigeration system: a) Pre-condenser b) Subcooler c) Desuperheater [136]. Reprinted from Applied Thermal Engineering, 27, Wang, F., Maidment, G., Missenden, J., Tozer, R., The novel use of phase change materials in refrigeration plant. Part 1: Experimental investigation, 2893–2901, Copyright (2007), with permission from Elsevier.

improvement in COP was observed for alternative C. The performance benefit of reduced refrigerant superheat provided by the PCM-HEX was counteracted by the effect of an increased pressure drop in the suction line caused by the PCM-HEX. The potential energy savings for UK climatic conditions were obtained by numerical optimisation of the system. It was shown that alternative B provided the highest improvement in COP (8%) for the UK climate [142,143]. Alternatives A and C were found to be beneficial for the system stabilization by lowering the condenser pressure and reducing the peak inlet temperature to the compressor, respectively.

Similarly, Korth et al. [144] carried out theoretical modelling and experimental tests of a tube-in-tank LHS with paraffin Parafol 16–97 as a PCM [145] having a melting point of 18 °C. The objective of the storage was to increase the peak refrigeration capacity by acting as a subcooler integrated after the condenser in a 6 kW AC system. The experimental results have shown an increase in the evaporation capacity of 18% for a condensing temperature of 35 °C. A PCM-HEX integrated into a multi-split AC system has been investigated by Korth et al. [146]. The selected PCM was paraffin RT28HC [90] and integrated into a tube-in-tank storage unit. The CTES unit was operating in parallel with the evaporators during the charging process, and in series between two evaporators during the discharging process (see Fig. 14). The refrigerant condenses through the CTES unit and reduces the load on the compressor. The experimental results have shown that the storage could achieve a mean cooling capacity of 1.5 kW for 2.33 h with 3–4 K temperature difference during discharge. The main benefits of integrating a PCM-HEX unit are proven, but the system performance needs to be further investigated when implemented into a real scale AC system, and an associated control strategy should be established.

Selvnes et al. [139] have proposed a novel design of a CTES unit to be integrated into a pumped CO_2 circuit of an industrial NH_3/CO_2 cascade refrigeration system for a poultry processing plant. The unit is integrated into the return line of the −5 °C evaporation temperature level. The main aim of the unit is to achieve peak shaving of the refrigeration load during high-demand hours while using low-cost electricity to charge the CTES unit during the night. The experimental prototype of the CTES unit is shown in Fig. 15. It consists of a stack of pillow plates shown in Fig. 15b, immersed into a container filled with PCM. The selection of the PCM was based on the application temperature range (Condensing temperature of CO_2 at −5 °C) and consists of paraffin RT-9HC [90]. The pillow plates consist of two metal plates that are welded together in a pattern of spot welds and seam-welded at the edges. The plate is inflated by applying high pressure on the inside, creating flow channels for the refrigerant. The CO_2 circulates through the plate and the flow is directed by the path created by the spot welds while exchanging heat with the PCM. A 2D CFD model of the previously described CTES unit was developed using the Ansys Fluent software [147]. In the numerical analysis, water was selected as the PCM due to lack of temperature-dependent thermophysical data for the PCM RT-9HC. The results revealed that the current version of the software was unable to handle the buoyancy-induced movement of solid PCM in the liquid PCM. The discharging time was found sensitive to the value of a modelling

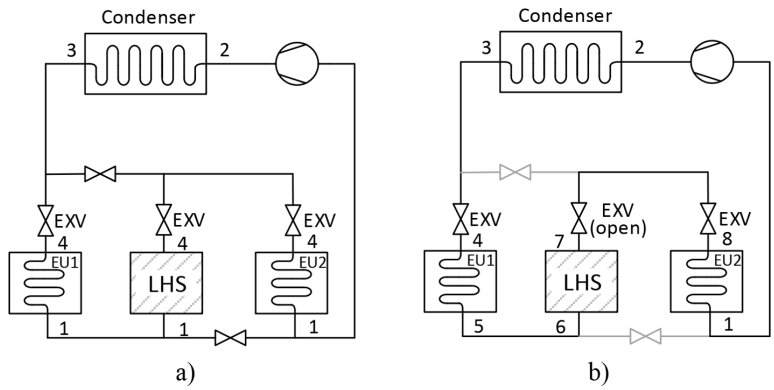

Fig. 14. PCM-HEX integrated into a multi-split AC system: a) Charging of the PCM-HEX b) Discharging of the PCM-HEX [146]. Copyright ©IIF/IIR. Published with the authorization of the International Institute of Refrigeration (IIR): www.iifiir.org.

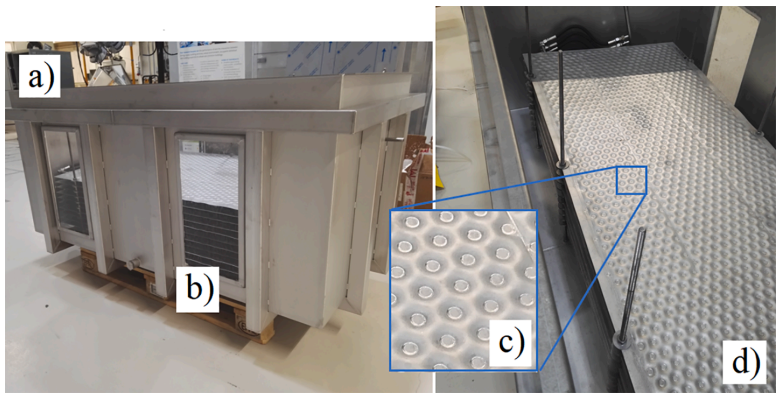

Fig. 15. Prototype CTES unit for a CO_2 refrigeration system: a) CTES unit before assembly b) PCM integration between the pillow plates c) Spot welds to direct the CO_2 flow d) Pillow plate HEX [139]. Copyright ©IIF/IIR. Published with the authorization of the International Institute of Refrigeration (IIR): www.iifiir.org.

constant used in the enthalpy-porosity method for melting/solidification in the software. Experimental investigations are currently being performed to complete this study. The total storage capacity of the CTES unit was found to be about 108 kWh. Selvnes et al. [141] developed a numerical model of the previously reported CTES unit with an increased capacity using Dymola software. The CTES unit was integrated into the −5 °C evaporation level of a pumped CO_2 refrigeration system. The main goal was to achieve peak shaving of the compressor power consumption by condensing the refrigerant through the storage during the discharging process. The system performance has revealed a reduction in the compressor peak power consumption of 19%. The model validations will soon be published by the authors of this review.

Yang et al. [138] proposed to implement PCM panels into a refrigerated warehouse along the walls and ceiling. The PCM panel consists of a tube-in-plate PCM-HEX. The refrigerant circulates inside the tubes to ensure the charging process of the PCM storage during the compressor ON periods. The refrigerated room is passively cooled by the PCM panels when they exchange the heat from the air during compressor OFF periods. The objective of the storage system was to benefit from a peak-valley electric pricing scheme by shifting the refrigeration load. Water was used as the storage medium. The system performance was numerically studied using Ansys Fluent software. A 3D CFD model of a refrigerated room was performed. It was found that PCM panels limited the increase in maximum air temperature to 2 K during the compressor OFF period. The payback time was calculated to be about 2.6 years. The model was not assuming the ambient heat transfer to the warehouse, therefore a complete numerical modelling taking into consideration the air infiltration should enhance the system performance predictions.

Other CTES concepts using solid CO_2 (dry ice) as the storage medium have been proposed. This technique is generally used for storage temperatures below −40 °C. Hafner et al. [148] numerically investigated a shell-and-tube HEX with dry ice as the storage medium. Referring to Fig. 16, the CTES unit was integrated into an NH_3/CO_2 cascade refrigeration system connected to a tunnel freezer for freezing of fish (Air temperature −30 °C). During the charging process, the CO_2 on the tube side sublimates while cooling the CO_2 on the shell side until solidification. During the discharging process, the dry ice on the shell side cools down and condenses the CO_2 gas on the tube side. Up to 30% energy savings were calculated for the same freezing capacity when applying the novel CTES design.

The same concept using a shell-and-tube PCM-HEX with dry ice was numerically studied by Verpe et al. [140]. It was integrated into a CO_2 refrigeration system for a plate freezer in a fishing vessel (CO_2 evaporation temperature down to −50 °C). The study indicates a reduction in the fish freezing time by 3.2% when integrating the storage into the

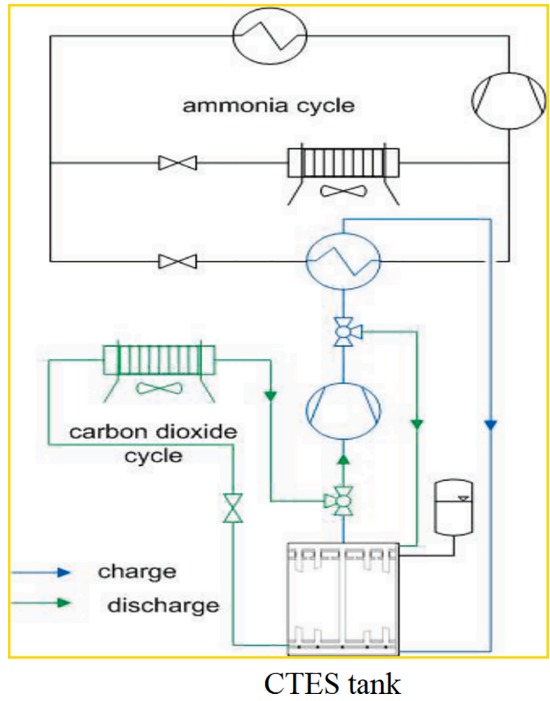

Fig. 16. CTES unit with dry ice as the storage medium in an NH_3/CO_2 cascade refrigeration system [148]. Reprinted from Procedia Food Science, 1, Hafner, A., Nordtvedt, T.S., Rumpf, I., Energy saving potential in freezing applications by applying cold thermal energy storage with solid carbondioxide, 448–454, Copyright (2011), with permission from Elsevier.

system. These findings suggest that dry ice can be an interesting option for energy savings in applications that require storage under −40 °C. Few other alternative PCMs are available below this temperature (see Table 4). However, there is very limited research on the behaviour of CO_2 during phase transition around the triple point [148]. More experimental research related to heat transfer of dry ice has to be carried out.

3.3.2. PCM-HEX integration into the secondary refrigerant circuit

Integration of CTES into the secondary refrigerant circuit of a refrigeration cycle has been an important research topic for two decades. Significant efforts were dedicated to improving the efficiency of CTES units that can be integrated into large capacity refrigeration systems through the secondary refrigerant circuit (Storage capacity up to 96 kWh [149]). Cylindrical tanks that are filled with macro-encapsulated water (e.g. spheres and small capsules) as the PCM has been a popular CTES configuration over the last 20 years [150–153,149]. In this configuration, the secondary refrigerant flows through the tank to exchange heat with the PCM capsules. Two commonly proposed CTES designs integrated into the secondary refrigerant circuit are the coil-in-tank (Fig. 17) and tube-in-tank designs (Fig. 18) [154–163]. The concept consists of one or multiple coils/tubes that are immersed into the PCM storage tank. The secondary refrigerant flows inside the tubes and exchanges heat with the surrounding PCM to ensure both the charging and the discharging processes.

The performance of a commercial coil-in-tank filled with 1450 kg of the paraffin PCM RT8 [90] was experimentally investigated by Torregrosa-Jaime et al. [161]. The CTES tank was connected to an 8 kW chiller by a secondary refrigerant circuit. The highest system COP during charging was obtained for the lowest refrigerant supply temperature (1 °C) and lowest refrigerant mass flow (1980 kg h^{-1}). It was also found that 40 kWh could be stored in the CTES tank after 6.5 h of charging.

Moreno et al. [165] compared the performance of an SHS tank using water as the storage medium and an LHS tank filled with macro-encapsulated S10 PCM [166]. The CTES tanks were connected to a 4.2 kW water-to-water heat pump for space cooling and heating of a small house. The experimental results demonstrated that the cold energy storage was enhanced by 35.5% when using the PCM as a storage medium. The charging process of the PCM tank was 4.55 times longer than for the SHS water tank. An experimental study of a tube-in-tank CTES integrated into the HTF circuit of a 15 kW AC chiller unit was presented by Allouche et al. [8]. A comparison between SHS and LHS was carried out using water and an MPCM paraffin suspension (45% concentration of RT15 [90]) in the tank, respectively. After 10 h of charging, it was found that the cold storage capacity was enhanced by 46.6% when using the PCM as a storage medium.

Recent theoretical studies on CTES integration in HTF circuits have focused on energy consumption and performance of the total system, exergy analysis and techno-economical calculations [167–169]. Mosaffa et al. [167] carried out a theoretical analysis of a refrigeration system and a CTES-HEX for an AC system of a building. The proposed design included a PCM-HEX which consists of PCM slabs installed in the main air duct of the ventilation system. The numerical analysis and evaluation of the thermal performance were carried out using COMSOL Multiphysics and EES software. A COP of 3.07 is calculated for the refrigeration system with CTES. The exergy analysis revealed that the CTES unit has the lowest relative irreversibility of all the components in the system with 6.0%. Rahdar et al. [168] made an exergetic, economic and environmental comparison between a standard 2000 kW AC chiller without storage, a chiller integrated with an ice-CTES and a chiller integrated with a PCM-CTES. Using multi-objective optimisation, the highest exergetic efficiency of 53.4% was reported for the PCM-CTES system. The annual energy consumption was reduced by 7.58% and 4.59% compared to the standard chiller for the PCM-CTES and ice-CTES, respectively. Due to higher investment costs of the PCM-CTES, the payback time was found to be shortest for the ice-CTES with 3.16 years. A techno-economical study of integrating a CTES tank into the AC system for a hypermarket was carried out by Erdemir and Altuntop [169]. Encapsulated ice/water was chosen as the PCM, and weather data from Turkey was used to calculate the peak cooling loads. The research considered the investment and operational costs to calculate the payback period and cost savings after ten years. Sizing strategies of the CTES from 10% partial storage to full storage was investigated. The shortest payback period was found for load levelling and 10 % partial storage with about 1.5 years. However, the highest cost savings were obtained by the full storage scenario with a total saving of 1.45 mill USD and a payback time of about 3.1 years.

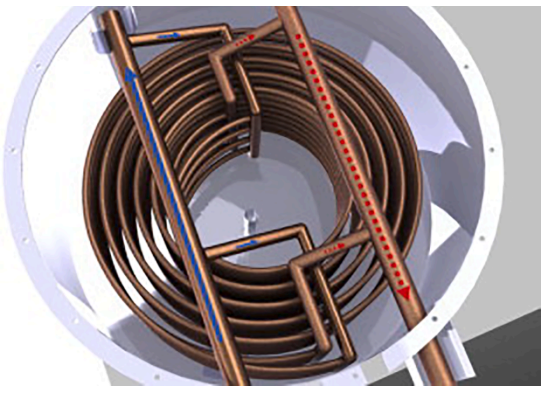

Fig. 17. Coil-in-tank CTES design [162]. Reprinted from Applied Energy, 119, López-Navarro, A., Biosca-Taronger, J., Corberán, J.M., Peñalosa, C., Lázaro, A., Dolado, P., Payá, J., Performance characterization of a PCM storage tank, 151–162, Copyright (2014), with permission from Elsevier.

A district cooling system is a large-scale cold energy production facility that can serve the cooling demand of multiple buildings. Integration of ice-CTES in this type of cooling system was theoretically investigated by Chan et al. [137] using TRNSYS software and compared to a chiller without storage. The results from several case studies have revealed that the annual cost savings range from 0% to 4% under different Chinese electricity tariff structures. The district cooling system with storage had about 30% higher investment cost compared to the standard system. The payback time of the system was calculated to be from 22 to 30 years and was found to be economically non-viable.

3.3.3. Summary and discussion

A summary of the reviewed literature utilising a PCM/two-phase fluid heat exchange and PCM/single-phase fluid heat exchange is given in Table 7 and 8, respectively. It can be clearly seen that the integration of CTES has been considered in various applications of the large industry (e.g. Industrial refrigeration, large AC installations, district cooling). LHS integration into AC application has been a key research area for more than two decades due to several aspects. First, the current share of AC in the peak electricity load for developed countries (e.g. The United States) can be up to 30% [4]. This share is predicted to rise sharply in certain hot-climate regions towards 2050 (E.g. from 10% to over 40% in India). Second, the number of AC units is growing and was estimated to be more than 1.6 billion units worldwide in 2016 [4]. Lastly, water as an available and affordable PCM storage medium has encouraged researches to dedicate significant efforts in developing efficient CTES units for integration into AC systems. Systems using a PCM/two-phase fluid heat exchange have also been a hot topic over the last few years. As it can be depicted in Table 7, these systems have been mainly applied into AC systems and low-temperature food processing plants. The reported benefits of CTES implementation in these systems are: The increased evaporator capacity for AC plants [144], a reduced peak load consumption [141,148] and a reduction in product freezing time for batch processes [140]. The concepts using PCM/two-phase fluid heat exchange were found to be promising due to the elimination of the secondary refrigerant circuit. This can reduce the overall cost of the storage system, especially for refrigeration systems where the ordinary refrigeration load is satisfied directly with the primary refrigerant. This concept allows the evaporation temperature of the primary refrigeration system to be increased during the charging process of the CTES, increasing the efficiency compared to using a secondary refrigerant

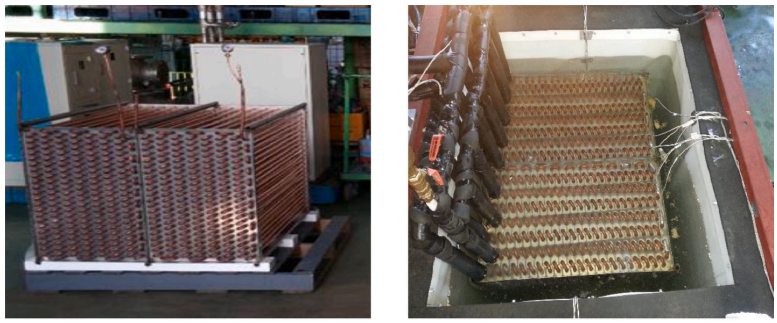

(a) (b)

Fig. 18. Tube-in-tank CTES design a) tube bundle b) finished CTES unit filled with water [164]. Reprinted from Energy and Buildings, 183, Abhishek, A., Kumar, B., Kim, M.H., Lee, Y.T., Chung, J.D., Kim, S.T., Kim,T., Lee, C., Lee, K., Comparison of the performance of ice-on-coil LTES tanks with horizontal and vertical tubes, 45–53, Copyright (2019), with permission from Elsevier.

system [146]. Several novel PCM-HEX designs were proposed, but many of them lack experimental validation to prove the performance of the storage units [147,139,140].

Looking at Table 8 one may note that the systems using a PCM/single-phase fluid heat exchange presented in this review only employ PCMs with a melting temperature above 0 °C. The reported benefits of integrating CTES in the secondary refrigerant circuit of a refrigeration system are: Avoiding part-load operation of the chiller [152], reduced operational costs [167–169] and peak load shifting [168]. The most commonly studied application for CTES integration is AC systems, where water/ice is frequently used as the PCM.

Significant research effort has been devoted to developing CTES units to be integrated into the secondary refrigerant circuit of refrigeration systems. CTES tanks with encapsulated water as the PCM have been extensively studied over the last two decades. The tube-in-tank and coil-in-tank designs have gained more attention over the last five to ten years, due to compact design and low cost. Most of these studies investigated the effect of the secondary refrigerant supply temperature and mass flow rate on the performance of the charging and discharging processes of the CTES unit. The storage capacity of the tested CTES units ranges from a few kWh up to around 40 kWh. To the authors best knowledge, the reported study by Torregrosa-Jaime et al.[161] is the highest amount which was experimentally tested for CTES applications (1450 kg and 40 kWh). Many real-life applications, such as industrial process plants and AC systems, require significant storage capacities to achieve peak shaving. Hence, experimental characterisation of larger lab-scale and prototype CTES units is a key factor to raise the attention on the application of cold storage into these refrigeration systems. For both PCM/two-phase fluid and PCM/single-phase fluid CTES units, there is a lack of detailed numerical modelling research, probably due to limited experimental data to validate the models.

4. Conclusions

This review aims to provide a solid background to the reader about the possible ways of implementation of CTES using PCM in various refrigeration systems. The focus of the review was to establish a state of the art on the PCM integration as cold storage application into refrigeration systems in food transport and packaging, commercial refrigeration, large scale industrial applications and various other refrigeration systems. A brief overview of the different types of PCMs was first given. A brief presentation including the most important material properties as well as their appropriate characterization methods was then given. The main findings from the literature are summarized as follows:

- There are mainly three different ways to integrate PCMs in food transport and packaging applications; PCM integration within the walls of the refrigerated vehicles, into the product container, or the installation of an active CTES system to replace the commonly used diesel-driven refrigeration system in the vehicle. Important research efforts have been dedicated to the development of multi-layer walls with PCM for refrigerated vehicles. The efficiency of this technique was proven by limiting peak heat flux from the external environment up to 29%. It was shown that PCMs integration into food packaging can provide better thermal protection than standard packaging during a breach in the cold chain.
- Two strategies to integrate PCM storage units in supermarket display cabinets are commonly investigated: In the product shelf or by implementing a PCM-HEX in the main air duct. The reported benefits of CTES integration are: The reduced and stabilized cabinet air temperature during the defrosting process, energy savings and product temperature reduction. Water/ice is frequently used as the storage medium in these applications. It should be highlighted that the integration of PCM-CTES into the supermarket refrigeration system has only been studied at a theoretical level using simplified models of the storage. Nevertheless, the studies show that CTES implementation is a promising technique as it allows for a peak shaving and a reduced compressor peak power consumption in supermarket refrigeration systems.
- The implementation of CTES in AC systems has been a hot topic over the last two decades. Significant research effort has been dedicated to developing performant CTES units. The use of encapsulated water as the latent storage medium have been frequently studied. The coil-in-tank and tube-in-tank designs have become very popular during the last ten years, offering a more compact and flexible design. One may distinguish two strategies to achieve an efficient heat transfer process between the refrigeration system and the CTES unit. The first method consists of integrating the PCM-CTES unit in the secondary refrigeration circuit commonly found in AC chiller systems (glycol/brine/water). The reported benefits of this strategy are: Reduced part-load operation of the chiller, reduced energy consumption and an increased storage capacity compared to SHS units. The second strategy found in literature is the direct integration of the CTES into the primary refrigerant circuit using a PCM-refrigerant heat exchange system. This integration strategy is commonly applied in refrigerated warehouses, AC systems and low-temperature food processing plants. Moreover, promising theoretical concepts were also found in the literature, such as using dry ice as the storage medium for low-temperature storage under −40 °C.

5. Recommendations for future investigations

From the summary carried out in the previous section, it is clear that the implementation of CTES technology provides many benefits to key parts of the food cold chain including processing plants, transport and packaging, cold storage facilities and supermarket refrigeration. The intensive research activities performed on PCMs and their integration into refrigeration over the last decade has promoted their utilization at a commercial level. However, various aspects still need further investigations in order to provide commercially viable cold storage techniques and improve their competitiveness. Some of them are presented as follows:

For CTES applications in food transport and packaging:

- The effect of combining different melting temperatures and the location of the PCM layer in the walls of refrigerated vehicles both need to be further investigated. The concept of copper pipes filled with PCM has demonstrated the highest heat transfer reductions, although most researchers have focused on including a PCM layer into the wall. Due to the limited research on this topic, the optimal combination is still not clear. Furthermore, a techno-economic evaluation of the different PCM wall configurations in comparison with a standard insulation wall would provide knowledge on the economic competitiveness of this concept.
- More experimental investigations should be carried out comparing PCM packaging and standard packaging using real temperature conditions experienced in the cold chain, i.e. by field tests or by replicating temperature profiles which have been obtained by measurements in actual transport routes. Further investigations should be performed to determine if the PCM packaging could provide a sufficient thermal buffer to replace the need for the on-board refrigeration system for typical transport routes in the cold chain. Moreover, the experience gained from the research carried out on PCM food packaging should be further applied to develop packaging for temperature-sensitive medical goods. This can ensure safe transport and delivery of goods in locations with limited access to electricity and refrigeration.
- Further development and experimental validation of the active CTES system are needed to replace the diesel-driven refrigeration system in refrigerated vehicles presented by Liu et al. [99]. This novel concept supports a phase-out of a conventional technology associated with significant CO_2 emissions and local pollution. Future research within this topic should include evaluation of energy and emission reductions in various climate conditions and extending the concept from frozen transport (−18 °C) to refrigerated transport (2 °C to 5 °C). Moreover, a detailed infrastructure for the charging of the PCM-HEX at the warehouse still needs to be developed.

For PCM applications in commercial refrigeration, future research should focus on:

- A proper design and a suitable integration scenario of the PCM-HEX unit into supermarket display cabinets are still challenging. Further developments should focus on the experimental validation of PCM-HEX units taking advantage of the available space in the display cabinets, e.g. on top of the cabinet.
- The development and experimental validation of PCM-HEX units that can be integrated into the supermarket refrigeration system to support the promising results from current analytical studies. Important tasks that need to be addressed are the design of the PCM-HEX unit, selection of the appropriate PCM, location for integration and capacity sizing.

For PCM applications in various other refrigeration systems, more research is required addressing the following aspects:

- More advanced research for the integration of CTES into multi-split and single AC units to achieve peak shaving, e.g. the concept presented by Korth et al. [146]. Due to the expected growth in the AC market worldwide in the coming years, future research needs to be focused on the total equivalent warming impact (TEWI) of refrigerants used in these units and introducing flexibility by CTES integration to avoid significant peak loads on the grid.
- Promising novel concepts applying a PCM/two-phase fluid heat exchange are emerging, but experimental validation needs to be carried out to prove the performance of these PCM-HEX units [139,147]. Increased focus on the development and testing of larger lab-scale and prototype CTES units, both for PCM/two-phase fluid and PCM/single-phase fluid heat exchange, is a key factor to encourage manufacturers considering this novel technology for a real scale industrial application.
- The use of the CO_2/dry ice as the storage material for CTES applications below −40 °C is promising, but a practical HEX design and pressure control of the system represent the main limitation of this technique [140,148].

Declaration of Competing Interest

The authors declare that they have no known competing financial interests or personal relationships that could have appeared to influence the work reported in this paper.

Acknowledgements

The work is part of HighEFF - Centre for an Energy Efficient and Competitive Industry for the Future, an 8-year Research Centre under the FME-scheme (Centre for Environment-friendly Energy Research, 257632). The first author gratefully acknowledges the financial support from the Research Council of Norway and user partners of HighEFF.

References

[1] International Energy Agency, Energy Efficiency 2018: Analysis and outlooks to 2040, IEA Publications, 2018a.
[2] W. Su, H. Eichi, W. Zeng, M.-Y. Chow, A survey on the electrification of transportation in a smart grid environment, IEEE Trans. Industr. Inf. 8 (1) (2011) 1–10.
[3] S. Lechtenböhmer, L.J. Nilsson, M. Åhman, C. Schneider, Decarbonising the energy intensive basic materials industry through electrification–Implications for future EU electricity demand, Energy 115 (2016) 1623–1631.
[4] International Energy Agency, The Future of Cooling: Opportunities for energy-efficient air conditioning, IEA Publications, 2018b.
[5] I. Dincer, M. Rosen, Thermal energy storage: systems and applications, John Wiley & Sons, 2002.
[6] P. Arce, M. Medrano, A. Gil, E. Oró, L.F. Cabeza, Overview of thermal energy storage (TES) potential energy savings and climate change mitigation in Spain and Europe, Appl. Energy 88 (8) (2011) 2764–2774.
[7] H. Mehling, L.F. Cabeza, Heat and cold storage with PCM, vol. 308, Springer, 2008.
[8] Y. Allouche, S. Varga, C. Bouden, A.C. Oliveira, Experimental determination of the heat transfer and cold storage characteristics of a microencapsulated phase change material in a horizontal tank, Energy Convers. Manage. 94 (2015) 275–285.
[9] F. Kuznik, D. David, K. Johannes, J.-J. Roux, A review on phase change materials integrated in building walls, Renew. Sustain. Energy Rev. 15 (1) (2011) 379–391.
[10] L.F. Cabeza, A. Castell, C. Barreneche, A. De Gracia, A. Fernández, Materials used as PCM in thermal energy storage in buildings: a review, Renew. Sustain. Energy Rev. 15 (3) (2011) 1675–1695.
[11] R. Baetens, B.P. Jelle, A. Gustavsen, Phase change materials for building applications: a state-of-the-art review, Energy Buildings 42 (9) (2010) 1361–1368.
[12] D. Zhou, C.-Y. Zhao, Y. Tian, Review on thermal energy storage with phase change materials (PCMs) in building applications, Appl. Energy 92 (2012) 593–605.
[13] M. Song, F. Niu, N. Mao, Y. Hu, S. Deng, Review on building energy performance improvement using phase change materials, Energy Buildings 158 (2018) 776–793.
[14] A. Crespo, C. Barreneche, M. Ibarra, W. Platzer, Latent thermal energy storage for solar process heat applications at medium-high temperatures–A review, Sol. Energy 192 (2019) 3–34.

[15] B. Xu, P. Li, C. Chan, Application of phase change materials for thermal energy storage in concentrated solar thermal power plants: a review to recent developments, Appl. Energy 160 (2015) 286–307.
[16] E. Oró, A. De Gracia, A. Castell, M. Farid, L. Cabeza, Review on phase change materials (PCMs) for cold thermal energy storage applications, Appl. Energy 99 (2012) 513–533.
[17] G. Li, Y. Hwang, R. Radermacher, H.-H. Chun, Review of cold storage materials for subzero applications, Energy 51 (2013) 1–17.
[18] M.M. Joybari, F. Haghighat, J. Moffat, P. Sra, Heat and cold storage using phase change materials in domestic refrigeration systems: The state-of-the-art review, Energy Buildings 106 (2015) 111–124.
[19] S. Bista, S.E. Hosseini, E. Owens, G. Phillips, Performance improvement and energy consumption reduction in refrigeration systems using phase change material (PCM), Appl. Therm. Eng. 142 (2018) 723–735.
[20] P. Moreno, C. Solé, A. Castell, L.F. Cabeza, The use of phase change materials in domestic heat pump and air-conditioning systems for short term storage: A review, Renewable and Sustainable Energy Rev. 39 (2014) 1–13.
[21] A. Sharma, V.V. Tyagi, C. Chen, D. Buddhi, Review on thermal energy storage with phase change materials and applications, Renew. Sustainable Energy Rev. 13 (2) (2009) 318–345.
[22] T. Silva, R. Vicente, F. Rodrigues, Literature review on the use of phase change materials in glazing and shading solutions, Renew. Sustain. Energy Rev. 53 (2016) 515–535.
[23] C. Amaral, R. Vicente, P. Marques, A. Barros-Timmons, Phase change materials and carbon nanostructures for thermal energy storage: A literature review, Renew. Sustain. Energy Rev. 79 (2017) 1212–1228.
[24] C. Zeng, S. Liu, A. Shukla, Adaptability research on phase change materials based technologies in China, Renew. Sustain. Energy Rev. 73 (2017) 145–158.
[25] M.A. Wahid, S.E. Hosseini, H.M. Hussen, H.J. Akeiber, S.N. Saud, A. T. Mohammad, An overview of phase change materials for construction architecture thermal management in hot and dry climate region, Appl. Therm. Eng. 112 (2017) 1240–1259.
[26] B. Zalba, J.M. Marın, L.F. Cabeza, H. Mehling, Review on thermal energy storage with phase change: materials, heat transfer analysis and applications, Appl. Thermal Eng. 23 (3) (2003) 251–283.
[27] H. Kumano, T. Asaoka, A. Saito, S. Okawa, Study on latent heat of fusion of ice in aqueous solutions, Int. J. Refrigeration 30 (2) (2007) 267–273.
[28] A. Abhat, Low temperature latent heat thermal energy storage: heat storage materials, Solar Energy 30 (4) (1983) 313–332.
[29] H. Nazir, M. Batool, F.J.B. Osorio, M. Isaza-Ruiz, X. Xu, K. Vignarooban, P. Phelan, A.M. Kannan, et al., Recent developments in phase change materials for energy storage applications: A review, Int. J. Heat Mass Transf. 129 (2019) 491–523.
[30] C. Castellón, E. Günther, H. Mehling, S. Hiebler, L.F. Cabeza, Determination of the enthalpy of PCM as a function of temperature using a heat-flux DSC–A study of different measurement procedures and their accuracy, Int. J. Energy Res. 32 (13) (2008) 1258–1265.
[31] C. Barreneche, A. Solé, L. Miró, I. Martorell, A.I. Fernández, L.F. Cabeza, Study on differential scanning calorimetry analysis with two operation modes and organic and inorganic phase change material (PCM), Thermochim. Acta 553 (2013) 23–26.
[32] A. Lazaro, C. Peñalosa, A. Solé, G. Diarce, T. Haussmann, M. Fois, B. Zalba, S. Gshwander, L.F. Cabeza, Intercomparative tests on phase change materials characterisation with differential scanning calorimeter, Appl. Energy 109 (2013) 415–420.
[33] G. Feng, K. Huang, H. Xie, H. Li, X. Liu, S. Liu, C. Cao, DSC test error of phase change material (PCM) and its influence on the simulation of the PCM floor, Renewable Energy 87 (2016) 1148–1153.
[34] H. Mehling, C. Barreneche, A. Solé, L.F. Cabeza, The connection between the heat storage capability of PCM as a material property and their performance in real scale applications, J. Energy Storage 13 (2017) 35–39.
[35] G. Ferrer, C. Barreneche, A. Solé, I. Martorell, L.F. Cabeza, New proposed methodology for specific heat capacity determination of materials for thermal energy storage (TES) by DSC, J. Energy Storage 11 (2017) 1–6.
[36] A. Frazzica, Recent Advancements in Materials and Systems for Thermal Energy Storage, Springer, 2018.
[37] W. Parker, R. Jenkins, C. Butler, G. Abbott, Flash method of determining thermal diffusivity, heat capacity, and thermal conductivity, J. Appl. Phys. 32 (9) (1961) 1679–1684.
[38] W.N. dos Santos, P. Mummery, A. Wallwork, Thermal diffusivity of polymers by the laser flash technique, Polym. Test. 24 (5) (2005) 628–634.
[39] J. Healy, J. De Groot, J. Kestin, The theory of the transient hot-wire method for measuring thermal conductivity, Physica B+ c 82 (2) (1976) 392–408.
[40] F. Frusteri, V. Leonardi, S. Vasta, G. Restuccia, Thermal conductivity measurement of a PCM based storage system containing carbon fibers, Appl. Thermal Eng. 25 (11–12) (2005) 1623–1633.
[41] S.E. Gustafsson, Transient plane source techniques for thermal conductivity and thermal diffusivity measurements of solid materials, Rev. Sci. Instruments 62 (3) (1991) 797–804.
[42] D. Cederkrantz, Measuring the thermal conductivity of PCMs - Dos and Don'ts, in: Book of extended abstracts and posters. Seminar PCMs4Buildings – PCMs: Thermophysical characterization and buildings' applications, Coimbra, Portugal, ADAI, 2018.
[43] S. Norman, G. Anthony, Measurement, Instrumentation and Sensors Handbook, Edited by John Webster, Florida: CRC Press LLC. Section (1999) 71–1.
[44] T. Oya, T. Nomura, M. Tsubota, N. Okinaka, T. Akiyama, Thermal conductivity enhancement of erythritol as PCM by using graphite and nickel particles, Appl. Therm. Eng. 61 (2) (2013) 825–828.
[45] S. Park, Y. Lee, Y.S. Kim, H.M. Lee, J.H. Kim, I.W. Cheong, W.-G. Koh, Magnetic nanoparticle-embedded PCM nanocapsules based on paraffin core and polyurea shell, Colloids Surf., A 450 (2014) 46–51.
[46] C. Vélez, M. Khayet, J.O. De Zárate, Temperature-dependent thermal properties of solid/liquid phase change even-numbered n-alkanes: n-Hexadecane, n-octadecane and n-eicosane, Applied Energy 143 (2015) 383–394.
[47] A. Sarı, A. Karaipekli, Thermal conductivity and latent heat thermal energy storage characteristics of paraffin/expanded graphite composite as phase change material, Appl. Therm. Eng. 27 (8–9) (2007) 1271–1277.
[48] I. Tavman, Effective thermal conductivity of granular porous materials, Int. Commun. Heat Mass Transfer 23 (2) (1996) 169–176.
[49] T. Boumaza, J. Redgrove, Use of the transient plane source technique for rapid multiple thermal property measurements, Int. J. Thermophysics 24 (2) (2003) 501–512.
[50] M. Li, A nano-graphite/paraffin phase change material with high thermal conductivity, Appl. Energy 106 (2013) 25–30.
[51] L. Xia, P. Zhang, R. Wang, Preparation and thermal characterization of expanded graphite/paraffin composite phase change material, Carbon 48 (9) (2010) 2538–2548.
[52] L. Boussaba, A. Foufa, S. Makhlouf, G. Lefebvre, L. Royon, Elaboration and properties of a composite bio-based PCM for an application in building envelopes, Constr. Build. Mater. 185 (2018) 156–165.
[53] R.J. Warzoha, A.S. Fleischer, Determining the thermal conductivity of liquids using the transient hot disk method. Part II: Establishing an accurate and repeatable experimental methodology, Int. J. Heat Mass Transfer 71 (2014) 790–807.
[54] Y.-X. Fu, Z.-X. He, D.-C. Mo, S.-S. Lu, Thermal conductivity enhancement with different fillers for epoxy resin adhesives, Appl. Thermal Eng. 66 (1–2) (2014) 493–498.
[55] M.M. Farid, A.M. Khudhair, S.A.K. Razack, S. Al-Hallaj, A review on phase change energy storage: materials and applications, Energy Conver. Manage. 45 (9–10) (2004) 1597–1615.
[56] Y. Allouche, PCM energy storage modelling: case study for a solar-ejector cooling cycle, Ph.D. thesis, National Engineering School of Tunis (ENIT), 2016.
[57] M. Delgado, A. Lázaro, J. Mazo, B. Zalba, Review on phase change material emulsions and microencapsulated phase change material slurries: materials, heat transfer studies and applications, Renew. Sustain. Energy Rev. 16 (1) (2012) 253–273.
[58] P. Hu, D.-J. Lu, X.-Y. Fan, X. Zhou, Z.-S. Chen, Phase change performance of sodium acetate trihydrate with AlN nanoparticles and CMC, Solar Energy Mater. Solar Cells 95 (9) (2011) 2645–2649.
[59] L.F. Cabeza, G. Svensson, S. Hiebler, H. Mehling, Thermal performance of sodium acetate trihydrate thickened with different materials as phase change energy storage material, Appl. Therm. Eng. 23 (13) (2003) 1697–1704.
[60] G. Li, B. Zhang, X. Li, Y. Zhou, Q. Sun, Q. Yun, The preparation, characterization and modification of a new phase change material: CaCl2·6H2O–MgCl2·6H2O eutectic hydrate salt, Solar Energy Materials and Solar Cells 126 (2014) 51–55.
[61] A. Efimova, S. Pinnau, M. Mischke, C. Breitkopf, M. Ruck, P. Schmidt, Development of salt hydrate eutectics as latent heat storage for air conditioning and cooling, Thermochim. Acta 575 (2014) 276–278.
[62] P.B. Salunkhe, P.S. Shembekar, A review on effect of phase change material encapsulation on the thermal performance of a system, Renew. Sustainable Energy Rev. 16 (8) (2012) 5603–5616.
[63] M. Jurkowska, I. Szczygieł, Review on properties of microencapsulated phase change materials slurries (mPCMS), Appl. Therm. Eng. 98 (2016) 365–373.
[64] T. Khadiran, M.Z. Hussein, Z. Zainal, R. Rusli, Encapsulation techniques for organic phase change materials as thermal energy storage medium: A review, Solar Energy Materials and Solar Cells 143 (2015) 78–98.
[65] Y.E. Milian, A. Gutierrez, M. Grageda, S. Ushak, A review on encapsulation techniques for inorganic phase change materials and the influence on their thermophysical properties, Renew. Sustain. Energy Rev. 73 (2017) 983–999.
[66] N. Beaupere, U. Soupremanien, L. Zalewski, Nucleation triggering methods in supercooled phase change materials (PCM), a review, Thermochim. Acta 670 (2018) 184–201.
[67] H. Kiani, D.-W. Sun, Water crystallization and its importance to freezing of foods: a review, Trends Food Sci. Technol. 22 (8) (2011) 407–426.
[68] M. Dalvi-Isfahan, N. Hamdami, E. Xanthakis, A. Le-Bail, Review on the control of ice nucleation by ultrasound waves, electric and magnetic fields, J. Food Eng. 195 (2017) 222–234.
[69] L. Liu, D. Su, Y. Tang, G. Fang, Thermal conductivity enhancement of phase change materials for thermal energy storage: A review, Renew. Sustain. Energy Rev. 62 (2016) 305–317.
[70] Y. Lin, Y. Jia, G. Alva, G. Fang, Review on thermal conductivity enhancement, thermal properties and applications of phase change materials in thermal energy storage, Renew. Sustainable Energy Rev. 82 (2018) 2730–2742.
[71] S. Wu, T. Yan, Z. Kuai, W. Pan, Thermal conductivity enhancement on phase change materials for thermal energy storage: A review, Energy Storage Materials.
[72] J. Khodadadi, L. Fan, H. Babaei, Thermal conductivity enhancement of nanostructure-based colloidal suspensions utilized as phase change materials for thermal energy storage: a review, Renew. Sustain. Energy Rev. 24 (2013) 418–444.

[73] P. Bose, V.A. Amirtham, A review on thermal conductivity enhancement of paraffinwax as latent heat energy storage material, Renew. Sustain. Energy Rev. 65 (2016) 81–100.
[74] N.I. Ibrahim, F.A. Al-Sulaiman, S. Rahman, B.S. Yilbas, A.Z. Sahin, Heat transfer enhancement of phase change materials for thermal energy storage applications: A critical review, Renew. Sustain. Energy Rev. 74 (2017) 26–50.
[75] H. Akeiber, P. Nejat, M.Z.A. Majid, M.A. Wahid, F. Jomehzadeh, I.Z. Famileh, J. K. Calautit, B.R. Hughes, S.A. Zaki, A review on phase change material (PCM) for sustainable passive cooling in building envelopes, Renew. Sustain. Energy Rev. 60 (2016) 1470–1497.
[76] F. Souayfane, F. Fardoun, P.-H. Biwole, Phase change materials (PCM) for cooling applications in buildings: A review, Energy Buildings 129 (2016) 396–431.
[77] A. Marques, G. Davies, G. Maidment, J. Evans, I. Wood, Novel design and performance enhancement of domestic refrigerators with thermal storage, Appl. Therm. Eng. 63 (2) (2014) 511–519.
[78] N. Ndraha, H.-I. Hsiao, J. Vlajic, M.-F. Yang, H.-T.V. Lin, Time-temperature abuse in the food cold chain: Review of issues, challenges, and recommendations, Food Control 89 (2018) 12–21.
[79] M. Rokka, S. Eerola, M. Smolander, H.-L. Alakomi, R. Ahvenainen, Monitoring of the quality of modified atmosphere packaged broiler chicken cuts stored in different temperature conditions: B. Biogenic amines as quality-indicating metabolites, Food Control 15 (8) (2004) 601–607.
[80] W. Tingman, Z. Jian, Z. Xiaoshuan, Fish product quality evaluation based on temperature monitoring in cold chain, African J. Biotechnol. 9 (37) (2010) 6146–6151.
[81] O. Laguerre, H.M. Hoang, D. Flick, Experimental investigation and modelling in the food cold chain: Thermal and quality evolution, Trends Food Sci. Technol. 29 (2) (2013) 87–97.
[82] E. Derens, B. Palagos, J. Guilpart, The cold chain of chilled products under supervision in France, in: 13th World Congress of Food Science & Technology 2006, 823–823, 2006.
[83] D. Smith, L. Sparks, Temperature Controlled Supply Chains, in: Food Supply Chain Management, Wiley-Blackwell, 179–198, 2007.
[84] P. Glouannec, B. Michel, G. Delamarre, Y. Grohens, Experimental and numerical study of heat transfer across insulation wall of a refrigerated integral panel van, Appl. Thermal Eng. 73 (1) (2014) 196–204.
[85] R. Fioretti, P. Principi, B. Copertaro, A refrigerated container envelope with a PCM (Phase Change Material) layer: Experimental and theoretical investigation in a representative town in Central Italy, Energy Conver. Manage. 122 (2016) 131–141.
[86] B. Copertaro, P. Principi, R. Fioretti, Thermal performance analysis of PCM in refrigerated container envelopes in the Italian context–Numerical modeling and validation, Appl. Thermal Eng. 102 (2016) 873–881.
[87] A. Tinti, A. Tarzia, A. Passaro, R. Angiuli, Thermographic analysis of polyurethane foams integrated with phase change materials designed for dynamic thermal insulation in refrigerated transport, Appl. Thermal Eng. 70 (1) (2014) 201–210.
[88] B. Michel, P. Glouannec, A. Fuentes, P. Chauvelon, Experimental and numerical study of insulation walls containing a composite layer of PU-PCM and dedicated to refrigerated vehicle, Appl. Therm. Eng. 116 (2017) 382–391.
[89] M. Ahmed, O. Meade, M.A. Medina, Reducing heat transfer across the insulated walls of refrigerated truck trailers by the application of phase change materials, Energy Convers. Manage. 51 (3) (2010) 383–392.
[90] Rubitherm Technologies GmbH, Phase change materials, https://www.rubitherm.eu/en//index.html, 2017.
[91] E. Oró, L.F. Cabeza, M.M. Farid, Experimental and numerical analysis of a chilly bin incorporating phase change material, Appl. Therm. Eng. 58 (1–2) (2013) 61–67.
[92] E. Oró, A. De Gracia, L.F. Cabeza, Active phase change material package for thermal protection of ice cream containers, Int. J. Refrig 36 (1) (2013) 102–109.
[93] D. Leducq, F. NDoye, G. Alvarez, Phase change material for the thermal protection of ice cream during storage and transportation, Int. J. Refrigeration 52 (2015) 133–139.
[94] PureTemp LLC, Phase Change Material, http://www.puretemp.com/, 2019.
[95] CRISTOPIA Energy Systems, The STL technology, http://www.cristopia.com/EN/index.html, 2013.
[96] H. Hoang, D. Leducq, R. Pérez-Masia, J. Lagaron, E. Gogou, P. Taoukis, G. Alvarez, Heat transfer study of submicro-encapsulated PCM plate for food packaging application, Int. J. Refrig 52 (2015) 151–160.
[97] U. Kartoglu, J. Milstien, Tools and approaches to ensure quality of vaccines throughout the cold chain, Expert Rev. Vaccines 13 (7) (2014) 843–854.
[98] D. Mondieig, F. Rajabalee, A. Laprie, H.A. Oonk, T. Calvet, M.A. Cuevas-Diarte, Protection of temperature sensitive biomedical products using molecular alloys as phase change material, Transfus. Apheres. Sci. 28 (2) (2003) 143–148.
[99] M. Liu, W. Saman, F. Bruno, Development of a novel refrigeration system for refrigerated trucks incorporating phase change material, Appl. Energy 92 (2012) 336–342.
[100] M. Liu, W. Saman, F. Bruno, Computer simulation with TRNSYS for a mobile refrigeration system incorporating a phase change thermal storage unit, Appl. Energy 132 (2014) 226–235.
[101] M. Liu, W. Saman, F. Bruno, Validation of a mathematical model for encapsulated phase change material flat slabs for cooling applications, Appl. Therm. Eng. 31 (14–15) (2011) 2340–2347.
[102] C. Sohrabi, Z. Alsafi, N. O-Neill, M. Khan, A. Kerwan, A. Al-Jabir, C. Iosifidis, R. Agha, World Health Organization declares global emergency: A review of the 2019 novel coronavirus (COVID-19), International Journal of Surgery.
[103] Y. Wu, S. Zhang, M. Li, Y. Ge, J. Shu, Y. Zhou, Y. Xu, J. Hu, H. Liu, L. Fu, et al., The challenge to NOx emission control for heavy-duty diesel vehicles in China, Atmos. Chem. Phys 12 (19) (2012) 9365–9379.
[104] Z. Mylona, M. Kolokotroni, S.A. Tassou, Frozen food retail: Measuring and modelling energy use and space environmental systems in an operational supermarket, Energy Buildings 144 (2017) 129–143.
[105] M. Kolokotroni, Z. Mylona, J. Evans, A. Foster, R. Liddiard, Supermarket energy use in the UK, Energy Procedia 161 (2019) 325–332.
[106] F. Alzuwaid, Y. Ge, S. Tassou, J. Sun, The novel use of phase change materials in an open type refrigerated display cabinet: A theoretical investigation, Appl. Energy 180 (2016) 76–85.
[107] P. Gullo, A. Hafner, K. Banasiak, Transcritical R744 refrigeration systems for supermarket applications: Current status and future perspectives, Int. J. Refrig 93 (2018) 269–310.
[108] N. Fidorra, A. Hafner, S. Minetto, J. Köhler, Low temperature heat storages in CO2 supermarket refrigeration systems, in: 24th IIR Refrigeration Congress of Refrigeration. IIF/IIR, Yokohama, Japan, 2015.
[109] Y. Lu, W. Zhang, P. Yuan, M. Xue, Z. Qu, W. Tao, Experimental study of heat transfer intensification by using a novel combined shelf in food refrigerated display cabinets (Experimental study of a novel cabinets), Appl. Therm. Eng. 30 (2–3) (2010) 85–91.
[110] F. Alzuwaid, Y. Ge, S. Tassou, A. Raeisi, L. Gowreesunker, The novel use of phase change materials in a refrigerated display cabinet: An experimental investigation, Appl. Therm. Eng. 75 (2015) 770–778.
[111] N. Fidorra, S. Minetto, A. Hafner, K. Banasiak, J. Köhler, Analysis of cold thermal energy storage concepts in CO2 refrigeration systems, Refrigeration Sci. Technol. (2016) 495–502.
[112] P.D. Gaspar, L.C. Gonçalves, R. Pitarma, Experimental analysis of the thermal entrainment factor of air curtains in vertical open display cabinets for different ambient air conditions, Appl. Therm. Eng. 31 (5) (2011) 961–969.
[113] S. Tassou, Y. Ge, A. Hadawey, D. Marriott, Energy consumption and conservation in food retailing, Appl. Therm. Eng. 31 (2–3) (2011) 147–156.
[114] S. Estrada-Flores, Market analysis for energy savings in the cold chain, Packaging, Storage Transport Report 51 (2007) 1–75.
[115] M. Kauffeld, J. Harnisch, J. Rhiemeier, Environmental impact of various alternative supermarket refrigeration systems, in: 8th IIR Gustav Lorentzen Conference on Natural Working Fluids, Copenhagen, Denmark, vol. 8, 2008.
[116] B. Fricke, B. Becker, Comparison of Vertical Display Cases: Energy and Productivity Impacts of Glass Doors Versus Open Vertical Display Cases., ASHRAE Transactions 117 (1).
[117] X. Wu, W. Li, Y. Wang, Z. Chang, C. Wang, C. Ding, Experimental investigation of the performance of cool storage shelf for vertical open refrigerated display cabinet, Int. J. Heat Mass Transf. 110 (2017) 789–795.
[118] W. Lu, S. Tassou, Characterization and experimental investigation of phase change materials for chilled food refrigerated cabinet applications, Appl. Energy 112 (2013) 1376–1382.
[119] R. Ben-Abdallah, D. Leducq, H. Hoang, L. Fournaison, O. Pateau, B. Ballot-Miguet, A. Delahaye, Experimental investigation of the use of PCM in an open display cabinet for energy management purposes, Energy Convers. Manage. 198 (2019), 111909.
[120] A. Sevault, K. Banasiak, J. Bakken, A. Hafner, A novel PCM accumulator for refrigerated display cabinet: design and CFD simulations, in: 12th IIR/IIF International Conference on Phase-Change Materials and Slurries for Refrigeration and Air Conditioning-PCM 2018: book of proceedings, International Institute of Refrigeration, 2018.
[121] M. Jokiel, K. Banasiak, H. Hauko, A. Sevault, Dynamic modelling of a refrigerated cabinet with integrated phase change material thermal storage, in: Proceedings of the 25th ICR International Congress of Refrigeration Conference, Montreal, Canada, 3403–3410, 2019.
[122] C. Ferrandi, M. Orlandi, Theoretical analysis of cold storage devices in a CO2 transcritical/subcritical supermarket refrigeration plant, in: Proceedings of the 23rd IIR International Congress of Refrigeration: Prague, Czech Republic, 2011.
[123] C. Ferrandi, M. Orlandi, Theoretical analysis of cold storage device effects on the performance and regulation of a CO2 supermarket refrigeration plant, in: Proceedings of the 10th IIR-Gustav Lorentzen Conference on Natural Working Fluids (GL2012); Delft, The Netherlands, 2012.
[124] A. Polzot, P. D–agaro, P. Gullo, G. Cortella, Water storage to improve the efficiency of CO2 commercial refrigeration systems, in: Proceedings of the 24th IIR International Congress of Refrigeration; Yokohama, Japan, 2015.
[125] A. Polzot, P. D'Agaro, P. Gullo, G. Cortella, Modelling commercial refrigeration systems coupled with water storage to improve energy efficiency and perform heat recovery, Int. J. Refrig. 69 (2016) 313–323.
[126] A. Polzot, P. D. Agaro, G. Cortella, P. Gullo, Supermarket refrigeration and air conditioning systems integration via a water storage, in: Proceedings of the 4th IIR Conference on Sustainability and the Cold Chain; Auckland, New Zealand, 2016b.
[127] Calmac Corp., Thermal energy storage in supermarkets, http://www.calmac.com/stuff/contentmgr/files/0/a2c6d5b156fea7639cd0cd619f36c95a/pdf/ib_155_supermarket_market_brochure_160811.pdf, 2015.
[128] Viessmann Refrigeration Solutions, ESyCool green - Sustainable energy systems for food retailing, https://cooling.viessmann.co.uk/en-gb/our-products/esycool-green, 2018.
[129] C. Heerup, T. Green, Load shifting by ice storage in retail CO2 systems, in: 11th IIR Gustav Lorentzen Conference on Natural Refrigerants, Hangzhou, China, 2014.

[130] M.V. Beek, H.D. Jong, Reducing display bottle cooler energy consumption using PCM as active thermal storage, in: 15th International Refrigeration and Air Conditioning Conference at Purdue, 2014.
[131] M.A. Ezan, E.O. Doganay, F.E. Yavuz, I.H. Tavman, A numerical study on the usage of phase change material (PCM) to prolong compressor off period in a beverage cooler, Energy Conver. Manage. 142 (2017) 95–106.
[132] D. Maerić, B. Pavković, K. Lenić, An experimental research on energy efficiency of a beverage cooler with the latent heat storage, Appl. Therm. Eng. 148 (2019) 270–277.
[133] R. Manescu, A. Hafner, N. Fidorra, S. Försterling, J. Köhler, A new approach for cold thermal energy storages in supermarket refrigeration systems, in: Proceedings of the 7th IIR Ammonia and CO2 Refrigeration Technologies Conference, Ohrid, Macedonia, 11–13, 2017.
[134] Á. Á. Pardiñas, A. Hafner, K. Banasiak, Integrated R744 ejector supportet parallel compression racks for supermarkets: experimental results, in: Proceedings of the 13th IIR Gustav Lorentzen Conference, Valencia, 2018, IIR, 2018a.
[135] Á.Á. Pardiñas, A. Hafner, K. Banasiak, Novel integrated CO2 vapour compression racks for supermarkets. Thermodynamic analysis of possible system configurations and influence of operational conditions, Appl. Thermal Eng. 131 (2018) 1008–1025.
[136] F. Wang, G. Maidment, J. Missenden, R. Tozer, The novel use of phase change materials in refrigeration plant. Part 1: Experimental investigation, Applied Thermal Engineering 27 (17–18) (2007a) 2893–2901.
[137] A.L. Chan, T.-T. Chow, S.K. Fong, J.Z. Lin, Performance evaluation of district cooling plant with ice storage, Energy 31 (14) (2006) 2750–2762.
[138] T. Yang, C. Wang, Q. Sun, R. Wennersten, Study on the application of latent heat cold storage in a refrigerated warehouse, Energy Procedia 142 (2017) 3546–3552.
[139] H. Selvnes, A. Hafner, H. Kauko, Design of a cold thermal energy storage unit for industrial applications using CO2 as refrigerant, in: 25th IIR International Congress of Refrigeration Proceedings, International Institute of Refrigeration, 2019a.
[140] E.H. Verpe, I. Tolstorebrov, A. Sevault, A. Hafner, Y. Ladam, Cold thermal energy storage with low-temperature plate freezing of fish on offshore vessels, in: Proceedings of the 25th IIR International Congress of Refrigeration. Montréal, Canada, August 24–30, 2019, International Institute of Refrigeration, 2019.
[141] H. Selvnes, A. Hafner, H. Kauko, Cold thermal storage integration in a large industrial refrigeration system, in: Proceedings of the 13th IIR Gustav Lorentzen Conference, Valencia, 2018, International Institute of Refrigeration, 2018.
[142] F. Wang, G. Maidment, J. Missenden, R. Tozer, The novel use of phase change materials in refrigeration plant. Part 2: Dynamic simulation model for the combined system, Applied Thermal Engineering 27 (17–18) (2007b) 2902–2910.
[143] F. Wang, G. Maidment, J. Missenden, R. Tozer, The novel use of phase change materials in refrigeration plant. Part 3: PCM for control and energy savings, Applied Thermal Engineering 27 (17–18) (2007c) 2911–2918.
[144] T. Korth, F. Loistl, A. Storch, R. Schex, A. Krönauer, C. Schweigler, Capacity enhancement of air conditioning systems by direct integration of a latent heat storage unit, Appl. Therm. Eng. 167 (2020), 114727.
[145] Sasol Chemicals, Parafol 16–97, https://products.sasol.com/pic/products/home/grades/AS/5parafol-16-97/index.html/, 2020.
[146] T. Korth, F. Loistl, C. Schweigler, Novel integration of latent heat storage in multi-split air conditioning systems, in: 25th IIR International Congress of Refrigeration Proceedings, International Institute of Refrigeration, 2019.
[147] H. Selvnes, Y. Allouche, A. Sevault, A. Hafner, CFD modeling of ice formation and melting in horizontally cooled and heated plates, in: Eurotherm Seminar# 112-Advances in Thermal Energy Storage, Edicions de la Universitat de Lleida Lleida, Spain, 2019b.
[148] A. Hafner, T.S. Nordtvedt, I. Rumpf, Energy saving potential in freezing applications by applying cold thermal energy storage with solid carbon dioxide, Procedia Food Science 1 (2011) 448–454.
[149] J. Wu, B. Tremeac, M.-F. Terrier, M. Charni, E. Gagnière, F. Couenne, B. Hamroun, C. Jallut, Experimental investigation of the dynamic behavior of a large-scale refrigeration–PCM energy storage system. Validation of a complete model, Energy 116 (2016) 32–42.
[150] S.-L. Chen, C.-L. Chen, C.-C. Tin, T.-S. Lee, M.-C. Ke, An experimental investigation of cold storage in an encapsulated thermal storage tank, Exp. Thermal Fluid Sci. 23 (3–4) (2000) 133–144.
[151] T. Kousksou, J.-P. Bédécarrats, J.-P. Dumas, A. Mimet, Dynamic modelling of the storage of an encapsulated ice tank, Appl. Therm. Eng. 25 (10) (2005) 1534–1548.
[152] M. Cheralathan, R. Velraj, S. Renganarayanan, Performance analysis on industrial refrigeration system integrated with encapsulated PCM-based cool thermal energy storage system, Int. J. Energy Res. 31 (14) (2007) 1398–1413.
[153] J.-P. Bédécarrats, J. Castaing-Lasvignottes, F. Strub, J.-P. Dumas, Study of a phase change energy storage using spherical capsules. Part I: Experimental results, Energy Conver. Manage. 50 (10) (2009) 2527–2536.
[154] A. Castell, M. Belusko, F. Bruno, L.F. Cabeza, Maximisation of heat transfer in a coil in tank PCM cold storage system, Appl. Energy 88 (11) (2011) 4120–4127.
[155] N. Tay, M. Belusko, F. Bruno, An effectiveness-NTU technique for characterising tube-in-tank phase change thermal energy storage systems, Appl. Energy 91 (1) (2012) 309–319.
[156] N. Tay, M. Belusko, F. Bruno, Experimental investigation of tubes in a phase change thermal energy storage system, Appl. Energy 90 (1) (2012) 288–297.
[157] N. Tay, F. Bruno, M. Belusko, Experimental validation of a CFD and an ε)NTU model for a large tube-in-tank PCM system, Int. J. Heat Mass Transf. 55 (21–22) (2012) 5931–5940.
[158] N. Tay, F. Bruno, M. Belusko, Experimental validation of a CFD model for tubes in a phase change thermal energy storage system, Int. J. Heat Mass Transf. 55 (4) (2012) 574–585.
[159] A. López-Navarro, J. Biosca-Taronger, B. Torregrosa-Jaime, J. Corberán, J. Bote-García, J. Payá, Experimental investigations on the influence of ice floating in an internal melt ice-on-coil tank, Energy Buildings 57 (2013) 20–25.
[160] A. López-Navarro, J. Biosca-Taronger, B. Torregrosa-Jaime, I. Martínez-Galván, J. M. Corberán, J. Esteban-Matías, J. Paya, Experimental investigation of the temperatures and performance of a commercial ice-storage tank, Int. J. Refrig. 36 (4) (2013) 1310–1318.
[161] B. Torregrosa-Jaime, A. López-Navarro, J.M. Corberán, J. Esteban-Matías, L. Klinkner, J. Payá, Experimental analysis of a paraffin-based cold storage tank, Int. J. Refrig. 36 (6) (2013) 1632–1640.
[162] A. López-Navarro, J. Biosca-Taronger, J. Corberán, C. Peñalosa, A. Lázaro, P. Dolado, J. Payá, Performance characterization of a PCM storage tank, Appl. Energy 119 (2014) 151–162.
[163] F. Bosholm, A. López-Navarro, M. Gamarra, J. Corberán, J. Payá, Reproducibility of solidification and melting processes in a latent heat thermal storage tank, Int. J. Refrig. 62 (2016) 85–96.
[164] A. Abhishek, B. Kumar, M.H. Kim, Y.T. Lee, J.D. Chung, S.T. Kim, T. Kim, C. Lee, K. Lee, Comparison of the performance of ice-on-coil LTES tanks with horizontal and vertical tubes, Energy Buildings 183 (2019) 45–53.
[165] P. Moreno, A. Castell, C. Solé, G. Zsembinszki, L.F. Cabeza, PCM thermal energy storage tanks in heat pump system for space cooling, Energy Buildings 82 (2014) 399–405.
[166] PCM Products Ltd, PlusICE Range, http://www.pcmproducts.net/files/S%20range-2018.pdf, 2018.
[167] A. Mosaffa, L.G. Farshi, C.I. Ferreira, M. Rosen, Advanced exergy analysis of an air conditioning system incorporating thermal energy storage, Energy 77 (2014) 945–952.
[168] M.H. Rahdar, A. Emamzadeh, A. Ataei, A comparative study on PCM and ice thermal energy storage tank for air-conditioning systems in office buildings, Appl. Therm. Eng. 96 (2016) 391–399.
[169] D. Erdemir, N. Altuntop, Effect of encapsulated ice thermal storage system on cooling cost for a hypermarket, Int. J. Energy Res. 42 (9) (2018) 3091–3101.

Paper II

H. Selvnes, Y. Allouche, A. Hafner (2021). "Experimental characterisation of a cold thermal energy storage unit with a pillow-plate heat exchanger design." *Applied Thermal Engineering* Volume 199, 11750
DOI: https://doi.org/10.1016/j.applthermaleng.2021.117507

Applied Thermal Engineering 199 (2021) 117507

Contents lists available at ScienceDirect

Applied Thermal Engineering

journal homepage: www.elsevier.com/locate/apthermeng

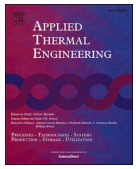

Experimental characterisation of a cold thermal energy storage unit with a pillow-plate heat exchanger design

Håkon Selvnes *, Yosr Allouche, Armin Hafner

Norwegian University of Science and Technology, Department of Energy and Process Engineering, Kolbjørn Hejes vei 1B, NO-7491 Trondheim, Norway

ARTICLE INFO

Keywords:
Cold thermal energy storage
Phase change materials
CO_2 refrigeration
Industrial refrigeration

ABSTRACT

Cold Thermal Energy Storage (CTES) technology can be introduced to refrigeration systems for air conditioning and process cooling to reduce the peak power consumption by decoupling the supply and demand of refrigeration. In these systems, the refrigeration demand can vary significantly over a day, resulting in a challenging peak and valley load pattern on the electrical grid. This paper presents the design, development, and experimental performance investigations of a novel plates-in-tank CTES unit design intended for integration into pump-circulated CO_2 industrial refrigeration systems. The CTES unit is composed of a stainless steel container filled with water as the latent storage medium and fitted with a pillow plate heat exchanger. The refrigerant (CO_2) circulates within the heat exchanger to transfer heat with the storage medium. The current study demonstrates the feasibility of implementing a latent CTES unit directly into the primary refrigerant circuit for peak shaving of the refrigeration load. The results show that the evaporation and condensation temperatures of the refrigerant are the most critical parameters influencing the performance of the charging and discharging cycles, respectively. The unit demonstrated a mean discharge rate of 7.90 kW over a total discharging cycle time of approximately 4.5 h. The resulting maximum discharged energy was calculated to 35.29 kWh.

1. Introduction

The demand for electricity in modern society is high. The peak and valley consumption pattern that is dominating today is a challenge for the grid. Also, the demand pattern is becoming more distinct due to the decarbonisation of industry, transport and the building sector [1–4]. The energy demand for space cooling in the building sector has more than tripled since 1990, making space cooling the fastest-growing end-use in buildings [5]. Furthermore, space cooling for residential and commercial buildings is expected to contribute significantly to the increase in peak power demand towards 2050 [6]. With the current growth in the air-conditioning market, the IEA predicts that over 40% of the total peak power demand in hot climates will be caused by space cooling in 2050 [6]. Consequently, there is undoubtedly a need to introduce new technologies that can reduce the peak load on the electrical grid. Thermal Energy Storage (TES) can represent one solution, as it allows for peak shaving of the thermal demand, ranging from several cycles per day to a seasonal timescale depending on the application [7]. A term often used to designate TES systems operating at sub-ambient temperatures is Cold Thermal Energy Storage (CTES). CTES integrated into Air-Conditioning (AC) systems for buildings have shown good performance by enabling peak shifting of up to 100% of the cooling load to off-peak hours depending on system design [8]. This approach has been particularly popular for commercial buildings occupied only during working hours, which causes a substantial difference in the peak and off-peak cooling load [9]. TES systems employing the sensible heat storage principle is considered mature technology. Commonly used storage materials for sensible heat storage are chilled/hot water, glycol mixtures, rock and concrete. However, the main limitation of these materials is their limited storage capacity over the operating temperature range of the systems in which they are integrated. Chilled water systems for AC commonly use a 7 °C supply temperature and 12 °C return temperature, resulting in a high volume requirement for storing the energy in a chilled water tank. Latent heat storage is considered a developing solution that has demonstrated improved storage performance compared with sensible heat storage solutions. Latent heat storage provides high energy density storage, a tailored phase change temperature and a near-constant storage temperature during the charging and discharging processes [10].

Selvnes et al. [11] proposed a classification of latent CTES with Phase Change Material (PCM) applied to refrigeration systems into two categories; CTES units integrated into the primary refrigerant circuit and

* Corresponding author.
E-mail address: hakon.selvnes@ntnu.no (H. Selvnes).

https://doi.org/10.1016/j.applthermaleng.2021.117507
Received 7 May 2021; Received in revised form 22 July 2021; Accepted 26 August 2021
Available online 3 September 2021

Nomenclature

Abbreviations

COP	Coefficient Of Performance
CTES	Cold Thermal Energy Storage
HEX	Heat Exchanger
HTF	Heat Transfer Fluid
P&ID	Piping and Instrumentation Diagram
PCM	Phase Change Material
PP	Pillow Plate
PWM	Pulse-Width Modulation
TES	Thermal Energy Storage
ACC	Auxiliary CO_2 Circuit
GHC	Glycol Heating Circuit
PCC	Primary CO_2 Circuit
SCC	Secondary CO_2 Circuit

Symbols

$\dot{E}$	energy flow [kW]
$\dot{m}$	mass flow rate [kg/s]
b	thickness [m]
d	diameter [m]
E	energy [kWh]
h	enthalpy [kJ/kg]
L	length [m]
n	number [–]
s	welding spot pitch [m]
T	temperature [K]
t	time [s]
W	width [m]

Greek letters

δ	height [m]
ρ	density [kg/m^3]

Subscripts

CO_2	carbondioxide
PCM	phase change material
PP	Pillow Plate
SW	Spot Weld
C	charging
D	discharging
fus	fusion
g	glycol
i	inner
in	inlet
L	longitudinal
lat	latent
o	outer
out	outlet
s	solid
sat	saturation
T	transversal
th	theoretical
w	wall

CTES units integrated into the secondary refrigeration circuit. In the first category, the CTES unit is directly integrated into the main refrigeration circuit employing a PCM/two-phase fluid Heat Exchanger (HEX) design. The storage acts as an evaporator during the charging process and operates as a condenser for the refrigeration system during the discharging process. In the second category, the storage is integrated into the secondary refrigerant circuit employing a PCM/single-phase fluid HEX design. A secondary refrigerant circuit is commonly used in larger chiller applications, using chilled water, glycol or brine as the secondary refrigerant. During the charging process, the secondary refrigerant is pumped through the CTES unit, acting as a heat source. During the discharging process, the CTES unit acts as a heat sink for the system. Ice bank CTES systems have commonly been applied to high-capacity chiller systems for process cooling purposes, particularly in the dairy industry [12]. During the charging process, ice is formed gradually around the surface of the tubes in which the cold heat transfer fluid (glycol/brine) circulates. The most investigated configurations for CTES units integrated into the secondary refrigerant circuit are the tube-in-tank [13–18] and coil-in-tank designs [19–25], probably due to a relatively simple design and low cost. Despite the higher heat transfer characteristics, CTES units based on the plates-in-tank design are less frequently studied, probably due to the limited availability of plate designs suitable for this application. Furthermore, the higher cost and the lower feasibility of creating a suitable lab-scale test facility based on the plate-in-tank design are possible causes. Only a few recent studies investigating the novel plates-in-tank design were found in the literature and only for positive temperature applications [26,27].

The chiller energy efficiency is positively influenced by the direct integration of a CTES unit into the primary refrigeration circuit compared to a secondary refrigerant circuit because the evaporation temperature of the refrigeration system can be increased during the charging process [28]. Since the evaporation temperature of the refrigeration system is lifted, the pressure lift of the compressors is reduced. This configuration is still not thoroughly described in the literature but has received increased attention, especially over the last five years. The integration of a shell-and-tube PCM-HEX into a 5 kW air-to-air AC unit was experimentally and numerically investigated by Wang et al. [29–31]. The results have shown that integrating the PCM-HEX as a subcooler downstream the condenser could increase the Coefficient Of Performance (COP) by 8% in UK climate conditions. Korth et al. [28] suggested using a tube-in-tank PCM-HEX CTES design integrated into a multi-split AC system to reduce the load on the compressor in the system during peak hours. The experimental results have demonstrated that the PCM-HEX could achieve a mean discharge rate of 1.5 kW for 2.33 h. Furthermore, Korth et al. [32] carried out theoretical modelling and experimental tests on the same tube-in-tank PCM-HEX integrated as a subcooler downstream of the condenser in a 6 kW AC system. The paraffin Parafol 16–97 [33] was used as the PCM, which has a melting point of 18 °C. The experimental results have shown an increase in the evaporation capacity of the AC system by 18% when using the storage for a condensing temperature of 35 °C.

A novel type of HEX that has gained increased attention in industrial applications is the Pillow Plates (PP) HEX. Besides the high heat transfer exchange rate, the application of PP-HEX is interesting as it can be used as an immersed HEX in systems with high operating pressure on the inner flow channel (>80 bar) due to its fully welded design of each single PP. PP-HEX are therefore suitable for integration into the primary refrigerant circuit. The PPs can be manufactured to withstand operating pressures up to 120 bar, and the PP-HEX design is then appropriate for transcritical CO_2 refrigeration systems. Compared to conventional HEX types (e.g. shell and tube), the PP-HEX is a relatively young technology. The main limitations of the PP-HEX to date are the higher cost compared to conventional HEX and limited suppliers of these products. One PP is represented in Fig. 1a. It consists of two thin metal sheets spot-welded together in a particular repetitive pattern by a laser-welding machine. The spots form a defined channel where the refrigerant flows and exchange heat with the storage medium. The two metal plates are also seam-welded along the edges to ensure the sealing of the PP. Two pipes

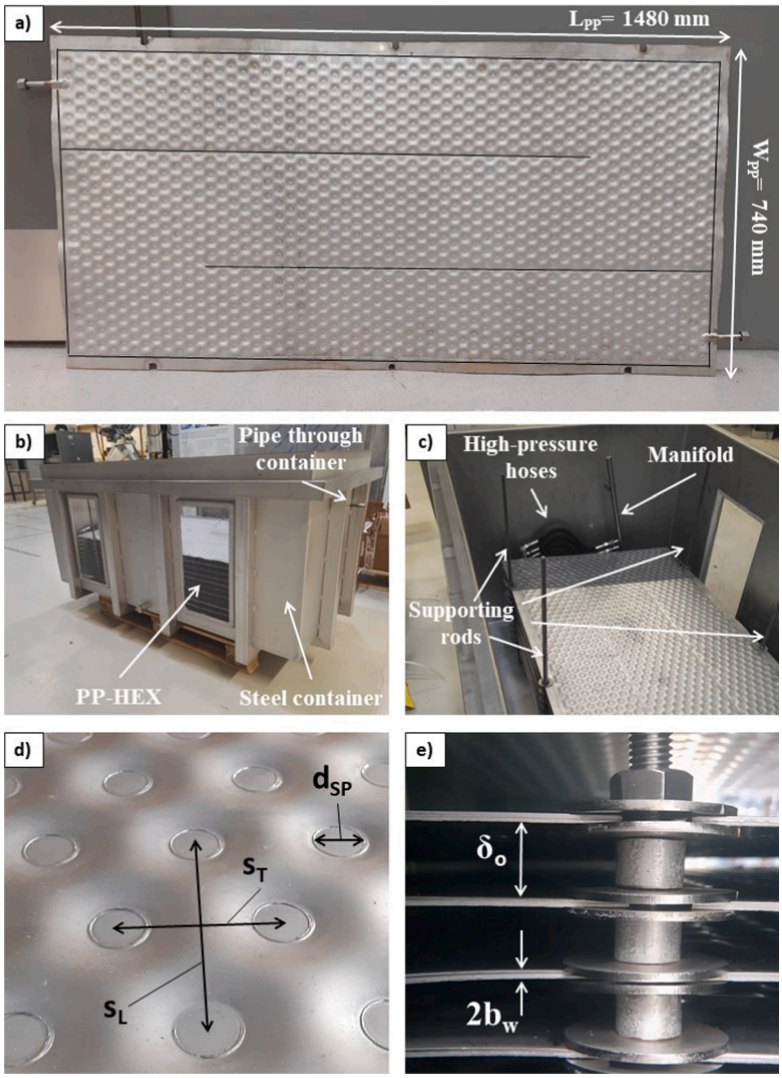

Fig. 1. Overview of the novel CTES unit showing the details of a) one PP for CO_2 refrigeration with inlet/outlet pipes and the seam welds marked with black lines b) the CTES unit before assembly in the test facility c) view of the PP-HEX inside the container d) the wavy PP surface characteristic with the welding pattern parameters e) the PP-HEX stack in the CTES unit with vertical plate pitch.

acting as refrigerant collectors are welded from both sides of the PP, ensuring the inlet and outlet of the refrigerant. After the welding process, the plate is inflated by a hydroforming process, applying high water pressure to the inside of the plate. This process creates the flow channels for the fluid inside the PP and its main wavy surface characteristic (see Fig. 1d). Any number of PP can then be stacked vertically or horizontally, forming a complete PP-HEX.

Although PP-HEX is an emerging design used in chemical and process applications, the published literature on design methods, heat transfer calculation and flow patterns in this type of HEXs remain limited. The mathematical description of the surface and the flow channel cross-section is more challenging than for conventional HEX due to the complex channel shape created by the hydroforming process and its periodicity. Until the date, the published literature on PP-HEX covers both experimental [34–36] and numerical investigations [37–42]. Most studies on PP-HEX use a configuration with a cold and hot stream pair; one stream flowing inside the PP channel and the other stream flowing over the external surface of the PP. Mitrovic and Peterson [34] performed an experimental study of a PP-HEX applied as a condenser for the process fluid located at the top of a distillation column. The experiments were carried out with Marlotherm oil (single-phase) and isopropanol (two-phase) as the hot stream flowing between the PPs, and cooling water as the cold stream flowing inside the PPs. The correlations for the heat transfer and the pressure drop occurring between the condensing isopropanol and the cooling water were developed. However, the application was limited to the specific HEX geometry and the fluid used in the study. Mitrovic and Maltic [37] numerically investigated the effect of the flow parameters and channel geometry on the thermo-hydraulic performance of PPs. It was shown that using a PP provides a heat transfer improvement up to four times compared to a flat

channel with plane walls. However, the PP generally generated a higher pressure drop than the corresponding flat channel geometry. Piper et al. [43] performed a numerical study of PP using forming simulations in the Finite-Element-Analysis software ABAQUS. The study aimed to establish a method of determining the hydraulic diameter, cross-sectional area and heat transfer area of PPs. The results show that the forming simulation could reproduce the PP surface shape with a deviation of less than 4%, and expressions for the design parameters of PP were provided based on the results. Tran et al. [35] carried out experimental investigations on both a lab-scale and a pilot-scale PP-HEX applied as condensers in distillation columns. In the pilot-scale PP-HEX, condensation of chlorobenzene occurred between the PP by flowing cooling water inside the PP. Piper et al. [38] numerically investigated the heat transfer and fluid dynamics in a periodic element of a PP for single-phase turbulent flow (water). The investigation showed that two distinct zones characterise the flow; the meandering core and the recirculating zone forming in the wake of the welding spots. The parametric study has revealed that a longitudinal welding pattern, a larger inflation height and a low Reynolds number generates the highest HEX efficiency (heat transfer to pressure loss ratio). Additionally, the results showed that using oval welding spots increased the HEX efficiency up to 37% compared to the conventional round type. For oval spot welds, the size of the recirculating zone was reduced, which was the main contributor to the pressure loss in the PP. In further work, Piper et al. [39] proposed different models to describe the heat transfer and pressure loss for single-phase turbulent forced convection flow in PPs. The equations were fitted with validated CFD data obtained in [38], achieving a relative deviation of less than 6% for the pressure loss and less than 15% for the heat transfer compared to the numerical data. To the authors best knowledge, only one study can be found in the literature on the two-phase heat transfer characterisation inside the PP channel. The evaporation of the refrigerant R134a was experimentally investigated inside a PP in both natural and forced circulation operations modes [36]. The two-phase heat transfer coefficient for the evaporation process inside the PP channel was determined. A numerical investigation on the influence of various geometrical parameters and flow conditions on the PP performance was performed by Shirzad et al. [41]. The results agreed with those obtained by Piper et al. [38], and here it was shown that a PP with a larger inflation height (from 3 mm to 7.5 mm) improves the HEX performance by up to 4 times due to a reduction in the pressure loss (Reynolds number of 1000). Additionally, increasing the longitudinal spot weld distance from 53 mm to 73 mm improved the efficiency by 5% at a Reynolds number of 6000. A similar study was performed by Kumar et al. [42], where increasing the PP channel height from 3 mm to 6 mm resulted in a decrease in specific pressure drop of 81% and an increase in the Nusselt number of 29%. Overall, this improved the HEX efficiency by a factor of 3. The results have also revealed that increasing the welding spot diameter have a negligible effect on the heat transfer in the channel. However, the pressure loss was found to be higher with larger welding spots. Consequently, the overall HEX efficiency was reduced. Arsenyeva et al. [40] established a method for the design of PP-HEX based on predefined process conditions of the cold and hot streams in addition to limits of pressure loss and heat transfer in the HEX. The proposed method evaluates the overall heat transfer coefficient and velocities in both the external channel (between each PP) and inner channels for several PP geometries. By fully exploiting the allowable pressure drop of the cold stream in the inner PP channel, the distance between each PP was varied to find the minimum heat transfer surface area that satisfies the operating conditions. The results show that the PP-HEX requires approximately 30% lower heat transfer area compared to a chevron type plate HEX when using water as both the hot and cold streams.

Natural refrigerants such as CO_2, ammonia and hydrocarbons are the most sustainable and environmentally friendly refrigerants [44,45]. CO_2 transcritical refrigeration systems have become the industry standard in supermarket refrigeration for cold and mild climates [46]. Furthermore, CO_2 is becoming a viable alternative in the industrial refrigeration sector with available system capacities in the range of 2–3 MW [47]. Other demonstrated and well-proven CO_2 refrigeration applications are residential water heaters [48] and systems for ice rinks [49]. Demonstration of the performance of HEX units for latent CTES is vital to increase the confidence in this technology by manufacturers and stakeholders in the refrigeration industry. Thorough experimental characterisation of promising PCM-HEX units at a laboratory scale is a measure that can contribute to establishing up-scaled pilot plants and demonstration sites in the refrigeration industry, increasing the market penetration of CTES technology. The design of a novel latent CTES unit based on the PP-HEX design intended as a peak shaving device was first presented by Selvnes et al. [50]. The unit could be integrated into the primary refrigeration circuit of an industrial size CO_2 refrigeration system. The CTES unit, experimental facility, and implementation strategy were described in detail. The initial results using water as the storage medium were then presented by Selvnes et al. [51]. In the current paper, the performance of the novel PP CTES unit is tested for various PP configurations and refrigerant parameters using water/ice as the PCM. During the charging process, heat is transferred from the PCM to the CO_2 so that the storage medium solidifies and the refrigerant evaporates. During the discharging cycle, heat is transferred from the CO_2 to the PCM so that the storage medium melts and the refrigerant condenses. First, a presentation of the CTES unit and the experimental setup is given, followed by a description of the experimental procedure for the charging and discharging cycles. Finally, the results from the experimental characterisation of the CTES unit are presented and discussed separately for the charging and discharging processes.

2. Experimental setup

2.1. Cold thermal energy storage unit

The novel CTES unit is shown in Fig. 1b. It is composed of a plates-in-tank HEX design immersed in water as the cold storage medium for industrial refrigeration applications (see Fig. 1c). Using water as the cold storage medium is suitable for peak shaving of the cooling load in refrigeration systems for AC or process cooling in the temperature range of 0 °C to 10 °C. Heat is transferred to/from the flowing refrigerant in the PP during the storage charging/discharging processes, respectively. The plates-in-tank design consists of a stack of ten PP constructed of stainless steel. The main design parameters for the PP-HEX are the overall PP length (L_{PP}), the width (W_{PP}), the maximum vertical distance between each PP (δ_o) and the number of plates (n_{PP}). One PP is represented in Fig. 1a. It is composed of two metal sheets of stainless steel with a thickness of 1 mm welded together by a laser-welding machine.

The main geometrical design parameters of one PP are the following (see Fig. 1d-e): the spot weld diameter (d_{SW}), the transversal spot weld pitch (s_T), the longitudinal spot weld pitch (s_L), the channel maximum inflation height (δ_i) and the PP wall thickness (b_w). In this study, a longitudinal welding spot pattern was applied to the PP. It has a longitudinal welding spot pitch of 50 mm and a transversal welding spot pitch of 30 mm. This parameter selection results in a triangular configuration commonly found in the PP industry. The detailed view of the PP surface in Fig. 1d clearly shows the staggered spot-weld pattern of the PP, which promotes the mixing of the flow as well as an improving heat transfer between the refrigerant and the storage medium [38]. Two longitudinal seam welds are performed on the plate, as indicated in Fig. 1a. It generates three flow passes for the refrigerant to flow between the inlet and outlet pipe. This technique is used to direct the refrigerant flow and ensure a better distribution through the channels to maximise the heat exchange between both mediums. The plate stack is mounted on a support frame of square steel tube for convenient installation and removal of the stack into the container. The PPs are fixed in the frame by six metal supporting rods, three along each side of the plates (see Fig. 1c). The distance (pitch) between the PPs in the PP-HEX can be varied using different lengths of cylindrical spacers and washers on the

metal rods, shown in Fig. 1e. The plate pitch is a key parameter for the proper design of the CTES unit. The selection of the PP pitch is based on the thermal properties of the PCM, the required storage capacity and the refrigeration load profile of the process. In the current investigation, the experimental performance characterisation of the CTES unit is carried out with three vertical plate-to-plate pitches (δ_o): 15 mm, 30 mm, and 45 mm. The same number of PPs (10) in the stack was used for all the tests. The total heat exchange area for all test campaigns was 21.90 m^2. The inlet and outlet pipe to/from each PP is connected to a manifold by a high-pressure braided hose at their respective ends of the PP-HEX (see Fig. 1c). The CTES unit is connected to the experimental test facility by a pipe from the manifold that passes through the container wall, shown in Fig. 1b. The stack of PP is placed into a stainless-steel container which is supported by a frame of square steel tube. The PCM is filled into the container so that the PP-HEX is completely immersed in liquid. A lid is placed at the top of the container to prevent the evaporation of the PCM. The CTES unit is equipped with two windows of thick acrylic plexiglass on each side for visual observation of the melting and freezing process of the PCM as shown in Fig. 1b. The container is insulated using 50 mm polystyrene plates. The container is fitted with a service valve to drain the PCM when needed. The main geometrical parameters of the CTES unit are summarised in Table 1.

2.2. Experimental test facility

An experimental test facility is designed by the authors and constructed to test the performance of the CTES unit [50]. A simplified Piping and Instrumentation Diagram (P&ID) of the test facility is shown in Fig. 2. The purpose of the facility is to set and monitor the thermo-hydraulic conditions of the refrigerant at the inlet of the CTES unit during the charging and discharging processes. The facility is operated in two different modes: Charging mode (indicated with green lines in Fig. 2) and discharging mode (indicated with purple lines in Fig. 2). Four circuits can be identified in the facility: The Primary CO_2 Circuit (PCC), the Secondary CO_2 Circuit (SCC), the Glycol Heating Circuit (GHC), and the Auxiliary CO_2 Circuit (ACC). During the charging mode, the PCC and the ACC are in operation. When the facility is operating in discharging mode, the SCC and the GHC are active. The total charge of refrigerant in the PCC/SCC is approximately 50 kg.

The location of sensors for mass flow rate, temperature, pressure and differential pressure are indicated in Fig. 2. The pressure of the PCC/SCC is measured by an absolute pressure transmitter (P1) calibrated in the pressure range 0–70 bar. Three differential pressure transmitters calibrated in the pressure range 0.03–3 bar are installed to measure the pressure drop across the evaporator HEX (DP1), the CTES unit (DP2) and the condenser HEX (DP3). The refrigerant temperature through both the charging and discharging processes in the PCC/SCC is measured by five RTD Pt100 temperature sensors as follows: inlet and outlet of the CTES unit (T1 and T2), outlet of condenser HEX (T3), outlet of CO_2 pump (T4) and outlet of the evaporator (T5). The water temperature in the CTES unit is measured by T-type thermocouples (TC) located on the top surface of the PPs. A top view of one PP showing the main geometrical characteristics and position of the thermocouples is represented in Fig. 3. Three PPs are selected according to their height in the plate stack. Each of these PPs is equipped with nine consecutively numbered thermocouples distributed on its surface as follows: The thermocouples TC00-TC08 are mounted on PP 2, TC09-TC17 are mounted on PP 5 and TC18-TC26 are mounted on PP 9. The control of the test facility and the collection of the measurement data are achieved using a data acquisition system coupled with LabView software [52]. An overview of the measurement equipment is given in Table 2.

Table 1
Main geometrical parameters of the novel CTES unit.

Parameter	Value
s_L	50 mm
s_T	30 mm
d_{SW}	10 mm
δ_i	4.3 mm
b_w	1.0 mm
L_{PP}	1480 mm
W_{PP}	740 mm
δ_o	15/30/45 mm
n_{PP}	10

The charging process is carried out through the PCC. All CO_2 tubing is K65 copper tubes with brazed joints, while all service valves (V1-V4) are manual ball valves (Refrigera Industriale [53]). The circulation of the refrigerant is assured by a hermetic centrifugal refrigerant pump (CO_2 pump) that is fitted with an inverter for frequency control to control the refrigerant flow rates (CAMh 2/4, AGX3.0 PN60, Hermetic Pumpen GmbH [54]). From the outlet of the CO_2 pump, the refrigerant flow is separated into two pipes: A recirculation pipe back to the receiver and a pipe going to the CTES unit. The recirculation pipe is included according to the specification of the pump manufacturer to assure the minimum flow requirement of the CO_2 pump. A Coriolis flowmeter (FT2) is used to measure the inlet CO_2 mass flow rate to the CTES unit. The refrigerant enters the CTES at a liquid state through valve 2 (V2). The refrigerant evaporates as it flows through the CTES unit as heat is transferred from the storage medium to the refrigerant. At the outlet of the CTES, the refrigerant is a mixture of liquid and vapour. The CO_2 mixture is then circulated through the condenser plate HEX (CBXP52, Alfa Laval), which is connected to the ACC to condense the refrigerant in the PCC to the liquid state. From the outlet of the condenser, the liquid CO_2 is circulated to the refrigerant receiver. Then the liquid is drawn from the bottom of the receiver, and the cycle continues until the charging process is completely achieved.

The ACC has a double function. First, it provides the cooling of the PCC during the charging process. The cooling is achieved by supplying liquid refrigerant through an electronic expansion valve (EEV 1, CCMT-2, Danfoss). Second, it also maintains the desired pressure in the PCC during standstill by supplying cooling in the subcooler through EEV 2 (AKVH 10-3, Danfoss). Both valves are operated by fully automatic Danfoss superheat controllers (EKD 316C and AK-CC550A, respectively). The ACC is connected to the liquid line and suction lines of a CO_2 booster refrigeration system in the laboratory to accomplish these two functions. This refrigeration system has three evaporation levels (−10 °C, −30 °C and −50 °C) that can be chosen by operating a valve station (see Fig. 2). A stepper-type valve (V5, CCMT42, Danfoss) is fitted in the suction side of the ACC. This valve is operating as a back pressure valve to manually control the evaporation pressure of the ACC if an evaporation pressure between the fixed levels is required. By decreasing the evaporation pressure of the ACC, the pressure of the PCC will also decrease. Consequently, experiments with a wider range of evaporation temperatures in the PCC can be carried out.

The discharging process is carried out through the SCC, which is connected to a GHC to simulate the thermal load. Liquid CO_2 is drawn from the bottom of the receiver by the CO_2 pump and circulated to the evaporator plate HEX (CBXP112, Alfa Laval) through valve 1 (V1). In the evaporator, heat is transferred from the glycol to the refrigerant so that the CO_2 exits the evaporator as a liquid/vapour mixture. The two-phase CO_2 then circulates through the CTES unit, where heat is transferred to the storage medium and the refrigerant condenses to a fully liquid state. The liquid then returns to the refrigerant receiver through valve 3 (V3), completing the cycle. The Heat Transfer Fluid (HTF) in the GHC consists of a mixture of 30% propylene glycol and water (DowCal 200, [55]). The glycol is supplied to the evaporator by a circulation pump (UPS25-125, Grundfos). The glycol mass flow rate is measured by a Coriolis mass flow meter (FT 1). The heat input to the GHC is achieved by two 9 kW electric immersion heaters. One of the heaters is fitted with pulse-width modulation (PWM) control for precise regulation of the

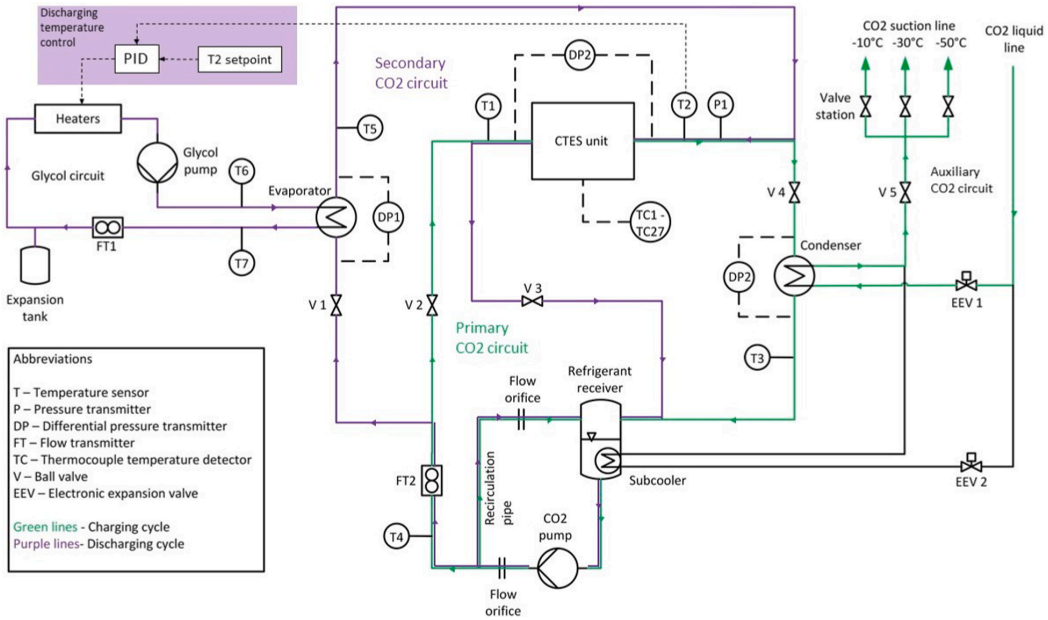

Fig. 2. Piping and instrumentation diagram (P&ID) of the test facility.

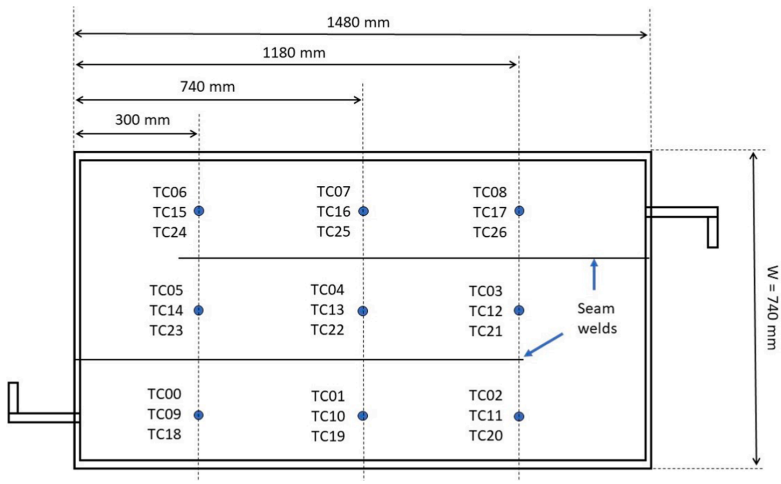

Fig. 3. Top view of a PP: Locations of thermocouples on three selected PPs.

power output from 0 to 100%. Furthermore, two RTD Pt100 temperature sensors are mounted in the inlet (T6) and outlet (T7) pipe of the evaporator to measure the inlet and outlet temperature of the glycol, respectively.

3. Experimental procedure

3.1. Charging process

The charging process consists of extracting heat from the PCM storage medium to the refrigerant. Consequently, the PCM solidifies (heat release) and the refrigerant evaporates (heat absorption). During the charging process (see Fig. 2), valve 1 (V1) and valve 3 (V3) is closed so that the CO_2 refrigerant circulates through the PCC as described in Section 2.2. In this study, a series of experiments considering various refrigerant mass flow rates and evaporation temperatures were conducted for each plate pitch. The refrigerant evaporation temperature was varied from −2.5 °C to −15 °C, and the mass flow rate was varied from 4 kg/min to 10 kg/min. The charging process in each test was run until completion to compare storage capacities and charging time of the different HEX configurations and operating conditions. The charging process starts when the average value given by the first placed TC on each plate is measured below 5 °C. TC00, TC09 and TC17 are the closest sensors to the refrigerant inlet on PP2, PP5 and PP9, respectively. As the

Table 2
Measurement equipment utilised in the test facility.

Component	Model	Producer	Indicated accuracy
Absolute pressure transmitter	Cerabar S PMP71	Endress+Hauser	±0.25% of set span
Differential pressure transmitter	Deltabar S PMD75	Endress+Hauser	±0.15% of set span
Temperature sensor CO_2 and glycol	Class B RTD Pt100	RS PRO	±0.1 K
Temperature sensor water	Thermocouple type T	RS PRO	±0.2 K
Mass flow meter glycol	RHM 15 Coriolis meter	Rheonik	±0.2% of reading
Mass flow meter CO_2	RHM 06 Coriolis meter	Rheonik	±0.2% of reading

charging process takes place, an ice layer on each plate is formed and becomes thicker as the charging process progresses. The charging process ends when an ice block is formed between two adjacent PPs, i.e. when the ice layer on the two PPs has overlapped. At this point, energy storage is carried out through a sensible energy storage process until the temperature of the ice block approaches the inlet refrigerant temperature. In the tests, the end of the charging cycle is that corresponding to a temperature difference between the mean value of the last-placed TC on each instrumented PP (TC8, TC17 and TC26) and the refrigerant saturation temperature, is lower than 0.2 K. This period from the first temperature sensors (TC00, TC09 and TC17) measures a storage medium temperature below 5 °C and the last temperature sensors (TC8, TC17 and TC26) approaches the refrigerant evaporation temperature by 0.2 K is defined as the charging time. The progress of the charging cycle can also be easily observed by following the ice block thickness through the four windows on the CTES unit (see Fig. 1b). The theoretical maximum latent storage capacity of the CTES unit depends on the PP size and the vertical plate-to-plate pitch. Due to the pillow-like surface of the plates, the vertical distance between two plates varies across the surface. The mean vertical plate-to-plate pitch $\delta_{o,mean}$ is approximated as the mean value between the maximum (δ_o) and the minimum (δ_o - δ_i) distance between two adjacent plates, as given by Eq. 1:

$$\delta_{o,mean} = \frac{1}{2}((\delta_o - \delta_i) + \delta_o). \quad (1)$$

The maximum theoretical latent storage capacity is calculated considering only the PCM volume between the PPs as the active PCM volume. Furthermore, it is assumed that the ice layer below PP1 and above PP10 has grown to a thickness of half the vertical plate pitch when the charging cycle is complete (see Fig. 1e). The theoretical maximum latent storage capacity can be calculated as follows:

$$E_{lat,th} = h_{fus,\mathrm{PCM}} \cdot \rho_{s,\mathrm{PCM}} \cdot (W_{\mathrm{PP}} \cdot L_{\mathrm{PP}} \cdot \delta_{o,mean} \cdot n_{\mathrm{PP}}) \quad (2)$$

where $E_{lat,th}$ is the theoretical maximum latent storage capacity of the CTES unit, $h_{fus,\mathrm{PCM}}$ is the specific enthalpy of fusion of the PCM, and $\rho_{s,\mathrm{PCM}}$ is the solid density of the PCM. The last term of Eq. 2 ($W_{\mathrm{PP}} \cdot L_{\mathrm{PP}} \cdot \delta_{o,mean} \cdot n_{\mathrm{PP}}$) is the total active volume of PCM in the CTES unit. The mass flow rate of the CO_2 in the PCC is adjusted by controlling the frequency output of the inverter for the CO_2 pump in the range 35–50 Hz. If a lower mass flow rate is required than the minimum frequency, the flow is throttled by partly closing valve 2 (V2, see Fig. 2). The evaporation temperature of the CO_2 in the CTES unit is set by adjusting the cooling rate of the ACC in the condenser. The pressure in the primary CO_2 is kept constant as the same extracted heat rate from the CTES unit is rejected through the condenser. When a higher cooling rate is provided to the condenser, the pressure of the PCC is lowered.

3.2. Discharging process

The discharging process consists of the heat transfer from the refrigerant to the storage medium. As the refrigerant flows inside the PPs, heat is rejected to the storage medium until the refrigerant is completely condensed at the outlet of the PP manifold. Consequently, the PCM temperature increases until it is completely melted. During the discharging process, valve 2 (V2) and valve 4 (V4) are closed (see Fig. 2) so that the SCC is active. The flow direction through the CTES unit is reversed compared to the charging cycle so that the inlet and outlet are swapped. The refrigerant mass flow rate is controlled in the same manner as described in Section 3.1. The heat input to the CO_2 from the GHC controls the pressure in the SCC during the discharging cycle. If the heat transferred to the CO_2 in the evaporator equals the heat rejected to the storage medium in the CTES unit, the pressure in the SCC remains constant. In this case, the pressure can be controlled by supplying more or less heat to the secondary circuit. As described in Section 2.2, the output of the electric heaters can be controlled with high precision as one of the heaters is equipped with PWM control. A PI-controller in the LabVIEW software adjusts the output of the PWM-controlled heater from 0% to 100% according to the set point temperature of the refrigerant at the inlet of the CTES unit. Since the discharging cycle is a highly transient process, the PI controller continuously adjusts the heater output to keep the pressure level constant in the secondary circuit. The discharging process continues until all the ice blocks have melted or until the refrigerant is not able to reject any more heat to the CTES unit without increasing the pressure. The discharging time is defined as the period from the start of the discharging cycle until one of these criteria occurs.

For each PP-HEX configuration, a series of experiments considering various CO_2 mass flow rates and condensing temperatures were conducted. The refrigerant condensing temperature was varied from 2.5 °C to 10 °C, and the mass flow rate was varied from 4 kg/min to 10 kg/min. The discharging capacity of the CTES unit is calculated based on the heat flow from the glycol to the CO_2 in the evaporator, assuming there is no heat loss to the ambient. The energy balance for the evaporator is presented in Eq. 3. The thermodynamic properties of the glycol mixture were taken from the data sheet of the manufacturer, assuming a constant specific heat capacity in the relevant temperature range. The refrigerant enters the CTES unit as a two-phase mixture and exits the CTES unit in a subcooled condition. Consequently, the heat transferred from the glycol to the CO_2 in the evaporator is that rejected to the PCM during the discharging process as formulated in Eq. 3 and 4:

$$\dot{E}_{\mathrm{CO_2}} - \dot{E}_g = 0, \quad (3)$$

$$\dot{E}_{\mathrm{CO_2}} = \dot{m}_g \cdot cp_g \cdot (T_{g,out} - T_{g,in}), \quad (4)$$

where $\dot{E}_{\mathrm{CO_2}}$ is the heat flow to the refrigerant in the evaporator, $\dot{E}_g$ is the heat flow from the glycol, $\dot{m}_g$ is the glycol mass flow rate, cp_g is the specific heat capacity of the glycol and $(T_{g,out} - T_{g,in})$ is the temperature difference of the glycol between the inlet and the outlet in the evaporator.

4. Uncertainty analysis and repeatability

The output of the temperature sensors were checked with an ice water bath and validated to operate at within ±0.2 K (thermocouples TC01-TC27, see Fig. 2) and ±0.1 K (RTD100 T1-T7, see Fig. 2) at 0 °C. The uncertainty analysis was carried out by the method elaborated in [56], using a confidence level of 95% (coverage factor of 2). The formulation used for propagation of uncertainty is summarised below. Uncertainty for the mean PCM temperature on PP2, PP5, and PP9 ($T_{\mathrm{PP2,mean}}$, $T_{\mathrm{PP5,mean}}$, and $T_{\mathrm{PP9,mean}}$):

$$u(T_{PCM}) = \sqrt{(1/9)^2 \cdot \sum_{i=1}^{9} u(T_i)}. \quad (5)$$

Uncertainty for the refrigerant saturation temperature:

$$u(T_{CO_2,sat}) = \sqrt{\left(\frac{\partial T_{CO_2,sat}}{\partial P_{CO_2,sat}}\right)^2 \cdot u(P_{CO_2,sat})^2}. \quad (6)$$

From the Antoine equation the relationship between saturation temperature and saturation pressure can be found. By derivation and inserting the coefficients for CO_2, it can be written as:

$$\frac{\partial T_{CO_2,sat}}{\partial P_{CO_2,sat}} = \frac{2273.66}{P_{CO_2,sat} \cdot (17.9834 - \ln(P_{CO_2,sat}))^2}. \quad (7)$$

Uncertainty in the heat flow from the glycol to the refrigerant in the evaporator:

$$u(\dot{E}_{CO_2}) = \sqrt{(cp_g \cdot \Delta T_g \cdot u(\dot{m}_g))^2 + (\dot{m}_g \cdot cp_g \cdot u(\Delta T_g))^2}. \quad (8)$$

Uncertainty in the glycol temperature difference from inlet to outlet in the evaporator:

$$u(\Delta T_g) = \sqrt{u(T_{g,in})^2 + u(T_{g,out})^2}. \quad (9)$$

The uncertainty in the discharged energy over the cycle is estimated by integrating the uncertainty in the heat flow from the glycol (Eq. 8 from the start to the end of the cycle. To investigate the repeatability of the experiments, tests with identical test conditions were carried out for the 30 mm and 45 mm plate pitches. The charging time was used as the indicator for the charging cycle. The resulting range of charging time was found to be <10 min for both the 30 mm and 45 mm plate pitch. This corresponds to a repeatability of the charging time within ±5.9% and ±3.3% at $T_{sat} = -5$ °C and $\dot{m}_{CO_2} = 7$ kg/min for the 30 mm and 45 mm plate pitch, respectively. For the discharging process, the mean discharge rate and discharged energy over the cycle were chosen as indicators for repeatability. The obtained range for the discharged energy over the cycle was <1 kWh for both configurations, corresponding to <5% and <3% of the discharged energy for the 30 mm and 45 mm plate pitch, respectively. For the mean discharge rate, the obtained range was <0.25 kW for both configurations.

5. Results and discussion

5.1. Charging cycle

This section presents the results obtained from the charging tests described in Section 3.1. The mean refrigerant evaporation temperature is calculated using the REFPROP 10 database [57] based on the mean pressure in the CTES unit between the inlet and outlet using transmitter P1 and DP2 (see Fig. 2). The mean pressure drop across the CTES unit during the charging process as a function of the CO_2 evaporation temperature for three mass flow rates ($\dot{m}_{CO_2} = 4$ kg/min, $\dot{m}_{CO_2} = 7$ kg/min and $\dot{m}_{CO_2} = 10$ kg/min) is shown in Fig. 4. The presented values of the pressure drop are the mean value over the complete charging cycle. From Fig. 4 it can be observed that the mean pressure drop increases when the evaporation temperature of the refrigerant is reduced. For a given mass flow rate, as the CO_2 evaporation temperature is reduced, more refrigerant is evaporated in the PP due to the higher temperature difference between the storage medium (water/ice) and the refrigerant. Thus the mean refrigerant density decreases and the mean refrigerant velocity increases, resulting in a higher pressure drop across the CTES unit. An increasing pressure drop difference is observed for the higher refrigerant mass flow rate for the studied evaporation temperature range (-1.5 °C to −10 °C). The pressure drop difference between −1.5 °C and −10 °C was calculated to be approximately 91%, 113% and 138% for $\dot{m}_{CO_2} = 4$ kg/min, $\dot{m}_{CO_2} = 7$ kg/min and $\dot{m}_{CO_2} = 10$ kg/min, respectively.

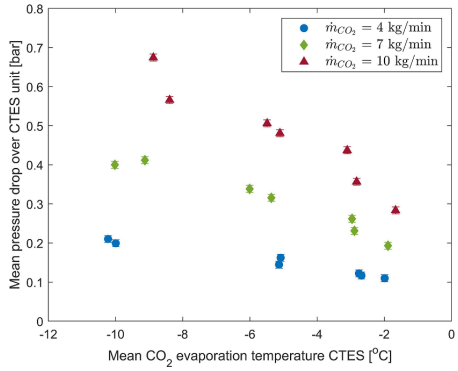

Fig. 4. Mean pressure drop over CTES unit during charging cycle as a function of the refrigerant evaporation temperature for various refrigerant mass flow rates.

The refrigeration capacity of the ACC limited the evaporation temperature to approximately −8.9 °C for the highest refrigerant mass flow rate ($\dot{m}_{CO_2} = 10$ kg/min). Furthermore, increasing the refrigerant mass flow rate increases the mean pressure drop for a given evaporation temperature. At a refrigerant evaporation temperature of −5 °C, the mean pressure drop increases by about 118% and 232% when increasing the refrigerant mass flow rate from 4 kg/min to 7 kg/min and 10 kg/min, respectively. The increase in pressure drop with increasing mass flow rate is caused by an increased mean velocity of the refrigerant in the PP channel.

The mean storage medium temperature adjacent to the PPs in the stack (PP2, PP5 and PP9, see Section 2.2) during the charging process as well as the CO_2 evaporation temperature represented in Fig. 5c using refrigerant mass flow rates of $\dot{m}_{CO_2} = 4$ kg/min, $\dot{m}_{CO_2} = 7$ kg/min and $\dot{m}_{CO_2} = 10$ kg/min, respectively. All three experiments use a plate pitch of 30 mm, an initial temperature of the storage medium of 9 °C and a refrigerant evaporation temperature of −5 °C. For a given refrigerant mass flow rate, as the charging process progresses, the water temperature decreases from the initial temperature to 0 °C (sensible heat storage). When the water temperature reaches 0 °C, the phase change process starts, and the storage medium solidifies. During the phase change process, energy is stored as latent heat, and the charging process progresses with a constant temperature difference between the evaporating refrigerant and the solidifying storage medium. A plateau can then be observed in the temperature profiles to describe the latent heat storage (indicated in Fig. 5a to c). The measured water temperatures on PP2, PP5, and PP9 are approaching the refrigerant evaporation temperature during the latent heat storage period because the thermocouple sensors become embedded in the solid ice layer as the charging progresses. There is a temperature gradient within the solid ice layer in the perpendicular direction of the PP surface, where the temperature ranges from the refrigerant evaporation temperature at the PP surface to the PCM phase change temperature at the liquid-solid interface. After the latent storage period, the storage medium temperature decreases at a higher rate, indicating that the charging process continues as sensible heat storage. The mean storage medium temperature approaches the refrigerant evaporation temperature to denote the end of the charging cycle.

It can be seen from Fig. 5a to c that the experiment time increases for decreasing refrigerant mass flow rates. Compared to a flow rate of $\dot{m}_{CO_2} = 10$ kg/min, the experiment time (from the initial storage temperature to completion) is approximately 8% and 19% longer using a refrigerant mass flow rate of $\dot{m}_{CO_2} = 7$ kg/min and $\dot{m}_{CO_2} = 4$ kg/min, respectively. Furthermore, the storage medium temperature is reduced more rapidly from the initial temperature (9 °C) to the phase change temperature

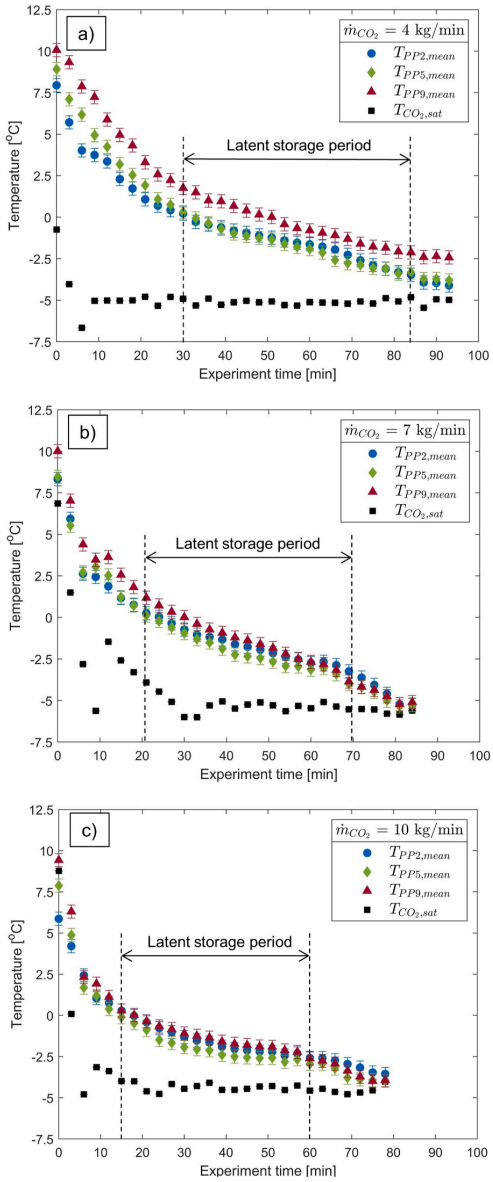

Fig. 5. The mean PCM temperature close to PP 2, 5 and 9 in the stack during the charging cycle with plate pitch $\delta_o = 30$ mm for a refrigerant mass flow rate of a) 4 kg/min b) 7 kg/min and c) 10 kg/min.

using a higher refrigerant mass flow rate. Also, observing the temperature difference through the height of the PP-HEX (T_{PP2}, T_{PP5} and T_{PP9}), a more distinct temperature stratification of the storage medium is observed for the lowest refrigerant mass flow rate (Fig. 5a). These observations are explained by an inadequate refrigerant supply to the PP-HEX to carry out the heat transfer process using the lowest refrigerant mass flow rate. For the flow rate of $\dot{m}_{CO_2} = 4$ kg/min, it was measured varying degree of superheated refrigerant at the outlet of the PP-HEX during the first 20–30 min of the charging process. This observation means that all refrigerant supplied to the CTES unit has been evaporated inside the PPs before reaching the manifold at the outlet. Superheated refrigerant is generally unwanted, as ensuring a vapour/liquid refrigerant mixture throughout the length of the PPs (flooded condition) ensures the best utilization of the heat transfer area and high heat transfer [58–60]. Furthermore, it was visually observed that the lowest refrigerant mass flow rate resulted in a less uniform ice layer on the PP surface, giving less ice growth at the outer edges of the PPs. Consequently, it can be concluded that a refrigerant mass flow rate of $\dot{m}_{CO_2} = 7$ kg/min and $\dot{m}_{CO_2} = 10$ kg/min are more appropriate to produce a uniform ice layer on each PP in the plate stack.

The charging time as a function of the mean refrigerant evaporation temperature and mass flow rates ($\dot{m}_{CO_2} = 4$ kg/min, $\dot{m}_{CO_2} = 7$ kg/min, and $\dot{m}_{CO_2} = 10$ kg/min) for the different configurations are presented in Fig. 6 ($\delta_o = 15$ mm), Fig. 7 ($\delta_o = 30$ mm), and Fig. 8 ($\delta_o = 45$ mm). See Section 3.1 for the definition of the charging time presented here. It can be clearly seen that for all three configurations, the lower the refrigerant evaporation temperature is, the lower the charging time. Indeed, the conduction heat transfer between the PP surface and the solidifying storage medium is the dominant heat transfer mechanism. During the charging process, heat is transferred by conduction from the storage medium to the refrigerant. A solid ice layer is formed on both sides of each PP as the heat transfer progresses. The thickness of the ice layer increases as the charging process is carried out. The charging process ends when a uniform block of ice is developed between each PP. The ice layer growth is the main indicator showing the satisfying progress of the charging process. Nevertheless, the heat transfer will be increasingly limited as the ice layer is developed since it acts as additional thermal resistance to the heat transfer process. One solution to compensate for this phenomenon and decrease the charging time is to increase the temperature difference between the solidifying storage medium and the refrigerant, increasing the driving forces and enhancing the heat transfer. As the phase change temperature of the storage medium is fixed, the temperature difference can only be increased by decreasing the refrigerant evaporation temperature. However, reducing the evaporation temperature increases the required temperature lift of the refrigeration system and directly affects the charging COP. It is established that reducing the evaporation temperature by 1 K will reduce the COP of the refrigeration system by 2–3% [61]. Therefore, it is advisable to operate the system with the highest possible evaporation temperature. However, the optimal evaporation temperature should be selected considering the complete refrigeration system in which the CTES unit is implemented and other factors such as the electricity price and the number of hours available to operate the charging process.

It can also be observed that the charging time is generally reduced by

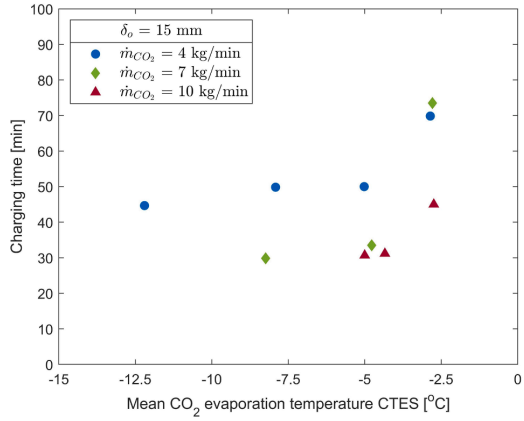

Fig. 6. Charging time for of CTES unit with plate-to-plate pitch of 15 mm as a function of the refrigerant evaporation temperature for various refrigerant mass flow rates.

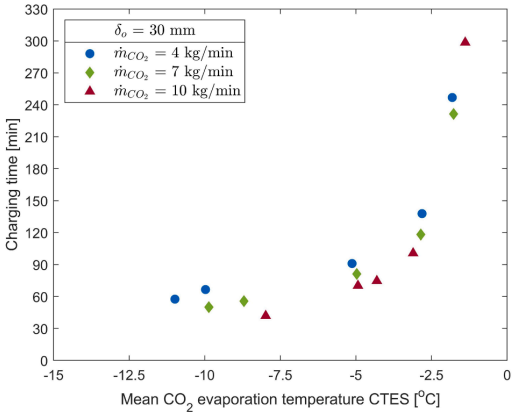

Fig. 7. Charging time for of CTES unit with plate-to-plate pitch of 30 mm as a function of the refrigerant evaporation temperature for various refrigerant mass flow rate.

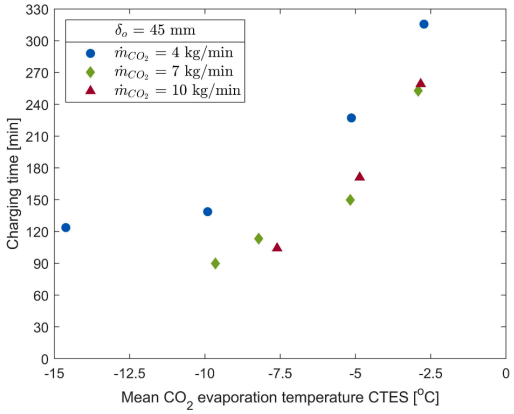

Fig. 8. Charging time for of CTES unit with plate-to-plate pitch of 45 mm as a function of the refrigerant evaporation temperature for various refrigerant mass flow rate.

increasing the refrigerant mass flow rate for the same evaporation temperature and plate pitch. Increasing the flow rate from $\dot{m}_{CO_2} = 4$ kg/min to $\dot{m}_{CO_2} = 7$ kg/min yields the largest reduction in charging time, while only a marginal decrease in charging time is observed when further increasing the flow rate to $\dot{m}_{CO_2} = 10$ kg/min. This observation is explained by the insufficient refrigerant supply to the CTES unit when using the lowest flow rate, as described in detail above. Using a flow rate of $\dot{m}_{CO_2} = 7$ kg/min provides sufficient refrigerant for the charging process and increasing to a higher mass flow rate does not provide any further benefits. In fact, a higher refrigerant mass flow rate is associated with higher pressure drop through the CTES unit (see Fig. 4. Therefore a refrigerant mass flow rate of $\dot{m}_{CO_2} = 7$ kg/min is recommended to operate the charging process. Comparing the charging time between the three plate pitches (Figs. 6–8) for the same evaporation temperature level and mass flow rate, it is clear that the shortest charging time is recorded for the smallest plate pitch ($\delta_o = 15$ mm). This result is expected because increasing the plate pitch increases the amount of storage medium between every PP. Consequently, more energy needs to be stored to complete the charging cycle. For an evaporation temperature of about −8.5 °C and mass flow rate of 7 kg/min, the charging time increases by 87% and 297% when increasing the plate pitch from 15 mm to 30 mm and 45 mm, respectively. For a pitch of 30 mm (Fig. 7), an additional CO_2 evaporation temperature level of approximately −1.7 °C was tested for all three refrigerant mass flow rates. It was found that the charging time has increased by 95% compared to an evaporation temperature of −2.7 °C for a refrigerant mass flow rate of 7 kg/min. Since increasing the evaporation temperature by 1 K resulted in almost double the charging time, this evaporation temperature level was excluded for the 15 mm and 30 mm configurations. Therefore, the recommended upper limit for the evaporation temperature during the charging process is −2.5 °C when implementing the CTES unit into a refrigeration system.

Table 3 shows the approximate active volume of the storage medium and the calculated maximum theoretical latent storage capacity of the CTES unit for the three configurations using Eq. 2. The density of ice is 916.74 kg/m^3, and the enthalpy of fusion is 333.43 kJ/kg [62]. Furthermore, the charging time for each configuration for a refrigerant evaporation temperature of −5 °C and mass flow rate of 7 kg/min is indicated as a reference. Increasing the plate-to-plate pitch from 15 mm to 30 mm yielded an increase of about 116% in latent storage capacity and the charging time by about 142%. By increasing the plate-to-plate pitch from 15 mm to 45 mm, the theoretical latent storage capacity increased by about 233% and the charging time increased by about 347%.

5.2. Discharging cycle

This section presents the results obtained from the discharging tests described in Section 3.2. The discharging rate for tests using a refrigerant mass flow rate of 7 kg/min and a condensing temperature varying from 5 °C to 10 °C for a PP pitch of 15 mm, 30 mm, and 45 mm are presented in Fig. 9a, b, and c, respectively. One may clearly note that the discharging cycles start with a high discharge rate (18–16 kW) for the first 20–35 min due to adjacency of ice to the PP surface and a high temperature difference between the refrigerant inside the PPs and the storage medium (initial temperature about −5 °C). However, the discharge rate is limited during this initial phase by the maximum installed heating capacity of the electric heaters in the glycol system that provides the heat load to the refrigerant (18 kW, see Section 2.2). This initial phase of high discharge rate is the longest for the highest CO_2 condensing temperature. This period constitutes a higher fraction of the total discharging time for the shortest plate pitch (15 mm) due to the melting of a significant share of the ice block. As the discharging process progresses, the discharging rates decrease towards zero, denoting the end of the process. From the ice melting process point of view, a large amount of heat (16–18 kW) is absorbed by the ice block formed between the plates, the ice melts, and thin liquid layers are formed from both sides of the PP. As the discharging process advances, the liquid layers become thicker while the ice block becomes thinner. This water layer between the ice block and the PP surface constitutes a thermal resistance to the heat transfer process, and the growth of the liquid layer results in a decrease in the discharge rate. Furthermore, the highest mean discharging rates of 7.97 kW ($\delta_o = 15$ mm), 9.82 kW ($\delta_o = 30$ mm) and 7.90 kW ($\delta_o = 45$ mm) are achieved using the highest refrigerant condensing temperatures for each plate pitch (7.9 °C, 8.5 °C and 9.0 °C), due to the larger difference between the refrigerant inlet temperature and the storage medium. For the 15 mm configuration (Fig. 9a) the discharging

Table 3
Calculated maximum theoretical latent storage capacity of the CTES unit in various configurations. Charging time is given for a refrigerant mass flow rate of 7 kg/min and a evaporation temperature of −5 °C.

δ_o [mm]	$\delta_{o,mean}$ [mm]	$V_{PCM,tot}$ [m^3]	$E_{lat,th}$ [kWh]	t_C [min]
15	12.85	0.1271	10.80	34
30	27.85	0.2755	23.40	81
45	42.85	0.4240	36.00	150

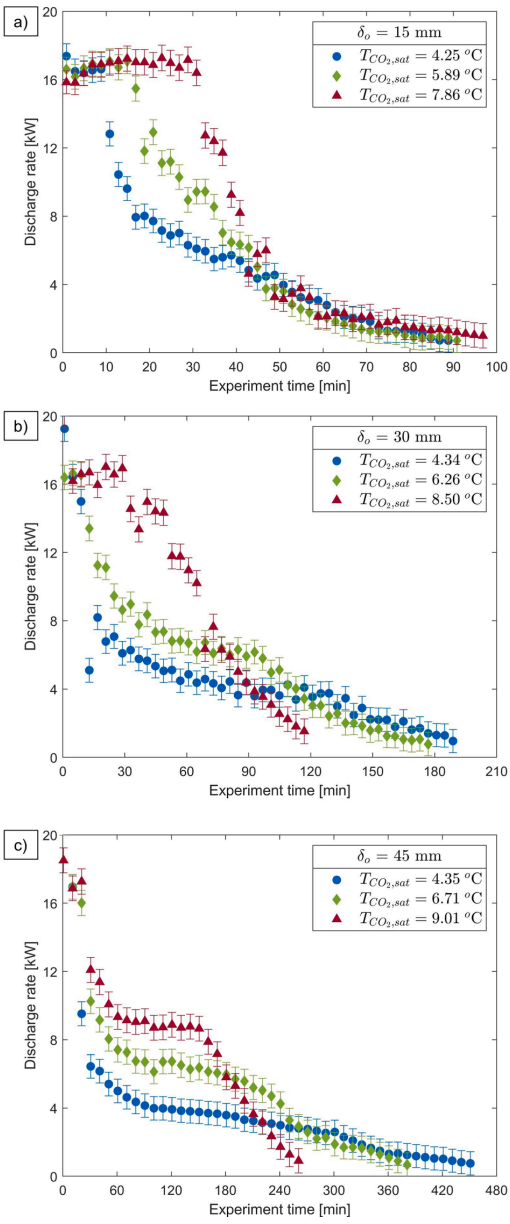

Fig. 9. Discharging rate of the CTES unit over the discharging cycle using a refrigerant mass flow rate of 7 kg/min for various refrigerant condensation temperatures for plate-to-plate pitch of a) 15 mm b) 30 mm c) 45 mm.

time is similar for the three condensing temperatures (4.25 °C, 5.89 °C and 7.86 °C). In contrast, the discharging time using a pitch of 30 mm (Fig. 9b) and 45 mm (Fig. 9c) is significantly shorter for the highest condensing temperature (8.50 °C and 9.01 °C, respectively) compared to the middle and low condensing temperatures. The most significant difference in the discharging time when varying T_{CO_2} is observed for the largest plate-to-plate pitch ($\delta_o = 45$ mm).

The mean discharge rate and discharged energy over the discharging cycle as a function of the refrigerant mass flow rate when using a condensation temperature of 6 °C is presented in Fig. 10 and 11, respectively. From Fig. 10 the general observation is that increasing the refrigerant mass flow rate increases the mean discharge rate for all plate pitches. The one exception is for the 15 mm configuration, where 4 kg/min and 7 kg/min show similar discharge rates. For the 30 mm configuration, the mean discharge rate increases by 21.6% and 58.2% when increasing the refrigerant mass flow rate from 4 kg/min to 7 kg/min and 10 kg/min, respectively. Furthermore, the mean discharge rate decreases when increasing the plate-to-plate pitch. For a refrigerant mass flow rate of 10 kg/min, the mean discharge rate is reduced by 17.8% and 36.5% when increasing the plate pitch from 15 mm to 30 mm and 45 mm, respectively. From Fig. 11 it can be observed that the discharged energy over the cycle is increasing when increasing the plate-to-plate pitch. The higher amount of discharged energy is due to a thicker ice block between each plate that gives more thermal energy stored in the PP-HEX. Furthermore, a mass flow rate of 7 kg/min results in the highest amount of discharged energy over the cycle for all three plate pitches. The difference in discharged energy by varying the mass flow rate is most pronounced for the largest plate pitch with a difference in stored energy of 8.2%, 18.8% and 23.0% for the 15 mm, 30 mm and 45 mm configuration, respectively.

Table 4 give a summary and comparison of the discharging performance of the CTES unit for the three plate-to-plate configurations for a refrigerant mass flow rate of 7 kg/min. For the 30 mm and 45 mm plate-to-plate pitch, the discharging time is significantly reduced by increasing the condensing temperature of the refrigerant. On the other hand, the condensing temperature has no considerable effect on the discharging time for the 15 mm HEX configuration. Consequently, the thermal energy of the CTES unit is discharged over a shorter period. As discussed before, a larger temperature difference between the condensing refrigerant and the storage medium increases the driving force for the heat transfer process during the discharging cycle. This effect is particularly important for the larger plate-to-plate pitches (30 mm and 45 mm) because of the increased thermal resistance caused by the thicker liquid layer forming on the PP surface compared to the 15 mm plate pitch. Table 4 includes the ratio of total discharged energy to the maximum theoretical latent storage capacity. It can be observed that the discharged energy is lower than the theoretical maximum capacity of the unit, except for the highest condensing temperature using a pitch of 15 mm. For the total discharge energy measured in the experiments (E_D), the contribution from both the latent heat storage and sensible heat storage in the CTES is included. Since the theoretical maximum latent storage capacity ($E_{lat,th}$) includes only the latent heat storage, the ratio of the total discharged energy to the maximum theoretical latent storage

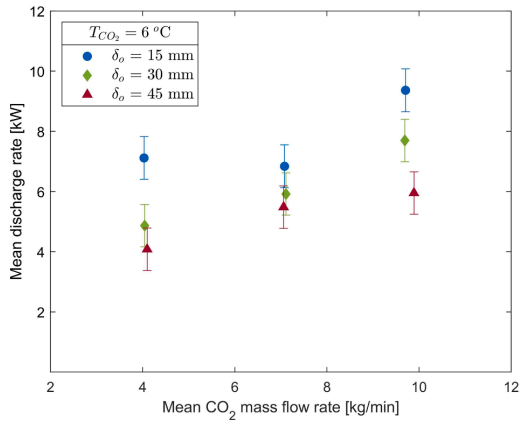

Fig. 10. Mean discharge rate as a function of refrigerant mass flow rate for a refrigerant condensation temperature of 6 °C.

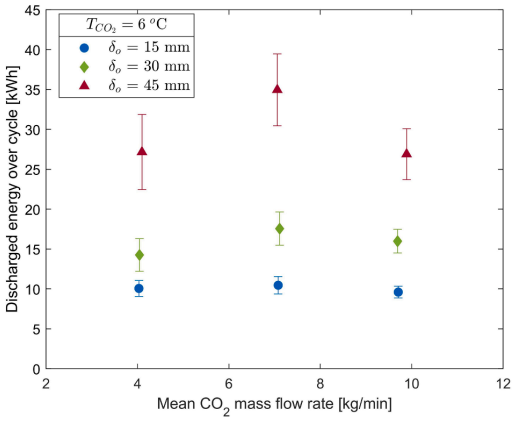

Fig. 11. Discharged energy as a function of refrigerant mass flow rate for a refrigerant condensation temperature of 6 °C.

Table 4
Summary of the discharging performance employing a refrigerant mass flow rate of $\dot{m}_{CO_2} = 7$ kg/min for various plate-to-plate configurations.

δ_o [mm]	T_c [°C]	$\dot{E}_r$ [kW]	E_D [kWh]	$E_D/E_{lat,th}$	t_D [min]
15	4.26	5.82 ± 0.687	8.62 ± 1.02	0.799	89
15	5.89	6.84 ± 0.712	10.46 ± 1.09	0.969	92
15	7.86	7.97 ± 0.725	12.91 ± 1.17	1.20	97
30	4.34	4.67 ± 0.690	14.76 ± 2.18	0.680	190
30	6.26	5.92 ± 0.702	17.56 ± 2.09	0.809	178
30	8.50	9.82 ± 0.732	19.69 ± 1.47	0.907	121
45	4.35	3.55 ± 0.687	26.90 ± 5.21	0.747	455
45	6.71	5.48 ± 0.705	34.95 ± 4.50	0.971	383
45	9.01	7.90 ± 0.725	35.29 ± 3.24	0.980	268

capacity can be larger than one. It can also be observed that the 15 mm configuration had the highest ratio of discharged energy to theoretical storage capacity for all refrigerant condensing temperatures due to the proximity of the ice block to the PP over the whole cycle. There are multiple explanations why the ratio of the discharged energy to the theoretical storage capacity generally is lower than one. Indeed, when calculating the theoretical latent storage capacity, the entire surface of the PP is assumed to be covered by solid ice. When the charging tests are completed, no ice around the outer edges of the PP was completely formed. This edge effect will be less critical for a full-size CTES unit using larger PP sizes than in the present study. Moreover, at the locations where the refrigerant turns around the longitudinal seam welds to start the next flow pass, the ice did not form at the outer edge (see Fig. 3). This effect was most visible for the lowest refrigerant mass flow rate, indicating a poor refrigerant distribution in this section of the PP. Possible solutions to this issue are to increase the length of the longitudinal seam welds or manufacture the PP with more refrigerant flow passes. The latter will improve the refrigerant distribution by creating narrower channels and a longer flow length for the refrigerant at the cost of increasing the pressure loss. Overall, it can be concluded that a refrigerant flow rate of 7 kg/min is convenient to ensure adequate refrigerant distribution for the current design of the PP. However, the refrigerant distribution can be improved by including more flow passes for the refrigerant for future work.

Table 4 can be used as a design guide for the practical implementation of this type of CTES unit into a refrigeration plant. Given that peak shaving of the refrigeration demand is the aim of the CTES implementation, the designer must have an accurate prediction of the load curve of the refrigeration plant. Based on the desired peak reduction and peak duration, the adequate CTES configuration and operating conditions can be selected based on Table 4. As a general recommendation, the 15 mm configuration will be a good fit for reducing a peak with a short duration (1–1.5 h) and a relatively high refrigeration load. To achieve peak shaving for a peak with a lower magnitude and a duration in the range of 4 to 6 h, the 45 mm configuration is the appropriate selection. If more storage capacity or a higher discharge rate is required than provided by a single CTES unit, two or more units can be installed in parallel. Furthermore, this CTES unit can also be installed as a subcooler in a similar configuration as presented by Korth et al. [32]. Using a thermal energy storage unit as a subcooler has been proven to effectively increase the COP of the refrigeration cycles by increasing the evaporation capacity or by reducing the throttling losses in the case of CO_2 systems [11].

6. Conclusions

This paper presents the development of a novel Cold Thermal Energy Storage (CTES) unit and the associated experimental test facility. Inside the CTES unit, the Heat Exchanger (HEX) employs Pillow Plates (PP) to exchange heat between the latent storage medium (ice/water) and the refrigerant (CO_2). It is designed to be integrated directly into the primary refrigerant circuit to achieve peak shaving of the refrigeration demand. This work is one of the very few experimental demonstrations of a CTES unit that couples the isothermal phase change process of the latent storage medium with the isothermal phase change process of the refrigerant. The work provides important knowledge on the performance of latent CTES units in refrigeration systems. The main results from the experimental characterisation are summarised as follows:

- The main parameter affecting the charging time of the CTES unit was found to be the refrigerant evaporation temperature. Reducing the charging temperature is associated with an increase in the energy consumption of the refrigeration system due to increased pressure lift of the compressor. For the 15 and 30 mm HEX configurations, a refrigerant evaporation temperature of −5 °C is a suitable option. A more linear dependency between the charging time and the evaporation temperature was observed for the 45 mm plate-to-plate pitch. The evaporation temperature should be selected based on the time available for charging in the system where the unit is installed. A refrigerant mass flow rate of 7 kg/min resulted in an adequate refrigerant distribution within the ten PP in the plate stack, ensuring flooded operation during the whole charging process.
- The discharging rate of the CTES unit was highly transient during the discharging process, yielding a high discharge rate during the initial phase that continuously decreases towards the end. The refrigerant condensing temperature is the main parameter affecting the mean discharge rate of the discharging process. The highest amount of energy discharged for the 45 mm configuration was 35.29 kWh in approximately 4.5 h, with a mean discharge rate of 7.90 kW.
- The flexible construction of the PP-HEX inside the CTES unit enables the designer to match the discharging rate and storage capacity of the CTES unit to the refrigeration load curve of the system to be considered. For a system with relatively short peaks with high magnitude, the 15 mm configuration is the best choice. If the load peak lasts up to 6 h and requires higher latent storage capacity, the 45 mm configuration is a suitable alternative.

Further experimental work could include an investigation of partial charging and discharging cycles of the CTES unit and the resulting consequences for the performance. A continuation of present work is ongoing with replacing the storage medium ice/water with an organic Phase Change Material (PCM) that is suitable to achieve peak shaving in refrigeration systems used in an industrial food processing plant.

Declaration of Competing Interest

The authors declare that they have no known competing financial interests or personal relationships that could have appeared to influence the work reported in this paper.

Acknowledgements

The work is part of HighEFF - Centre for an Energy Efficient and Competitive Industry for the Future, an 8-year Research Centre under the FME-scheme (Centre for Environment-friendly Energy Research, 257632). The first author gratefully acknowledges the financial support from the Research Council of Norway and user partners of HighEFF. The authors would also like to acknowledge the financial and technical support of Skala Fabrikk AS, Hermetic Pumpen GmbH, Alfa Laval, HB Products and Danfoss regarding the test facility.

References

[1] K.J. Dyke, N. Schofield, M. Barnes, The impact of transport electrification on electrical networks, IEEE Trans. Industr. Electron. 57 (2010) 3917–3926.
[2] L.P. Fernandez, T.G. San Roman, R. Cossent, C.M. Domingo, P. Frias, Assessment of the impact of plug-in electric vehicles on distribution networks, IEEE Trans. Power Syst. 26 (2010) 206–213.
[3] W. Su, H. Eichi, W. Zeng, M.-Y. Chow, A survey on the electrification of transportation in a smart grid environment, IEEE Trans. Industr. Inf. 8 (2011) 1–10.
[4] S. Lechtenböhmer, L.J. Nilsson, M. Åhman, C. Schneider, Decarbonising the energy intensive basic materials industry through electrification–implications for future eu electricity demand, Energy 115 (2016) 1623–1631.
[5] International Energy Agency, Cooling, IEA, Paris, 2020.
[6] International Energy Agency, The Future of Cooling: Opportunities for energy-efficient air conditioning, IEA Publications, 2018.
[7] I. Dincer, M. Rosen, Thermal energy storage: systems and applications, John Wiley & Sons, 2002.
[8] Y. Yau, B. Rismanchi, A review on cool thermal storage technologies and operating strategies, Renew. Sustain. Energy Rev. 16 (2012) 787–797.
[9] Y. Sun, S. Wang, F. Xiao, D. Gao, Peak load shifting control using different cold thermal energy storage facilities in commercial buildings: A review, Energy Convers. Manage. 71 (2013) 101–114.
[10] E. Oró, A. De Gracia, A. Castell, M.M. Farid, L.F. Cabeza, Review on phase change materials (pcms) for cold thermal energy storage applications, Appl. Energy 99 (2012) 513–533.
[11] H. Selvnes, Y. Allouche, R.I. Manescu, A. Hafner, Review on cold thermal energy storage applied to refrigeration systems using phase change materials, Therm. Sci. Eng. Prog. 22 (2021) 100807.
[12] A.L. Gómez, Review of Energy Efficient Technologies in the Refrigeration Systems of the Agrofood Industry, Institut Català d'Energia (1995).
[13] N. Tay, M. Belusko, F. Bruno, An effectiveness-ntu technique for characterising tube-in-tank phase change thermal energy storage systems, Appl. Energy 91 (2012) 309–319.
[14] N. Tay, M. Belusko, F. Bruno, Experimental investigation of tubes in a phase change thermal energy storage system, Appl. Energy 90 (2012) 288–297.
[15] N. Tay, F. Bruno, M. Belusko, Experimental validation of a cfd and an ϵ-ntu model for a large tube-in-tank pcm system, Int. J. Heat Mass Transf. 55 (2012) 5931–5940.
[16] N. Tay, F. Bruno, M. Belusko, Experimental validation of a cfd model for tubes in a phase change thermal energy storage system, Int. J. Heat Mass Transf. 55 (2012) 574–585.
[17] Y. Allouche, S. Varga, C. Bouden, A.C. Oliveira, Experimental determination of the heat transfer and cold storage characteristics of a microencapsulated phase change material in a horizontal tank, Energy Convers. Manage. 94 (2015) 275–285.
[18] A. Abhishek, B. Kumar, M.H. Kim, Y.T. Lee, J.D. Chung, S.T. Kim, T. Kim, C. Lee, K. Lee, Comparison of the performance of ice-on-coil ltes tanks with horizontal and vertical tubes, Energy Build. 183 (2019) 45–53.
[19] A. Castell, M. Belusko, F. Bruno, L.F. Cabeza, Maximisation of heat transfer in a coil in tank pcm cold storage system, Appl. Energy 88 (2011) 4120–4127.
[20] M.A. Ezan, A. Erek, I. Dincer, Energy and exergy analyses of an ice-on-coil thermal energy storage system, Energy 36 (2011) 6375–6386.
[21] A. López-Navarro, J. Biosca-Taronger, B. Torregrosa-Jaime, J. Corberán, J. Bote-García, J. Payá, Experimental investigations on the influence of ice floating in an internal melt ice-on-coil tank, Energy Build. 57 (2013) 20–25.
[22] A. López-Navarro, J. Biosca-Taronger, B. Torregrosa-Jaime, I. Martínez-Galván, J. M. Corberán, J. Esteban-Matías, J. Paya, Experimental investigation of the temperatures and performance of a commercial ice-storage tank, Int. J. Refrig. 36 (2013) 1310–1318.
[23] B. Torregrosa-Jaime, A. López-Navarro, J.M. Corberán, J. Esteban-Matías, L. Klinkner, J. Payá, Experimental analysis of a paraffin-based cold storage tank, Int. J. Refrig. 36 (2013) 1632–1640.
[24] A. López-Navarro, J. Biosca-Taronger, J. Corberán, C. Peñalosa, A. Lázaro, P. Dolado, J. Payá, Performance characterization of a pcm storage tank, Appl. Energy 119 (2014) 151–162.
[25] F. Bosholm, A. López-Navarro, M. Gamarra, J. Corberán, J. Payá, Reproducibility of solidification and melting processes in a latent heat thermal storage tank, Int. J. Refrig. 62 (2016) 85–96.
[26] R.M. Saeed, J.P. Schlegel, R. Sawafta, V. Kalra, Plate type heat exchanger for thermal energy storage and load shifting using phase change material, Energy Convers. Manage. 181 (2019) 120–132.
[27] W. Lin, W. Zhang, Z. Ling, X. Fang, Z. Zhang, Experimental study of the thermal performance of a novel plate type heat exchanger with phase change material, Appl. Therm. Eng. 178 (2020) 115630.
[28] T. Korth, F. Loistl, C. Schweigler, Novel integration of latent heat storage in multi-split air conditioning systems, in: 25th IIR International Congress of Refrigeration Proceedings, International Institute of Refrigeration, 2019.
[29] F. Wang, G. Maidment, J. Missenden, R. Tozer, The novel use of phase change materials in refrigeration plant. part 1: Experimental investigation, Appl. Therm. Eng. 27 (2007) 2893–2901.
[30] F. Wang, G. Maidment, J. Missenden, R. Tozer, The novel use of phase change materials in refrigeration plant. part 2: Dynamic simulation model for the combined system, Appl. Therm. Eng. 27 (2007) 2902–2910.
[31] F. Wang, G. Maidment, J. Missenden, R. Tozer, The novel use of phase change materials in refrigeration plant. part 3: Pcm for control and energy savings, Appl. Therm. Eng. 27 (2007) 2911–2918.
[32] T. Korth, F. Loistl, A. Storch, R. Schex, A. Krönauer, C. Schweigler, Capacity enhancement of air conditioning systems by direct integration of a latent heat storage unit, Appl. Therm. Eng. 167 (2020) 114727.
[33] Sasol Chemicals, Parafol 16-97, 2020. URL: https://products.sasol.com/pic/products/home/grades/AS/5parafol-16-97/index.html/.
[34] J. Mitrovic, R. Peterson, Vapor condensation heat transfer in a thermoplate heat exchanger, Chem. Eng. Technol. Ind. Chem. Plant Equip. Process Eng. Biotechnol. 30 (2007) 907–919.
[35] J. Tran, S. Sommerfeld, M. Piper, E. Kenig, Investigation of pillow-plate condensers for the application in distillation columns, Chem. Eng. Res. Des. 99 (2015) 67–74.
[36] J. Tran, M. Linnemann, M. Piper, E. Kenig, On the coupled condensation-evaporation in pillow-plate condensers: Investigation of cooling medium evaporation, Appl. Therm. Eng. 124 (2017) 1471–1480.
[37] J. Mitrovic, B. Maletic, Numerical simulation of fluid flow and heat transfer in thermoplates, Chem. Eng. Technol. 34 (2011) 1439–1448.
[38] M. Piper, A. Zibart, J. Tran, E. Kenig, Numerical investigation of turbulent forced convection heat transfer in pillow plates, Int. J. Heat Mass Transf. 94 (2016) 516–527.
[39] M. Piper, A. Zibart, E. Kenig, New design equations for turbulent forced convection heat transfer and pressure loss in pillow-plate channels, Int. J. Therm. Sci. 120 (2017) 459–468.
[40] O. Arsenyeva, J. Tran, M. Piper, E. Kenig, An approach for pillow plate heat exchangers design for single-phase applications, Appl. Therm. Eng. 147 (2019) 579–591.
[41] M. Shirzad, M.A. Delavar, S.S.M. Ajarostaghi, K. Sedighi, Evaluation the effects of geometrical parameters on the performance of pillow plate heat exchanger, Chem. Eng. Res. Des. 150 (2019) 74–83.
[42] S. Kumar, B. Premachandran, P. Subbarao, Study on thermo–hydraulics in a pillow plate channel, Int. J. Therm. Sci. 145 (2019) 106020.
[43] M. Piper, A. Olenberg, J. Tran, E. Kenig, Determination of the geometric design parameters of pillow-plate heat exchangers, Appl. Therm. Eng. 91 (2015) 1168–1175.
[44] G. Lorentzen, The use of natural refrigerants: a complete solution to the cfc/hcfc predicament, Int. J. Refrig. 18 (1995) 190–197.
[45] R. Ciconkov, Refrigerants: There is still no vision for sustainable solutions, Int. J. Refrig. 86 (2018) 441–448.
[46] P. Gullo, A. Hafner, K. Banasiak, Transcritical r744 refrigeration systems for supermarket applications: Current status and future perspectives, Int. J. Refrig. 93 (2018) 269–310.
[47] K.Z. Skačanová, M. Battesti, Global market and policy trends for co2 in refrigeration, Int. J. Refrig. 107 (2019) 98–104.
[48] P. Nekså, H. Rekstad, G.R. Zakeri, P.A. Schiefloe, Co2-heat pump water heater: characteristics, system design and experimental results, Int. J. Refrig. 21 (1998) 172–179.
[49] J. Rogstam, Evolution of co2 as refrigerant in ice rink applications, in: 12th IIR Gustav Lorentzen Natural Working Fluids Conference, Edinburgh, UK, Aug 2016, pp. 21–24.
[50] H. Selvnes, A. Hafner, H. Kauko, Design of a cold thermal energy storage unit for industrial applications using co2 as refrigerant, in: 25th IIR International Congress of Refrigeration Proceedings, IIR, 2019.
[51] H. Selvnes, V. Büttner, A. Hafner, Evaluation of a pillow-plate heat exchanger for a pump-circulated CO2 refrigeration system, in: Proceedings of the 14th IIR-Gustav Lorentzen Conference on Natural Refrigerants, International Institute of Refrigeration, 2020.
[52] C. Elliott, V. Vijayakumar, W. Zink, R. Hansen, National instruments labview: a programming environment for laboratory automation and measurement, JALA, J. Assoc. Lab. Autom. 12 (2007) 17–24.
[53] Refrigera Industriale, Refrigera 2-way ball valves, 2015. URL: https://www.refrigera.eu/en/ball-valves/2-way-ball-valve.
[54] HERMETIC Pumpen GmbH, HERMETIC refrigeration pumps, 2021. URL: https://kaelte.hermetic-pumpen.com/en/pump-types.

[55] DOW Chemical Company, DOWCAL 200 Heat Transfer Fluid Technical Data Sheet, 2021. URL: https://www.dow.com/en-us/document-viewer.html?ramdomVar=2372344082032526391&docPath=/content/dam/dcc/documents/en-us/productdatasheet/180/180-01589-01-dowcal-200-heat-transfer-fluid-tds.pdf.
[56] I. ISO, B. OIML, Guide to the expression of uncertainty in measurement, Geneva, Switzerland 122 (1995) 16–17.
[57] E. Lemmon, I. Bell, M. Huberm, M. McLinden, NIST Standard Reference Database 23: Reference Fluid Thermodynamic and Transport Properties-REFPROP, Version 10.0, National Institute of Standards and Technology, 2018. URL: https://www.nist.gov/srd/refprop.
[58] S. Minetto, R. Brignoli, C. Zilio, S. Marinetti, Experimental analysis of a new method for overfeeding multiple evaporators in refrigeration systems, Int. J. Refrig. 38 (2014) 1–9.
[59] S. Bortolin, M. Rossato, S. Bernardinello, D. Del Col, Investigation of evaporator performance with and without liquid overfeeding (2016).
[60] G. Mitsopoulos, E. Syngounas, D. Tsimpoukis, E. Bellos, C. Tzivanidis, S. Anagnostatos, Annual performance of a supermarket refrigeration system using different configurations with co2 refrigerant, Energy Convers. Manage. X 1 (2019) 100006.
[61] A. Tambovtsev, H. Quack, Cop improvement by transfer of the superheating into the internal heat exchanger, in: International Congress of Refrigeration, Beijing, China, 2007.
[62] R. Feistel, W. Wagner, A new equation of state for h 2 o ice ih, J. Phys. Chem. Ref. Data 35 (2006) 1021–1047.

Paper III

H. Selvnes, Y. Allouche, A. Hafner, C. Schlemminger, I. Tolstorebrov (2022). "Cold thermal energy storage for industrial CO_2 refrigeration systems using phase change material: An experimental study" *Applied Thermal Engineering* Volume 212, 118543. DOI: https://doi.org/10.1016/j.applthermaleng.2022.118543

Applied Thermal Engineering 212 (2022) 118543

Contents lists available at ScienceDirect

Applied Thermal Engineering

journal homepage: www.elsevier.com/locate/ate

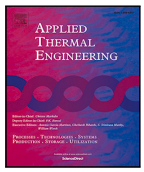

Research paper

Cold thermal energy storage for industrial CO_2 refrigeration systems using phase change material: An experimental study

Håkon Selvnes [a,*], Yosr Allouche [a], Armin Hafner [a], Christian Schlemminger [b], Ignat Tolstorebrov [a]

[a] Norwegian University of Science and Technology, Department of Energy and Process Engineering, Kolbjørn Hejes vei 1B, NO-7491, Trondheim, Norway
[b] Sintef Energy Research, Kolbjørn Hejes vei 1D, NO-7465, Trondheim, Norway

ARTICLE INFO

Keywords:
Cold thermal energy storage
Phase change material
CO_2 refrigeration
Industrial refrigeration

ABSTRACT

Refrigeration systems in industrial food processing plants are large users of electric energy and often show high peak power consumption. Cold thermal energy storage (CTES) technology integrated into refrigeration systems can reduce the peak power requirement and achieve peak shifting by decoupling the supply and demand of the refrigeration load. This paper presents the design and performance of a CTES unit consisting of a pillow plate heat exchanger (PP-HEX) immersed into a low-temperature phase change material (PCM) as the storage medium. It is one of the first experimental investigations featuring a large-scale technical solution that allows for coupling the evaporation and condensation processes of the refrigeration system with the melting and solidification of a low-temperature PCM in the same heat exchanger. The charging and discharging performance of the plates-in-tank CTES unit was extensively tested using CO_2 as the refrigerant and a commercial PCM with phase change temperature of -9.6 °C. The charging time was found to be mainly affected by the refrigerant evaporation temperature, while the discharging rate and discharged energy over the cycle was higher when increasing the refrigerant condensing temperature. Using a plate pitch of 30 mm resulted in the highest mean discharge rate and total discharged energy over the cycle with 9.79 kW and 17.04 kWh, respectively. The flexible CTES-PCM unit can be adapted to fit several refrigeration load characteristics and temperature levels by changing the PP-HEX geometry and type of PCM used as the storage medium.

1. Introduction

Refrigeration demands in industrial food processing plants can vary significantly over a day or week, depending on the production schedules. As a result, the electric power consumption of such plants is characterised by peaks and valleys. Cold thermal energy storage (CTES) technology has received increased interest for the past two decades from researchers and stakeholders in the refrigeration sector as a measure to reduce the peaks in the cooling load that occurs in many refrigeration systems, e.g. in food processing plants and air-conditioning systems. Furthermore, CTES technology plays an important role to provide higher flexibility and enabling demand-side management in refrigeration systems [1]. In addition to CTES applications in air-conditioning [2] and domestic refrigeration [3], the current research on CTES applications focuses on the different links in the food cold chain, such as food transport and packaging, commercial and supermarket refrigeration systems, and industrial food processing plants [4]. More research on CTES technology has been identified as an important factor for further market penetration of environment-friendly CO_2 supermarket refrigeration systems across the world [5]. CTES technology using a phase change material (PCM) as the storage medium is of particular interest due to the high volumetric energy storage capacity of latent heat storage (LHS) systems compared to sensible heat storage (SHS) systems [6]. PCMs are materials that utilise the phase transition between the solid and liquid state for storing energy. As an example, Allouche et al. [7] showed that using an LHS with microencapsulated PCM slurry for CTES application for implementation into an air-conditioning system provided a storage capacity enhancement of up to 53% compared to using the equivalent volume of water as the SHS medium. PCMs can be divided into two main categories, organic PCMs and inorganic PCMs [8]. The two most studied groups of PCMs for CTES applications are paraffins (organic PCM, primarily consisting of mixtures of alkanes) and eutectic salt-water solutions (inorganic PCM), which have become readily available commercially the last ten years [4,6,9]. Eutectic salt-water solutions are mixtures of different salt hydrates and water with high volumetric storage capacity compared to most organic PCMs due to the high density and latent heat capacity of these PCMs. The thermal conductivity of eutectic water-salt solutions is also considerably higher than for most organic PCMs, comparable

* Corresponding author.
E-mail address: hakon.selvnes@ntnu.no (H. Selvnes).

https://doi.org/10.1016/j.applthermaleng.2022.118543
Received 14 November 2021; Received in revised form 10 March 2022; Accepted 16 April 2022
Available online 22 April 2022

Nomenclature

Abbreviations

ACC	Auxiliary CO_2 circuit
$CTES$	Cold thermal energy storage
GHC	Glycol heating circuit
HEX	Heat exchanger
PCC	Primary CO_2 circuit
PCM	Phase change material
PID	Process and instrumentation diagram
PP	Pillow plate
SCC	Secondary CO_2 circuit

Symbols

$\dot{E}$	Energy flow
$\dot{m}$	Mass flow rate
b	Thickness
d	Diameter
E	Energy
h	Enthalpy
L	Length
n	Number
s	Welding spot pitch
T	Temperature
t	Time
W	Width

Greek letters

δ	Height, distance
η	Apparent viscosity
γ	Shear rate
ρ	Density

Subscripts

C	Charging
CO_2	Carbondioxide
$cond$	Condensation
D	Discharging
$evap$	Evaporation
fus	Fusion
g	Glycol
L	Longitudinal
o	Outer
PCM	Phase change material
PP	Pillow plate
s	Solid
sat	Saturation
SP	Welding spot
T	Transversal
th	Theoretical
w	Wall

to the thermal conductivity of water (approximately 0.6 W/(m K)). However, some significant drawbacks of these PCMs are their high rate of supercooling, incongruent melting, and being corrosive to certain metals [10]. Paraffins are substances that consist of chains of saturated hydrocarbons that can be produced from either fossil or bio-based sources [11], where the latter is offered by a few producers such as PureTemp LLC [12] and Croda International Plc [13]. Producing PCM from non-edible plant oils or waste cooking oil instead of fossil sources could be a measure to increase the sustainability of TES technology, and organic PCMs in particular [14]. Paraffins have some favourable properties when used as an LHS medium, such as not being corrosive to metals, low supercooling, stable and non-reactive behaviour and no phase segregation issues [15]. The most important drawback of PCMs in general, and organic PCM in particular, is the low thermal conductivity of these materials, limiting the heat transfer rate when used in a CTES system. Extensive research has been carried out to enhance the conductivity of various PCMs by adding highly conductive inserts such as metal particles, carbon materials and metal foams [16,17], but the cost of these enhanced materials remains a limitation for widespread implementation.

When considering the integration of PCM heat exchanger (PCM-HEX) units into a refrigeration system, Selvnes et al. [4] proposed a classification into two groups; CTES units integrated into the secondary refrigerant circuit and CTES units integrated into the primary refrigeration circuit. In the first group, the PCM-HEX is integrated into the secondary refrigeration circuit (glycol/water/brine) using a PCM/single-phase fluid heat exchanger (HEX) design. In the second group, the PCM-HEX unit is designed to be integrated directly into the primary refrigerant circuit, employing a PCM/two-phase fluid HEX design. For this design, the CTES unit will act as an evaporator during the charging process and it operates as a condenser for the refrigeration system during the discharging process. Most experimental research on CTES units to date has focused on CTES units integrated into the secondary refrigeration circuit, likely because of the focus on CTES applied to air-conditioning systems in the past, where secondary refrigerant circuits are common. Furthermore, integrating the CTES unit into the primary refrigerant circuit involves much stricter requirements of the CTES unit in terms of often increased refrigerant charge and the pressure class of the equipment, governed by relevant standards such as the European Standard EN-378 and the EU Pressure Equipment Directive (PED) [18]. On the other hand, integration of the CTES unit into the primary refrigerant circuit allows for raising the evaporation temperature during the charging process, increasing the system efficiency compared to using a secondary refrigerant circuit [19].

Demonstration of performance of heat exchanger (HEX) units using PCM as the storage medium is vital to increase the confidence in this CTES technology by manufacturers and stakeholders in the refrigeration industry. Thorough experimental characterisation of promising PCM-HEX units at a laboratory scale is a measure that can contribute to establishing up-scaled pilot plants and demonstration sites in the refrigeration industry, increasing the market penetration of CTES technology. The coil-in-tank, tube-in-tank and plate-in-tank designs are the most frequently investigated PCM-HEX configurations to date. The coil-in-tank and tube-in-tank constitute the major share of past studies. This is probably due to the relatively simple design, simple construction and low cost of these PCM-HEX units for testing at a laboratory scale, particularly when using a single-phase refrigerant inside the pipes. Experimental investigations on the three CTES unit design have been carried out using various storage media including water/ice [20–26], inorganic PCMs [21,27] and organic PCMs [7,28–33]. Furthermore, several manufacturers of CTES systems also use the coil-in-tank design for their commercial products, e.g. the systems from Calmac [34] and Viessmann [35] for thermal energy storage purposes in supermarket refrigeration systems.

Abhishek et al. [24] investigated a coil-in-tank PCM-HEX using water as the PCM and a brine as secondary refrigerant. A study on the effect on the charging and discharging performance by vertical and horizontal tube orientation, tube outlet location and tube size was performed, showing that a vertical tube orientation was generally preferable with up to about 30% improvement for the discharging process. Ballot-Miguet et al. [36] reported the performance of a 500 kWh-capacity ice-on-coil CTES unit integrated into a glycol circuit for

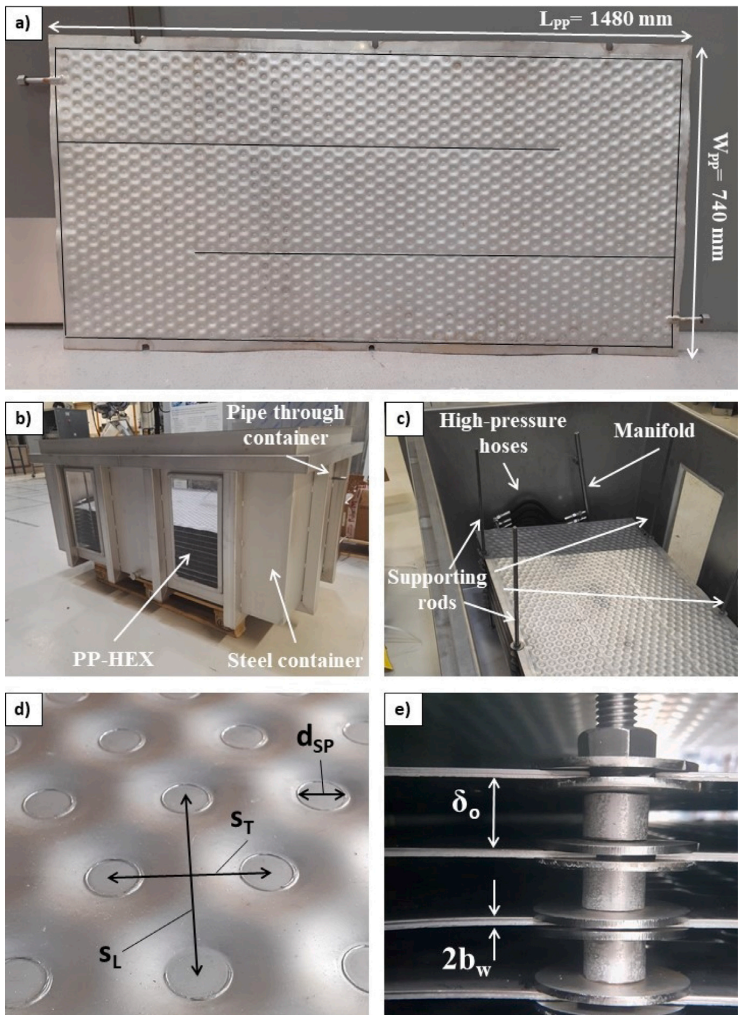

Fig. 1. Overview of the novel CTES unit showing the details of (a) one PP for CO_2 refrigeration with inlet/outlet pipes and the seam welds marked with black lines (b) the CTES unit before assembly in the test facility (c) view of the PP-HEX inside the container (d) the wavy PP surface characteristic with the welding pattern parameters (e) the PP-HEX stack in the CTES unit with vertical plate pitch. Figure first presented in [26].

medium temperature cooling purposes in a supermarket CO_2 refrigeration system. The CTES unit was installed in a supermarket in France and operated as a subcooler for the refrigeration system during high ambient temperatures to improve its performance, reducing the annual electricity consumption by 6%. A plates-in-tank PCM-HEX unit using hexadecane (18 °C) as the PCM, targeted for load shifting purposes in data centres and server rooms was presented by Saeed et al. [32]. The modular PCM-HEX unit was experimentally tested under various conditions, and the unit demonstrated an effectiveness of over 80 % with a mean discharge rate of 4.8 kW. Verpe et al. [37] proposed and numerically investigated the integration of a shell and tube PCM-HEX into a CO_2 refrigeration system for a plate freezer on a fishing vessel. Using dry ice (solid CO_2) as the PCM for storing the cold energy lower than −40 °C, a reduction in the freezing time of the fish by 3.2% was calculated. Qu et al. [31] proposed using a fin-and-tube PCM-HEX (PCM RT10, melting temperature 9.4 °C) to solve the issue of defrosting of the evaporator in a cascade air-source heat pump. The PCM-HEX acted as the heat source for both the high-temperature circuit (providing heat to condenser) and the low-temperature circuit (for hot gas defrost) in the heat pump during the defrosting process. The experimental results show that the PCM-HEX unit was able to supply a mean discharge rate of 5.09 kW for the defrosting period of about 9 min. Korth et al. [33] experimentally investigated the use of a tube-in-tank PCM-HEX unit as a subcooler to increase the refrigeration capacity of an air conditioning system. The PCM-HEX unit was utilising the direct PCM/refrigerant heat exchange principle and an organic PCM with a melting temperature of 18 °C. An 18% capacity increase of the refrigeration system was demonstrated during the discharge of the PCM-HEX.

The design of a novel modular CTES unit based on the plates-in-tank principle intended for peak shaving of refrigeration load was first presented by Selvnes et al. [38]. The PCM-HEX unit was designed for integration into pump-circulated CO_2 circuits found in many industrial refrigeration systems and large chiller applications. The initial experimental test results and proof of concept were presented by Selvnes

et al. [25] using water/ice as the storage medium, making the PCM-HEX unit suitable for process cooling and air conditioning purposes. The CO_2 was evaporating/condensing inside the plates, while the PCM was freezing/melting on the surface of the plates during the charging and discharging processes, respectively. The work was continued by an extensive investigation of various HEX configurations and a variation of the refrigerant parameters, still using water/ice as the PCM [26]. It was shown that the evaporation and condensation temperature of the CO_2 were the most influencing parameters for the charging and discharging cycles, respectively. For the HEX configuration resulting in the largest storage capacity, the mean discharge rate was found to be 7.90 kW over a cycle time of 4.5 h. From the reviewed literature, it is clear that experimental research on PCM-HEX units covering the temperature range below 0 °C to date is very limited, a temperature area of high importance for refrigeration systems in the food cold chain. It is estimated that 40% of all food products need refrigeration [39], while refrigeration is estimated to account for up to 15% of electricity consumption worldwide [40]. More research on low-temperature PCM-HEX units suitable for large-scale installations in refrigeration plants is therefore of key importance to improve energy efficiency, provide flexibility and achieve peak shifting in this sector.

In the current paper, the plates-in-tank PCM-HEX unit presented in earlier studies using water/ice as the PCM [25,26,38] is modified to fit the application of industrial refrigeration plants, specifically for integration into the pump-circulated CO_2 circuit used in CO_2/NH_3 cascade refrigeration systems. To adapt to the temperature requirement of the food processing industry, the available commercial PCMs on the market was mapped and an organic PCM with a melting point of −9.6 °C was selected as the storage medium in the PCM-HEX. First, a presentation of the CTES unit and the experimental setup is given, followed by a description of the experimental procedure for the charging and discharging cycles. Second, the thermo-physical properties of the commercial PCM are characterised, presented and discussed. Finally, the results from the extensive experimental campaign are presented and discussed separately for the charging and discharging processes. The overall performance of the novel PCM-HEX unit is reported and recommendations for future studies are given.

2. Experimental setup

2.1. Cold thermal energy storage unit

The novel CTES unit is presented in Fig. 1b. The design of the unit follows the plates-in-tank principle, and it is composed of a stack of HEX plates placed into a welded stainless steel container filled with an organic PCM (see Fig. 1c). The container is supported on the outside by a frame of square steel tube (see Fig. 1b). It has been shown that stainless steel is the most suitable material for CTES units using PCMs, even for salt hydrate mixtures [41]. The use of a container of polymer materials to hold the PP-HEX and the PCM is generally less expensive, but these were found to be not compatible with certain paraffin PCMs in a long term perspective [29]. The container is filled with PCM to ensure the complete immersion of the PP-HEX into the storage medium. The container is fitted with a lid to prevent the evaporation of the PCM as well as two 1 cm thick windows of acrylic plexiglass on each side to observe the melting and solidification process (see Fig. 1b). The container is insulated with 50 mm polystyrene plates to limit the heat transfer loss from the storage unit to the environment. The HEX consists of a set of plates called pillow plates (PP) due to their characteristic pillow-like surface. These novel type of HEX plates has gained increased attention in both research and the industry due to their compact design and ability to operate under high pressures. Literature on this novel PP-HEX design as well as its performance has been limited compared to other conventional HEX types, e.g. brazed plate HEX or shell and tube HEX. However, several important studies on PP-HEX have been published in the last seven years. For more details on the main characteristics of the PP geometry, the reader is directed to Piper et al. [42]. To date, most research on PP-HEX has been carried out using a single-phase flow of cooling water inside the PPs [43–47]. The literature on two-phase heat transfer inside the PP remains very limited. To the authors best knowledge, Tran et al. [43] is the only study considering two-phase heat transfer inside the PP channel, where the two-phase heat transfer coefficient of refrigerant R134a was experimentally determined using both natural and forced circulation flows.

Fig. 1a shows one PP used in the PP-HEX for this study. The PP consists of two thin stainless steel metal sheets that are spot-welded together in a particular repetitive pattern by a laser-welding machine. The welding spots form a defined channel where the refrigerant flows and exchange heat with the PCM. The two metal plates are seam-welded along the edges to ensure the sealing of the PP. One pipe is welded to the PP at each end, serving as the inlet and outlet of the refrigerant. Furthermore, two longitudinal seam welds are performed on the plate, as indicated in Fig. 1a. These seam welds generate three flow passes for the refrigerant to flow between the inlet and outlet pipe. This technique is used to direct the refrigerant flow and ensure a better distribution of refrigerant through the PP channels. After the welding process, the PP is inflated by a hydroforming process, applying high water pressure to the inside of the plate. The hydroforming process creates the flow channels for the refrigerant inside the PP and the pillow-like surface characteristic (see Fig. 1d). Any number of PP can then be stacked together to form a complete PP-HEX. The geometrical design parameters of a PP are as follows (see Fig. 1d and e): the spot weld diameter (d_{SP}), the transversal spot weld pitch (s_T), the longitudinal spot weld pitch (s_L), the channel maximum inflation height (δ_i) and the PP wall thickness (b_w). In the current study, a longitudinal welding spot pattern was selected to define the flow channels in the PP, using a longitudinal welding spot pitch of 50 mm and a transversal welding spot pitch of 30 mm. The welding spot arrangement results in a triangular configuration commonly found in the PP industry. The staggered spot-weld pattern of the PP can be seen in Fig. 1d, allowing for heat transfer enhancement between the refrigerant and the storage medium by promoting mixing of the flow inside the PP channel [44]. Important design parameters of PP-HEX are the overall PP length (L_{PP}), the width (W_{PP}), the maximum vertical distance between each PP (δ_o) and the number of plates (n_{PP}), see Fig. 1a and e. The PP-HEX is mounted on a frame of square stainless steel tube for convenient removal and refitting of the stack into the container. The PP-HEX is mounted to the frame by six metal supporting rods, three along each side of the PPs as shown in Fig. 1c. The vertical distance between each PP (plate pitch) in the stack can be selected by using different lengths of cylindrical spacers and washers on the metal rods (see Fig. 1e). The plate pitch is an important parameter because it directly determines the storage capacity of the CTES unit. In this study, the experimental characterisation of the CTES unit was carried out for a plate pitch of 15 mm and 30 mm. Ten PPs were used in the PP-HEX in both plate pitch configurations, resulting in a total heat transfer area of 21.90 m^2. The pipes welded to each end of the PPs are connected to a manifold by high-pressure braided hoses at their respective ends of the PP-HEX. The CTES unit is connected to the experimental test facility by a tube from the manifold that passes through the container wall as shown in Fig. 1a. Approximately 460 kg of liquid PCM was required to completely immerse the PP-HEX for a plate pitch of 30 mm. To handle the expansion of the PCM transitioning between the solid and liquid states, a clearance volume between the container wall and the PP-HEX is included. From the initial testing, the clearance volume (about 10 cm) ensures there is always liquid towards the wall. The thermal expansion of the PCM is then handled through an elevated liquid height in the container, which has atmospheric air above the PCM liquid level. This effectively limits the mechanical stress on both the PP-HEX and the container. The selected geometrical parameters of the PPs and PP-HEX are given in Table 1.

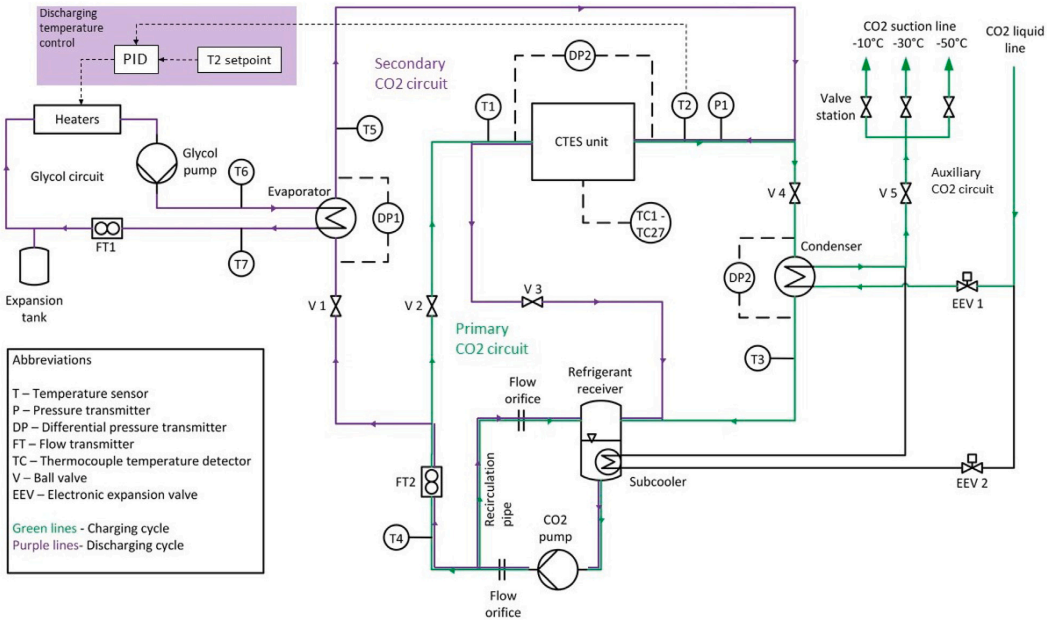

Fig. 2. Piping and instrumentation diagram (PID) of the test facility. Figure first presented in [26].

Table 1
Main geometrical parameters of the PPs and PP-HEX in the novel CTES unit.

Parameter	Value
s_L	50 mm
s_T	30 mm
d_{SP}	10 mm
δ_i	4.3 mm
b_w	1.0 mm
L_{PP}	1480 mm
W_{PP}	740 mm
δ_o	15/30 mm
n_{PP}	10

2.2. Experimental test facility

The experimental test facility was designed by the authors and constructed to test the performance of the CTES unit, previously described in Selvnes et al. [26]. A piping and instrumentation diagram (P&ID) of the test facility is shown in Fig. 2. The facility enables the operator to set and monitor the operating parameters of the refrigerant (e.g. temperature, pressure and flow rate) at the inlet of the CTES unit during both the charging and discharging processes. The test facility can be operated in two different modes: Charging mode (indicated with green lines in Fig. 2) and discharging mode (indicated with purple lines in Fig. 2). Four circuits can be identified in the facility: The primary CO_2 circuit (PCC), the secondary CO_2 circuit (SCC), the glycol heating circuit (GHC) and the auxiliary CO_2 circuit (ACC). During the charging mode, the PCC and the ACC are in operation. During the discharging mode, the SCC and the GHC are in operation.

Fig. 2 indicates the location of sensors for monitoring the mass flow rate, temperature, pressure and differential pressure in the test facility. The pressure of the PCC and SCC is measured by an absolute pressure transmitter (P1) calibrated in the pressure range 0–70 bar. Three differential pressure (DP) transmitters (calibrated in the range of 0.03–3 bar) are installed to measure the pressure loss across evaporator HEX (DP1), CTES unit (DP2) and condenser HEX (DP3). The refrigerant temperature through both the charging and discharging processes in the primary and SCC is measured by five RTD Pt100 temperature sensors as follows: inlet and outlet of the CTES unit (T1 and T2), outlet of condenser HEX (T3), outlet of CO_2 pump (T4) and outlet of the evaporator (T5). The PCM temperature in the CTES unit is measured by T-type thermocouples (TC), located on the top surface of three selected PPs. Fig. 3 shows a top view of one PP indicating the position of each TC. The three PPs are selected according to their height in the plate stack, namely PP 2, PP 5 and PP 9. Each of these PPs is equipped with a set of nine consecutively numbered TC, which are distributed on the surface as follows: TC00–TC08 are mounted on PP 2, TC09–TC17 are mounted on PP 5 and TC18–TC26 are mounted on PP 9. The operator control of the test facility and the collection of the measurement data are achieved using a data acquisition system coupled with LabVIEW software [48]. An overview of the measurement equipment is given in Table 2.

The charging process is carried out through the PCC. The process consists of extracting heat from the PCM storage medium to the refrigerant. Consequently, the PCM solidifies (heat release) and the refrigerant evaporates (heat absorption). The circulation of the CO_2 is assured by a hermetic centrifugal refrigerant pump (CO_2 pump) with an inverter to control the refrigerant flow rate (Hermetic Pumpen GmbH [49]). From the outlet of the CO_2 pump, the refrigerant flow is split into two pipes: One pipe is used to recirculate the liquid refrigerant to the receiver of the CO2 refrigeration system and another one is used to feed the CTES. The recirculation pipe is required to assure the minimum flow requirement of the CO_2 pump. A Coriolis flowmeter (FT2) is used to measure the inlet CO_2 mass flow rate to the CTES unit. During the charging process, valves V1 and V3 are closed so that the PCC is active. The refrigerant enters the CTES at a liquid state through valve V2, then evaporates as it flows through the CTES unit as heat is transferred from the storage medium to the refrigerant. At the outlet of the CTES, the refrigerant is a mixture of liquid and vapour. The CO_2 mixture is then condensed to the liquid state in a plate HEX (condenser) connected to the auxiliary CO_2 cooling circuit. The liquid CO_2 is then brought from the outlet of the condenser to the

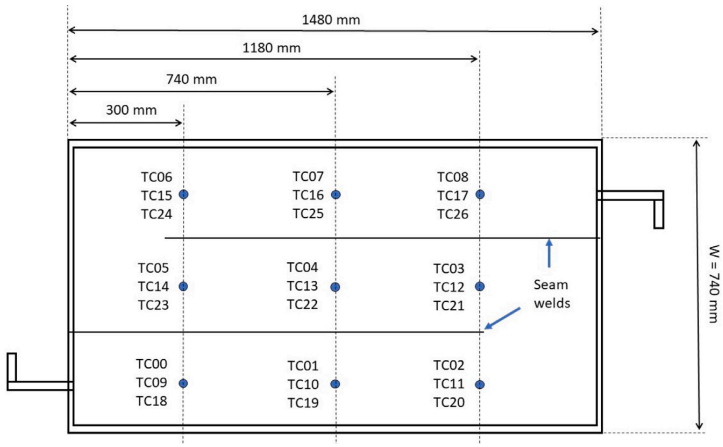

Fig. 3. Top view of a PP: Locations of thermocouples on three selected PPs. Figure first presented in [26].

refrigerant receiver. It is then drawn from the bottom of the receiver, and the cycle continues until the charging process is completed. The ACC provides the cooling of the PCC during the charging process. The cooling is achieved by supplying liquid refrigerant to the plate HEX (condenser) in the PCC through an electronic expansion valve (EEV 1). Furthermore, it maintains standby pressure in the PCC when the system is not in operation by supplying refrigerant to the subcooler through EEV 2. Both EEVs are operated by Danfoss superheat controllers. The auxiliary circuit is connected to the liquid and suction lines of a CO_2 booster refrigeration system in the laboratory to accomplish these two functions. The operator can select an evaporation level of −10 °C, −30 °C and −50 °C for the ACC by acting on a valve station (see Fig. 2). The evaporation pressure in the ACC can be modified by operating valve V5 located on the suction side of the ACC. This valve serves as a back-pressure valve, and reducing its opening degree will therefore increase the evaporation pressure in the ACC.

The discharging process is carried out through the SCC and consists of heat transfer from the refrigerant to the PCM. When the refrigerant flows inside the PPs, heat is rejected to the storage medium until the refrigerant is completely condensed at the manifold outlet. Consequently, the PCM absorbs the heat until it is completely melted. The SCC is connected to the GHC by the evaporator HEX, simulating the thermal load on the refrigeration system. During the discharging process, valve V2 and valve V4 are closed (see Fig. 2) so that the SCC is active. The flow direction through the CTES unit is reversed compared to the charging cycle so that the inlet and outlet are swapped. During the discharging cycle, the same DP transmitter used in the charging cycle measures the total pressure loss over the CTES unit. Two small manual ball valves are operated to exchange the high-pressure and low-pressure sides on the sensor. In the discharging process, liquid CO_2 is drawn from the bottom of the receiver by the CO_2 pump and circulated to the evaporator through valve V1. In the evaporator, heat is transferred from the glycol to the refrigerant so that the CO_2 exits the evaporator as a liquid/vapour mixture. The two-phase CO_2 is then circulated through the CTES unit, where heat is transferred to the storage medium and the refrigerant condenses to a fully liquid state. The cycle is then completed by returning the liquid refrigerant to the receiver through valve V3. The heat transfer fluid in the GHC is a mixture of 47% ethylene glycol (DowCal 100, DOW Chemicals) and water. The concentration of the ethylene glycol is measured with an ATAGO Master refractometer. The glycol is supplied to the evaporator by a Grundfos circulation pump. The glycol mass flow rate is measured by a Coriolis mass flow meter (FT 1). The heat input to the GHC is achieved by two 9 kW electric immersion heaters installed in the GHC, which gives the possibility to simulate a thermal load up to 18 kW. One of the heaters is fitted with pulse-width modulation (PWM) control for precise regulation of the power output from 0 to 100%. Furthermore, two RTD Pt100 temperature sensors are mounted in the inlet (T6) and outlet (T7) pipe of the HEX to measure the inlet and outlet temperature of the glycol, respectively.

Table 2
Measurement equipment utilised in the test facility.

Component	Model	Producer	Indicated accuracy
Absolute pressure transmitter	Cerabar S PMP71	Endress+Hauser	±0.25% of set span
Differential pressure transmitter	Deltabar S PMD75	Endress+Hauser	±0.15% of set span
Temperature sensor CO_2 and glycol	Class B RTD Pt100	RS PRO	±0.1 K
Temperature sensor PCM	Thermocouple type T	RS PRO	±0.2 K
Mass flow meter glycol	RHM 15 Coriolis meter	Rheonik	±0.2% of reading
Mass flow meter CO_2	RHM 06 Coriolis meter	Rheonik	±0.2% of reading

3. Experimental procedure

3.1. Charging process

For the charging process, vertical plate pitches (δ_o) of 15 mm and 30 mm in the PP-HEX are considered. A series of experiments considering various refrigerant mass flow rates and evaporation temperatures were conducted for each plate pitch. The CO_2 evaporation temperature was varied from −12 °C to −23 °C, while the CO_2 mass flow rate was varied from 4 kg/min to 10 kg/min. The charging process in each test was run until completion to compare CO_2 pressure loss, PCM temperature and charging time for the different operating conditions and plate pitches. The charging cycle is initiated with the PCM in the CTES unit in the liquid phase. The start of the charging process takes place when the average PCM temperature (mean of TC00 to TC26) is measured below 0 °C. When the charging process is initiated, a layer of solid PCM is formed on the PP surface and it becomes thicker as the charging process progresses. This phenomenon continues until a complete block of solid PCM is formed between two adjacent PPs, i.e. when the solid PCM layer on the two PPs has overlapped (see

Fig. 10). At this point, the charging process continues as sensible energy storage until the temperature of the solid PCM block approaches the inlet refrigerant temperature. The charging process is completed when the difference between the mean PCM temperature and the refrigerant saturation temperature is less than 0.2 K. The charging time is defined as the period from the mean PCM temperature is measured below 0 °C and to the point where the temperature difference of the PCM and the refrigerant is less than 0.2 K. During the charging process, the formation of solid PCM can be easily visually observed through the plexiglass windows. The CTES is equipped with a camera that captures the formation of the solid PCM during the charging process at a fixed time interval. The mass flow rate of the CO_2 in the PCC is adjusted by controlling the frequency output of the inverter for the CO_2 pump (35–50 Hz). If the required mass flow rate is lower than the minimum frequency, the flow is throttled by partly closing valve V2 (see Fig. 2). The evaporation temperature of the CO_2 in the PCC (and thereby in the CTES unit) is set by adjusting the cooling rate of the ACC in the condenser HEX as explained in Section 2.2. The pressure in the PCC is maintained at a constant level when the same heat rate is extracted the CTES unit is rejected to the ACC in the condenser. When a higher cooling rate is provided by the ACC in the condenser than extracted from the PCM in the CTES unit, the pressure of the PCC will decrease.

3.2. Discharging process

For the discharging cycle, a plate pitch of 15 mm and 30 mm was applied. A series of experiments considering various CO_2 mass flow rates and condensing temperatures were conducted for each plate pitch. The CO_2 mass flow rate was varied from 4 kg/min to 10 kg/min and the CO_2 refrigerant condensing temperature was varied from −6.5 °C to 3.7 °C. The discharging process is initiated immediately when the charging cycle is completed, as described in Section 3.1. The refrigerant mass flow rate is controlled by frequency control of the CO_2 pump and throttling of the flow using valve V1, similar to the procedure applied in the charging process. The heat input to the CO_2 from the GHC controls the pressure in the SCC during the discharging cycle. If the heat transferred to the CO_2 in the evaporator equals the heat rejected to the storage medium in the CTES unit, the pressure in the SCC remains constant. Consequently, the pressure in the SCC can be set to the required value by supplying more or less heat to the SCC. Since one of the heaters is equipped with PWM control, the output of the electric heaters can be controlled with high precision by the operator. The discharging cycle is a highly transient process, and a PI controller is therefore implemented in the LabVIEW software to continuously adjust the heater output and keep a constant pressure in the SCC according to the specifications of the experiment. The discharging process continues until all the solid PCM blocks have completely melted or until the CO_2 is not able to reject any more heat to the CTES unit without increasing the pressure. The discharging time is defined as the time from the start of the discharging cycle until one of the two aforementioned criteria occurs. The discharging rate of the CTES unit is obtained by calculating the total heat transfer rate from the refrigerant to the PCM in the CTES unit. The heat is transferred from the GHS to the SCC in the evaporator, assuming no heat loss to the ambient occurs in the evaporator HEX. The CO_2 enters the evaporator at a saturated liquid state, delivered from the liquid receiver (see Section 2.2). Then the refrigerant enters the CTES unit as a two-phase mixture and exits the CTES unit in a subcooled condition. Consequently, it can be assumed that all the heat which is transferred from the glycol to the refrigerant in the evaporator HEX is rejected to the PCM in the CTES unit. The energy balance for the evaporator is given in Eq. (1). The thermodynamic properties of the ethylene glycol mixture were taken from the datasheet of the manufacturer [50], assuming a constant specific heat capacity of the fluid in the relevant temperature range.

$$\dot{E}_{CO_2,evap} = \dot{E}_g = \dot{m}_g\, cp_g\, (T_{g,outlet} - T_{g,inlet}) \tag{1}$$

where $E_{CO_2,evap}$ is the heat flow to the refrigerant in the evaporator, $\dot{E}_g$ is the heat flow of the glycol, $\dot{m}_g$ is the mass flow rate of the glycol, cp_g is the specific heat capacity of the glycol and $(T_{g,outlet} - T_{g,inlet})$ is the temperature difference from the inlet to the outlet of the glycol in the evaporator. Furthermore, the heat transfer required to cool the refrigerant from the condensation temperature (saturation temperature) to the outlet temperature (subcooled condition) is given in Eq. (2).

$$\dot{E}_{CO_2,subcool} = \dot{m}_{CO_2}\, cp_{CO_2}\, (T_{CO_2,sat} - T_{CO_2,outlet}) \tag{2}$$

where $E_{CO_2,subcool}$ is heat flow from the refrigerant to the PCM due to subcooling, $\dot{m}_{CO_2}$ is the mass flow rate of the refrigerant, cp_{CO_2} is the specific heat capacity of the refrigerant and $(T_{CO_2,sat} - T_{CO_2,outlet})$ is the difference between the saturation temperature and the outlet temperature of the refrigerant. The total discharge rate is then obtained by adding Eqs. (1) and (2) together, as presented in Eq. (3).

$$\dot{E}_{CO_2,tot} = \dot{E}_{CO_2,evap} + \dot{E}_{CO_2,subcool} \tag{3}$$

where $E_{CO_2,tot}$ is the total heat flow from the refrigerant to the PCM in the CTES unit. The total energy discharged over the cycle is obtained by numerical integration of the total discharge rate given in Eq. (3). All thermo-physical properties of the CO_2 are obtained using the thermodynamic database REFPROP 10 [51].

4. Uncertainty analysis and repeatability

The output of the temperature sensors was checked with an ice water bath and validated to operate at within ±0.2 K (thermocouples TC01–TC27, see Fig. 2) and ±0.1 K (RTD100 T1–T7, see Fig. 2) at 0 °C. The uncertainty analysis was carried out by the method elaborated in [52], using a confidence level of 95% (coverage factor of 2). The formulation used for the propagation of uncertainty is summarised below. Uncertainty for the mean PCM temperature on PP2, PP5, and PP9 ($T_{PP2,mean}$, $T_{PP5,mean}$, and $T_{PP9,\ mean}$):

$$u(T_{PCM}) = \sqrt{(1/9)^2 \cdot \sum_{i=1}^{9} u(T_i)}\ . \tag{4}$$

Uncertainty for the refrigerant saturation temperature:

$$u(T_{CO_2,sat}) = \sqrt{\left(\frac{\partial T_{CO_2,sat}}{\partial P_{CO_2,sat}}\right)^2 \cdot u(P_{CO_2,sat})^2}. \tag{5}$$

From the Antoine equation, the relationship between saturation temperature and saturation pressure can be found. By derivation and inserting the coefficients for CO_2, it can be written as:

$$\frac{\partial T_{CO_2,sat}}{\partial P_{CO_2,sat}} = \frac{2273.66}{P_{CO_2,sat} \cdot (17.9834 - \ln(P_{CO_2,sat}))^2}. \tag{6}$$

Uncertainty in the heat flow from the glycol to the refrigerant in the evaporator:

$$u(\dot{E}_{CO_2,\ evap}) = \sqrt{(cp_g \cdot \Delta T_g \cdot u(\dot{m}_g))^2 + (\dot{m}_g \cdot cp_g \cdot u(\Delta T_g))^2}. \tag{7}$$

Uncertainty in the glycol temperature difference from inlet to outlet in the evaporator:

$$u(\Delta T_g) = \sqrt{u(T_{g,in})^2 + u(T_{g,out})^2}. \tag{8}$$

Uncertainty in the heat flow from the refrigerant to the PCM due to subcooling of the refrigerant:

$$u(\dot{E}_{CO_2,\ subcool}) = \sqrt{(cp_{CO_2,liq} \cdot \Delta T_{CO_2} \cdot u(\dot{m}_{CO_2}))^2 + (\dot{m}_{CO_2} \cdot cp_{CO_2,liq} \cdot u(\Delta T_{CO_2}))^2}. \tag{9}$$

Uncertainty in the refrigerant temperature difference from the saturation temperature to the outlet temperature from the CTES:

$$u(\Delta T_{CO_2}) = \sqrt{u(T_{CO_2,sat})^2 + u(T_{CO_2,\ out})^2}. \tag{10}$$

Uncertainty in the total heat flow from the refrigerant to the PCM in the CTES unit:

$$u(\dot{E}_{CO_2,tot}) = \sqrt{u(\dot{E}_{CO_2,\ evap})^2 + u(\dot{E}_{CO_2,\ subcool})^2}. \quad (11)$$

The uncertainty in the discharged energy over the cycle is estimated by integrating the uncertainty in the heat flow from the refrigerant to the PCM (Eq. (3)) from the start to the end of the cycle. To investigate the repeatability of the experiments, tests with identical test conditions were carried out for both plate configurations. The charging time was used as the indicator for the charging cycle. The resulting range of charging time was found to be <5 min for the 15 mm plate pitch <10 min for the 30 mm configuration. This corresponds to a repeatability of the charging time within ±6.7% and ±5.1% at T_{sat} = −15.5 °C and $\dot{m}_{CO_2}$ = 8 kg/min for the 15 mm and 30 mm plate pitch, respectively. For the discharging process, the mean discharge rate and discharged energy over the cycle were chosen as indicators for repeatability. The obtained range for the discharged energy over the cycle was <0.3 kWh for both configurations, corresponding to <4% and <3% of the discharged energy at the tested conditions for the 15 mm and 30 mm plate pitch, respectively. For the mean discharge rate, the obtained range was <0.25 kW for both configurations.

5. Characterisation of the PCM

In this study, the selected PCM consists of the commercial paraffin PCM RT-9HC (Rubitherm Technologies GmbH [53]) which has a phase change temperature in the range of −9 °C and −10 °C [53]. The selection of RT-9HC as the PCM was based on the temperature requirement for a CTES system designed to be integrated into CO_2 refrigeration systems in the food processing industry (typically −15 °C to 0 °C). The PCM was selected among other potential candidates as it has the highest latent heat capacity. Moreover, RT-9HC was selected thanks to its compatibility with the materials used in the CTES unit in this study. A thorough experimental characterisation of the PCM is required in order to fully explore and understand the behaviour of the heat transfer process from the PCM to the refrigerant and vice versa. Several experimental characterisation techniques are applied to determine the latent heat capacity, phase transition temperature, thermal conductivity, density and viscosity of the PCM. The applied methods and the results for each property are described in detail in the following paragraphs.

The Differential Scanning Calorimetry (DSC) technique is used to determine the latent heat capacity and the phase transition temperature of the PCM. DSC is found to be the appropriate technique to identify the storage capacity characteristics and phase change range for organic PCM according to the German quality label PCM-RAL (RAL-GZ 896 [54]). Several authors emphasise the importance of low heating/cooling rates (typically 1 K/min or lower) to obtain reliable and accurate results when using DSC for PCM characterisation [55–58]. Feng et al. [57] showed that the sample mass has less influence on the measured latent heat capacity and melting temperature than the heating rate. The apparatus used in the current study is a TA Instruments Q2000 DSC equipped with liquid nitrogen cooling, and the standard 40 μL aluminium crucibles were used to host the material samples. The DSC is calibrated and checked with indium. The obtained results of the melting temperature and melting enthalpy of indium were within 0.5% of the reference values provided by the manufacturer [59,60]. Furthermore, a 10 mg sample of deionised water was tested and found to give melting enthalpy with less than 0.2% deviation of tabulated values (333.55 kJ/kg). Two samples of RT-9HC were prepared and weighed using a Mettler Toledo laboratory scale with a precision of ±0.01 mg. The samples were then cycled from 30 °C to −40 °C using a constant heating/cooling rate ranging from 10 to 1 K/min, often referred to as the dynamic method. For more in-depth information and description of DSC methods applicable to PCM characterisation, the reader is directed to Barreneche et al. [55]. The samples were subject to temperature equilibration and a 5-minute isothermal stage before and after each heating/cooling segment. The results are presented in Table 3. It can be seen that the onset melting temperature is slightly shifted to a higher temperature by reducing the heating rate, namely from −9.80 °C to −9.58 °C in the case of the smallest sample mass. Furthermore, the peak melting temperature is shifted towards a lower temperature with lower heating rates. This effect is more pronounced for higher sample mass due to the higher thermal inertia of the larger sample when applying a high heating rate to the sample. The latent heat capacity is not significantly influenced by neither the heating rate change nor the sample weight. A mean value of 202.6 kJ/kg was obtained considering all the DSC tests. For the solidification process, a supercooling phenomenon was observed. This is an unwanted behaviour as the temperature of the PCM needs to be decreased below the freezing point to start the crystallisation process [61]. However, it is expected that the supercooling effect will not be as pronounced when the PCM is cycled at full scale in the CTES unit. The crystallisation onset ranged from −12.32 °C to −12.83 °C for the largest sample and between −13.22 °C and −13.51 °C for the smallest sample. The supercooling effect was greater when applying the highest cooling rate.

The heat transfer process within the PCM in the CTES unit is expected to be dominated by conduction heat transfer because the PCM is not subject to mechanical stirring or any other form of forced circulation. Therefore, the thermal conductivity of the PCM will have a significant impact on the heat transfer rate for both the charging and the discharging processes. The thermal conductivity of the PCM used in this study is measured by a thermal constants analyser (TPS 2500s, Hotdisk AB) which is based on the transient plane source technique [62]. It was identified for both liquid and solid phases of the PCM. A liquid sample holder specially designed by the manufacturer of the thermal constants analyser (Hotdisk AB) was utilised to perform the measurements on the liquid PCM and ensure adequate test conditions of the sample. The liquid test cell consists of a block of aluminium with a small sample volume inside where the sensor is vertically inserted. The manufacturer recommends using a small sensor, applying low sensor heating power and limiting the measurement time to a few seconds to ensure the reliability and repeatability of the tests. These recommendations are given to avoid initiating natural convection in the sample that affects the measurements when measuring the thermal conductivity of low-viscosity liquids. A sensor with a radius of 2.0 mm (Kapton sensor 7577, Hotdisk AB), a sensor heating power of 25 mW and a measurement time of 2 s were then applied to perform the measurements. The liquid test cell was put into a metal sample holder and placed into a thermal bath. A Pt100 temperature sensor was used to measure the sample temperature during the temperature stabilisation period. The temperature of the thermal bath was varied from 25 °C to −9 °C, and a 6-hour stabilisation period was introduced at each temperature stage before the measurements were taken to ensure a thermal equilibrium within the sample. The measurements were performed four times at each temperature step with a 20 min holding time between each measurement. The mean value and standard deviation were calculated. For the measurements in the solid phase, a sensor with a radius of 6.4 mm (Kapton sensor 5501, Hotdisk), a sensor heating power of 25 mW and a measurement time of 80 s were selected to perform the measurements. The Kapton sensor was centred in a cylindrical sample holder that was filled with solid PCM. The solidified sample was then placed into the thermal bath to achieve thermal equilibrium. A test series using distilled water in the liquid sample holder was first carried out in the temperature range 5 °C to 30 °C for verification of the instrument. The thermal conductivity obtained for distilled water was then compared to the correlation proposed by Dixon [63]. The results were found to be within 3% and 6.5% of the correlation for a sample temperature below and above 20 °C, respectively. It is suspected that there is some onset of convection within the sample for temperatures above 20 °C due to decreased viscosity of the water, resulting in an

Table 3
Results of DSC thermal analysis of PCM RT-9HC.

Sample mass [mg]	Heating rate [°C/min]	$T_{onset,melt}$ [°C]	$T_{peak,melt}$ [°C]	Melting enthalpy [kJ/kg]
7.941	10	−9.80	−8.11	203.8
7.941	5	−9.71	−8.50	204.2
7.941	2.5	−9.63	−8.74	204.0
7.941	1	−9.58	−8.82	202.0
13.351	10	−9.87	−7.99	201.9
13.351	5	−9.77	−8.43	202.2
13.351	2.5	−9.68	−8.52	201.6
13.351	1	−9.59	−8.37	201.1

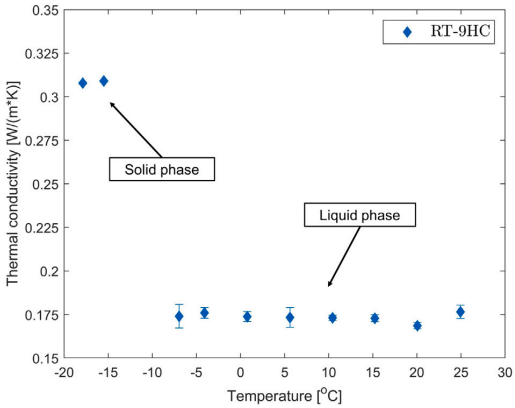

Fig. 4. Thermal conductivity of PCM RT-9HC in the liquid and solid phases as a function of temperature.

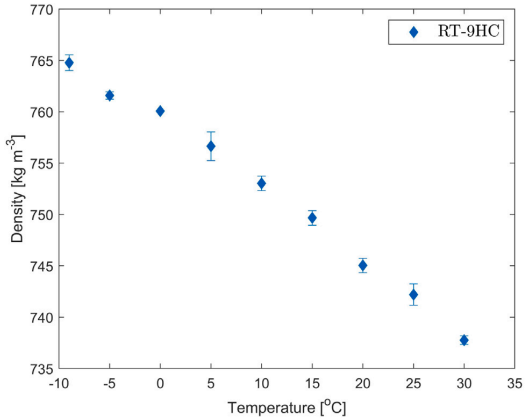

Fig. 5. Liquid density of RT-9HC depending on the temperature. Standard deviation of the measurements are indicated as error bars.

overestimation of the thermal conductivity. The results were within the acceptable limit of 5% for sample temperatures below 20 °C, which is the typically expected accuracy of the apparatus. The results of the thermal conductivity measurements for RT-9HC is presented in Fig. 4. It can be observed that in the applied temperature range −7 °C to 25 °C thermal conductivity in the liquid phase was approximately constant (≈ 0.174 W/(m K)). Furthermore, it can be observed that the thermal conductivity of the PCM in the solid phase is about 75% higher compared to that in the liquid phase (0.309 W/(m K) at −15.5 °C). It is expected that the thermal conductivity of the solid phase is higher than the liquid phase, as the lattice structure in solids fixes the position of the molecules, which increases the thermal conductivity of the material. It was also found that the thermal conductivity of the water is ≈ 235% higher than for the PCM at 5 °C, confirming that low thermal conductivity is one of the main limitations of using organic PCMs as the storage material [7].

Natural convection within the liquid PCM can be a significant contribution to the overall heat transfer in a PCM-HEX. The significance of natural convection in the liquid PCM is mainly dependent on three factors: the temperature variation within the PCM to drive the natural convection process, the change of density with change in temperature and the viscosity of the PCM. The density change of the liquid PCM was calculated by measuring the volumetric expansion of the liquid PCM in a 25 ml measuring cylinder placed in a thermal bath. The temperature was varied from 30 to −9 °C, with 5 K intervals and a holding time of 30 min per step. The procedure was repeated for three samples with a mass of 14.82 g, 16.38 g and 17.90 g, respectively. The sample mass was measured with a laboratory scale with a precision of 0.01 g (ME4002, Mettler Toledo). The mean value of the liquid density depending on temperature is presented in Fig. 5. It can be observed that the liquid density shows a nearly linear increase with temperature in the investigated range. The density of the solid phase was determined by placing a liquid sample (39.8 g), which was kept in a 100 ml measuring cylinder, into a thermal bath at −15 °C to solidify. The volume of the solid sample was registered, and the density was calculated to 880 kg m^{-3}. Due to the precision of reading the PCM volume in the measuring cylinders, an uncertainty of ±10% is assumed for the density results.

The viscosity of the PCM in the liquid phase is determined using a rotational rheometer (Haake Mars III, Thermo Fischer Scientific) having a concentric cylinder geometry (DIN Z40, 8 mm gap). The rheometer geometry is connected to a thermal bath to control the temperature of the sample. The apparent viscosity of the PCM was determined by varying the shear rate from γ = 10 1/s to γ = 100 1/s within the temperature application range. Each test series was repeated three times, and the results with the standard deviation are presented in Fig. 6. It can be seen that the apparent viscosity of the PCM is nearly constant for the investigated range of shear rate, demonstrating a near-Newtonian behaviour of the PCM for the considered range of shear rate. Moreover, it was observed that the apparent viscosity of the PCM increases as the temperature is reduced. The mean value of the viscosity is η_{PCM} = 5.57 mPa s, η_{PCM} = 2.53 mPa s and η_{PCM} = 1.98 mPa s for a temperature of −8.05 °C, −0.06 °C and 7.78 °C, respectively. At a temperature of ≈ 0 °C, the viscosity of the PCM was found to be 41.3% higher compared to that of liquid water (η_{H_2O} = 1.79 mPa s at T = 0.01 °C [64]). A summary of the PCM characterisation with complementary data from the datasheet of the manufacturer is presented in Table 4.

6. Results and discussion

6.1. Charging cycle

This section presents the results obtained from the charging tests described in Section 3.1. The purpose of the first test series is to

Table 4
Summary of PCM characterisation and comparison with data from manufacturer [53].

Property	Measured	Datasheet	Comments; Rubitherm (R) and measurements (M)
Melting temperature	−9.6 °C	between −9 °C and −10 °C	R: using a 3-layer-calorimeter
Latent heat capacity	202.6 kJ/kg	250 kJ/kg	R: ±7.5%, including sensible heat −16 °C to −1 °C
Thermal conductivity liquid	0.174 W/(m K)	0.2 W/(m K)	R: Same value for both phases
Thermal conductivity solid	0.309 W/(m K)	0.2 W/(m K)	R: Same value for both phases
Density liquid	745 kg/m^3	770 kg/m^3	M: ±10%. Both values at 20 °C
Density solid	880 kg/m^3	880 kg/m^3	M ±10%. Both values at 20 °C
Flash point	–	70 °C	–
Maximum operating temperature	–	30 °C	–

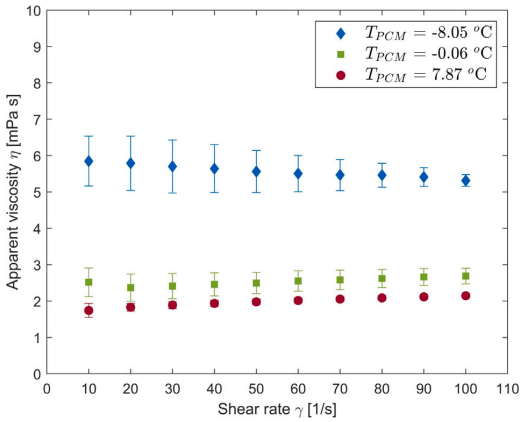

Fig. 6. Apparent viscosity of the PCM RT-9HC depending on the temperature. The standard deviation of each measurement point is indicated.

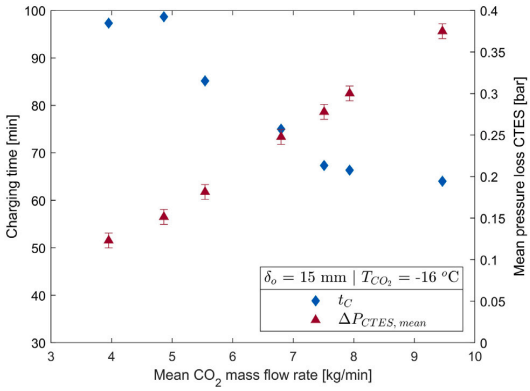

Fig. 7. The effect of refrigerant mass flow rate on charging time and pressure loss through the CTES unit using a CO_2 evaporation temperature of −16 °C and a plate pitch of 15 mm.

determine the appropriate refrigerant flow rate supplied to the CTES unit to operate the charging cycle effectively. The selected HEX design is relative to a plate pitch of 15 mm. The refrigerant evaporation temperature was kept constant at −16 °C for all tests, while the total mass flow rate was varied from 4 kg/min to ≈ 9.5 kg/min. The refrigerant pressure loss through the CTES is measured using the differential pressure sensor (DP2) shown previously in Fig. 2. Both the charging time and the mean pressure loss over the CTES unit are represented in Fig. 7 for a set of applied CO_2 mass flow rates. It can be observed that the charging time decreases when the refrigerant mass flow rate is increased. Increasing the flow rate from $\dot{m}_{CO_2}$ = 5 kg to $\dot{m}_{CO_2}$ = 8 kg/min has decreased the charging time by 33%. A further increase of the flow rate further from $\dot{m}_{CO_2}$ = 8 kg/min to $\dot{m}_{CO_2}$ = 9.5 kg/min was observed to have no significant enhancement on the charging time which has decreased only by 5%. The increase in the charging time for the lowest mass flow rate can be explained by inadequate refrigerant supply to operate the charging cycle. In fact, for $\dot{m}_{CO_2}$ = 4 kg/min and $\dot{m}_{CO_2}$ = 5 kg/min, superheated refrigerant was measured at the outlet of the CTES unit during the first 10–15 min of the charging process. This observation means that all the refrigerant supplied to the CTES unit during this period had been fully evaporated inside the PPs before reaching the manifold at the outlet.

Operating the charging cycle under superheated conditions is found to decrease the efficiency of the charging cycle as the heat transfer from the PCM to the refrigerant is ensured by sensible heat (elevation of the refrigerant vapour temperature), and no more by the evaporation of the liquid refrigerant. Applying vapour/liquid refrigerant mixture conditions along the full length of the HEX (often referred to as flooded conditions) is a key factor for the proper use of the available heat transfer area and thus increase the heat transfer process [65–68]. It was also observed that for the experiments using a CO_2 flow rate less than 7.5–8 kg/min the thickness of the solid PCM layer on the PP surface was less uniform, particularly close to the outer edges and corners of the PPs (dead zones) where the refrigerant shifts direction (see Fig. 1a). Consequently, a higher refrigerant flow rate improves the refrigerant distribution in the PP channels. Moreover, these observations indicate that the turbulence occurring in the dead zones by the higher refrigerant flow rates also promotes the heat exchange between the PCM and the refrigerant in these areas, leading to a shorter and more efficient charging process. It can also be depicted from Fig. 7 that the mean refrigerant pressure loss through the PPs increases when increasing the refrigerant mass flow rate. Indeed, a higher mass flow rate increases the mean velocity of the refrigerant inside the PP channel, which in turn increases the pressure loss. The pressure loss increases nearly linearly from 0.123 bar for $\dot{m}_{CO_2}$ = 4 kg/min to 0.3749 bar for $\dot{m}_{CO_2}$ = 9.5 kg/min. The pressure loss is an unwanted phenomenon since it increases the required pressure lift of the compressors in the refrigeration system, consequently increasing the energy consumption. However, for the investigated range of flow rates, the pressure loss is less than the typical maximum allowable pressure drop in PP-HEX (0.4–0.6 bar [69]). By increasing the mass flow rate from 8 kg/min to 9.5 kg/min, the pressure loss increases by 25 %, while the corresponding reduction in charging time is less than 4%. This indicates that the heat transfer process is limited from the PCM side. Based on the analysis above, a mass flow rate of 8 kg/min resulting in a lower charging time, a pressure loss lower than 0.4 bar and promoting a satisfying heat transfer in the CTES dead zones was selected for further investigations on the charging cycle.

A series of tests were performed using a CO_2 mass flow rate of 8 kg/min and a CO_2 evaporation temperature ranging from −12 °C to −23 °C for both plate pitches of 15 mm and 30 mm. The tests

were carried out to investigate the effect of the refrigerant evaporation temperature on the charging cycle performance. The charging time and mean pressure loss as a function of the refrigerant evaporation temperature are presented in Fig. 8a and b, respectively. It can be clearly seen from Fig. 8a that the same refrigerant evaporation temperature and comparing the 15 mm and 30 mm plate pitch designs, the charging time for δ_o = 15 mm results in a faster charging process than that of δ_o = 30 mm as the theoretical latent storage capacity of the CTES unit is doubled for the 30 mm configuration. For an evaporation temperature ($T_{CO_2,evap}$) of −13 °C, the charging time has increased by ≈ 150% for the 30 mm configuration compared to the 15 mm configuration. For a $T_{CO_2,evap}$ = −20 °C the recorded increase in the charging time for δ_o = 30 mm was ≈ 161%.

The results also show that the charging time is reduced when operating the charging cycle with lower refrigerant evaporation temperatures. Decreasing the evaporation temperature from −13 °C to −15.5 °C yields a reduction in the charging time by 40.7 % for the 15 mm configuration and by 44.0% for the 30 mm configuration. A further reduction in the evaporation temperature from −15.5 °C to −17.5 °C reduces the charging time by 21.0% and 23.7% for the 15 mm and 30 mm plate pitch, respectively. As heat is removed from the PCM during the charging cycle, a layer of solid PCM is formed on both sides of each PP. For two successive PPs, the liquid PCM volume comprised between the formed solid PCM blocks is reduced, and the thickness of the solid PCM layer increases. As the solid PCM layer grows, the charging process decelerates as the solid PCM layer acts as additional thermal resistance to the heat transfer process. This effect is even more pronounced for the 30 mm configuration compared to the 15 mm configuration due to the thicker solid PCM layer required to complete the charging process. The temperature difference between the solidifying PCM and the refrigerant can be increased by reducing the refrigerant evaporation temperature to increase the driving forces for the heat transfer process. Although significant reductions in the charging time can be achieved by reducing the evaporation temperature, the energy consumption of the compressors in the refrigeration system will also increase due to the increased pressure lift of the system. Previous studies have shown that lowering the evaporation temperature of 1 °C will reduce the coefficient of performance (COP) of the system by about 2%–3% [65]. Based on the discussion above, a significant reduction in the charging time is achieved using a temperature difference between the phase change temperature of the PCM and the refrigerant of 5–6 K for both plate pitches. Nevertheless, a parametric study to identify the appropriate refrigerant evaporation temperature and plate pitch should be carried out for each CTES installation using the present HEX design, considering the required storage capacity and cost of electricity as the design parameters.

Fig. 8b presents the mean refrigerant pressure loss across the CTES unit during the charging cycle for both 15 mm and 30 mm plate pitch for different refrigerant evaporation temperatures. It can be seen that the mean pressure loss tends to increase for a fixed refrigerant flow rate as the evaporation temperature decreases. In fact, a reduction in the evaporation temperature strengthens the driving forces for the heat transfer process, and thus more refrigerant is evaporated in the PP channels. Consequently, the mean density of the vapour/liquid refrigerant mixture decreases and the mean velocity of the refrigerant increases, generating a higher pressure loss. A nearly linear increase in the pressure loss is recorded in the studied refrigerant temperature range. The pressure loss increased by 156% (from 0.214 bar to 0.548 bar) for δ_o = 15 mm and by 103% (from 0.211 bar to 0.428 bar) for δ_o = 30 mm when decreasing the refrigerant temperature from −12 °C to −22.5 °C. The recorded mean pressure loss for the 15 mm configuration was higher than for the 30 mm configuration as the charging cycle for the former design is shorter than that for the latter. For δ_o = 30 mm, the heat transfer is decelerated due to the solid PCM layer formation on the PP as the charging process progresses, as explained earlier in this section. Consequently, less refrigerant is evaporated in the PP channels, and the mean density of the refrigerant increases gradually during the charging cycle. The refrigerant velocity is then reduced and decreases the mean refrigerant pressure loss over the cycle.

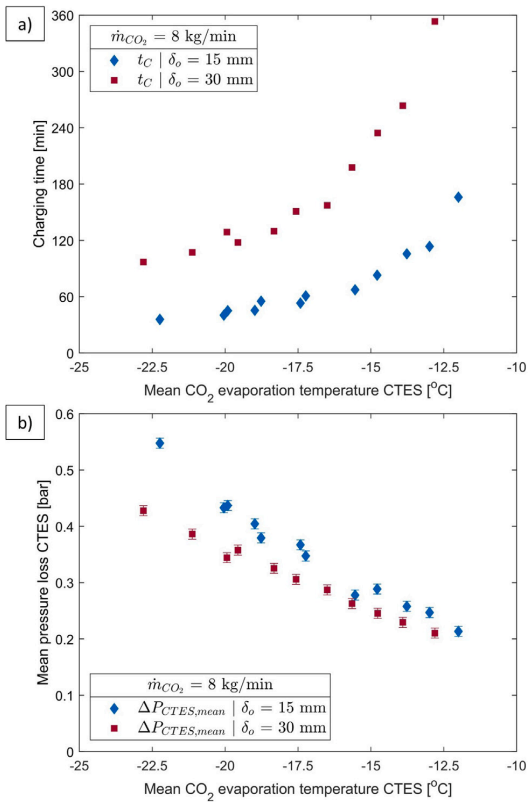

Fig. 8. The effect of refrigerant evaporation temperature for the 15 mm and 30 mm configuration using a refrigerant mass flow rate of 8 kg/min on (a) the charging time (b) mean pressure loss.

During the charging process, both the bulk PCM temperature (mean of TC00–TC26, see Fig. 3) near to PP2, PP5 and PP9 as well as their relative refrigerant temperature evolution are recorded for three selected experiments ($T_{CO_2,evap}$ = −13 °C, $T_{CO_2,evap}$ = −16 °C and $T_{CO_2,evap}$ = −22 °C). They are represented for δ_o = 30 mm plate pitch as shown in Fig. 9. For all experiments, the initial temperature of the storage medium was set to ≈ 4 °C and a refrigerant mass flow rate of 8 kg/min. The phase change temperature (onset melting temperature) of the PCM RT-9HC was determined by DSC measurements to $T_{pc,PCM}$ = −9.58 C. At first glance, it can be observed that the duration of the charging cycle significantly decreases when decreasing the refrigerant evaporation temperature. The charging time of the CTES unit is reduced from 354 min to 110 min when the CO_2 evaporation temperature is reduced from −13 °C to −22 °C. For the three experiments, a rapid decrease in the PCM bulk temperature was observed in the first 15–20 min of the charging cycle, denoting an SHS process. After this initial period, the charging process continues as an LHS process with a constant temperature difference between the evaporating CO_2 inside the PP channels and the phase change temperature of the PCM that solidifies at the solid–liquid interface. During this period, a "plateau" can be observed in the PCM bulk temperature profile describing a latent heat storage, most notable for the highest CO_2 evaporation temperatures ($T_{CO_2,evap}$ =

Table 5
The calculated maximum theoretical latent storage capacity of the CTES unit in various configurations.

δ_o [mm]	$\delta_{o,mean}$ [mm]	m_{PCM} [kg]	$E_{lat,th}$ [kWh]	t_C @ $T_{CO_2,evap}$ = −15.5 °C [min]
15	12.85	111.88	6.31	67
30	27.85	225.07	12.69	198

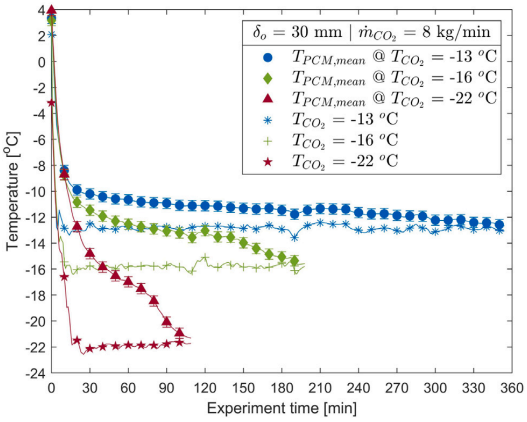

Fig. 9. Bulk PCM temperature and refrigerant evaporation temperature evolution during the charging cycle for three different refrigerant evaporation temperatures ($T_{CO_2,evap}$ = −13 °C, $T_{CO_2,evap}$ = −16 °C and $T_{CO_2,evap}$ = −22 °C) using a refrigerant mass flow rate of 8 kg/min and δ_o = 30 mm.

−13 °C and $T_{CO_2,evap}$ = −16 °C). The measured bulk PCM temperature is approaching the refrigerant evaporation temperature during the LHS period because the thermocouple sensors become embedded in the solid PCM layer as the charging progresses. There is a temperature gradient within the solid PCM layer in the perpendicular direction of the PP surface, where the temperature ranges from the refrigerant evaporation temperature at the PP surface to the PCM phase change temperature at the liquid–solid interface. The LHS period continues until the solid PCM layer formed on the PP surface overlaps with the solid PCM layer on the neighbouring PP (see Fig. 10), forming a solid block of PCM between the PPs. The PCM temperature decreases more rapidly and approaches the refrigerant temperature, and energy is then stored by an SHS process. From Fig. 9, this condition occurs at ≈ 293 min for $T_{CO_2,evap}$ = −13 °C, at ≈ 145 min for $T_{CO_2,evap}$ = −16 °C and at ≈ 77 min for $T_{CO_2,evap}$ = −22 °C. The development of the charging process and growth of the solid PCM layer on the PP surface after 30, 50 and 90 min for three CO_2 evaporation temperatures (−13 °C, −17 °C and −21 °C) are shown in Fig. 10. The pictures clearly show that operating the charging process with lower refrigerant evaporation temperature results in faster growth of the solid PCM layer. It can be observed that after 90 min, the charging cycle using an evaporation temperature of −21 °C is nearly finished, i.e. the PCM layers from neighbouring PPs have nearly grown together.

Table 5 presents the calculated useful mass of PCM in the CTES unit, i.e. the PCM that occupies the volume between the PPs that is cycled through its phase change process. Furthermore, the theoretical latent storage capacity of the CTES unit and the resulting charging time using an evaporation temperature of −15.5 °C for the 15 mm and 30 mm plate pitches are presented. It can be seen that the theoretical storage capacity is doubled when the plate pitch is increased from 15 mm to 30 mm. However, the charging time increases by 194% from 67 min to 198 min for the same evaporation temperature ($T_{CO_2,evap}$ = −15.5).

6.2. Discharging cycle

This section presents the results obtained for the discharging tests following the procedure described in Section 3.2. The first test series are performed to identify the appropriate refrigerant flow rate for the discharging cycle. During these experiments, the CO_2 condensation temperature ($T_{CO_2,cond}$) was kept at −1 °C and the mass flow rate was varied from 4 kg/min to 10 kg/min for a plate pitch δ_o = 30 mm. The discharging rate profiles for the tests using a refrigerant mass flow rate of 4, 7 and 10 kg/min are presented in Fig. 11. It is observed that the discharging cycle follows the same general trend for all of the considered flow rates. A high discharging rate (24–16 kW) is recorded during the first 10–15 min. A gradual decrease in the discharging rate is then observed towards zero to denote the end of the discharging cycle. At the beginning of this process, the adjacent solid PCM to the PP surface starts to melt. As the condensation heat from the CO_2 is transferred to the PCM, a thin layer of liquid PCM is formed between the PP surface and the solid PCM block. As the discharging process progresses, the liquid PCM layer becomes thicker, and thus, the thermal resistance to the heat transfer process is also increased. This process is analogous to the growth of the solid PCM layer during the charging process, which is also limiting the heat transfer between the PCM and the refrigerant. As the liquid PCM layer increases in thickness, the discharging rate decreases gradually towards ≈ zero, denoting the end of the discharging cycle. It can also be seen from Fig. 11 that a mass flow rate of 7 kg/min yields the highest overall discharge rate during the first 60 min of the discharging cycle, approximately 2–3 kW higher than for the flow rate of 4 kg/min.

The mean discharging rate and discharged energy over the cycle for the considered range of refrigerant mass flow rates (4 kg/min to 10 kg/min) for $T_{CO_2,cond}$ = −1 °C and δ_o = 30 mm are presented in Fig. 12. The figure shows that the mean discharging rate is continually increasing in a nearly linear behaviour from 5.09 kW to 7.76 kW when the mass flow rate increases from 4 kg/min to 10 kg/min, respectively. The total discharged energy (E_D) over the cycle is increasing from 12.19 kWh at a flow rate of 4 kg/min to the maximum value of 13.86 kWh at 7 kg/min. For a mass flow rate of $\dot{m}_{CO_2}$ = 10 kg/min, E_D decreases to 11.87 kWh. Although the highest refrigerant mass flow rate resulted in the highest mean discharge rate, it yielded the lowest amount of discharged energy over the cycle. This is because using lower mass flow rates (<8 kg/min) it was possible to sustain the discharging cycle for a longer time, see Fig. 11. Using a flow rate of 4 and 7 kg/min resulted in a longer discharging time (40–50 min) than using the flow rate of 10 kg/min, and the discharge rate is less than 2.5 kW during this period. Consequently, the mean discharge rate over the cycle will be lower for the tests with a longer discharging time. Based on the discussions above, the mass flow rate that yielded the highest amount of discharged energy over the cycle (7 kg/min) was selected for further investigations.

The effects of the CO_2 condensation temperature variation ($T_{CO_2,cond}$ = −4.59 °C, $T_{CO_2,cond}$ = −0.88 °C and $T_{CO_2,cond}$ = 2.46 °C) on the evolution in the discharging rate have also been studied and presented in Fig. 13. The selected refrigerant mass flow rate was $\dot{m}_{CO_2}$ = 7 kg/min as it has provided the highest discharged energy (see the previous paragraph). It was observed that the discharging rate is higher as the $T_{CO_2,cond}$ is increased. During the discharging process, the mean discharging rate for $T_{CO_2,cond}$ = −4.59 °C, $T_{CO_2,cond}$ = −0.88 °C and $T_{CO_2,cond}$ = 2.46 °C are 3.67 kW, 6.22 kW and 9.01 kW, respectively. Furthermore, operating the discharging cycle with higher $T_{CO_2,cond}$ results in a decrease in the discharging time because of the higher discharge rate. As the PCM melting temperature is fixed at −9.6 °C, increasing the $T_{CO_2,cond}$ increases the driving forces for the heat transfer process from the refrigerant to the PCM. Also, increasing the temperature difference between the storage medium and the refrigerant

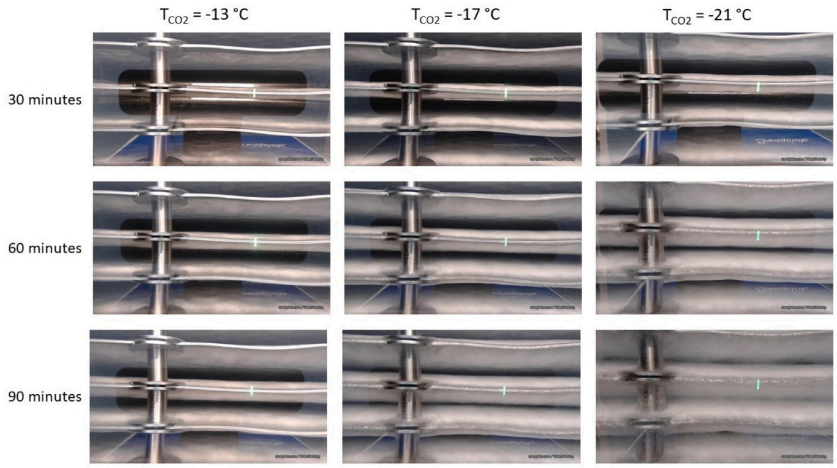

Fig. 10. Development of the solid PCM layer on the PP surface after 30, 60 and 90 min when using a CO_2 evaporation temperature of −13 °C, −17 °C and −21 °C and using a refrigerant mass flow rate of 8 kg/min and a plate pitch of 30 mm.

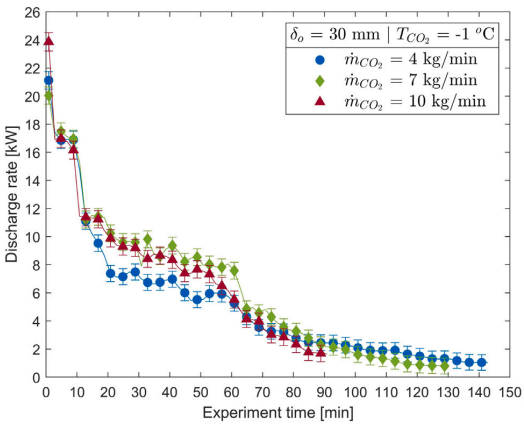

Fig. 11. Discharging rates for three refrigerant mass flow rates (4, 7 and 10 kg/min) for a refrigerant condensation temperature $T_{CO_2,cond}$ = −1 °C and a plate pitch δ_o = 30 mm.

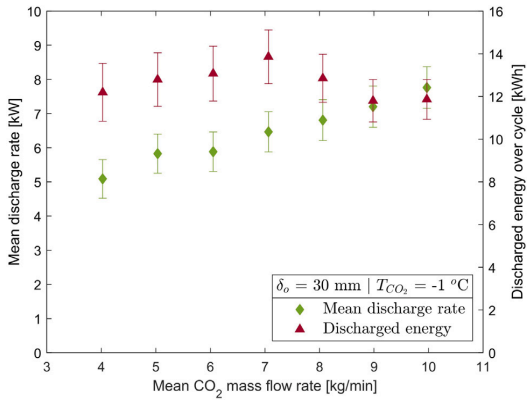

Fig. 12. Mean discharging rate and discharged energy variation with the refrigerant mass flow rate for a refrigerant condensation temperature $T_{CO_2,cond}$ = −1 °C and a plate pitch δ_o = 30 mm.

compensates to some extent the thermal resistance that occurs when the liquid PCM layer is formed between the solid PCM block and the PP surface, and thus ensures a higher discharge rate throughout the cycle. Consequently, a clear "plateau" in the discharging rate curve is observed for the first 45 min using $T_{CO_2,cond}$ = 2.46 °C. This effect is also observed for $T_{CO_2,cond}$ = −0.88 °C for the first 65 min, but is less pronounced compared to $T_{CO_2,cond}$ = 2.46 °C. For $T_{CO_2,cond}$ = −4.59 °C, the discharging rate is slowly decreasing from about 6.4 kW at 12 min to zero at 162 min, denoting the end of the cycle. For the first 60 min of the discharging cycle, the mean discharging rate for $T_{CO_2,cond}$ = −4.59 °C, $T_{CO_2,cond}$ = −0.88 °C and $T_{CO_2,cond}$ = 2.46 °C are 5.94 kW, 10.58 kW and 13.80 kW, respectively.

The mean discharging rate and discharged energy over the cycle as a function of the CO_2 condensation temperature in the range of −6.49 °C to 3.67 °C are presented in Fig. 14. It can be observed that the mean discharging rate over the cycle increases in a nearly linear trend from 2.50 kW to 9.79 kW as the $T_{CO_2,cond}$ increases from −6.49 °C to 3.67 °C. Increasing the difference between the $T_{PCM,pc}$ and $T_{CO_2,cond}$ by 327% has enhanced the driving forces for the heat transfer process from the refrigerant to the PCM and generated an increase of 292% in the discharging rate. It can also be seen from Fig. 14 that the discharged energy over the cycle increases with higher CO_2 condensation temperature. A higher $T_{CO_2,cond}$ (and thereby high driving forces for the heat transfer) ensures that all solid PCM is melted during the discharging cycle. It was also visually observed that for the lowest CO_2 condensation temperature ($T_{CO_2,cond}$ = −6.49 °C), a significant share of the solid PCM did not melt even when the discharging cycle ended. This phenomenon is an unwanted behaviour of the storage medium as it clearly limits the discharging capacity of the storage. The smallest solid PCM fraction left by the end of the discharging cycle was observed around the edges of the PP for the highest refrigerant condensation temperature. The complete melt of the PCM block at the end of the discharging cycle was depicted for $T_{CO_2,cond}$ higher than −2.58 °C. The discharged energy over the cycle was E_D = 10.05 kWh, E_D = 13.92 kWh and E_D = 17.03 kWh when using a CO_2 condensation temperature of $T_{CO_2,cond}$ = −4.59 °C, $T_{CO_2,cond}$= −0.83 °C and $T_{CO_2,cond}$ = 3.67 °C, respectively. The discharged energy over the cycle is further enhanced

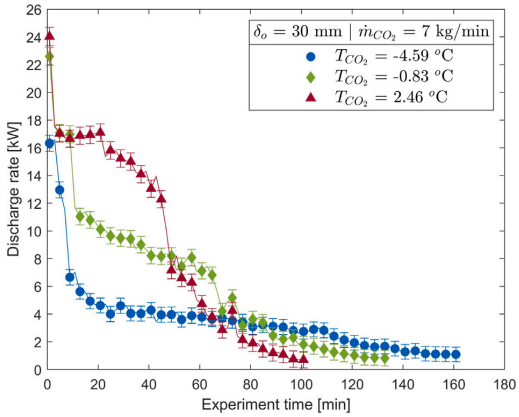

Fig. 13. Discharging rates for various refrigerant condensation temperatures ($T_{CO_2,cond}$ = −4.59 °C, $T_{CO_2,cond}$ = −0.88 °C and $T_{CO_2,cond}$ = 2.46 °C) for $\dot{m}_{CO_2}$ = 7 kg/min and a δ_o = 30 mm.

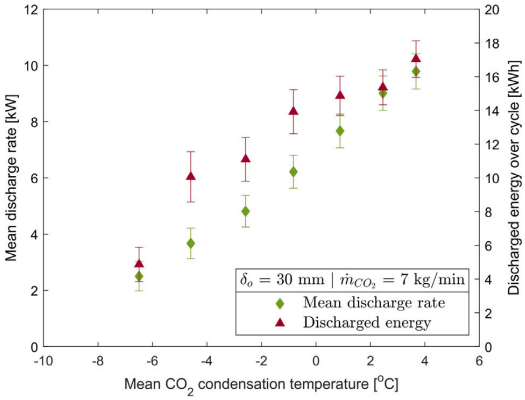

Fig. 14. Mean discharging rate and discharged energy as a function of the refrigerant condensation temperature using a refrigerant mass flow rate of $\dot{m}_{CO_2}$ = 7 kg/min and plate pitch δ_o = 30 mm.

by sensible heat when the phase change process is completed: for higher $T_{CO_2,cond}$, the final PCM temperature reached at the end of the process are also higher towards the refrigerant temperature. For a condensation temperature of −0.8 °C, the theoretical sensible heat discharged over the cycle was calculated to about 7% of the total theoretical discharged energy (latent heat + sensible heat) when considering the volume of PCM between the PPs in the PP-HEX.

The same experiments were reproduced for pitch plate δ_o = 15 mm as for δ_o = 30 mm, using $T_{CO_2,cond}$ = −1 °C to determine the appropriate refrigerant mass flow rate that results in the best performance of the cycle. It was found that the refrigerant mass flow rate of $\dot{m}_{CO_2}$ = 5 kg/min provided the highest amount of discharged energy (kWh) and thus selected for the rest of the test campaign. The mean discharging rate and the discharged energy over the cycle by variation of the refrigerant condensation temperature from $T_{CO_2,cond}$ = −7.70 °C to $T_{CO_2,cond}$ = 2.71 °C are presented in Fig. 15. The same observations can be made as for the δ_o = 30 mm configuration, both the discharged energy over the cycle and the mean discharging rate increases as the condensation temperature of the refrigerant increases. The maximum discharged energy (9.32 kWh) and mean discharge rate (kW) were obtained using $T_{CO_2,cond}$ = 0.84 °C. It was found that a $T_{CO_2,cond}$ higher

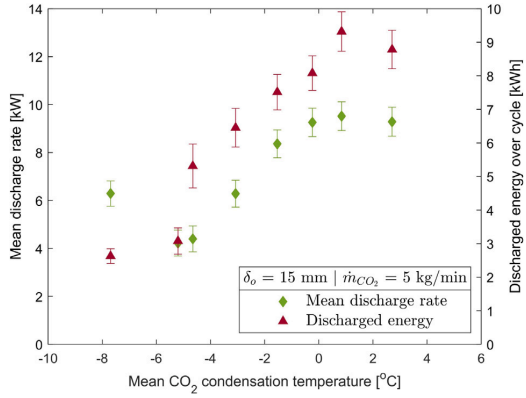

Fig. 15. Mean discharging rate and discharged energy as a function of the refrigerant condensation temperature using a refrigerant mass flow rate of $\dot{m}_{CO_2}$ = 5 kg/min and plate pitch δ_o = 15 mm.

than −4.65 °C is required to ensure the entire melting of the solid PCM fraction by the end of the discharging cycle, compared to $T_{CO_2,cond}$ = −2.58 °C for the δ_o = 30 mm configuration. This shows that the discharging process for the δ_o = 15 mm configuration can be operated effectively with approximately 2 K lower difference in $T_{CO_2,cond}$ and $T_{PCM,pc}$ compared to the δ_o = 30 mm due to the shorter plate pitch. For the lowest $T_{CO_2,cond}$ (−7.70 °C), the temperature difference between the $T_{CO_2,cond}$ and $T_{PCM,pc}$ was not sufficient to sustain the discharging cycle and ended after the initial period of the cycle (where the discharge rate is high, see Fig. 15).

Table 6 presents a summary of the discharging performance of the CTES unit for both δ_o = 15 mm and δ_o = 30 mm plate configurations. Three tests using different CO_2 condensation temperatures are selected to represent the performance of the whole temperature range. For δ_o = 15 mm, a 90% increase in the mean discharging rate and 41% increase in the discharged energy over the cycle are obtained when increasing the difference between the $T_{CO_2,cond}$ and $T_{PCM,pc}$ by 63% (from 4.95 K to 8.07 K). A further increase of the condensation temperature by 2.37 K to $T_{CO_2,cond}$ = 0.84 °C results in just a 14% and 24% increase in the discharge rate and discharged energy, respectively. In summary, the relatively small plate pitch of 15 mm allows for an efficient discharging process of the CTES unit by using a temperature difference between the melting point of the PCM and condensing refrigerant of about 8 K. It is concluded that the CTES design consisting of δ_o = 15 mm using $\dot{m}_{CO_2}$ = 5 kg/min and $T_{CO_2,cond}$ = −1.53 °C is appropriate to ensure peak shaving of the refrigeration load in a refrigeration process characterised by load peaks which last ≈ 1 h. For the 30 mm plate pitch, the increase in the discharging rate and discharged energy over the cycle has a more linear profile than that for the 15 mm plate pitch. This behaviour is expected as the increased distance between the PPs results in more thermal resistance to the heat transfer process as the discharging cycle progresses. Consequently, the discharging performance of the CTES unit is more sensitive to higher $T_{CO_2,cond}$ when using δ_o = 30 mm compared to δ_o = 15 mm. When the condensation temperature is increased from −4.59 °C to −0.83 °C (3.76 K), an increase of 67% in the mean discharge rate and an increase of 38% in the discharged energy over the cycle is observed. A further increase in the $T_{CO_2,cond}$ by 4.5 K (from −0.83 °C to 3.67 °C) results in a 57% and 22% increase in the discharging rate and discharged energy, respectively. The discharging time (t_D) was found to be more influenced by the $T_{CO_2,cond}$ for the δ_o = 30 mm configuration than for δ_o = 15 mm. For δ_o = 30 mm, t_D is reduced by ≈ 30 min when increasing $T_{CO_2,cond}$ from −4.59 °C to −0.83 °C and further reduced by ≈ 30 min when increasing $T_{CO_2,cond}$ from −0.83 °C to 3.67 °C.

Table 6
Summary of the discharging performance for the CTES unit for various CO_2 condensation temperature for a plate pitch of 15 mm and 30 mm.

δ_o [mm]	$\dot{m}_{CO_2}$ [kg/min]	T_c [°C]	$\dot{E}_r$ [kW]	E_D [kWh]	t_D [min]
15	5.0	−4.65	4.40 ± 0.540	5.31 ± 0.653	73
15	5.0	−1.53	8.36 ± 0.583	7.51 ± 0.523	54
15	5.0	0.84	9.52 ± 0.601	9.32 ± 0.589	59
30	7.0	−4.59	3.67 ± 0.542	10.06 ± 1.49	165
30	7.0	−0.83	6.22 ± 0.584	13.92 ± 1.31	135
30	7.0	3.67	9.79 ± 0.625	17.04 ± 1.09	105

The results for the discharging process summarised in Table 6 can be used as a design guide to engineer similar CTES units to be implemented in the industry. The results from the discharging process have demonstrated that peak shifting of the refrigeration demand is feasible when integrating this novel CTES unit into a CO_2 refrigeration system. The flexible design of the CTES unit allows the designer to select a discharge characteristic of the CTES unit that matches the refrigeration load curve in different refrigeration systems. It was found that the 15 mm plate pitch is the appropriate choice to reduce load peak with high magnitude and a duration of approximately one hour. On the other hand, it was found that the 30 mm plate pitch is most suitable when the peak has a longer duration and a lower magnitude. However, it is possible to install several of these CTES units in parallel to increase the overall energy storage capacity or increase the total discharge rate of the CTES system.

7. Conclusions

This paper presents the design and thorough experimental performance testing of a CTES unit based on a pillow plate heat exchanger with a low-temperature commercial PCM as the storage medium. It is one of the first experimental investigations to couple the phase change process of a subzero PCM (solidification/melting) with the phase change process of the refrigerant (evaporation/condensation) in the same heat exchanger. The results from the experimental testing have demonstrated the feasibility of using the CTES unit with PCM for peak shifting of the refrigeration load. The main findings can be summarised as follows:

- The charging time of the CTES unit was mainly affected by reducing the CO_2 evaporation temperature, effectively increasing the temperature difference between the CO_2 refrigerant and the phase change temperature of the PCM. Decreasing the $T_{CO_2,evap}$ from −13 °C to −15.5 °C yielded a reduction in the charging time by 44% for $\delta_o = 30$ mm.
- The discharging rate was found to be generally high during the initial phase of the cycle and continually decreasing towards the end of the cycle, and was mainly affected by increasing the $T_{CO_2,cond}$. The maximum discharged energy was found to be 17.04 kWh using $\delta_o = 30$ mm with $T_{CO_2,cond} = 3.67$ °C, yielding a mean discharge rate of 9.79 kW.
- The flexible design of the CTES unit allows the designer to select a discharge characteristic of the CTES unit that matches the refrigeration load curve of the refrigeration plant by changing the plate pitch. A plate pitch of $\delta_o = 15$ mm was found as the appropriate choice to reduce a peak with a high magnitude and duration of approximately one hour, while $\delta_o = 30$ mm is most suitable for peaks of about 2 h with a lower magnitude.

The demonstrated module-based CTES technology is versatile and is expected to be scaleable for implementation in industrial refrigeration plants with various temperature requirements and load characteristics. The planned future studies on the technology are the development and validation of a dynamic numerical model to investigate the impact of integrating CTES technology into a complete refrigeration plant. Furthermore, it is relevant to investigate any performance degradation of the CTES unit over time, as well as partial charging and discharging cycles.

Declaration of competing interest

The authors declare that they have no known competing financial interests or personal relationships that could have appeared to influence the work reported in this paper.

Acknowledgements

The work is part of HighEFF - Centre for an Energy Efficient and Competitive Industry for the Future, an 8-year Research Centre under the FME-scheme (Centre for Environment-friendly Energy Research, 257632). The first author gratefully acknowledges the financial support from the Research Council of Norway and user partners of HighEFF. The authors would also like to acknowledge the financial and technical support of Skala Fabrikk, Norway, Hermetic Pumpen, Germany, Alfa Laval, Sweden, HB Products, Denmark and Danfoss regarding the test facility.

References

[1] A. Arteconi, F. Polonara, Demand side management in refrigeration applications, Int. J. Heat Technol. 35 (1) (2017) 58–63.
[2] P. Moreno, C. Solé, A. Castell, L.F. Cabeza, The use of phase change materials in domestic heat pump and air-conditioning systems for short term storage: A review, Renew. Sustain. Energy Rev. 39 (2014) 1–13.
[3] M.M. Joybari, F. Haghighat, J. Moffat, P. Sra, Heat and cold storage using phase change materials in domestic refrigeration systems: The state-of-the-art review, Energy Build. 106 (2015) 111–124.
[4] H. Selvnes, Y. Allouche, R.I. Manescu, A. Hafner, Review on cold thermal energy storage applied to refrigeration systems using phase change materials, Therm. Sci. Eng. Prog. 22 (2021) 100807.
[5] P. Gullo, A. Hafner, K. Banasiak, Transcritical R744 refrigeration systems for supermarket applications: Current status and future perspectives, Int. J. Refrig. 93 (2018) 269–310.
[6] G. Li, Y. Hwang, R. Radermacher, H.-H. Chun, Review of cold storage materials for subzero applications, Energy 51 (2013) 1–17.
[7] Y. Allouche, S. Varga, C. Bouden, A.C. Oliveira, Experimental determination of the heat transfer and cold storage characteristics of a microencapsulated phase change material in a horizontal tank, Energy Convers. Manage. 94 (2015) 275–285.
[8] A. Abhat, Low temperature latent heat thermal energy storage: heat storage materials, Sol. Energy 30 (4) (1983) 313–332.
[9] E. Oró, A. De Gracia, A. Castell, M.M. Farid, L.F. Cabeza, Review on phase change materials (PCMs) for cold thermal energy storage applications, Appl. Energy 99 (2012) 513–533.
[10] A. Safari, R. Saidur, F. Sulaiman, Y. Xu, J. Dong, A review on supercooling of phase change materials in thermal energy storage systems, Renew. Sustain. Energy Rev. 70 (2017) 905–919.
[11] Y.J. Zhou, E.J. Kerkhoven, J. Nielsen, Barriers and opportunities in bio-based production of hydrocarbons, Nat. Energy 3 (11) (2018) 925–935.
[12] PureTemp LCC, PureTemp phase change materials, 2020, URL: https://www.puretemp.com/stories/puretemp-safety-data-sheets.
[13] Croda International Plc, CrodaTherm phase change materials, 2020, URL: https://www.crodaenergytechnologies.com/en-gb/applications/thermal-energy-storage.
[14] O. Okogeri, V.N. Stathopoulos, What about greener phase change materials? A review on biobased phase change materials for thermal energy storage applications, Int. J. Thermofluids 10 (2021) 100081.
[15] B. Zalba, J.M. Marın, L.F. Cabeza, H. Mehling, Review on thermal energy storage with phase change: materials, heat transfer analysis and applications, Appl. Therm. Eng. 23 (3) (2003) 251–283.
[16] L. Liu, D. Su, Y. Tang, G. Fang, Thermal conductivity enhancement of phase change materials for thermal energy storage: A review, Renew. Sustain. Energy Rev. 62 (2016) 305–317.

[17] S. Wu, T. Yan, Z. Kuai, W. Pan, Thermal conductivity enhancement on phase change materials for thermal energy storage: A review, Energy Storage Mater. 25 (2020) 251–295.

[18] EU, Directive 2014/68/EU of the European Parliament and of the Council of 15 May 2014 on the harmonisation of the laws of the Member States relating to the making available on the market of pressure equipmen, Off. J. Eur. Union (2014).

[19] T. Korth, F. Loistl, C. Schweigler, Novel integration of latent heat storage in multi-split air conditioning systems, in: 25th IIR International Congress of Refrigeration Proceedings, International Institute of Refrigeration, 2019.

[20] M.A. Ezan, A. Erek, I. Dincer, Energy and exergy analyses of an ice-on-coil thermal energy storage system, Energy 36 (11) (2011) 6375–6386.

[21] N. Tay, M. Belusko, F. Bruno, Experimental investigation of tubes in a phase change thermal energy storage system, Appl. Energy 90 (1) (2012) 288–297.

[22] A. López-Navarro, J. Biosca-Taronger, B. Torregrosa-Jaime, J. Corberán, J. Bote-García, J. Payá, Experimental investigations on the influence of ice floating in an internal melt ice-on-coil tank, Energy Build. 57 (2013) 20–25.

[23] A. López-Navarro, J. Biosca-Taronger, B. Torregrosa-Jaime, I. Martínez-Galván, J.M. Corberán, J. Esteban-Matías, J. Paya, Experimental investigation of the temperatures and performance of a commercial ice-storage tank, Int. J. Refrig. 36 (4) (2013) 1310–1318.

[24] A. Abhishek, B. Kumar, M.H. Kim, Y.T. Lee, J.D. Chung, S.T. Kim, T. Kim, C. Lee, K. Lee, Comparison of the performance of ice-on-coil LTES tanks with horizontal and vertical tubes, Energy Build. 183 (2019) 45–53.

[25] H. Selvnes, V. Büttner, A. Hafner, Evaluation of a pillow-plate heat exchanger for a pump-circulated CO2 refrigeration system, in: Proceedings of the 14th IIR-Gustav Lorentzen Conference on Natural Refrigerants, International Institute of Refrigeration, 2020.

[26] H. Selvnes, Y. Allouche, A. Hafner, Experimental characterisation of a cold thermal energy storage unit with a pillow-plate heat exchanger design, Appl. Therm. Eng. (2021) 117507.

[27] A. Castell, M. Belusko, F. Bruno, L.F. Cabeza, Maximisation of heat transfer in a coil in tank PCM cold storage system, Appl. Energy 88 (11) (2011) 4120–4127.

[28] B. Torregrosa-Jaime, A. López-Navarro, J.M. Corberán, J. Esteban-Matías, L. Klinkner, J. Payá, Experimental analysis of a paraffin-based cold storage tank, Int. J. Refrig. 36 (6) (2013) 1632–1640.

[29] A. López-Navarro, J. Biosca-Taronger, J. Corberán, C. Peñalosa, A. Lázaro, P. Dolado, J. Payá, Performance characterization of a PCM storage tank, Appl. Energy 119 (2014) 151–162.

[30] F. Bosholm, A. López-Navarro, M. Gamarra, J. Corberán, J. Payá, Reproducibility of solidification and melting processes in a latent heat thermal storage tank, Int. J. Refrig. 62 (2016) 85–96.

[31] M. Qu, Y. Tang, T. Zhang, Z. Li, J. Chen, Experimental investigation on the multi-mode heat discharge process of a PCM heat exchanger during TES based reverse cycle defrosting using in cascade air source heat pumps, Appl. Therm. Eng. 151 (2019) 154–162.

[32] R.M. Saeed, J.P. Schlegel, R. Sawafta, V. Kalra, Plate type heat exchanger for thermal energy storage and load shifting using phase change material, Energy Convers. Manage. 181 (2019) 120–132.

[33] T. Korth, F. Loistl, A. Storch, R. Schex, A. Krönauer, C. Schweigler, Capacity enhancement of air conditioning systems by direct integration of a latent heat storage unit, Appl. Therm. Eng. 167 (2020) 114727.

[34] Calmac Corp., Thermal energy storage in supermarkets, 2015, URL: http://www.calmac.com/stuff/contentmgr/files/0/a2c6d5b156fea7639cd0cd619f36c95a/pdf/ib_155_supermarket_market_brochure_160811.pdf.

[35] Viessmann Refrigeration Solutions, ESyCool green - Sustainable energy systems for food retailing, 2018, URL: https://cooling.viessmann.co.uk/en-gb/our-products/esycool-green.

[36] B. Ballot-Miguet, G. Dejardins, B. Quaro, A. Defruit, D. Rousset, Increasing the performances of a CO2 refrigeration system using cool thermal energy storage for subcooling: a supermarket application, in: Proceedings of the 25th IIR International Congress of Refrigeration, 2019, pp. 1062–1069.

[37] E.H. Verpe, I. Tolstorebrov, A. Sevault, A. Hafner, Y. Ladam, Cold thermal energy storage with low-temperature plate freezing of fish on offshore vessels, in: Proceedings of the 25th IIR International Congress of Refrigeration. Montréal, Canada, August 24-30, 2019, IIR, 2019.

[38] H. Selvnes, A. Hafner, H. Kauko, Design of a cold thermal energy storage unit for industrial applications using CO2 as refrigerant, in: 25th IIR International Congress of Refrigeration Proceedings, IIR, 2019.

[39] S. James, C. James, The food cold-chain and climate change, Food Res. Int. 43 (7) (2010) 1944–1956.

[40] D. Coulomb, Refrigeration and cold chain serving the global food industry and creating a better future: two key IIR challenges for improved health and environment, Trends Food Sci. Technol. 19 (8) (2008) 413–417.

[41] E. Oró, L. Miró, C. Barreneche, I. Martorell, M.M. Farid, L.F. Cabeza, Corrosion of metal and polymer containers for use in PCM cold storage, Appl. Energy 109 (2013) 449–453.

[42] M. Piper, A. Olenberg, J. Tran, E. Kenig, Determination of the geometric design parameters of pillow-plate heat exchangers, Appl. Therm. Eng. 91 (2015) 1168–1175.

[43] J. Tran, S. Sommerfeld, M. Piper, E. Kenig, Investigation of pillow-plate condensers for the application in distillation columns, Chem. Eng. Res. Des. 99 (2015) 67–74.

[44] M. Piper, A. Zibart, J. Tran, E. Kenig, Numerical investigation of turbulent forced convection heat transfer in pillow plates, Int. J. Heat Mass Transfer 94 (2016) 516–527.

[45] M. Piper, A. Zibart, E. Kenig, New design equations for turbulent forced convection heat transfer and pressure loss in pillow-plate channels, Int. J. Therm. Sci. 120 (2017) 459–468.

[46] M. Shirzad, M.A. Delavar, S.S.M. Ajarostaghi, K. Sedighi, Evaluation the effects of geometrical parameters on the performance of pillow plate heat exchanger, Chem. Eng. Res. Des. 150 (2019) 74–83.

[47] S. Kumar, B. Premachandran, P. Subbarao, Study on thermo–hydraulics in a pillow plate channel, Int. J. Therm. Sci. 145 (2019) 106020.

[48] C. Elliott, V. Vijayakumar, W. Zink, R. Hansen, National instruments LabVIEW: a programming environment for laboratory automation and measurement, JALA: J. Assoc. Lab. Autom. 12 (1) (2007) 17–24.

[49] HERMETIC Pumpen GmbH, HERMETIC refrigeration pumps, 2021, URL: https://kaelte.hermetic-pumpen.com/en/pump-types.

[50] DOW Chemical Company, DOWCAL 100 heat transfer fluid technical data sheet, 2021, URL: https://www.dow.com/en-us/document-viewer.html?ramdomVar=5550034686195609151&docPath=/content/dam/dcc/documents/en-us/productdatasheet/180/180-01588-01-dowcal-100-heat-transfer-fluid-tds.pdf.

[51] E. Lemmon, I. Bell, M. Huberm, M. McLinden, NIST Standard Reference Database 23: Reference Fluid Thermodynamic and Transport Properties-REFPROP, Version 10.0, National Institute of Standards and Technology, 2018, URL: https://www.nist.gov/srd/refprop.

[52] IEC ISO and BIPM OIML, Guide to the Expression of Uncertainty in Measurement, Vol. 122, Geneva, Switzerland, 1995, pp. 16–17.

[53] Rubitherm Technologies GmbH, Data sheet RT-9HC, 2020, URL: https://www.rubitherm.eu/media/products/datasheets/Techdata_-RT-9HC_EN_29092020.PDF.

[54] German Institute for quality assurance and certification, Phase change materials, quality assurance RAL-GZ 896, 2018, URL: https://www.pcm-ral.org/pdf/RAL_GZ_896_Phase_Change_Material_Edition_March_2018.pdf.

[55] C. Barreneche, A. Solé, L. Miró, I. Martorell, A.I. Fernández, L.F. Cabeza, Study on differential scanning calorimetry analysis with two operation modes and organic and inorganic phase change material (PCM), Thermochim. Acta 553 (2013) 23–26.

[56] S. Gschwander, T. Haussmann, G. Hagelstein, C. Barreneche, G. Ferrer, L. Cabeza, G. Diarce, W. Hohenauer, D. Lager, C. Rathgeber, et al., Standardization of PCM characterization via DSC, in: Proceedings of SHC 2015 International Conference on Solar Heating and Cooling for Buildings and Industry, 2015, pp. 2–4.

[57] G. Feng, K. Huang, H. Xie, H. Li, X. Liu, S. Liu, C. Cao, DSC test error of phase change material (PCM) and its influence on the simulation of the PCM floor, Renew. Energy 87 (2016) 1148–1153.

[58] M.N. Sam, A. Caggiano, C. Mankel, E. Koenders, A comparative study on the thermal energy storage performance of bio-based and paraffin-based PCMs using DSC procedures, Materials 13 (7) (2020) 1705.

[59] K.-H. Breuer, W. Eysel, The calorimetric calibration of differential scanning calorimetry cells, Thermochim. Acta 57 (3) (1982) 317–329.

[60] TA Instruments, Enthalpy of melting for standards, 2021, URL: https://www.tainstruments.com/pdf/literature/TN11.pdf.

[61] Y. Liu, X. Li, P. Hu, G. Hu, Study on the supercooling degree and nucleation behavior of water-based graphene oxide nanofluids PCM, Int. J. Refrig. 50 (2015) 80–86.

[62] S.E. Gustafsson, Transient plane source techniques for thermal conductivity and thermal diffusivity measurements of solid materials, Rev. Sci. Instrum. 62 (3) (1991) 797–804.

[63] J.C. Dixon, The Shock Absorber Handbook, John Wiley & Sons, 2008.

[64] J. Sengers, J.T.R. Watson, Improved international formulations for the viscosity and thermal conductivity of water substance, J. Phys. Chem. Ref. Data 15 (4) (1986) 1291–1314.

[65] A. Tambovtsev, H. Quack, COP improvement by transfer of the superheating into the internal heat exchanger, in: International Congress of Refrigeration, Beijing, China, 2007.

[66] S. Minetto, R. Brignoli, C. Zilio, S. Marinetti, Experimental analysis of a new method for overfeeding multiple evaporators in refrigeration systems, Int. J. Refrig. 38 (2014) 1–9.

[67] S. Bortolin, M. Rossato, S. Bernardinello, D. Del Col, Investigation of evaporator performance with and without liquid overfeeding, in: International Refrigeration and Air Conditioning Conference, Purdue, US, 2016.

[68] G. Mitsopoulos, E. Syngounas, D. Tsimpoukis, E. Bellos, C. Tzivanidis, S. Anagnostatos, Annual performance of a supermarket refrigeration system using different configurations with CO2 refrigerant, Energy Convers. Manage.: X 1 (2019) 100006.

[69] O. Arsenyeva, J. Tran, M. Piper, E. Kenig, An approach for pillow plate heat exchangers design for single-phase applications, Appl. Therm. Eng. 147 (2019) 579–591.